National Library of Canada

Acquisitions and Bibliographic Services Branch

395 Wellington Street
Ottawa, Ontario
K1A 0N4

Bibliothèque nationale du Canada

Direction des acquisitions et des services bibliographiques

395, rue Wellington
Ottawa (Ontario)
K1A 0N4

Your file Votre référence

Our file Notre référence

NOTICE

The quality of this microform is heavily dependent upon the quality of the original thesis submitted for microfilming. Every effort has been made to ensure the highest quality of reproduction possible.

If pages are missing, contact the university which granted the degree.

Some pages may have indistinct print especially if the original pages were typed with a poor typewriter ribbon or if the university sent us an inferior photocopy.

Reproduction in full or in part of this microform is governed by the Canadian Copyright Act, R.S.C. 1970, c. C-30, and subsequent amendments.

AVIS

La qualité de cette microforme dépend grandement de la qualité de la thèse soumise au microfilmage. Nous avons tout fait pour assurer une qualité supérieure de reproduction.

S'il manque des pages, veuillez communiquer avec l'université qui a conféré le grade.

La qualité d'impression de certaines pages peut laisser à désirer, surtout si les pages originales ont été dactylographiées à l'aide d'un ruban usé ou si l'université nous a fait parvenir une photocopie de qualité inférieure.

La reproduction, même partielle, de cette microforme est soumise à la Loi canadienne sur le droit d'auteur, SRC 1970, c. C-30, et ses amendements subséquents.

Canada

UNIVERSITY OF ALBERTA

COLLAPSE BEHAVIOR OF VERY LOOSE SAND

BY

© SABANAYAGAM SASITHARAN

Ⓒ

A THESIS
SUBMITTED TO THE FACULTY OF GRADUATE STUDIES AND RESEARCH
IN PARTIAL FULFILLMENT OF THE REQUIREMENTS
FOR
THE DEGREE OF DOCTOR OF PHILOSOPHY.

IN

DEPARTMENT OF CIVIL ENGINEERING

EDMONTON, ALBERTA
SPRING, 1994

National Library
of Canada

Acquisitions and
Bibliographic Services Branch

395 Wellington Street
Ottawa, Ontario
K1A 0N4

Bibliothèque nationale
du Canada

Direction des acquisitions et
des services bibliographiques

395, rue Wellington
Ottawa (Ontario)
K1A 0N4

Your file Votre référence

Our file Notre référence

The author has granted an irrevocable non-exclusive licence allowing the National Library of Canada to reproduce, loan, distribute or sell copies of his/her thesis by any means and in any form or format, making this thesis available to interested persons.

The author retains ownership of the copyright in his/her thesis. Neither the thesis nor substantial extracts from it may be printed or otherwise reproduced without his/her permission.

L'auteur a accordé une licence irrévocable et non exclusive permettant à la Bibliothèque nationale du Canada de reproduire, prêter, distribuer ou vendre des copies de sa thèse de quelque manière et sous quelque forme que ce soit pour mettre des exemplaires de cette thèse à la disposition des personnes intéressées.

L'auteur conserve la propriété du droit d'auteur qui protège sa thèse. Ni la thèse ni des extraits substantiels de celle-ci ne doivent être imprimés ou autrement reproduits sans son autorisation.

ISBN 0-612-11356-6

Canada

UNIVERSITY OF ALBERTA

RELEASE FORM

NAME OF AUTHOR:	SABANAYAGAM SASITHARAN
TITTLE OF THESIS:	COLLAPSE BEHAVIOR OF VERY LOOSE SAND
DEGREE:	DOCTOR OF PHILOSOPHY
YEAR THIS DEGREE GRANTED:	SPRING, 1994

Permission is hereby granted to the University of Alberta to reproduce single copies of this thesis and to lend or sell such copies for private, scholarly or scientific research purpose only.

The author reserves all other publication and other rights in association with the copyright in the thesis, and except as hereinbefore provide neither the thesis nor any substantial portion thereof may be printed or otherwise reproduced in any material form whatever without the author's prior written permission.

S. Sasitharan.

S. Sasitharan

603 D, Michener Park
Edmonton, Alberta
T6H 5A1.

Date: Oct 13/93

UNIVERSITY OF ALBERTA

FACULTY OF GRADUATE STUDIES AND RESEARCH

THE UNDERSIGNED CERTIFY THAT THEY HAVE READ, AND RECOMMENDED TO THE FACULTY OF GRADUATE STUDIES AND RESEARCH FOR ACCEPTANCE, A THESIS ENTITLED **COLLAPSE BEHAVIOR OF VERY LOOSE SAND** SUBMITTED BY **SABANAYAGAM SASITHARAN** IN PARTIAL FULFILLMENT OF THE REQUIREMENTS FOR THE DEGREE OF DOCTOR OF PHILOSOPHY IN **CIVIL ENGINEERING**.

PK Robertson

Dr. P.K. Robertson, Supervisor

DC Sego.

Dr. D.C. Sego, Co-Supervisor

Dr. N.R. Morgenstern

Dr. A.E. Elwi

M. J. Dudas

Dr. M. Dudas

Poul Lade

Dr. P. Lade

Date: October 04, 1993

DEDICATION

"...to Appa, Amma and Acca"

and

"...to Vasantha and Saaranga"

ABSTRACT

Since the major earthquakes of 1964 in Niigata, Japan and Alaska, USA significant improvements have been made in the understanding of liquefaction of sand. Most of the early research was related to the behavior of sand under undrained cyclic loading (Seed and Lee, 1966). Castro (1969) showed that loose sands can collapse and strain soften during monotonic undrained loading and ultimately reach a steady state.

In this dissertation an experimental study of the collapse behavior of a loose sand is presented. This study is based on a variety of loading conditions that can lead to collapse. The stress paths were selected such that collapse was initiated using both drained and undrained loading. A framework based on the concept of a state boundary surface is proposed for describing both the drained and undrained collapse of the material tested. The influence of a state boundary surface on the drained behavior of loose saturated sand is investigated. Drained sand behavior for anisotropically and isotropically consolidated samples is compared with the proposed state boundary surface for the sand and the concept is also evaluated based on published results for various other sands. The practical implications of the state boundary surface on liquefaction behavior of sand are discussed.

It is shown that the shear wave velocity and the vertical effective stress can be used to identify sands that can show collapse behavior. It is also shown that this method based on shear wave velocity is consistence with the existing field methods based on SPT $(N)_{60}$ and CPT q_c. Further, the shear wave velocity interpretation is extended for sand containing small amount of fines. It is shown that shear wave velocity interpretation can be used for sands with small amount of fines without any correction for fines content.

ACKNOWLEDGMENTS

The work described in this thesis was carried out in the soil mechanics laboratory of University of Alberta and was supervised by Professors P.K. Robertson and D.C Sego. The research was supported by the natural science and engineering research council of Canada (NSERC) and Department of supplies and services contract N0 23420-0-M343/01-OSC. Thanks are due to both bodies for their financial support.

I wish to express my deepest gratitude to Drs. P.K. Robertson and D.C. Sego for their continuous encouragement, guidance and availability throughout this research. Their kindness and support will always be cherished. Working with them has been a valuable and pleasant experience.

I am deeply indebted to Dr. N.R. Morgenstern for his valuable advice regarding sand collapse process and relevant stress paths without which the investigation could not have achieved it's accomplishment.

I wish to express my sincere thanks to Dr. W.H. Gu and R. Dawson for their valuable discussion and suggestion during the testing program. I would also like to thank Professor K. Ishihara of University of Tokyo and Dr. K. Been of Golder Associates for providing Toyoura and Erksak sand data, respectively.

I would like to acknowledge the valuable assistance of the University of Alberta, Department of Civil Engineering technical staff G. Cyre, S. Gamble, C. Hereygess and J. Khajuria. G. Cyre provided prompt and invaluable support in the design, construction and maintenance of the apparatus used in the study. S. Gamble

helped with extensive experimental work. Graduate students Chan Zuge and T. Pitman provided helping hands during the experimental work.

Very special thanks with love must be expressed to my wife, Vasantha, who not only shared the difficult period of student life with me but also provided valuable moral and financial support. Mr. S. Thanigasalam and family provide inspiration and encouragement during our stay in Edmonton. I must also remember the affection and scarifies of my parents and my sister. They showed continuous interest in my career and insisted that I do post graduate study.

Last but not least, I would like to express my deepest gratitude to High school mathematics teacher A. Ratnasabapathy, to my undergraduate thesis supervisor Prof. A. Thurairaja, to my M.A.Sc supervisor Prof. Y.P. Vaid for their continuous encouragement.

TABLE OF CONTENTS

1. INTRODUCTION 1
Outline of Thesis 3
References 5

2. SAMPLE DISTURBANCE FROM SHEAR WAVE VELOCITY MEASUREMENTS

Introduction 7
Previous Laboratory Studies 10
Test Apparatus and Procedures 12
Sample Freezing 12
Shear Wave Velocity Measurements 13
Material Tested and Sample Preparation 15
Results and Discussion 15
Conclusions 17
References 18

3. COLLAPSE BEHAVIOR OF VERY LOOSE SAND

Introduction 31
Testing Apparatus 34
Experimental Problems 36
Sample Uniformity 36
Void Ratio Calculation 37
Test Program 38
Test Results 40

Constant Void Ratio Loading 40

Drained Collapse Behavior 40

State Boundary Surface for Interpretation of Test Results 43

Summary and Conclusions 46

4. A STATE BOUNDARY SURFACE FOR VERY LOOSE SAND

Introduction 66

Testing Program 68

Monotonic Undrained Loading 69

Monotonic Drained Loading 71

Test Results 73

Monotonic Undrained Loading 73

Monotonic Drained Loading 75

State Boundary Surface for Very Loose Sand 77

Interpretation of Drained Behavior of Loose Ottawa Sand

Using The State Boundary Surface 81

State Boundary Surface For Ottawa Sand 81

Monotonic Drained Loading 83

State Boundary Surface for Other Sands 85

Practical Implications 86

Summary and Conclusions 89

References 91

5. SHEAR WAVE VELOCITY TO EVALUATE FLOW LIQUEFACTION

Introduction 125

Testing Apparatus 131

Material Tested and Sample Preparation 133

Testing Program 134

Repeatability of Test Results.. 135

Results and Interpretation.. 135

Shear Wave Velocities During Consolidation 138

Evaluating The Potential for Flow Liquefaction Using Shear Wave Velocity 139

Field Application.. 144

Summary 146

References 148

6. PRELIMINARY EVALUATION OF FLOW LIQUEFACTION OF SILTY SANDS USING SHEAR WAVE VELOCITY

Introduction 172

Testing Program 175

Results and Interpretation.. 176

Summary and Conclusions.. 179

References 180

7. FABRIC STUDIES ON VERY LOOSE SAND

Introduction 191

Test Program 193

Results of Scanning Electron Microscope Analysis 194

Discussion 194

Conclusions 196

8. SUMMARY AND CONCLUSIONS.. 201

Recommendations for Future Work.. 204

APPENDIX A

Experimentation 206

APPENDIX B

Freeze Thaw Test Results 222

List of Figures

Figure 1.1. .... Schematic behavior of a cohesionless soil in monotonic undrained triaxial compression (after Robertson, 1993). 6

Figure 2.1. .... Relationship between the surface area index and fine mineralogy ratio for frost susceptibility boundary analysis (after Davila et al., 1992). 24

Figure 2.2. .... Schematic of a typical ground freezing system. 25

Figure 2.3. .... Schematic layout of freezing triaxial samples. 26

Figure 2.4. .... Bender element mounted on bottom pedestal. 27

Figure 2.5. .... Schematic layout of shear wave measuring system. 28

Figure 2.6. .... Typical axial strain behavior of a sample comprised of Ottawa sand and 5% Devon Silt. 29

Figure. 3.1. .... Typical stress-strain and resulting stress path for an undrained monotonic triaxial compression test. (a) stress path (b) stress-strain (c) pore pressure 51

Figure. 3.2. .... Steady state representation in e-p'-q space along with representation using e-p', e-q and p'-q planes. 52

Figure. 3.3. .... Collapse surface (modified from Sladen et al., 1985a). 53

Figure. 3.4. .... Effective stress paths for monotonic undrained loading and cyclic to monotonic undrained loading (modified from Ishihara et al., 1991). 54

Figure. 3.6. .... Schematic of testing apparatus. 56

Figure. 3.8. .... The deviator stress-axial strain response and resulting stress path of constant deviator stress (q=125 kPa) drained test. 58

Figure. 3.10. .... Stress paths of constant void ratio (0.804) test and constant deviator stress (q=125 kPa) drained test. 60

Figure. 3.11. .... State boundary defined by void ratio 0.804 and constant deviator stress (q=100 kPa) drained stress path. 61

Figure. 3.12. .... State boundary defined by void ratio 0.809 and constant deviator stress (q=100 kPa) drained stress path. 62

Figure. 3.13. .... Typical collapse surface in effective mean normal stress-deviator stress-void ratio space. 63

Figure. 3.14. .... Comparison of state boundary and collapse surface proposed by Sladen et al. (1985a) 64

Figure. 3.15 .... Monotonic undrained stress paths starting from various confining stresses for a given void ratio. (modified from Ishihara et al., 1991). 65

Figure 4.1 .... State boundary surface for remolded clay. 97

Figure 4.2 .... A schematic of a conventional drained triaxial compression stress path starting from an isotropic stress state. 98

Figure 4.3 .... A schematic of the drained constant effective mean normal stress path from the post peak portion of an undrained stress path. 99

Figure 4.4 .... A schematic of the drained constant effective minor principal stress path from the post peak portion of an undrained stress path. 100

Figure 4.5 .... The deviator stress-axial strain response and resulting stress paths for the monotonic undrained triaxial compression test on samples consolidated to an identical void ratio of 0.793. 101

Figure 4.6 .... The deviator stress- axial strain response and resulting stress path for the monotonic undrained triaxial compression test on samples connsolidated to an identical void ratio of 0.803. 102

Figure 4.7 .... Undrained stress paths of a very loose sample (e = 0.809) and a sample consolidated to a high stress (e= 0.758, p'o = 1470 kPa). 103

Figure 4.8(a) .... The deviator stress- axial strain behavior for the monotonic drained conventional triaxial compression test on a sample consolidated to an isotropic stress of 515 kPa and void ratio of 0.808. 104

Figure 4.8(b) .... The volumetric strain- axial strain behavior for the monotonic drained conventional triaxial compression test on a sample consolidated to an isotropic stress of 515 kPa and void ratio of 0.808. 105

Figure 4.9 .... Resulting stress path for the monotonic drained conventional triaxial compression test on a sample consolidated to an isotropic stress of 515 kPa and void ratio of 0.808. 106

Figure 4.10 .... The stress-strain behavior for the monotonic drained triaxial compression constant effective mean normal stress test performed from the post peak portion of an undrained stress path. 107

Figure 4.11 .... Resulting stress path for the monotonic drained triaxial compression constant effective mean normal stress test performed from the post peak portion of an undrained stress path. 108

Figure 4.12 .... The stress-strain behavior for the monotonic drained conventional triaxial compression test performed from the post peak portion of an undrained stress path. 109

Figure 4.13 .... Resulting stress path for the monotonic drained conventional triaxial compression test performed from the post peak portion of an undrained stress path. 110

Figure 4.14 .... A schematic of state boundary surface for very loose sand. 111

Figure 4.15 .... Projection of the state boundary surface in deviator stress-effective mean normal stress space. 112

Figure 4.16 .... Projection of the steady state curve in void ratio-effective mean normal stress space. 113

Figure 4.17 .... Steady state curve for loose Ottawa sand in deviator stress-effective mean normal stress space. 114

Figure 4.18 .... Steady state curve for loose Ottawa sand in void ratio-effective mean normal stress space. 115

Figure 4.19 .... Comparison of the conventional isotropically consolidated drained triaxial compression stress path with the state boundary defined by equation [4.6] for Ottawa sand. 116

Figure 4.20 .... Comparison of constant effective mean normal stress test performed from the post peak portion of an undrained stress path with the state boundary defined by equation [4.6] for Ottawa sand. 117

Figure 4.21 .... Comparison of conventional triaxial compression test performed from the post peak portion of an undrained stress path with the state boundary defined by equation [4.6] for Ottawa sand. 118

Figure 4.22 .... Comparison of the conventional isotropically consolidated drained triaxial compression stress path with the state boundary defined by equation [4.6] for Toyoura sand (Consolidation stress 197 kPa). 119

Figure 4.23 .... Comparison of the conventional isotropically consolidated drained triaxial compression stress path with the state boundary defined by equation [4.6] for Toyoura sand (Consolidation stress 394 kPa). 120

Figure 4.24 .... Comparison of the conventional isotropically consolidated drained triaxial compression stress path with the state boundary defined by equation [4.6] for Erksak sand (Consolidation stress 394 kPa, void ratio 0.820). 121

Figure 4.25 .... Comparison of the conventional isotropically consolidated drained triaxial compression stress path with the state boundary defined by equation [4.6] for Erksak sand (Consolidation stress 394 kPa, void ratio 0.815). 122

Figure 4.26 .... Schematic of two stress paths that can trigger collapse. 123

Figure 4.27 .... An element of sand with stress state on the state boundary. 124

Figure 5.1 .... Initial state of a soil relative to steady/critical state. 154

Figure 5.2 .... Flow chart for liquefaction evaluation. (After Robertson, 1993). 155

Figure 5.3 .... Schematic of testing apparatus. 156

Figure 5.4 .... Repeatability of water pluviated samples interms of void ratio and shear wave velocity. 157

Figure 5.5 .... Repeatability of moist tamped samples interms of void ratio and shear wave velocity. 158

Figure 5.6 .... Shear wave velocity and void ratio changes during consolidation of loose, medium dense and dense Ottawa sand. 159

Figure 5.7 .... Steady state shear wave velocities and void ratio for Ottawa sand. 160

Figure 5.8 .... Normalized shear wave velocity during consolidation for very loose Ottawa sand. 161

Figure 5.9 .... Normalized shear wave velocity during consolidation for very loose, medium dense and dense Ottawa sand. 162

Figure 5.10 .... Void ratio against logarithm of effective mean normal stress, showing the steady/critical state line and contours of shear wave velocity constructed using equation [5.10] as well as measured shear wave velocities. 163

Figure 5.11 .... Contours of shear wave velocity on a plot of void ratio against logarithm of effective mean normal stress over a wide range of void ratio and stress level. 164

Figure 5.12 .... The stress-strain behavior for the monotonic drained conventional triaxial compression test on a sample consolidated to an isotropic stress of 100 kPa and void ratio of 0.876. 165

Figure 5.13 .... The stress-strain behavior for the monotonic drained conventional triaxial compression test on a sample consolidated to an isotropic stress of 100 kPa and void ratio of 0.674. 166

Figure 5.14 .... The variation of Vsy calculated from the measured shear wave velocity and stresses with the state parameter calculated from the consolidation void ratio. 167

Figure 5.15 .... Boundary between contractive and dilative behavior at large strains based on shear wave velocity for Ottawa sand. 168

Figure 5.16 .... Boundary between contractive and dilative behavior at large strains using SPT (N)60 based on shear wave velocity criteria for Ottawa sand. 169

Figure 5.17 .... Comparison between contractive and dilative boundaries using SPT (N)60 based on shear wave velocity and those proposed by Ishihara (1993) and Robertson et al. (1992a). 170

Figure 5.18 .... Comparison between contractive and dilative boundaries using CPT (qc) based on shear wave velocity and those proposed by Sladen and Hewitt (1989), Robertson et al. (1992a) and Ishihara (1993). 171

Figure 6.1 .... The stress-strain behavior and resulting stress path for the monotonic undrained triaxial compression test performed on very loose Ottawa sand with 5% Kaolinite (isotropic consolidation stress of 650 kPa and void ratio of 0.800) 183

Figure 6.2 .... The stress-strain behavior and resulting stress path for the monotonic undrained triaxial compression test performed on very loose Ottawa sand with 5% Kaolinite (isotropic consolidation stress of 500 kPa and void ratio of 0.817) 184

Figure 6.3 .... The stress-strain behavior and resulting stress path for the monotonic undrained triaxial compression test performed on very loose Ottawa sand with 5% Kaolinite (isotropic consolidation stress of 250 kPa and void ratio of 0.890) 185

Figure 6.4 .... The stress-strain behavior and resulting stress path for the monotonic drained conventional triaxial compression test performed on very loose Ottawa sand with 5% Kaolinite. 186

Figure 6.5 .... Normalized shear wave velocity during consolidation for very loose Ottawa sand with 5% Kaolinite. 187

Figure 6.6 .... Normalized shear wave velocity at steady state vs. intergranular void ratio for Ottawa sand with 5% Kaolinite. 188

Figure 6.7 .... Steady state line in terms of intergranular void ratio against logarithm of effective mean normal stress for Ottawa sand with 5% Kaolinite. 189

Figure 6.8 .... Boundary between contractive and dilative behavior at large strain based on shear wave velocity for clean Ottawa sand and Ottawa sand with 5% Kaolinite. 190

Figure 7.1. .... SEM photographs of very loose Ottawa sand after consolidation. 199

Figure 7.2. .... SEM photographs of very loose Ottawa sand at steady state. 200

Figure A1.................... Schematic of the monotonic and cyclic triaxial testing system. 221

Figure B.1.................. Typical axial strain and water explusion behavior of a Ottawa sand sample at 100 kPa confining stress during freezing and thawing. 223

Figure B.2.................. Typical axial strain and water explusion behavior of a Ottawa sand sample at 50 kPa confining stress during freezing and thawing. 224

Figure B.3.................. Typical axial strain and water explusion behavior of a sample comprised of Ottawa sand and 5% Devon silt during freezing and thawing. 225

Figure B.4.................. Typical axial strain and water explusion behavior of a sample comprised of Ottawa sand and 12.5% Devon silt during freezing and thawing. 226

Figure B.5.................. Typical axial strain and water explusion behavior of a sample comprised of Ottawa sand and 5% Kaolinite during freezing and thawing. 227

Figure B.6.................. Typical axial strain and water explusion behavior of a sample comprised of Ottawa sand and 10% Kaolinite during freezing and thawing. 228

List of Tables

Table 2.1.................... Properties of fines. 22

Table 2.2.................... Summary of results from freeze-thaw tests 23

Table 4.1 .... Void ratio and stress state for undrained triaxial compression tests. 95

Table 4.2.................... State boundary surface constants for various sands. 96

Table 5.1.................... Summary of shear wave velocity measured during consolidation. 153

Table 6.1 .... Summary of Test Results from Ottawa sand with 5% Kaolinite. 182

CHAPTER 1

INTRODUCTION

To evaluate either the response of existing structures or to design new structures on or with soil that may liquefy it is important to understand the soil behavior under the appropriate loading condition. In engineering practice, the generic term liquefaction is used to describe different mechanisms. Seed and Lee (1966), using the results of extensive cyclic triaxial testing, defined liquefaction as the condition of zero effective confining stress due to cyclic loading with shear stress reversal. At zero effective stress a cohesionless soil has very little stiffness and large deformations can develop during the cyclic loading. Castro (1969) defined liquefaction as the strain softening and collapse of a loose sand to an ultimate state of constant effective stress and deformation.

During monotonic undrained loading a loose sand can reach a peak resistance and then rapidly strain soften to a constant resistance at which the effective stress state remains constant. Castro (1969) termed this ultimate constant state as the steady state and showed that it represents a state in the void ratio-effective mean normal stress-deviator stress space. If the gravitational shear stresses are larger than the ultimate strength at steady state, large flow deformations can occur. Been *et al.* (1991) showed that the ultimate steady state achieved during monotonic undrained loading is also a critical state implying that steady state is independent of the stress path followed, i.e., steady state is unique for a void ratio regardless of whether it was reached via drained or undrained loading.

Figure 1.1 shows a schematic summary of the behavior of a granular soil loaded in undrained triaxial compression. A soil with an initial state higher than the steady state will be strain softening (SS) at large strains, whereas a soil with an initial state lower than the steady state will be strain hardening (SH) at large strains. It is possible to have a soil with an initial state higher than the steady state but close to steady state. For this soil state the response can show limited strain softening (LSS), but eventually at large strains the response becomes strain hardening to the ultimate steady state. For a soil with limited strain softening (LSS) there can be a quasi-steady state before strain hardening occurs to the ultimate steady state.

If a soil structure, such as, an earth dam or tailings dam, is composed entirely of a strain softening soil and the *in-situ* gravitational shear stresses are larger than the ultimate steady state strength (i.e. a relatively steep slope), a catastrophic collapse and flow slide can occur if the soil is triggered to strain soften.

If a soil structure is composed entirely of a limited strain softening soil and the *in-situ* gravitational shear stresses are larger than the quasi-steady state strength, a catastrophic flow slide is unlikely. However, large deformations can occur before the soil stiffens as it strain hardens towards its ultimate state.

If a soil structure is composed entirely of strain hardening soil, undrained collapse and flow slide can not occur and deformations will, in general, be small.

Hence, the first step in any liquefaction analysis is to eveluate the material characteristic in terms of strain softening or strain hardening response (Robertson, 1993). The preferred method to evaluate the response of a soil to a given loading is to obtain high quality undisturbed samples and perform relevant laboratory testing following appropriate stress paths. However, obtaining high quality undisturbed samples is difficult in cohesionless soils such as sand. The disturbance during the sampling process induces void ratio change and structural rearrangements of the soil particles. Therefore, there have been several studies on reconstituted cohesionless soils to evaluate material characteristic in terms of strain softening or strain hardening response to estimate the field loading response of these materials. If the material response is strain softening, then the strength at the moment of collapse is important for any safety evaluation.

Outline of Thesis

This thesis is presented in a paper format and consequently each chapter describes aspects that is identified with the collapse behavior of granular material.

The second chapter presents the results of a study to evaluate sample disturbance due to artificial ground freezing using shear wave velocity measurements. The triaxial freezing setup and the shear wave velocity measuring systems are described. Test results on cohesionless soil samples prepared with various amounts of fines and type of fines (< 74 μm) are presented. These samples were prepared to ensure that some would be disturbed (heaved) and others would remain undisturbed by the freezing. For these samples, shear wave velocities measured before freezing were compared with the shear wave velocities measured after the sample was frozen and subsequently thawed.

A preliminary study of the collapse behavior of a loose sand is presented in the third chapter. This study is based on a variety of loading conditions which can lead to collapse. The stress paths were selected such that collapse was initiated using both slow (drained) and rapid (undrained) loading. A framework based on a state boundary surface is proposed for describing both the drained and undrained collapse of the material tested and which may be applicable for other cohesionless materials.

The influence of a state boundary surface on the drained behavior of loose saturated sand is investigated in the fourth chapter. Drained sand behavior for anisotropically and isotropically consolidated samples is compared with the proposed state boundary surface for the sand. The proposed state boundary surface concept is also evaluated based on published results for various other sands. Finally practical implications of the state boundary surface on the collapse behavior of sand is discussed.

The fifth chapter presents results of an experimental study performed to evaluate whether shear wave velocity can be used to identify the behavior of a sand at large strain. It is shown that the shear wave velocity can be related to the effective confining stresses and void ratio regardless of the soil fabric in a loose sand. Further, the shear wave velocity can be used to identify whether a given sand is contractant or dilatant at large strains. The next chapter, six, presents results of an experimental study performed to evaluate whether shear wave velocity can be used to identify the behavior of a sand with a small amount of fines content (< 5%) at large strain.

The seventh chapter describes results of fabric analysis performed using scanning electron microscope. The very loose sand fabric after consolidation is compared with the sand fabric at steady state. Conclusions and recommendations for further studies are presented in the eighth chapter.

REFERENCES

Been. K., Jefferies. M. G. and Hachey. J. 1991. The critical state of sand. Geotechnique, **41**: 365-381.

Castro, G. 1969. Liquefaction of sands. Harvard Soil Mechanics Series No. 81. 112 pp.

Robertson, P.K. 1993. Design consideration for liquefaction. US-Japan Workshop, June 1993.

Seed, H. B. and Lee, K. L. 1966. Liquefaction of saturated sands during cyclic loading. Journal of Soil mechanics and Foundation Engineering, American Society of Civil Engineering, **92**(6): 105-134.

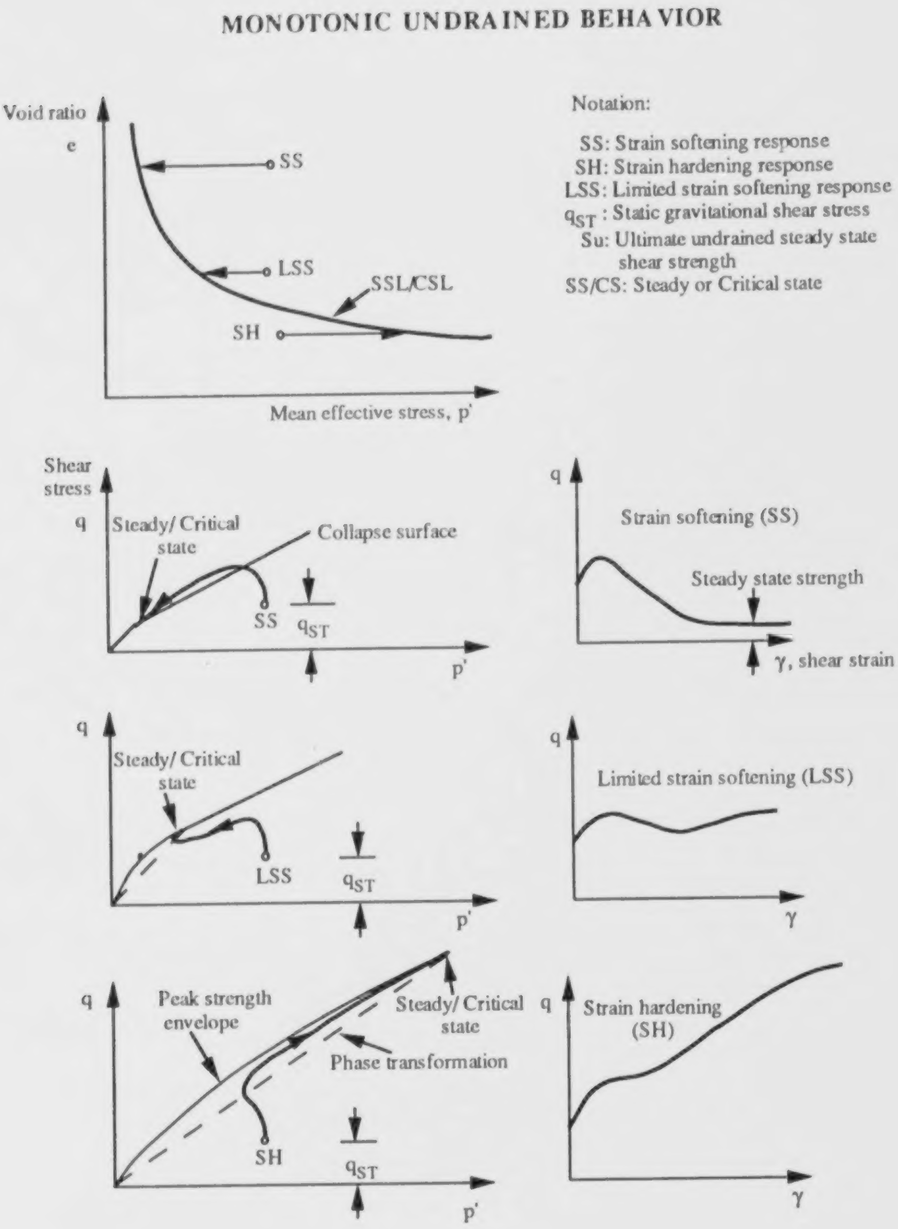
MONOTONIC UNDRAINED BEHAVIOR
Void ratio
e
SS
LSS
SSL/CSL
SH
Mean effective stress, p'
Notation:
SS: Strain softening response
SH: Strain hardening response
LSS: Limited strain softening response
q_ST : Static gravitational shear stress
Su: Ultimate undrained steady state shear strength
SS/CS: Steady or Critical state
Shear stress
q
Steady/ Critical state
Collapse surface
SS
q_ST
p'
q
Strain softening (SS)
Steady state strength
γ, shear strain
q
Steady/ Critical state
LSS
q_ST
p'
q
Limited strain softening (LSS)
γ
q
Peak strength envelope
Steady/ Critical state
Phase transformation
SH
q_ST
p'
q
Strain hardening (SH)
γ

Figure 1.1. Schematic behavior of a cohesionless soil in monotonic undrained triaxial compression (after Robertson, 1993).

CHAPTER 2

SAMPLE DISTURBANCE FROM SHEAR WAVE VELOCITY MEASUREMENTS*

INTRODUCTION

Techniques are currently available to obtain high quality undisturbed samples of cohesive soils. However, little advance had been made in the procurement of undisturbed samples of cohesionless soils such as sands, silty sands and clayey sands. Conventional sampling techniques of cohesionless soils induce void ratio changes and particle rearrangements due to mechanical disturbance, reduction in confining stress, poor handling during transportation and storage and while trimming prior to testing. The behavior of a cohesionless soil can change from strain softening to strain hardening during undrained loading when a small change in void ratio occurs due to this disturbance. Therefore, in the area of earthquake design and liquefaction researchers and practitioners are becoming more aware of the importance of obtaining high quality undisturbed samples of cohesionless soils.

---

* A version of this chapter has been published: Sasitharan, S., Robertson, P. K. and Sego. D. C. 1992. Sample disturbance from shear wave velocity measurements. 45th Canadian Geotechnical Conference, Toronto. 23:1-23:7.

Efforts have been made to evaluate the degree of disturbance that can take place during conventional sampling techniques (Marcuson *et al.*, 1977). However, there are inherent difficulties in correctly assessing the degree of disturbance of a natural sand deposit caused by conventional sampling techniques especially how disturbance affects the strain softening behavior of very loose cohesionless soils.

Ground freezing has been used as a soil stabilization method for underground excavations. However, there have been only a limited number of attempts to use ground freezing techniques to obtain undisturbed soil samples. The US. Corps of Engineers first reported the use of artificial ground freezing to obtain undisturbed samples in a study at Fort Peck Dam (1938, US. Army Corps). Following the work of the Corp. of Engineers, there have been several other attempts to use ground freezing to obtain undisturbed samples (Bishop, 1948; Hanzawa and Matsuda, 1977; Marcuson *et al.*, 1977).

Several factors affect whether a soil can be frozen without disturbance. The suction and expansion of the interstitial water at the time of phase change during the freezing process is the primary obstacle to obtaining an undisturbed soil sample. Hence, the water migration during the freezing process must be fully understood in order to determine whether the soil can be frozen without disturbance. These factors are also related to the frost heave susceptibility of the soil.

An excellent review of frost heave and frost susceptibility of soils was presented by Horne (1987). Konrad and Morgenstern (1980) presented an engineering model for frost heave that includes the effects of soil permeability, segregational freezing, temperature gradient, suction at the freezing front, rate of cooling and the vertical stress. Yoshimi *et al.* (1978) pointed out that neither the coefficient of permeability nor the gradation alone can count for the soil disturbance during freezing. They attempted to determine the frost heave behavior of sands with increasing fine content and concluded that for saturated sands the disturbance due to freezing increases proportionally to the percent fines.

Davila *et al.* (1992) defined the range of soils in which in-situ freezing can be applied to obtain undisturbed samples. They proposed a new criteria to distinguish between frost heaving and non frost heaving of a sandy soil based on the amount of clay minerals presented in the soil and the specific surface area of the clay in the fine portion of the sandy soil. From uniaxial freezing tests performed on sandy soils with different amount and type of fines, they established an approximate boundary between soil that can or cannot be frozen without disturbing its matrix. A summary of the proposed relationship is shown in Figure 2.1.

A sketch of a freezing system is shown in Figure 2.2. The freezing system consists of an inner freezing pipe and an outer freezing pipe. Coolant is supplied through the inner pipe and flows to the surface via the outer pipe. While the coolant flows upward in contact with the outer pipe, heat is removed from the ground by conduction through the wall of the freeze pipe. Coolants used can be liquid nitrogen (-196 °C), ethanol and dry ice (-70 °C) or brine (liquid calcium chloride -30 °C).

There have been several attempts to obtain undisturbed samples by using a freezing system shown in Figure 2.2 (Yoshimi *et al.*, 1984; Hatanaka *et al.*, 1985; Yoshimi *et al.*, 1989; Sego *et al.*, 1993). In most of these attempts of artificial ground freezing, the quality of the samples was estimated by visual examination of the trimmed samples and comparing the laboratory measured densities with *in-situ* densities measured using geophysical methods. Although these samples appeared to have retained their *in-situ* densities, it was not shown conclusively that the sand structure was undisturbed by the freezing and subsequent thawing.

The shear wave velocity reflects the *in-situ* state of a soil in terms of; soil structure, void ratio (density), consolidation history and effective confining stress (Hardin *et al.*, 1972; Tokimatsu *et al.*, 1986). Sample disturbance induces changes in density and soil particle arrangement (structure). Hence, the shear wave velocity may be used to reveal changes in the *in-situ* state and hence, sample disturbance.

This chapter presents the results of a study to evaluate sample disturbance due to artificial ground freezing using shear wave velocity measurements. The triaxial freezing setup and the shear wave velocity measuring systems are described. Test results on reconstituted cohesionless soil samples prepared with various amounts of fines and type of fines (< 74 μm) are presented. These samples were prepared to ensure that some would be disturbed (heaved) and others would remain undisturbed by the freezing. For these samples, shear wave velocities measured before freezing were compared with the shear wave velocities measured after the sample was frozen and thawed.

PREVIOUS LABORATORY STUDIES

Yoshimi *et al.* (1978) conducted a series of radial freezing tests to study the effect of surcharge pressure on vertical strains during freezing. They observed that for sands containing less than 5% fines, the expansive strains due to freezing were less than 0.1% when the vertical effective stress exceeded about 30 kPa. They also showed that freezing and thawing had negligible effect on the drained shear strength and deformation characteristics at large strains near failure. However, Yoshimi *et al.*

(op. cit.) did not provide information regarding the effect of artificial ground freezing on the small strain behavior (< $10^{-4}\%$) and the dynamic characteristics of the samples.

Singh *et al.* (1982) presented a series of unidirectional freezing test results on Monterey #0 sand. They studied the possible effects of removal of confining pressure (after freezing the sample) and frozen storage (24 hours) on the dynamic characteristics of the sand. Singh *et al.* (op. cit.) reported no difference between the dynamic characteristics of the unidirectionally frozen and thawed samples and those of unfrozen samples. The carefully prepared laboratory samples were not subjected to the effect of coring associated with *in-situ* freezing and sampling. Therefore, in addition Singh *et al.* (1982) performed tests on samples cored from a large diameter (304.8 mm) unidirectionally frozen specimen. They reported that the dynamic characteristics of the sand remained essentially unchanged by freezing and coring. Further, they concluded that the effectiveness of freezing depends on the coolant temperature, the percentage fines and the depth of sampling. However, Singh et al. (op. cit.) did not study the effect of variations in fines content. Singh *et al.* (1982) like Yoshimi *et al.* (1978), compared the effects of freezing on soil behavior near failure and did not compare the effect of freezing in the small strain range. Recent research has illustrated the importance of the small strain response of soils and the sensitivity of the small strain response to disturbance. The following describes the triaxial freezing and small strain measurement apparatus build at the University of Alberta, as well as, the laboratory program to evaluate the influence of the freeze thaw cycle on the small strain behavior.

TEST APPARATUS AND PROCEDURES

All tests were performed using a triaxial apparatus. Important features of the testing system are:

Sample freezing

A schematic layout of the freezing set up is shown in Figure 2.3. The base of the triaxial cell was modified such that a freezing plate can be attached. By circulating coolant through this plate various temperature gradients can be obtained across the sample. Further, the heat loss to the frame was minimized by keeping the complete triaxial frame in a cooler maintained at 4 °C. During freezing, it is essential to maintain constant cell pressure, therefore, an industrial oil Faxam 22 that has a freezing temperature of -60°C was used as the cell fluid.

Liquid Nitrogen at -196°C was circulated through the base freezing plate for this study. When liquid Nitrogen is circulated through the freezing plate the soil sample starts to freeze one-dimensionally from the bottom upwards. The temperature at the bottom pedestal and the fluid temperature around the top cap were measured using Resistance Temperature Devices (RTD). When the top RTD measured 0°C the circulation of liquid Nitrogen was stopped and then the sample was allowed to thaw for approximately 15 hours.

During freezing and thawing, the top drainage line was kept open to allow an open drainage system. The change in volume of the sample and height was measured continuously by an automatic volume measuring device and a linear displacement transducer (LVDT). All other test variables were measured using electronic transducers which were also collected and stored on a microcomputer.

Shear wave velocity measurements

Shear waves were generated and received using bender elements (Shirley, 1978). The bender element consists of two thin plates of ceramic material rigidly bonded together. Hamdi and Taylor-Smith (1982) used bender elements to measure shear wave velocities in oedometer and triaxial apparatus. Dynik and Madshu (1985) evaluated and compared shear modulus obtained using the resonant column tests and using bender elements and reported excellent agreement between these methods. The introduction of bender elements facilitates shear wave velocity measurements in most laboratory testing apparatus.

The bender elements are high impedance devices that cannot be exposed to moisture since it will electrically short the transducers. Therefore, the bender element must be cased in a water proof material. Clear epoxy (PF 5-7B Marine sealant) casing was used to prevent exposure to moisture. The cased bender elements were then placed in a slot in both the bottom and top cap of the triaxial cell. The slot was then filled with epoxy to approximately 10 mm height such that one third of the bender element protrudes into the specimen. The rest of the slot was then filled with sealant to prevent soil grains from entering between the bender elements and the bottom pedestal or top cap. A schematic of the bender element arrangement is shown in Figure 2.4.

A schematic layout of the shear wave velocity measuring system is shown in Figure 2.5. A pulse from the wave form generator provides the electrical pulse (± 15 V, 20 Hz) to the driving bender element and triggers the oscilloscope (Philips

PM 3365A digital storage oscilloscope). The polarization of the ceramic material in each bender and the electrical connection are such that when a driving voltage is applied to the bender element, one plate elongates and the other shortens. Hence, one edge of the bender element protrudes into the specimen as a cantilever and deforms as shown on Figure 2.4. The surrounding soil particles move in the same direction as the tip of the bender element. This generates a shear wave which propagates vertically in the sample.

The bender element can also be used as a receiver. When the shear wave reaches the receiving bender element it creates a mechanical vibration, which causes one layer of the bender element to undergo tension while the other undergoes compression, hence, generating an electrical pulse that is displayed on the oscilloscope screen. The travel time of the shear wave through the soil sample is determined from the time lag of the pulse of the receiving bender element. Hence the shear wave velocity is calculated by;

$$V_S = \frac{L}{t} \tag{2.1}$$

where;

L = the travel length

t = the travel time.

MATERIAL TESTED AND SAMPLE PREPARATION

Ottawa (C 109) sand obtained from Ottawa, Illinois was used in this study. Ottawa sand is a uniform sand with a mean grain size (D_{50}) of 0.35 mm and comprised primarily of quartz with a specific gravity of 2.67. Various amounts of fines were mixed with the Ottawa sand to obtain various sample gradation curves. Properties of the two types of fines added are given in Table 2.1. The slurry deposition method described by Kurbies *et al.* (1989) was used to make the samples of sand and fines mixture. This method of sample preparation simulates the natural deposition of sand through water and yields homogeneous cohesionless samples.

Davila *et al.* (1992) showed that the amount and type of fines influences the generation of disturbance caused during the freezing process. They showed that sandy soils can be frozen with no heave (no disturbance) if the fines contain limited amounts of clay minerals. Davila *et al* (1992) developed a criterion to define a boundary between heaving and non-heaving soils based on the amount and type of fines. The amount and type of fines used in this study was selected such that samples were on both sides of the heave boundary defined by Davila *et al.* (op. cit.).

RESULTS AND DISCUSSION

Typical axial strain behavior of a sample comprised of Ottawa sand and 5% Devon silt (by weight) during freezing and thawing is shown in Figure 2.6. Here, time begins at the start of freezing and compressive axial strain is assumed to be positive. It may be observed that it took 4 hours to freeze the entire sample and then the sample was allowed to thaw for 15 hours. It may also be observed that this cohesionless sample did not heave (zero axial strain) during freezing. The intergranular void ratio e_g before freezing and after freezing and thawing remained essentially unchanged ($e_g = 0.75$). Here the intergranular void ratio is given by;

$$[2.2] \qquad e_g = \frac{\text{Volume of voids + Volume of fines}}{\text{Volume of granular phase}}$$

The shear wave velocity measured before freezing ($(V_s)_{before}$) was 175 m/s and after freezing and thawing ($(V_s)_{after}$) was 178 m/s. For all practical purposes the velocity can be considered unchanged. Therefore, when the sample suffered no disturbance (did not heave) due to freezing the shear wave velocity remained essentially unchanged from before freezing to after freezing and thawing.

Figure 2.7 presents the axial strain response of a sample comprised of Ottawa sand and 12.5% Devon silt (by weight) during freezing and thawing. Here again, the compressive strain is assumed to be positive and time represents the time lapsed from the start of freezing. It may be observed that the sample starts to heave when the freezing begins and continued to heave until the entire sample was frozen. Then the sample was allowed to thaw for 14 hours. During thawing the sample height did not decrease, i.e., the sample never returned to its original height after freezing and thawing. The intergranular void ratio before freezing ((e_g) before) was 0.757 and after freezing and thawing ((e_g) after) was 0.763. The shear wave velocity measured before freezing was 155 m/s and the shear wave velocity measured after freezing and thawing was 138 m/s. Therefore, there was a change in shear wave velocity by 17 m/s, which represents a decrease of 10.9%. This variation in shear wave velocity reflects the change in void ratio and stress history as well as the change in soil particle rearrangement due to freezing and thawing.

Table 2.2 summarizes the results of all the tests performed. These results represent tests on samples with the following percentages of fines; 0% fines (pure sand), 5% and 12.5% Devon silt and 5% and 10% Kaolinite. According to Davila *et al.* (1992) samples with 0% fines and 5% Devon silt should not heave and samples with 12.5% Devon silt, 5% Kaolinite and 10% Kaolinite should heave. It may be observed from Table 2.2 that the results from this study confirm Davila *et al.*'s (op. cit.) observations. The non heaving (undisturbed) samples had essentially no change in intergranular void ratio and the measured change in shear wave velocities did not exceed 2% of the initial value. However, for the heaving samples (disturbed) the intergranular void ratio changed and the measured shear wave velocities changed considerably due to freezing and thawing. The change in the shear wave velocity reflects the change in void ratio and stress history as well as, the change in soil structure. The amount of change in measured shear wave velocity appears to be related to the degree of disturbance.

CONCLUSIONS

Based on the limited number of tests performed in this study, the following conclusions can be made;

(1) Shear wave velocities are essentially unchanged for samples that do not heave during a one-dimensional, drained freeze-thaw cycle.

(2) Samples that showed heave (disturbance) also showed an associated change in shear wave velocity.

Hence, it appears feasible that shear wave velocities measured in the laboratory can be compared with in-situ shear wave velocities to estimate the quality of samples obtained using *in-situ* ground freezing. Although the present study is confined to determining the quality of samples obtained using *in-situ* ground freezing, the comparison of laboratory and field shear wave velocities may also be extended to determine the degree of disturbance using conventional sampling procedures.

REFERENCES

Bishop, 1948. A new sampling tool for use in cohesion less sands below ground water level. Geotechnique, **1**: 125-131.

Davila, R.S. 1992. The influence of fines content and specific surface area on freezing of sandy soils. M. Sc. Thesis, Department of Civil Engineering, The University of Alberta, Edmonton, Alberta.

Davila, R.S., Sego, D.C. and Robertson, P.K., 1992. Undisturbed sampling of sandy soils by freezing. 45th Canadian Geotechnical Conference, Toronto, paper 13A.

Dynik, R. and Madshu, C., 1985. Laboratory. measurements of G_{max} using bender elements. Proceedings, Advances in the art of testing soils under cyclic conditions, American Society of Civil Engineering, Detroit, MI, pp. 186-196.

Hamdi, F and Taylor-Smith, D., 1982. The influence of permeability on compressional wave velocity in marine sediments. Geophysical Prospecting, **30**: 622-640.

Hanzawa and Matsuda, 1977. Density of alluvial sand deposits obtained from sand sampling. Proceedings, specialty session on sampling, 9th International Conference on Soil Mechanics and Foundation Engineering, Tokyo. pp. 7-14.

Hardin, B.O. and Drnevich, V. P., 1972. Shear modulus and damping of soils: measurements and parameter effects, Journal of the Soil Mechanics and Foundation Division, American Society of Civil Engineering, **98**(6): 603-624.

Hatanaka, M., Sugimato, M. and Suzudi, Y., 1985. Liquefaction resistance of alluvial volcanic soils sampled by in situ freezing. Soils and Foundations, **25**(3): 49-63.

Horne, W.T., 1987. Prediction of Frost Heave Using the Segregational Potential Theory. M.Sc. Thesis, Department of Civil Engineering, The University of Alberta, Edmonton, Alberta, Canada.

Konrad, J.M. and Morgenstern, N.R., 1980. A mechanistic theory of ice lens formation in fine-grained soils. Canadian Geotechnical Journal. **17**: 473-486.

Konrad, J.M. and Morgenstern, N.R., 1983. Frost susceptibility of soils in terms of their segregation potential. Proceeding of 4th International Conference on Permafrost, Fairbanks, National Academy of Science, Washington, DC. pp. 473-486.

Konrad, J.M., 1990. Sampling of saturated and unsaturated sands by freezing. ASTM, Geotechnical Testing Journal. **13**(2): 88-96.

Kuerbis, R.H. and Vaid, Y.P., 1989. Undrained behavior of clean and silty sands. Proc. of discussion session on influence of local conditions on seismic response, XII International Conference on Soil Mechanics and Foundation Engineering, Rio de Janeiro, pp. 91-100.

Marcuson, W.F., Cooper, S.S. and Bieganouskey, W.A. 1977. Laboratory sampling study conducted on fine sands. Proceedings, specialty session on sampling, 9th International Conference on Soil Mechanics and Foundation Engineering, Tokyo, pp. 15-22.

Shirley, E.T. 1978. An improved shear wave transducer. Journal of Acoustical Society of America. **63**: 1643-1645.

Singh, S., Seed, H.B. and Chan, C.K. 1982. Undisturbed sampling of saturated sands by freezing. Journal of the Geotechnical Engineering Division American Society of Civil Engineers, **108**(2):247-264.

Tokimatsu,. K. and Yoshinori, H., 1986. Effect of sample disturbance on dynamic properties of sand. Soils and Foundations, **26**(1):55-63.

U.S. Army Corps. Report on slide of a portion of up stream face of Fort Peck Dam, 1938. U.S. Army Corps of Engineers, U.S. Government Printing Office Washington D.C. pp. 17-21.

Yoshimi, Y., Hatanaka, M. and Oh-Oka, H., 1978. Undisturbed Sampling of Saturated Sands by Freezing. Soils and Foundations, **18**(3):59-71.

Yoshimi, Y. Tokimatsu, K., Kaneko, O. and Makihara, Y., 1984. Undrained cyclic shear strength of a dense Niigata sand. Soils and Foundations, **24**(4):131-145.

Yoshimi, Y. Tokimatsu, K. and Hosaka, Y., 1989. Evaluation of liquefaction resistance of clean sands based on high quality undisturbed samples. Soils and Foundations, **29**(1):93-104.

TABLE 2.1

Properties of fines

Fines	Plasticity Index PI (%)	Liquid Limit LL (%)	Specific Gravity Gs	Mineralogy
Devon silt	21.0	39.0	2.74	78 % non clay mineral
Kaolinite	32.0	50.0	2.6	100 % clay minerals

TABLE 2.2

Summary of results from freeze-thaw tests

Isotropic confining stress (kPa)	Type of Fines	Fines (by weight) (%)	Response During Freezing	Axial strain (%)	Inter-granular void ratio (e_g)before	Inter granular void ratio (e_g)after	SHEAR WAVE VELOCITY		
							(V_s) before (m/s)	(V_s) after (m/s)	% Change in V_s
100	-	0	no heave	0	0.715	0.706	239	237	-0.8
50	-	0	no heave	0	0.706	0.703	200	204	+2.0
50	Devon silt	5	no heave	0	0.750	0.750	175	178	+1.7
50	Devon silt	12.5	heave	1.80	0.757	0.763	155	138	-10.9
50	Kaolinite	5	heave	0.21	0.747	0.723	174	191	+9.8
50	Kaolinite	10	heave	1.04	0.622	0.584	264	342	+29.5

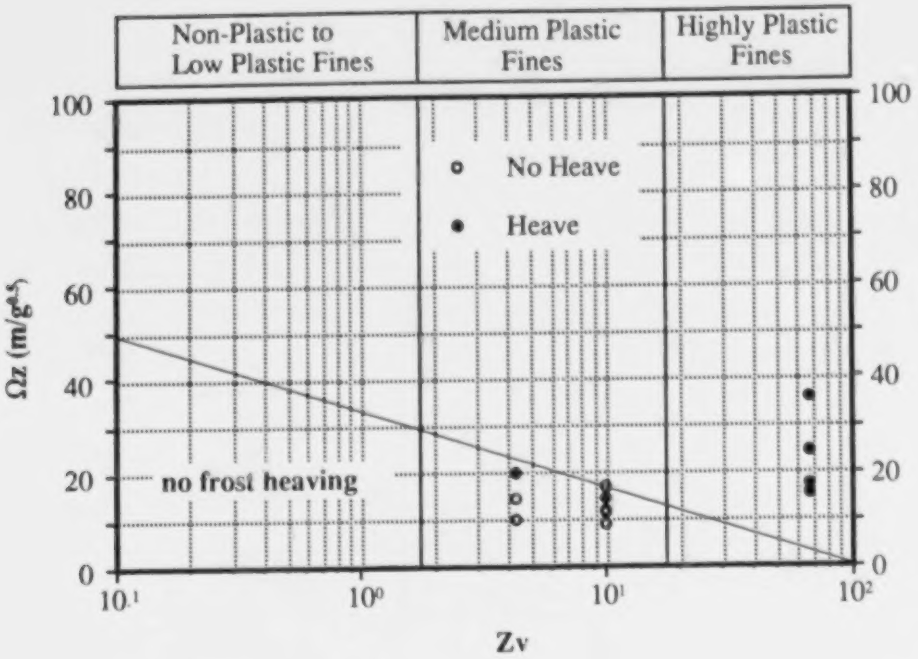

Test Boundary Conditions:

Temperature Gradient = 0.4 °C/cm
Minimum Time Period = 50 hours

1) The Fines Mineralogy Ratio $Zv = \frac{CM_f}{I_{SSA}}$

CMf = Clay Mineral Fraction < 75 µm (%)
ISSA = Intensity of the Specific Surface Area $I_{SSA} = \frac{S_c}{S_f}$

Sc = Specific Surface Area Fines < 2 µm

2) Surface Area Index $\Omega z = \sqrt{CM \times S_f}$

CM = Clay Mineral Fraction in the Soil (%)
S_f = Specific Surface Area Fines < 75 µm

Figure 2.1. Relationship between the surface area index and fine mineralogy ratio for frost susceptibility boundary analysis (after Davila *et al.*, 1992).

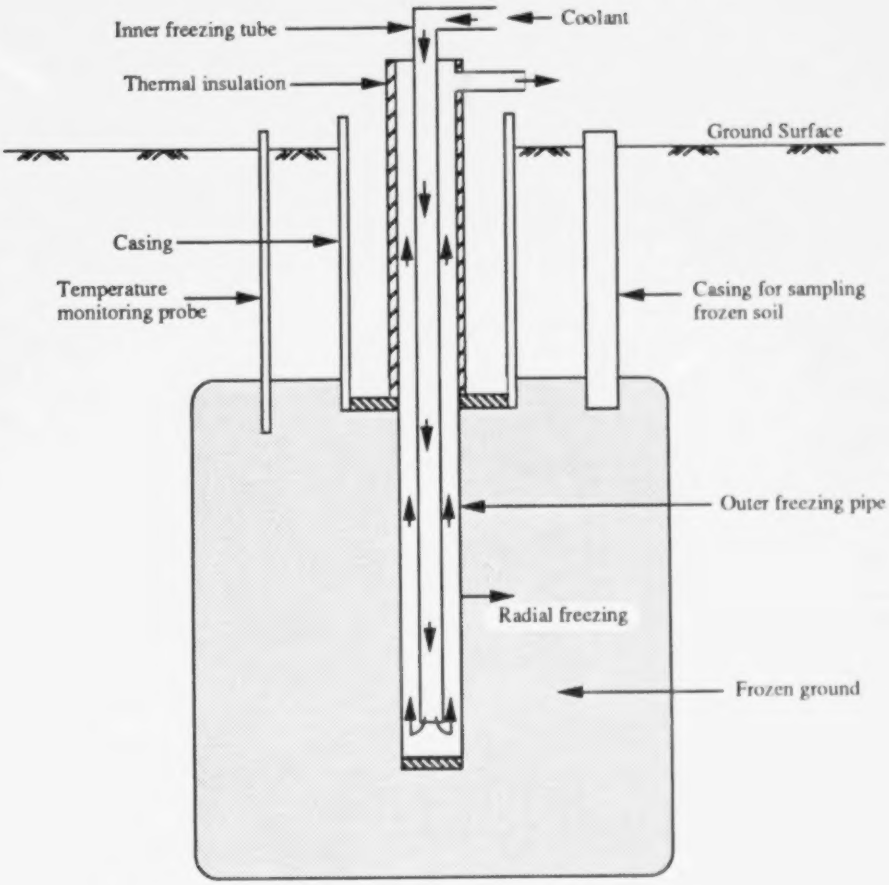

Figure 2.2. Schematic of a typical ground freezing system.

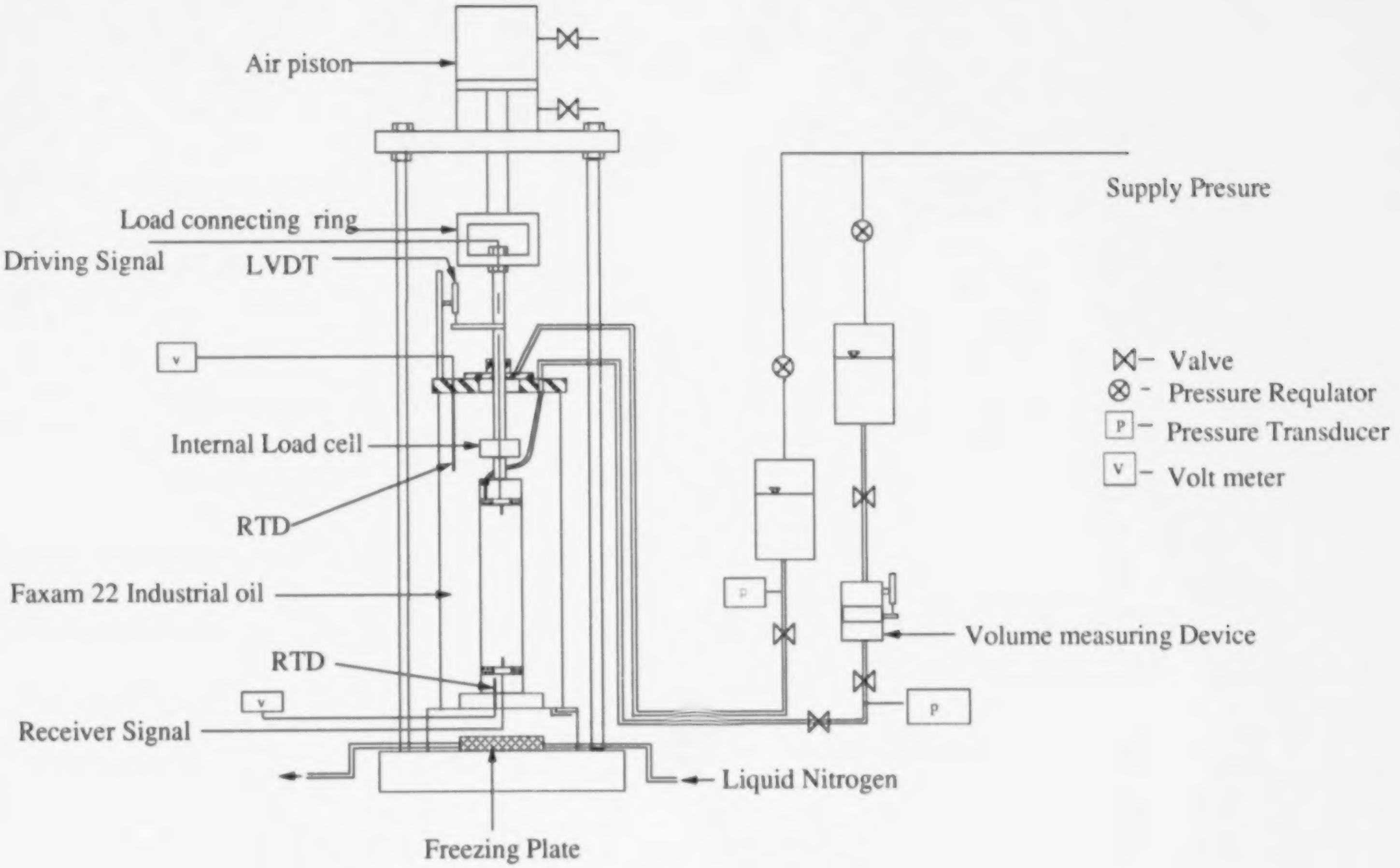

Figure 2.3 Schematic layout of freezing triaxial samples

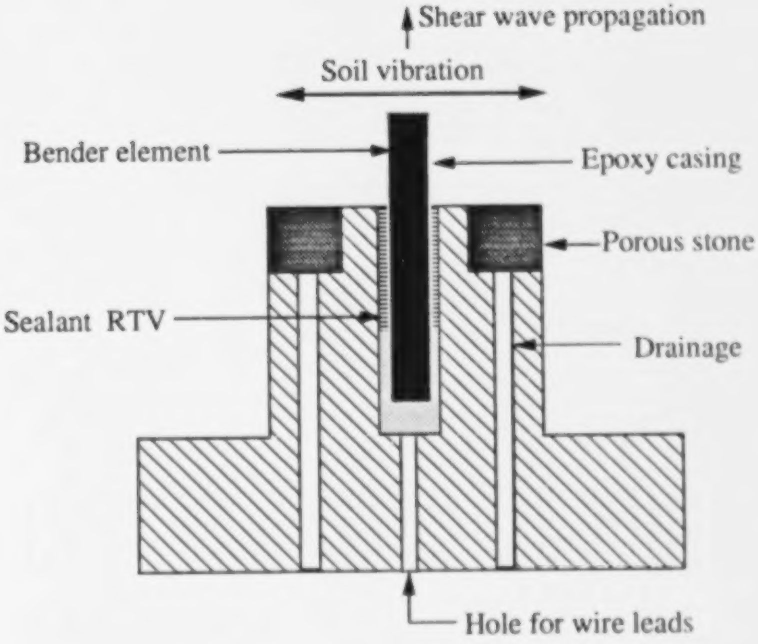

Figure 2.4. Bender element mounted on bottom pedestal.

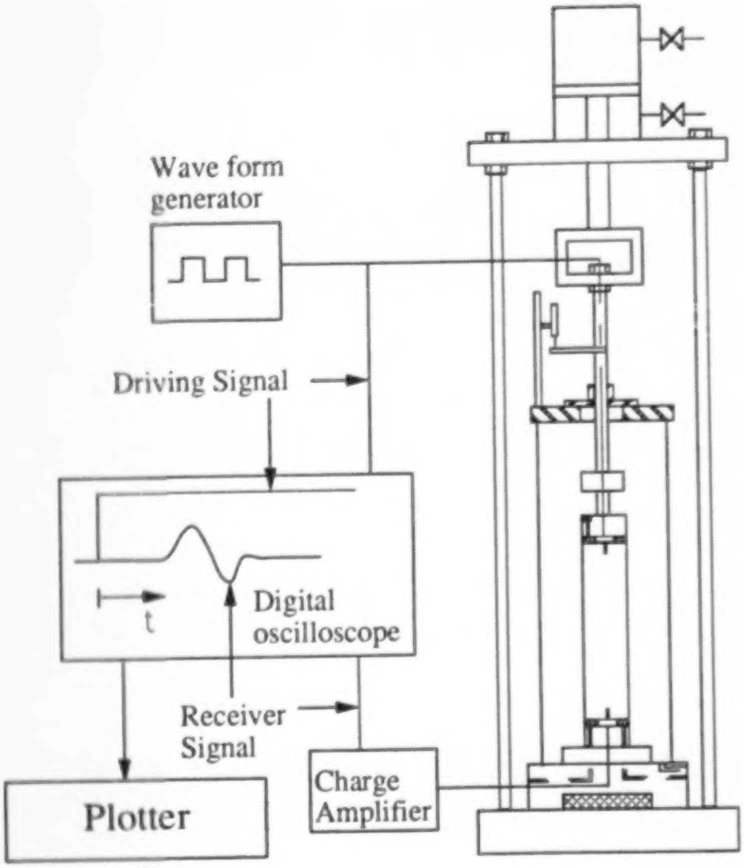

Figure 2.5. Schematic layout of shear wave measuring system.

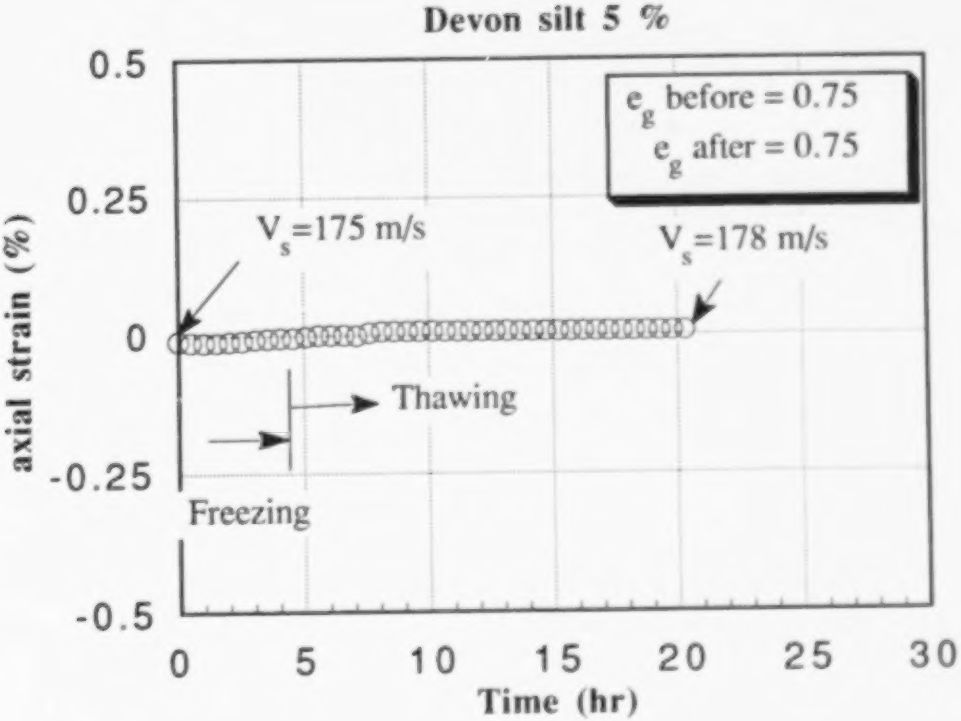

Figure 2.6. Typical axial strain behavior of a sample comprised of Ottawa sand and 5% Devon Silt.

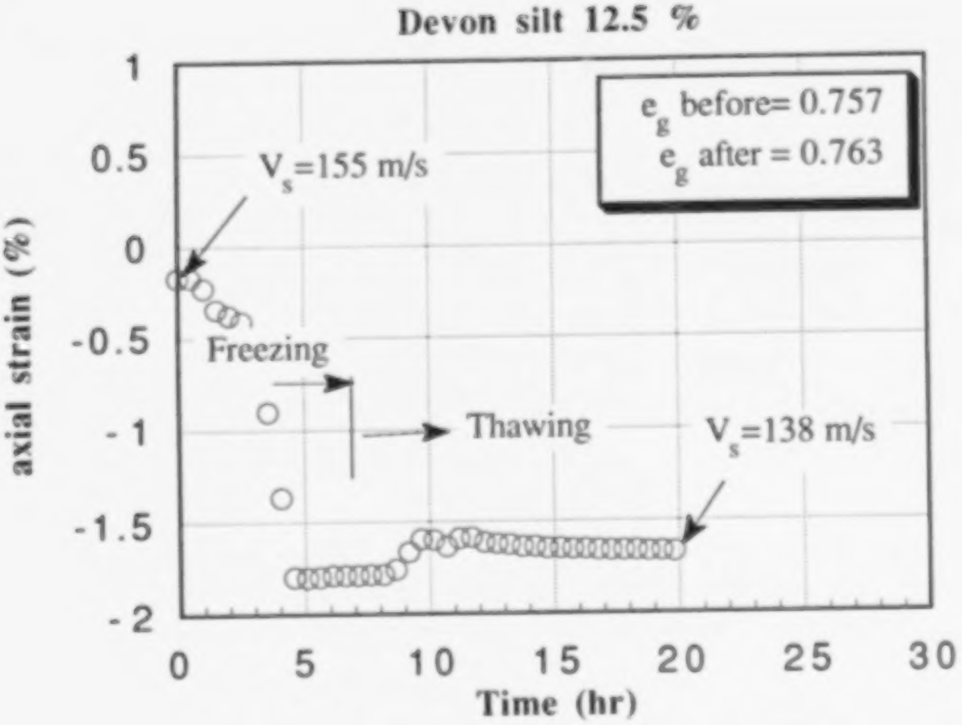

Figure 2.7. Typical axial strain behavior of a sample comprised of Ottawa sand and 12.5% Devon Silt.

CHAPTER 3

COLLAPSE BEHAVIOR OF VERY LOOSE SAND*

INTRODUCTION

Since the major earthquakes of 1964 in Niigata, Japan and Alaska, USA significant improvements have been made in the understanding of liquefaction of sand. Most of the early research was related to the behavior of sand under undrained cyclic loading (Seed and Lee, 1966). Castro (1969) showed that loose sands can collapse and strain soften during monotonic undrained loading and ultimately reach a steady state. Figure 3.1 shows a typical stress-strain response and resulting stress path in effective mean normal stress ($p' = ((\sigma'_1+2\sigma'_3)/3)$) - deviator stress ($q = (\sigma'_1-\sigma'_3)$) space for an undrained monotonic triaxial compression test on a loose sand. After reaching a peak resistance, the sand rapidly strain softens to a constant resistance during which the effective stress state remains constant. Castro (1969) termed the constant state as steady state and showed that steady state varied with void ratio as shown schematically in Figure 3.2. Steady state represents a state in the void ratio-effective mean normal stress-deviator stress space, as shown in Figure 3.2.

---

* A version of this chapter has been published: Sasitharan, S., Robertson, P.K., Sego, D.C. and Morgenstern, N.R. 1993. Collapse behavior of sand. Canadian Geotechnical Journal. August 1993.

Sladen *et al.* (1985a) suggested that a surface exists that defines the trigger of collapse and strain softening of loose sands leading to steady state under undrained loading. Figure 3.3 shows a series of monotonic undrained triaxial compression tests on a loose sand showing the collapse surface as defined by Sladen *et al.* (1985a) as a surface connecting the peak points to steady state. Several studies (Alarcon-Guzman *et al.*, 1988; Ishihara *et al.*, 1991) have shown that a collapse surface defined by the post peak portion of monotonic undrained stress paths forms a critical surface that can trigger collapse and strain softening during undrained cyclic loading, as illustrated by the results in Figure 3.4. The collapse surface proposed by Sladen *et al.* (1985a) is compared with the collapse surface observed by Alarcon-Guzman *et al.* (1988) and Ishihara *et al.* (1991) in Figure 3.5. It may be observed that the collapse surface proposed by Sladen *et al.* (1985a) is a simple straight line approximation of the curved collapse surface observed by Alarcon-Guzman *et al.* (1988) and Ishihara *et al.* (1991). Both surfaces were defined in terms of undrained triaxial compression tests.

Catastrophic flow slides due to liquefaction have occurred in a variety of geological materials such as sensitive clays, residual soils and cohesionless materials. However, they are most frequently encountered in saturated deposits of loose cohesionless materials. Flow slides have occurred in natural structures (e.g., slopes and under water slopes) and in man made structures (e.g., mine waste and hydraulic fills). Flow failure due to liquefaction results from a sudden and dramatic loss of shear resistance. Collapse and flow is usually associated with some form of undrained loading to trigger the collapse. This undrained loading can be caused by either cyclic loading such as earthquakes, blasting and pile driving or a sudden static loading such as rapid construction or over steepening of a slope. Eckersley (1990) performed tests on a model dam prepared using loose coking coal. He found that liquefaction flow slides could be initiated when the slope was wetted by allowing the water table to slowly rise. Hence, he concluded that liquefaction flow slides could be initiated under static drained loading conditions. Although failure was initiated under drained conditions, the deformations associated with the failure caused undrained collapse and a large increase in pore pressure which drastically reduced the shear resistance of the coking coal resulting in flow. Eckersley (op. cit.) further observed that collapse occurred at a slope angle of 36° although the angle of repose of the coking coal was 40°. This suggested that loose cohesionless materials can collapse under drained loading conditions before fully mobilizing the friction associated with the angle of repose of the material.

Although most previous laboratory studies have involved undrained loading, this undrained condition may not be a prerequisite to initiate liquefaction flow slides (Eckersley op. cit.). It appears that loose cohesionless material can collapse and flow by following specific drained stress paths rather than the traditionally believed undrained path.

In this chapter a preliminary study of the collapse behavior of a loose sand is presented. This study is based on a variety of loading conditions that can lead to collapse. The stress paths were selected such that collapse was initiated using both drained and undrained loading. A framework based on a state boundary surface is proposed for describing both the drained and undrained collapse of the material tested and which may be applicable for other cohesionless materials.

TESTING APPARATUS

Very loose samples of sand were tested under triaxial conditions in order to simulate field stress conditions and to study the fundamental material response. Usually, triaxial tests are used to determine shear strength parameters when the vertical axial stress increases while the horizontal stress is maintained constant. The vertical stress can be increased in either a stress controlled or a strain controlled manner. Monotonic axial loading under controlled stress conditions has been used to study the time dependent deformation of soils. Earthquake effects have been simulated using stress controlled cyclic axial loading conditions. On the other hand, axial loading under strain controlled conditions has been used to study the post peak behavior of soils.

In this study a modified Wykeham Farrance strain controlled loading machine was used to study the post peak behavior of a loose sand. The machine was modified to allow load controlled testing by the addition of dead loads to the top of a sample. A schematic layout of the testing apparatus is shown in Figure 3.6. Triaxial specimens could be consolidated either isotropically or anisotropically. The axial load applied to the sample was measured using an internal load cell to eliminate the need to consider ram friction and other external loads when determining the axial stress acting on the sample. Test variables were measured using electronic transducers to collect and store data in a microcomputer.

MATERIAL TESTED AND SAMPLE PREPARATION

Ottawa (C109) sand obtained from Ottawa, Illinois was used in this study. Ottawa sand is a uniform, medium sand comprised primarily of round to subrounded quartz grains with a specific gravity of 2.67. The mean grain size (D_{50}) of Ottawa sand is 0.34 mm. The maximum and minimum void ratios of the sand determined using the ASTM method D2049 are 0.82 and 0.50 respectively.

The objective of this testing program was to study the response of very loose sand that may collapse during loading. Triaxial specimens 63 mm in diameter and approximately 125 mm long were reconstituted in the laboratory using a moist tamping technique. The unsaturated moist sand exhibits some apparent cohesion that allows a very loose sand structure to be maintained during sample preparation. A predetermined amount of oven-dried Ottawa sand was mixed with 5% water (by weight). This unsaturated sand was then compacted in layers in a membrane lined split mold using a small drop hammer. The number of drops was increased for each additional layer in an effort to form a sample with a uniform density. The samples were then saturated in two stages at a confining pressure of 30 kPa. Carbon dioxide and then de-aired water were percolated through the sample. After percolation a back pressure was applied to saturate the sample. During back pressure saturation the pore pressure and cell pressure were monitored simultaneously to continuously determine Skempton's pore pressure parameter B. When the B value reached 0.99 or greater, the sample was considered to be fully saturated and consolidation was allowed to proceed.

EXPERIMENTAL PROBLEMS

Two experimental problems are commonly encountered when very loose samples of sand are prepared by moist tamping; uniformity of the void ratio across the sample and calculation of the void ratio of the sample after consolidation.

Sample uniformity

Sample uniformity was evaluated using freezing techniques on a moist tamped sample of Ottawa sand. The density (void ratio) of a very loose sand sample can be compared at different locations by freezing the sand sample with no disturbance. The sample will remain undisturbed during freezing provided water can freely flow away from the advancing freezing front and the volume of water expelled equals the volume expansion of the ice forming in pores. Clean sands have sufficiently high permeability to allow drainage and can be frozen in one dimension with no disturbance (Davila *et al.* ,1992; Sasitharan *et al.*, 1992). A sample was formed using the same moist tamping technique described above. After the sample was saturated and consolidated to 350 kPa, the sample was frozen using the freezing technique described in chapter 2. The void ratio calculated from the moisture content of two sections obtained from the center of the top and of the bottom half of the frozen sample were determined and found to be 0.795 and 0.792, respectively. This indicated that the sample preparation technique produced a sample with a uniform void ratio after saturation and consolidation. Based on a careful visual inspection, the sample had a uniform structure throughout.

Void ratio calculation

The initial void ratio of the sample was basically determined from the initial height and diameter of the sample. The height of the sample was measured using a dial gauge and comparing the reading for the sample with the reference taken by placing a dummy aluminum sample of known height in the triaxial apparatus. The circumference of the sample was carefully measured along the length of the sample, accounting for the membrane thickness. During sample set up and saturation the volume of the sample changes continuously. Sladen and Handford (1987) suggested that potential error in the calculated void ratio may be large if the changes in sample volume during saturation are not measured and taken into account.

The average void ratio calculated from the moisture content of the frozen sample was found to be 0.794. The void ratio calculated from the initial dimension of the sample, taking into account the volume change during saturation and consolidation was 0.798 with a membrane penetration correction (Vaid and Negussey, 1984). Hence, for all practical purposes the void ratio of the Ottawa sand samples can be estimated from their initial dimensions provided that the initial dimensions and the change in volume during saturation and consolidation are carefully measured. The axial strain during saturation was carefully measured and an isotropic strain condition was assumed to calculate volume change during saturation. However, this may not be true for samples with a high fine content (>10 % by weight) and for well graded sands which may undergo large volume changes during saturation.

TEST PROGRAM

Samples were consolidated to an isotropic confining stress of 350 kPa. Samples were then loaded along the following stress paths until the sample exhibited strain weakening due to collapse: undrained triaxial compression stress path, a constant volume triaxial compression stress path and constant deviator stress drained stress path. The behavior of a soil under any loading condition is controlled by the effective stresses. In conventional triaxial compression tests the effective stress paths are controlled by maintaining the effective minor principal stress (σ'_3) constant and increasing the effective major principal stress (σ'_1). In this testing program a drained stress path was followed by changing the effective minor principal stress. This change in effective minor principal stress in a triaxial compression test can be achieved either by adjusting the cell confining pressure or by adjusting the back pressure applied to the sample. Details of each stress path are given below.

Undrained stress path

Loading was performed under strain controlled condition at a constant rate of deformation (0.15 mm/ min.) and the sample was not allowed to drain throughout the loading process.

Constant volume stress path

Loading was performed under a constant rate of deformation (0.15 mm/ min.). The sample was free to drain through the drainage port during the loading process. However, the effective minor principal stress applied to the sample was continuously adjusted by small manual increments of back pressure during loading to ensure that the volume of the sample measured by the volume measuring device remained unchanged. The constant volume stress path was performed to study the collapse mechanism of very loose sand. The drainage was carefully monitored to see if the drainage conditions would change during the strain softening phase of the test.

Constant deviator stress path

The isotropically consolidated triaxial samples were first loaded by adding axial dead loads to the sample under undrained conditions. When the desired deviator stress was reached, the application of the axial dead load was stopped and maintained constant. The back pressure applied to the sample was set to the current pore pressure to ensure no volume change of the sample would occur when the drainage port was opened to allow for a free draining condition. Hence, the void ratio of the sample remained unchanged from that achieved during the isotropic consolidation. Under these conditions, the sample was then sheared in a drained condition along a constant deviator stress path by reducing the effective confining stress. This was achieved by increasing the back pressure while the applied cell pressure was kept constant. This special stress path was performed to simulate the loading of soil elements within a slope or embankment subjected to a slow increase in pore pressure. This increase in pore pressure may occur slowly under drained conditions. The drainage was carefully monitored throughout the drained loading to see if drainage conditions would change. The test was also performed to evaluate what friction angle could be mobilized at failure.

TEST RESULTS

Constant void ratio loading

Constant void ratio loading of a loose sand can be achieved either by performing monotonic undrained loading or by decreasing the effective stress during a drained loading process such that the void ratio stays constant (constant volume loading). The deviator stress-axial strain response and resulting stress paths of identical samples loaded under both undrained and under constant volume conditions are shown in Figure 3.7. It may be observed that for samples which were consolidated to identical isotropic stress (350 kPa) and void ratio (0.804), the stress path remained essentially the same for the two different loading conditions. The free to drain constant volume stress path shows the same behavior as the undrained stress path. Both samples have the same peak resistance and show a marked strain softening to a constant resistance at steady state. These tests show that the stress paths and not the external drainage condition governs the strain softening or collapse behavior.

Drained collapse behavior

Figure 3.8 shows the results of a constant deviator stress path test on a sample with an initial void ratio of 0.804. After undrained loading the deviator stress (q) was maintained at q=125 kPa, resulting in an anisotropic stress state (q/p' = 0.536). This represents an *in-situ* $K_c = \sigma'_1/\sigma'_3 = 1.65$. The deviator stress-axial strain response and resulting stress path of this constant deviator stress drained test are shown in

Figure 3.8. It may be noticed that while the effective mean normal stress was decreased from 233 to 178 kPa, the deviator stress that was applied using dead load remained constant at 125 kPa (axial load=371 N). When the effective mean normal stress reached a value of 178 kPa there was a slight increase in pore pressure (6.7 kPa) followed by a catastrophic undrained failure or collapse of the sample. The axial strain during the drained portion of the test at initiation of collapse was only 0.4 % . The velocity of collapse was so rapid that it was not possible to collect detailed test data. However, it was clear that the sample failed undrained. The sample reached such a large momentum during collapse that when the loading head hit the restricting nuts (see Fig. 3.6) the entire laboratory felt the vibration. The mobilized internal friction angle (ϕ'_m) can be expressed in an effective mean normal stress (p')-deviator stress (q) space by;

$$\frac{q}{p'} = \frac{6 \sin \phi'_m}{(3 - \sin \phi'_m)} \tag{3.1}$$

From Figure 3.8 it can be observed that at collapse the stress ratio $q/p' = 0.768$ which corresponds to a mobilized internal friction angle of 19.9° (Eq. 3.1). At steady state for a sample with an identical void ratio ($e = 0.804$), the stress ratio $q/p' = 1.22$ (Fig. 3.7). This corresponds to a steady state friction angle of 30.6° (Eq. 3.1). Hence, this test demonstrates that loose Ottawa sand can collapse at a mobilized friction angle well below the steady state friction angle under a fully drained loading condition. In this test, the decrease in effective mean normal stress before collapse was about 55 kPa which corresponds to an increase in pore pressure equivalent to a rise of water of about 5.5 m. Hence, it may be possible to induce collapse of this sand under fully drained conditions.

A similar constant deviator stress drained stress path was performed at 100 kPa deviator stress starting with the same initial void ratio 0.804. Similar drained collapse behavior was observed at this smaller deviator stress. The deviator stress-axial strain response and resulting stress path of this test are shown in Figure 3.9. The anisotropic stress state at the start of drained loading was q/p' = 0.333. This represents an in-situ $Kc = \sigma'_1/\sigma'_3 = 1.375$. It may be observed that the deviator stress remained constant at 100 kPa (axial load= 285 N) until the effective mean normal stress was reduced to 140 kPa from 300 kPa. Then the sample immediately collapsed. The axial strain during the drained loading portion of the test at initiation of the collapse was 0.6%. From Figure 3.9 it may be observed that when collapse was initiated the stress ratio was q/p' = 0.677. This corresponds to a mobilized internal friction angle of 17.7^{o}. In this test, the decrease in effective mean normal stress was about 160 kPa before collapse was initiated. This corresponds to an increase in pore pressure equivalent to a rise of water of about 16 m in water head to initiate collapse.

The sample volume change during the drained portion of the constant deviator stress path was continuously measured by the volume measuring device. The volume of the sample for the constant deviator stress (q=125 kPa) test was essentially unchanged and remained at 0.804 before the sample collapsed. However, the constant deviator stress (q=100 kPa) test showed a small dilative volume change as a result of the unloading associated with the constant deviator stress and decreasing effective mean normal stress path. The void ratio of the sample changed from 0.804 to 0.809 before the sample collapsed.

STATE BOUNDARY SURFACE FOR INTERPRETATION OF TEST RESULTS

One of the main aims of this investigation was to study the conditions initiating the collapse behavior of very loose sand. It is evident from the test results that collapse can be initiated by either following specific drained stress paths or undrained stress paths. Alarcon-Guzman *et al.* (1988) showed that during torsional undrained cyclic shear, collapse was initiated when the stress state reached the effective stress path defined by the post peak portion of the monotonic undrained loading test. Thereafter, they found the two effective stress paths to be essentially the same. Many researchers have also found that the monotonic undrained stress path forms an envelope for the cyclic undrained stress path for a given void ratio (Ishihara *et al.*, 1991; Georgiannou *et al.*, 1991 and Symes *et al.*, 1984). These results show that, regardless of the test type, when the cyclic undrained stress path approaches the monotonic undrained stress path between the peak and the steady state, the deviator stress of the cyclic undrained test quickly reduces to the same steady state value reached by following the monotonic undrained stress path (Fig. 3.4).

It may be observed from Figure 3.7 that when the void ratio is kept constant and a sample is free to drain, the drained stress path is similar to that of the undrained stress path. Hence, this constant void ratio stress path may define a boundary from the peak to the steady state (post peak portion) beyond which it may not be possible to have a stress state for a cohesionless material at a given void ratio. A boundary above which no stress state is possible was defined as a state boundary by Roscoe *et al.* (1958). Therefore, the post peak portion of a constant void ratio stress path may represent a state boundary.

Figure 3.10 shows the constant deviator stress (q=125 kPa) drained stress path at a void ratio of 0.804 compared with the constant void ratio stress path at the same void ratio. It may be noticed that as soon as the stress state tries to cross the potential state boundary defined by the constant void ratio stress path, the sample collapsed. This constant deviator stress (q=125 kPa) drained test shows that the post peak portion of the constant void ratio stress path appears to represents a state boundary.

Figure 3.11 shows the constant deviator stress (q=100 kPa) drained stress path with initial void ratio 0.804 and the state boundary defined for void ratio of 0.804. It may be observed that the sample collapsed slightly before it reached the state boundary defined for a void ratio of 0.804. However, it may be noticed that at failure the void ratio of the sample was 0.809. Hence, it appears that the sample collapsed on a state boundary defined for a void ratio of 0.809. Figure 3.12 shows the state boundary defined for a void ratio of 0.809 and the constant deviator (q=100 kPa) drained stress path. It may be noticed, the sample collapsed as it tried to cross the state boundary defined for void ratio 0.809. This test provides valuable information regarding the state boundary with changing void ratio. These constant deviator stress tests show that very loose Ottawa sand can collapse in an undrained manner when the stress state tries to cross the state boundary defined for the current void ratio. Hence, this state boundary defines a surface in the effective mean normal stress-deviator stress-void ratio space.

Sladen *et al*. (1985a) defined a similar collapse surface in effective mean normal stress-deviator stress-void ratio space by connecting the locus of the peak deviator stress during monotonic undrained loading and the corresponding steady state stress by straight lines as shown schematically in Figure 3.13. Sladen *et al.* (1985b) used this approach to predict the failure of the Nerlerk hydraulic fills. The collapse surface approach was also used by Gu *et al.* (1993) to predict the lower San Fernando dam post earthquake failure of 1971. In these analyses, the collapse surface approach correctly predicted the undrained failures. The collapse surface defined by connecting the locus of peak points and the corresponding steady state strength for undrained monotonic loading is not strictly a state boundary surface. The actual stress paths can travel slightly above this assumed linear surface before collapse. It has been shown that the state boundary surface is defined by the post peak portion of a constant void ratio stress path. However, for a cohesionless material monotonic undrained loading would yield the shortest stress path before collapse. Other stress paths that try to cross the state boundary surface such as cyclic undrained loading or constant deviator stress path are required to travel farther to reach the state boundary. Hence, monotonic undrained loading would be the most unsafe stress path by which a cohesionless material can reach collapse. For monotonic undrained loading, the collapse conditions represented by the state boundary surface and Sladen's linear collapse surface would be essentially the same (Fig. 3.14). Hence, for practical safety evaluations, the linear collapse surface suggested by Sladen *et al.* (1985a) can be used to avoid the complexity associated with modeling the curved state boundary surface.

The above discussion was based on the observed response of loose cohesionless material starting from an identical confining stress. Figure 3.15 shows the monotonic undrained stress paths obtained by Ishihara *et al.* (1991) for Toyoura sand starting from various isotropic confining stresses for a void ratio of 0.916. It may be noticed that the post peak portion of these monotonic undrained or constant void ratio stress paths forms a straight line (Fig. 3.15). This straight line portion defines the state boundary for a void ratio of 0.916 regardless of the confining stress. However, this straight line approximation of the state boundary surface for various consolidation stresses may not be valid for all sands and must be verified experimentally. Alternatively, the state boundary can be obtained by using curve fitting techniques to fit a relation through a set of data at different void ratios and confining stresses. Hence, the state boundary for a given void ratio and confining stress could be obtained.

SUMMARY AND CONCLUSIONS

The constant void ratio stress path followed under drained constant volume and undrained conditions are identical. It has been shown that the post peak portion of a constant void ratio stress path defines a state boundary. This post peak portion at different void ratios forms a surface that defines the state boundary surface in effective mean normal stress-deviator stress-void ratio space. The two constant deviator stress drained tests performed in this study show that a state boundary surface defined by the post peak portion of constant void ratio stress paths cannot be crossed by any type of loading. If an attempt is made to force a loose cohesionless material to cross the state boundary surface, collapse and undrained strain softening can occur. Hence, flow failure and liquefaction under drained and undrained loading can be initiated when the loading of a loose cohesionless material attempts to cross the state boundary surface. The following main conclusions can be made:

(1) The post peak portion of a constant void ratio stress path defines the state boundary surface.

(2) Loose cohesionless material can collapse under any type of loading when the stress path followed during loading attempts to cross the state boundary surface.

The results of the two constant deviator stress drained tests show that slopes can fail undrained if the soil is very loose and the pore pressure rises, even if the pore pressure rise is slow and is taking place under drained condition. This type of test clearly shows how static liquefaction flow slides can occur without the need for some undrained loading.

Whether or not undrained collapse occurs depends on the direction of the stress path. It appears that the stress path must attempt to cross the state boundary to initiate collapse. The axial strain at failure for the samples tested was between 0.4 and 0.6% and the mobilized friction angle at collapse was between 17^o and 20^o. If failure were to occur in a loose sand deposit by following these stress paths, then it would not be possible to observe any major earth movements prior to the initiation of collapse and undrained flow. In conventional terms, even though a slope might have a Factor of Safety of about 2, it may be on the brink of undetectable catastrophic undrained failure.

REFERENCES

Alarcon-Guzman, A., Leonards, G. A. and Chameau, J. L. 1988. Undrained monotonic and cyclic strength of sands. Journal of Geotechnical Engineering American Society of Civil Engineering, **114**: 1089-1109.

ASTM 1969. Standard test method for relative density of cohesionless soils (D2049-69). In 1969 Annual Book of ASTM Standards. American Society of Testing Materials, Philadelphia, pp. 622-630.

Casagrande, A. 1936. Characteristics of cohesionless soils affecting the stability of slopes and earth fills. Journal of the Boston Society of Civil Engineers, Reprinted in contributions to soil mechanics 1925-1940, Boston society of Civil Engineering, October 1940. pp. 257-276.

Casagrande, A. 1975. Liquefaction and cyclic deformations of sands - A critical review. Fifth Pan-American Conference on Soil Mechanics and Foundation Engineering. Buenos Aries, Argentina. Vol. 5. pp. 76-133.

Castro, G. 1969. Liquefaction of sands. Harvard Soil Mechanics Series No. 81. 112 pp.

Castro, G ., Enos, J. L., France, J. W. and Poulos, S. J. 1982. Liquefaction induced by cyclic loading. Report to National Science Foundation, Washington, DC, No. NSF/CEE-82018. 79 pp.

Davila , R. S., Sego, D. C. and Robertson, P. K. 1992. Undisturbed sampling of sandy soils by freezing. 45th Canadian Geotechnical Conference, Toronto, paper 13A.

Eckersley, D. 1990. Instrumented laboratory flow slides. Geotechnique, **40**: 489-502.

Georgiannou, V. N., Hight, D. W. and Burland, J. B. 1991. Behavior of clayey sands under undrained cyclic triaxial loading. Geotechnique, **41**: 383-393.

Gu, W. H., Morgenstern, N. R. and Robertson, P. K. 1993. Progressive failure of lower San Fernando dam. Journal of Geotechnical Engineering American Society of Civil Engineering, **119**: 333-349.

Ishihara, K., Verdugo, R. and Acacio, A. A. 1991. Characterization of cyclic behavior of sand and post-seismic stability analysis. IX. Asian Regional Conference on Soil Mechanics and Foundation Engineering, Bangkok, Thailand. Vol. 2. pp. 45-68.

Poulos, S. 1981. The steady-state of deformation. Journal of Geotechnical Engineering, American Society of Civil Engineering, **107**: 553-561.

Roscoe, K. H., Schofield, A. N. and Wroth, C. P. 1958. On the yielding of soils. Geotechnique, **8**: 22-53.

Sasitharan, S., Robertson, P. K. and Sego. D. C. 1992. Sample disturbance from shear wave velocity measurements. 45th Canadian Geotechnical Conference, Toronto. 23:1-23:7.

Seed, H. B. and Lee, K. L. 1966. Liquefaction of saturated sands during cyclic loading. Journal of Soil mechanics and Foundation engineering, American Society of Civil Engineering, **92**(6): 105-134.

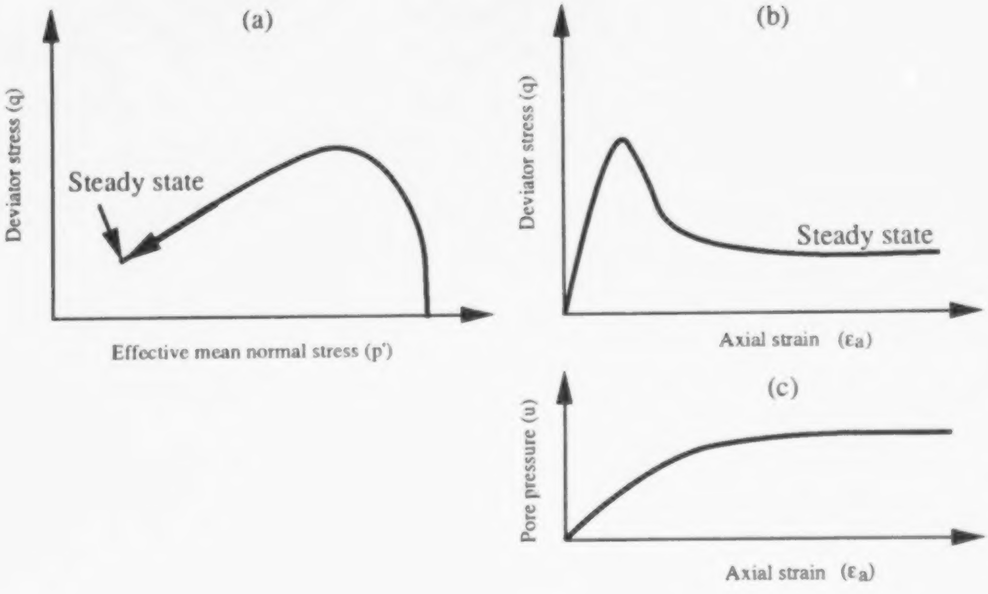

Figure. 3.1. Typical stress-strain and resulting stress path for an undrained monotonic triaxial compression test. (a) stress path (b) stress-strain (c) pore pressure

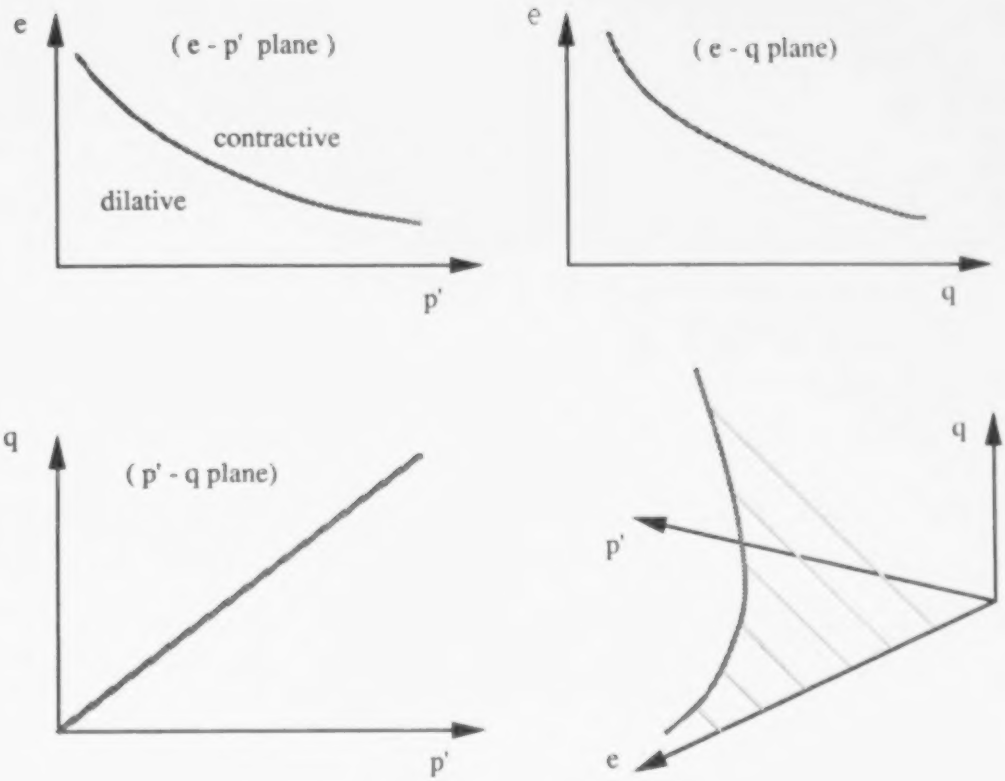

Figure. 3.2. Steady state representation in e-p'-q space along with representation using e-p', e-q and p'-q planes.

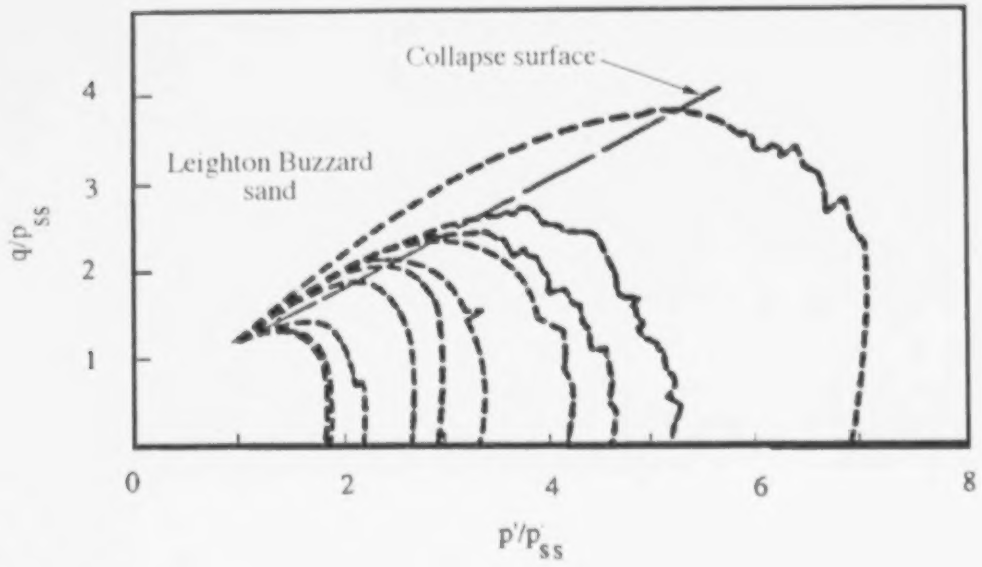

Figure. 3.3. Collapse surface (modified from Sladen *et al.*, 1985a). In this Figure p'_{ss} represents the effective mean normal stress at steady state.

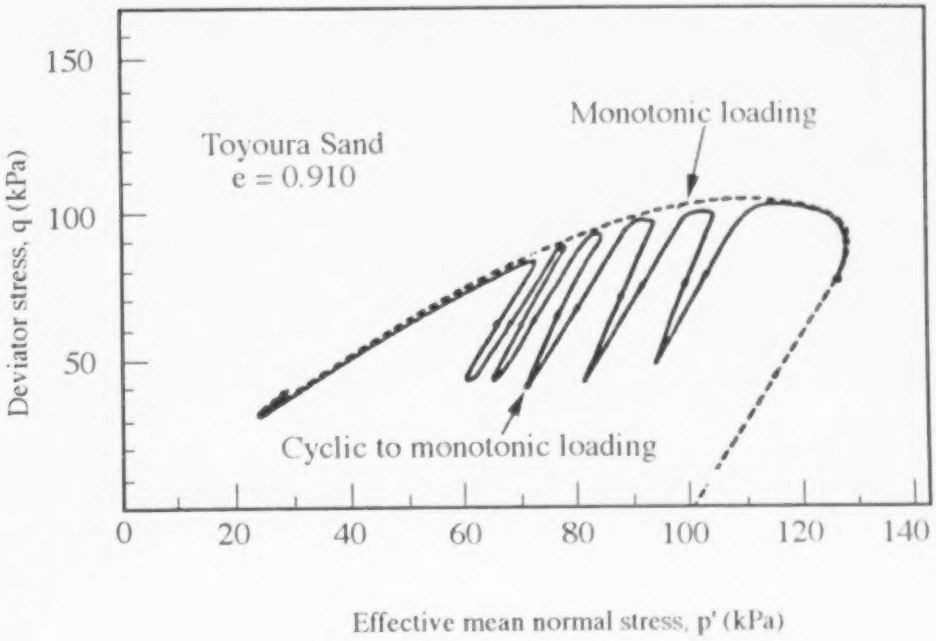

Figure. 3.4. Effective stress paths for monotonic undrained loading and cyclic to monotonic undrained loading (modified from Ishihara *et al*., 1991).

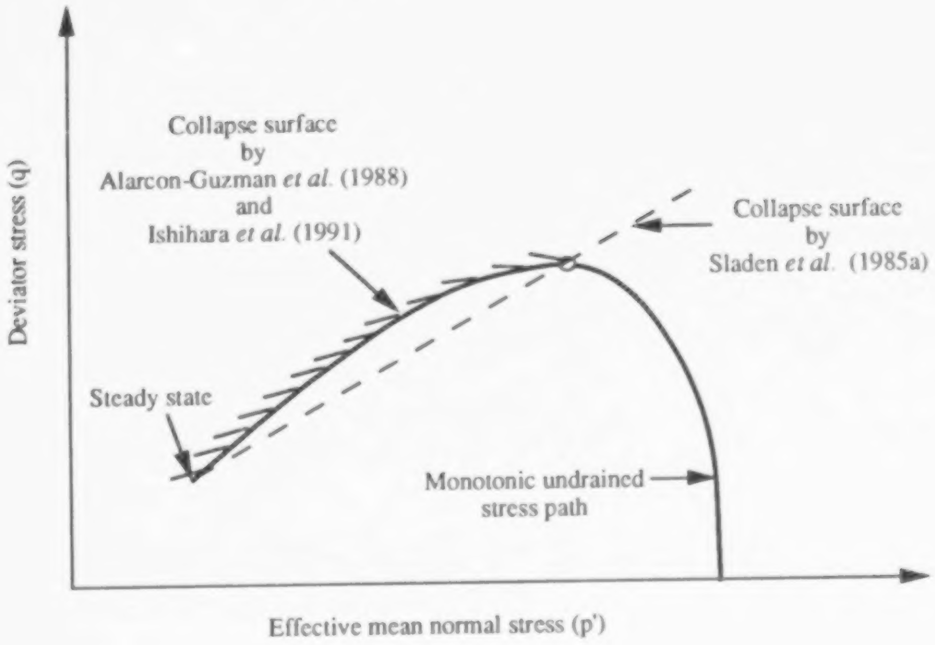

Figure. 3.5. Comparison of collapse surface proposed by Sladen *et al.* (1985a), Alarcon-Guzman *et al.* (1988) and Ishihara *et al.* (1991) for undrained loading condition.

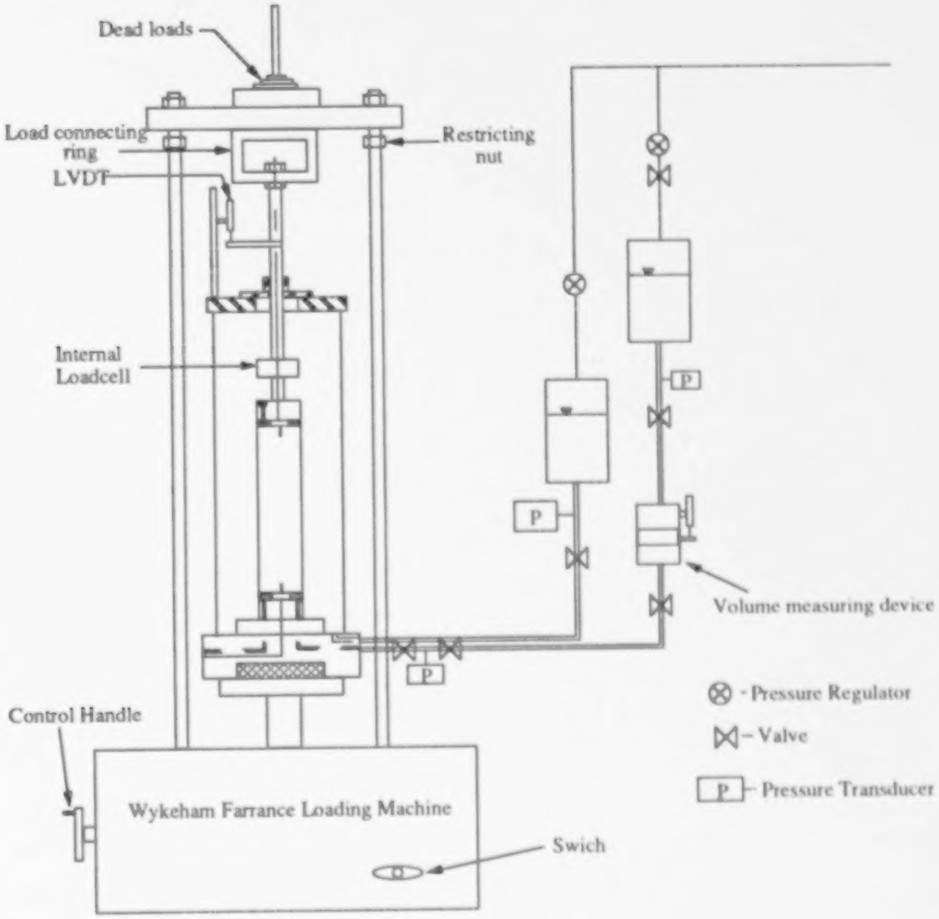

Figure. 3.6. Schematic of testing apparatus.

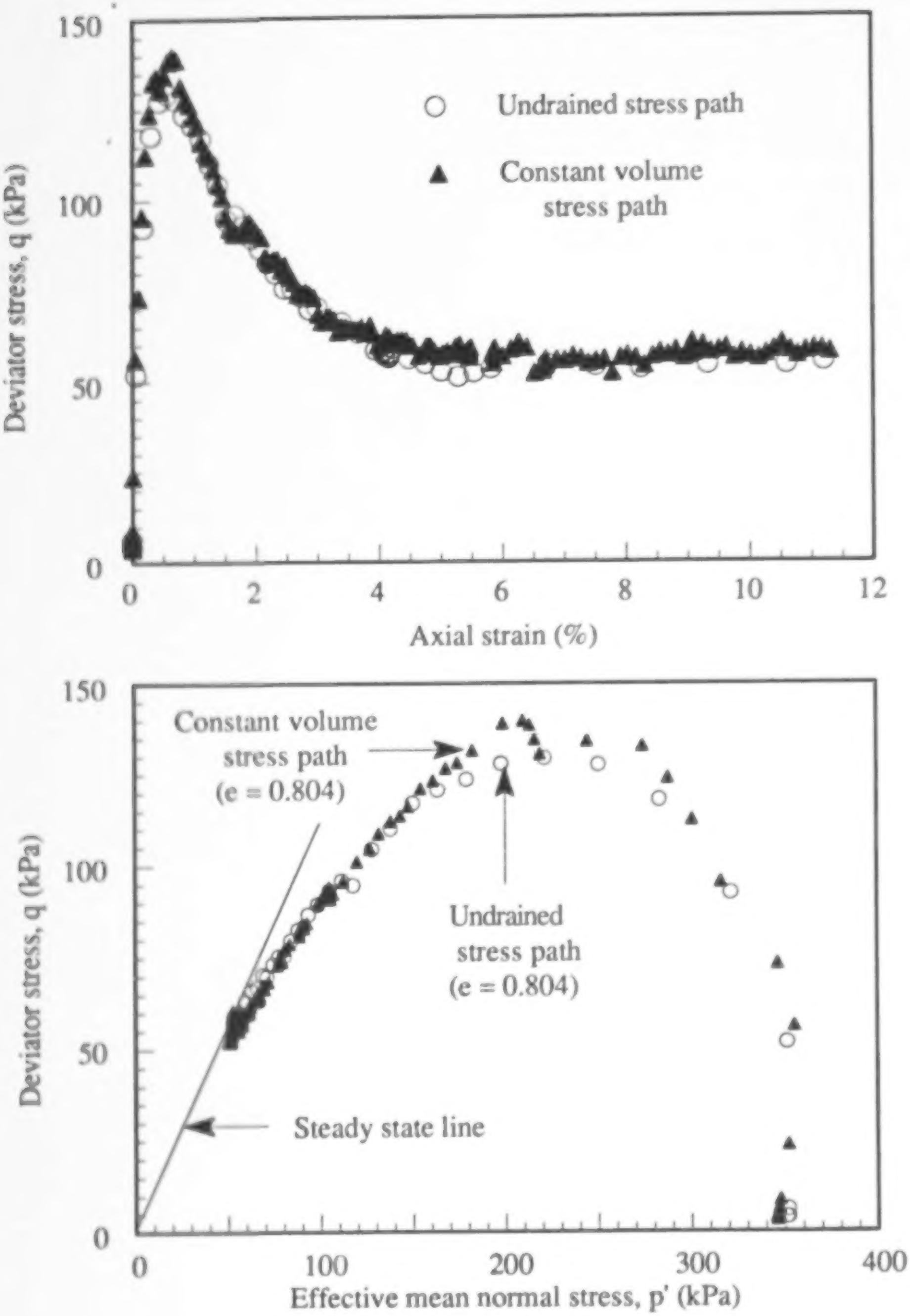

Figure. 3.7. Deviator stress-axial strain response and resulting stress paths of undrained and constant volume test.

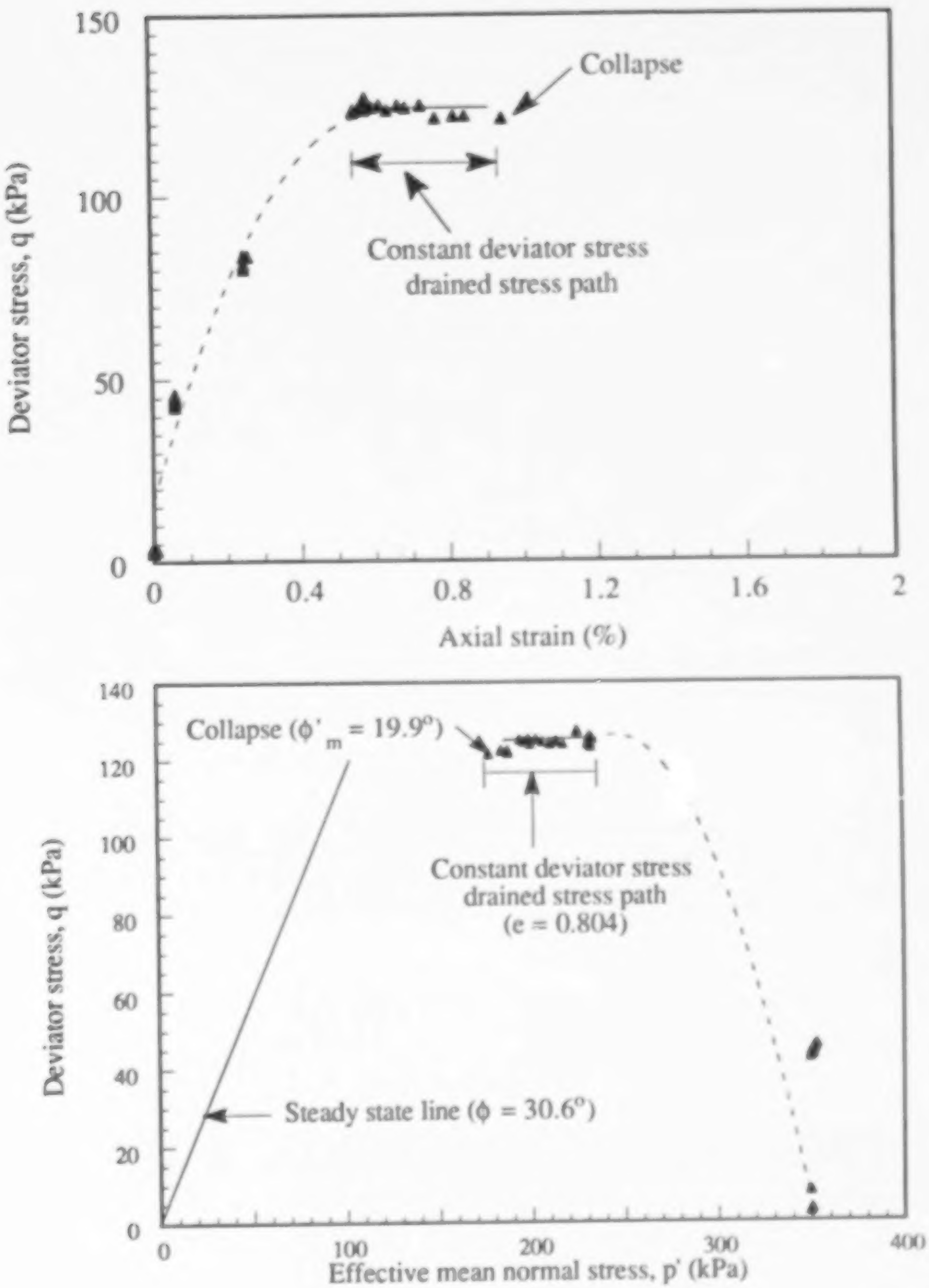

Figure. 3.8. The deviator stress-axial strain response and resulting stress path of constant deviator stress (q=125 kPa) drained test.

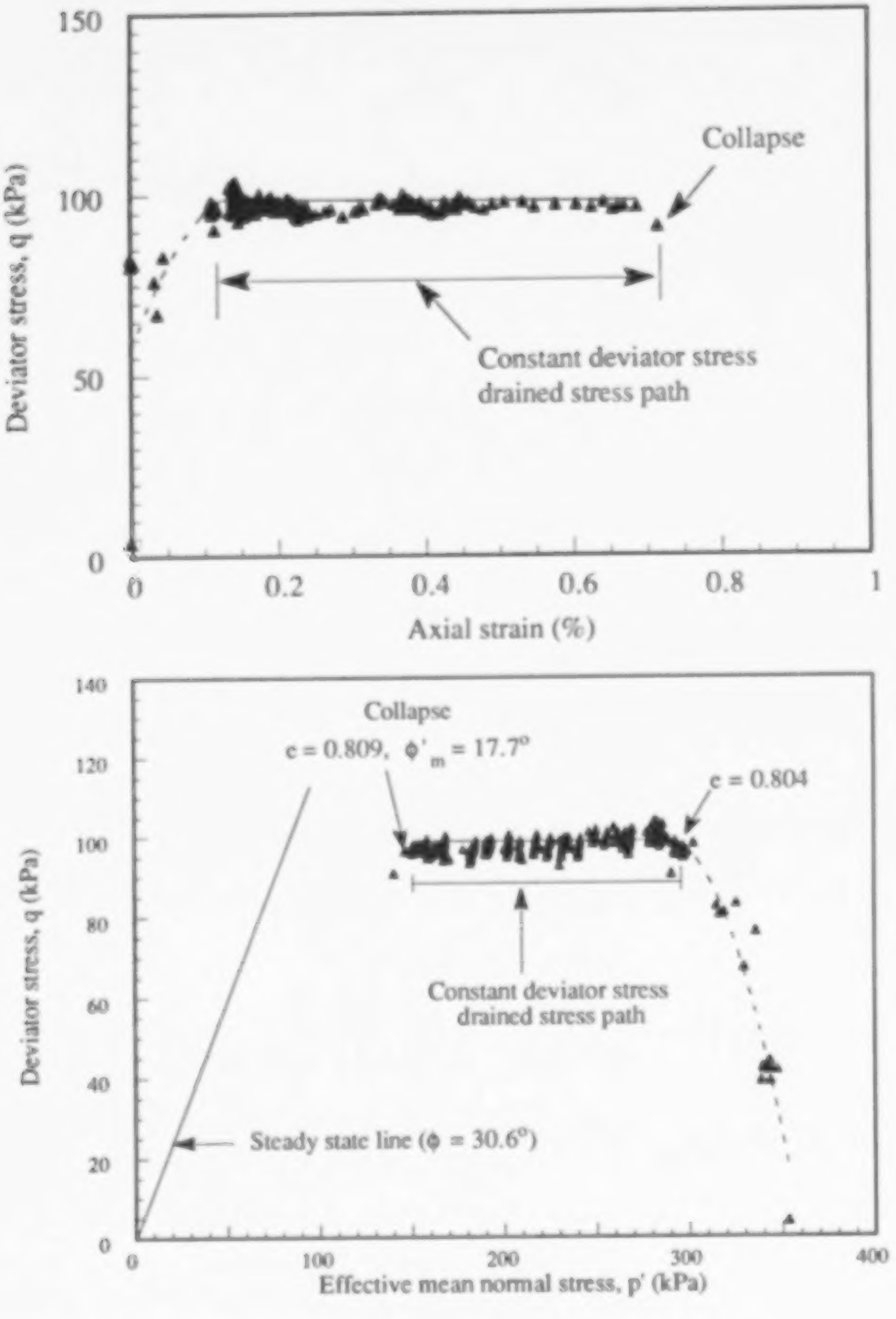

Figure. 3.9.The deviator stress-axial strain response and resulting stress path of constant deviator stress (q=100 kPa) drained test.

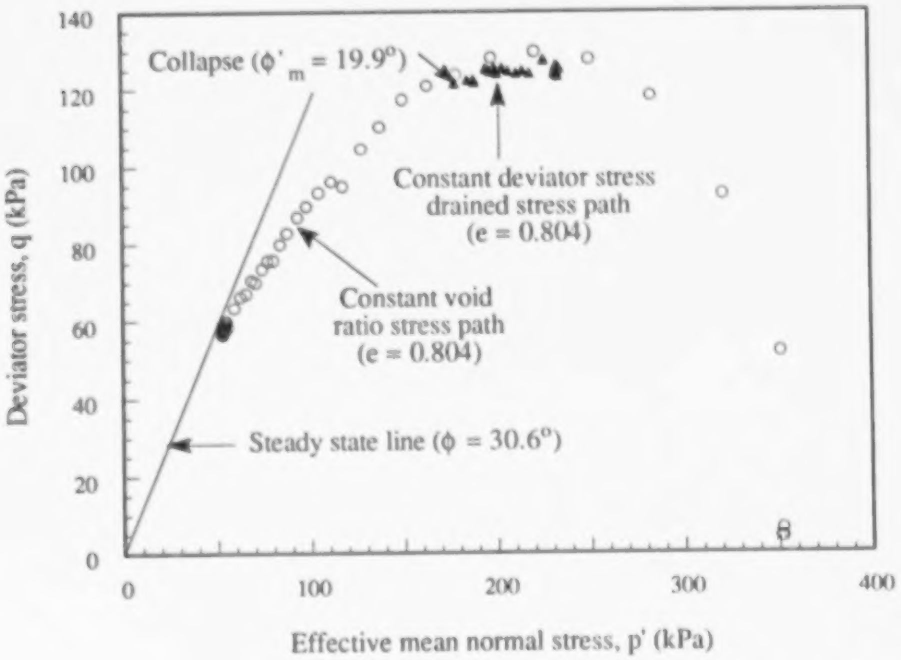

Figure. 3.10. Stress paths of constant void ratio (0.804) test and constant deviator stress (q=125 kPa) drained test.

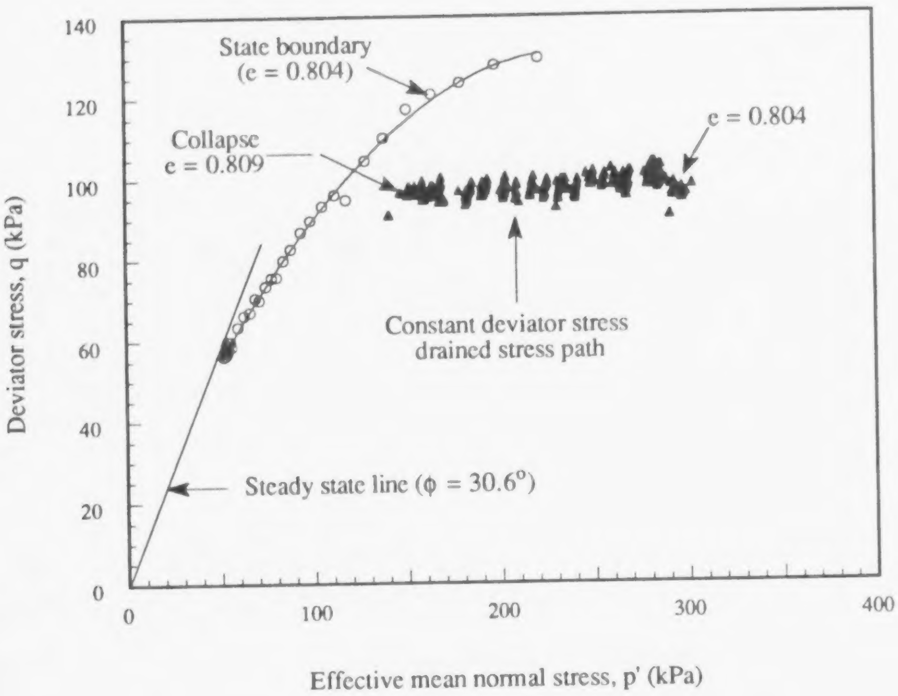

Figure. 3.11. State boundary defined by void ratio 0.804 and constant deviator stress (q=100 kPa) drained stress path.

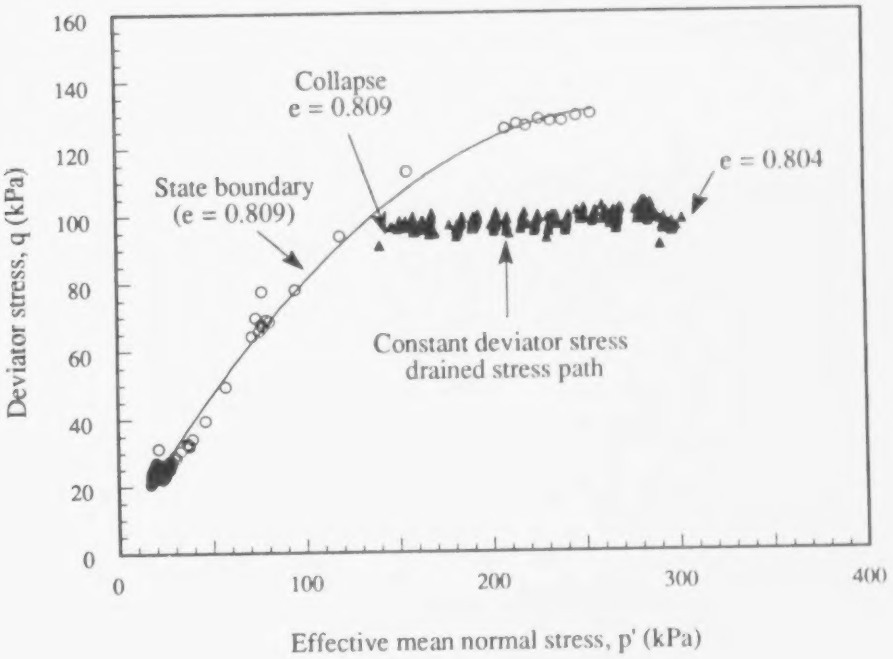

Figure. 3.12. State boundary defined by void ratio 0.809 and constant deviator stress (q=100 kPa) drained stress path.

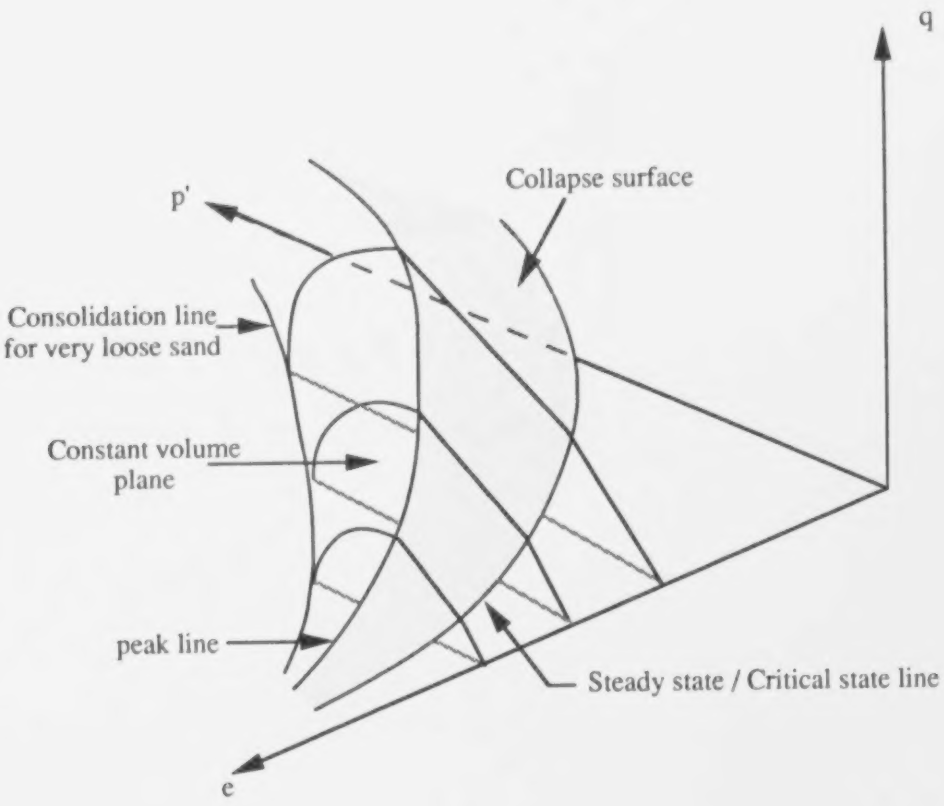
q
Collapse surface
p'
Consolidation line for very loose sand
Constant volume plane
peak line
Steady state / Critical state line
e

Figure. 3.13. Typical collapse surface in effective mean normal stress-deviator stress-void ratio space.

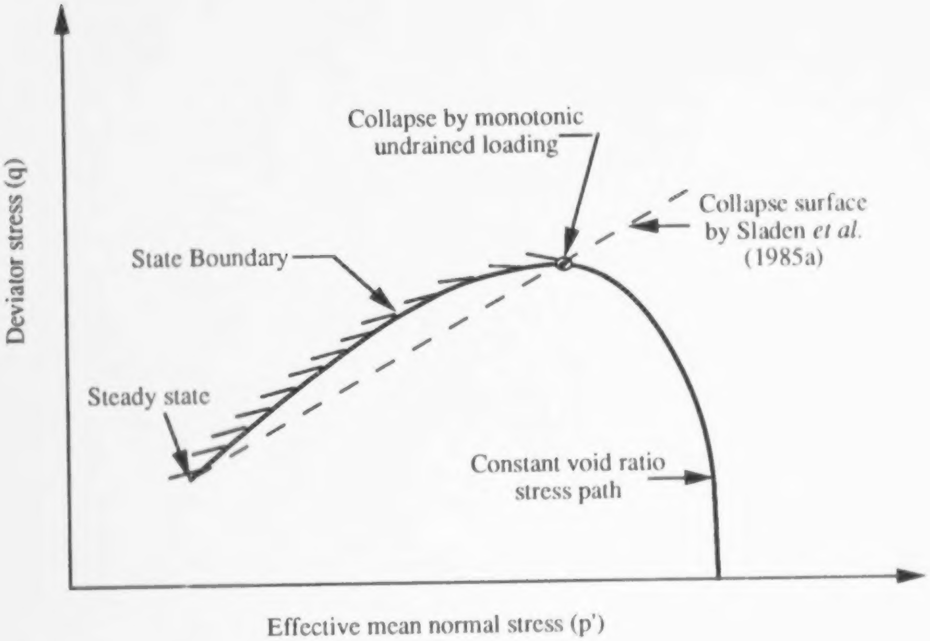
Deviator stress (q)
Effective mean normal stress (p')
Collapse by monotonic undrained loading
Collapse surface by Sladen *et al.* (1985a)
State Boundary
Steady state
Constant void ratio stress path

Figure. 3.14. Comparison of state boundary and collapse surface proposed by Sladen *et al.* (1985a)

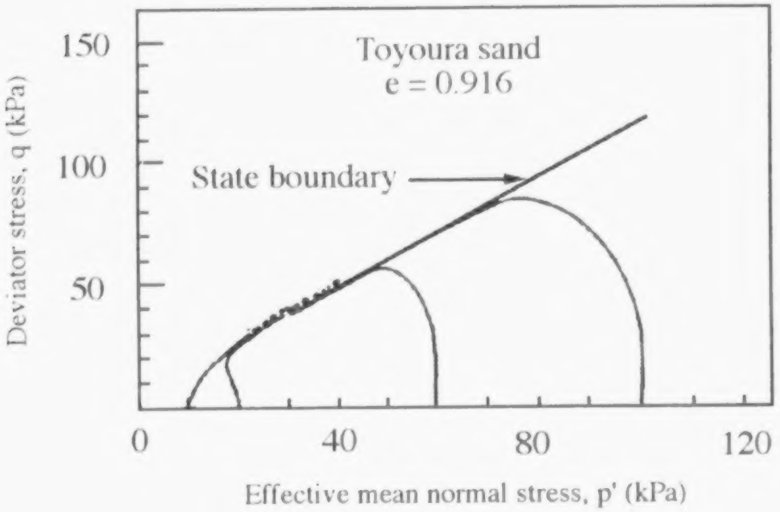

Figure. 3.15 Monotonic undrained stress paths starting from various confining stresses for a given void ratio. (modified from Ishihara *et al.*, 1991).

CHAPTER 4

A STATE BOUNDARY SURFACE FOR VERY LOOSE SAND AND ITS PRACTICAL IMPLICATIONS[*]

INTRODUCTION

According to critical state soil mechanics, (Roscoe *et al.*, 1958) the deviator stress ($q = (\sigma'_1 - \sigma'_3)$) effective mean normal stress ($p' = ((\sigma'_1 + 2\sigma'_3)/3)$) and void ratio (e) are uniquely related in the region between the normally consolidated state and a critical state. This forms a critical surface for a remolded clay, as shown schematically in Figure 4.1 which has often been referred to as the Roscoe surface. A normally consolidated remolded clay can have a stress state on the critical surface and an over consolidated remolded clay can have a stress state inside this critical surface. It separates states that samples can achieve from states which samples can never achieve. i.e. this critical surface is a state boundary surface.

---

[*] A version of this chapter has been submitted for publication: Sasitharan, S., Robertson, P.K., Sego, D.C. and Morgenstern, N.R. 1993. A State boundary surface for very loose sand and it's practical applications. Canadian Geotechnical Journal.

Following the development of critical state soil mechanics for remolded clays attention was also given to sands (e.g., Wroth and Bassett, 1965; Stroud, 1971). Application of critical state soil mechanics was less successful for sands mainly because there appeared to be no unique normally consolidated line defining the state boundary in the normal engineering range of stresses (0 - 700 kPa). Further, the concept of critical state soil mechanics for sand did not gain widespread attention because sands were generally not considered to be a difficult soil for design apart from the question of liquefaction.

Castro (1969) showed that loose sands can collapse and strain soften during monotonic undrained loading and ultimately reach a steady state. During monotonic undrained loading loose sand reaches a peak resistance and then rapidly strain softens to a constant resistance during which the effective stress state remains constant. Castro (1969) termed this constant state as steady state and showed that the steady state varied with void ratio. Steady state represents a state in the void ratio-effective mean normal stress-deviator stress space. Been *et al.* (1991) showed that the steady state achieved during monotonic undrained loading is also a critical state implying that steady state is independent of the stress path followed, i.e., steady state is unique for a void ratio regardless of whether it was reached by drained or undrained loading.

For very loose sand, Sladen *et al.* (1985) showed that a surface exists in deviator stress (q)- effective mean normal stress (p')- void ratio (e) space that can trigger collapse and strain softening leading to steady state under undrained loading. Several studies (Alarcon-Guzman *et al.*, 1988; Ishihara *et al.*, 1991; Georgiannou *et al.*, 1991; Symes *et al.*, 1984) have shown that a surface defined by the post peak portion of monotonic undrained stress paths forms a critical surface that can trigger collapse.

Although most pervious laboratory studies have involved undrained loading, this undrained condition is not a prerequisite to initiate liquefaction or collapse of cohesionless materials (Eckersley, 1990; Sasitharan *et al.*, 1993). In chapter 3 it was shown that saturated sand can collapse undrained during fully drained loading when the stress path tries to cross the collapse surface. Hence, it was shown that the post peak portion of an undrained stress path defines a state boundary above which it is not possible to have a stress state for a given void ratio and consolidation stress. Further, it was shown that liquefaction failure under drained and undrained loading can occur when the stress path tries to cross the state boundary surface of the sand. However, no attempt was made to study the shape of the state boundary surface and the behavior of saturated loose sand under drained loading conditions.

In this chapter, the influence of a state boundary surface on the drained behavior of loose saturated sand is investigated. Drained sand behavior for anisotropically and isotropically consolidated samples is compared with the proposed state boundary surface for the sand. The proposed state boundary surface concept is also evaluated based on published results for various other sands. Finally practical implications of the state boundary surface on liquefaction behavior of sand is discussed.

TESTING PROGRAM

A modified Wykeham Farrance triaxial testing apparatus and the moist tamping sample preparation technique described in chapter 3 was used throughout this study. The moist tamping technique was used to enable very loose samples of sand to be prepared. Ottawa (C109) sand obtained from Ottawa, Illinois was used. Ottawa sand is a uniform, medium sand comprised primarily of round to subrounded quartz grains with a specific gravity of 2.67. The mean grain size (D_{50}) of Ottawa sand is 0.34 mm. The maximum and minimum void ratios of the sand determined using the ASTM method D2049 are 0.82 and 0.50, respectively.

In all these tests the loading was performed under strain controlled conditions with a constant rate of deformation (0.15 mm/ min.).

Monotonic Undrained Loading

To determine the behavior of Ottawa sand under a constant void ratio stress path, seven monotonic undrained triaxial compression tests were performed on isotropically consolidated samples. The isotropic confining stress and void ratio after consolidation for these undrained tests are given in Table 4.1. Note that these samples were prepared at very high (loose) void ratios. These undrained tests include samples of 63 mm in diameter and approximately 125 mm long consolidated to an identical void ratio with different isotropic consolidation stresses. Identical void ratio for these samples was achieved by monitoring the void ratio change during increments of consolidation stress. When the sample reached the desired void ratio, the increases in consolidation stress was stopped and shearing proceeded. Full details of the sample preparation and testing procedures are given in chapter 3.

One of the undrained test was performed at an effective isotropic confining stress of 1470 kPa. The triaxial cell used for most of this study has a maximum cell pressure up to 1000 kPa. Hence, the high pressure test was performed in a high pressure triaxial cell in which samples of 37.5 mm diameter and 78.6 mm long can be sheared. In order to prepare a uniform loose sand sample of 37.5 mm and 78.6 mm long, a triaxial sample of 63 mm in diameter and approximately 125 mm long was reconstituted using the moist tamping technique described in chapter 3. The sample, confined by a split mold, was then saturated by percolating de-aired water. The saturated sample was then frozen by placing it in a cold room (-20 °C) and allowing open drainage to avoid changes in void ratio. The frozen sample was then removed from the split mold and machined to 37.5 mm diameter and approximately 78.6 mm long. This machined sample was then thawed and saturated by increasing the back pressure until the Skempton's B value was 0.99 in the high pressure testing cell. This sample was then consolidated to an isotropic confining stress of 1470 kPa and sheared undrained.

Monotonic Drained Loading

Three monotonic drained triaxial compression tests were performed. These tests were selected such that; one drained test was performed from an isotropic stress state and two drained tests were performed from anisotropic stress states. The anisotropic stress states were selected to be on the post peak strain softening portion of an undrained stress path, i.e., the initial stress state of the sample was on a constant void ratio stress path. Hence, the subsequent void ratio changes and stresses along the various drained stress paths can be compared with respective constant void ratio stress paths.

A loose sand sample was consolidated to an isotropic confining stress of 515 kPa and loaded in conventional drained triaxial compression. In a conventional drained triaxial compression test no pore pressures (u) are generated and the confining stress (σ_c) remains constant while the vertical stress increases. Hence, the effective minor principal stress ($\sigma'_3 = \sigma_c - u$) remains constant. Therefore, a constant effective minor principal stress path ($\Delta\sigma'_3 = 0$) was followed by loading the sample under a constant rate of deformation from an isotropic stress of 515 kPa. In a conventional drained triaxial compression test the stress path must lie on a plane defined by $\Delta q = 3 \Delta p'$. Figure 4.2 shows a schematic of a stress path in deviator stress (q)-effective mean normal stress (p') -void ratio (e) space for a compression test with the effective minor principal stress constant and starting from an isotropic consolidation state.

Anisotropically consolidated drained constant effective mean normal stress and constant effective minor principal stress (conventional) loading tests were also performed from the post peak portion of an undrained stress path. Initially, the samples were consolidated to an isotropic confining stress of 350 kPa. Then the samples were loaded undrained until the stress state reached the post peak strain softening portion. At this point the loading was stopped and the back pressure applied to the sample was adjusted to the current pore pressure to ensure no volume change of the sample would occur when the drainage port was opened to allow a free draining condition. Hence, the void ratio and the stress state remained unchanged from that achieved during the undrained loading. Under these anisotropic stress states and void ratio, the sample was then sheared in a fully drained condition along either a constant effective mean normal stress path or a constant effective minor principal stress path.

For the constant mean normal stress path, the back pressure applied to the sample was continuously adjusted such that during drained loading the effective mean normal stress remained constant. Figure 4.3 shows a schematic of the drained constant effective mean normal stress path from the post peak portion of an undrained stress path in q-p'-e space. In this figure A-B-C represents the undrained stress path and C-D represents the drained constant effective mean normal stress path.

From an anisotropic stress state (the post peak strain softening portion of an undrained stress path), the constant effective minor principal stress path was followed by the same procedure described above. It was shown that the constant effective minor principal stress path lies on a plane defined by $\Delta q = 3\ \Delta p'$. Figure 4. 4 shows a schematic of the drained constant effective minor principal stress path from the post peak portion of an undrained stress path in q-p'-e space. In this figure A-B-C represents the undrained stress path and C-D represents the drained constant effective minor principal stress path.

TEST RESULTS

Monotonic undrained loading

The deviator stress-axial strain response and resulting stress paths for the monotonic undrained triaxial compression tests on samples consolidated to an identical void ratio of 0.793 are shown in Figure 4.5. The stress path moves towards the zero effective stress state, until the process of deformation brings the sand to the steady state or critical state condition (see Fig. 4.5). It may be observed in Figure 4.5 that the deviator stress-axial strain response of these samples reached a peak deviator stress at a very small strain (0.4-0.6 %). Then the response showed a marked strain softening with increase in axial strain until the stress stabilized at the steady state strength. It may also be noticed that regardless of the initial consolidation stress all the samples of identical void ratio (e = 0.793) reached essentially the same steady state strength. This is consistent with the observation by Castro (1969) that steady state strength is uniquely related to void ratio regardless of the previous consolidation stresses, at least for samples that have an initial state considerably looser than that of steady state.

It may be observed from the resulting stress paths shown in Figure 4.5 that the locus of the peak deviator stress of these undrained stress paths can be represented by a straight line passing through the steady state strength. This straight line representation of the locus of peak strength was called a collapse surface by Sladen *et al.* (1985). Further, it may also be observed that the post peak portion of all these stress paths can be approximated by a straight line originating from steady state, as shown in Figure 4.5 with a slope of 0.8. This straight line forms an approximate boundary above which these undrained stress paths cannot travel.

A boundary above which no stress state is possible was defined as a state boundary by Roscoe *et al.*(1958). The straight line approximation of the post peak portion of the undrained stress paths shown in Figure 4.5 therefore defines a boundary above which undrained stress paths cannot travel. In chapter 3 it was shown that the post peak portion of an undrained stress path defines a state boundary for a given consolidation stress and void ratio. Hence, the straight line approximation of the post peak portion of the undrained stress path defines the state boundary for this void ratio (0.793) regardless of the confining stress. Such an approximation was postulated in chapter 3 by presenting undrained test results for Toyoura sand obtained by Ishihara *et al.* (1991). The results presented in Figure 4.5 confirms that a straight line approximation of the post peak portion of undrained stress paths is also true for Ottawa sand.

Figure 4.6 shows the deviator stress- axial strain response and resulting stress path of samples consolidated to an identical void ratio of 0.803. The deviator stress-axial strain response is similar to that observed for the void ratio of 0.793. After reaching a peak deviator stress, the sand rapidly strain softens to the same essentially constant deviator stress during which the effective stress state remained constant. It may be observed from the resulting stress paths that the post peak portion of these undrained stress paths can also be approximated by a straight line with a slope of 0.8. Figure 4.7 shows undrained stress paths of a very loose sample (e = 0.809) and a sample consolidated to a high stress (e= 0.758, p'_o = 1470 kPa). It may be noticed that a straight line with slope 0.8 forms an approximate envelope for the post peak portion of these undrained stress paths. Hence, from the results presented herein it appears that the post peak portion of undrained stress paths at different void ratio's can be approximated by a straight line regardless of the consolidation stress and that the slope of the straight line remains essentially constant regardless of the void ratio. These straight lines represent approximately the state boundary for each void ratio. There are an infinite number of these lines representing the complete state boundary in deviator stress (q)- effective mean normal stress (p')- void ratio (e) space. Hence, the state boundary can be approximated as a surface of constant slope straight lines for different void ratio's.

In reality the state boundary appears to flatten at larger stress and samples are less brittle (see Fig. 4.7). However, for very loose sands at typical engineering stress levels (0- 700 kPa), it appears reasonable to assume the surface to be planar with a constant slope.

Monotonic Drained Loading

Figure 4.8 shows the behavior of loose Ottawa sand tested under monotonic drained condition after consolidating to an isotropic stress of 515 kPa and void ratio of 0.808. It may be noticed that the deviator stress increases steadily until it reaches a constant value. The volume of the sand gradually decreases continuously until it reaches a constant value. This deformation under constant stress and volume was referred as steady state by Polous *et al.* (1981). Figure 4.9 shows the resulting stress path in deviator stress-effective mean normal stress and deviator stress-void ratio space.

Figure 4.10 shows the behavior of loose Ottawa sand tested under monotonic drained condition for the test with a constant effective mean normal stress performed from the post peak portion of an undrained stress path. In this figure A- B- C represents the undrained loading path and C-D represents the drained loading at constant effective mean normal stress. During the undrained loading, the deviator stress reaches a peak (point B) and then the deviator stress starts to reduce. Point C represents an anisotropic stress state on the post peak portion of the undrained stress path. Therefore, point C represents a stress state on the state boundary. From C to D the sample was loaded fully drained under constant effective mean normal stress conditions. During the drained phase of loading (C-D) the deviator stress increases continuously with increasing axial strain and reaches a constant value. The volume change-axial strain behavior shows that when axial strain was increased from A-B-C there was no volume change (undrained) and then from C-D the sample decreases in volume continuously until it reached a condition of constant volume and constant stress at D. Hence, the stress and void ratio at point D represents steady state conditions.

Figure 4.11 shows the resulting stress path of this constant effective mean normal stress loading in deviator stress - effective mean normal stress and deviator stress - void ratio space. In this figure the effective mean normal stress and void ratio axis are reversed in order to compare these stress paths with the schematic shown in Figure 4.3. Along C-D the mean normal stress remains constant and the deviator stress and void ratio changes continuously until steady state is reached at D.

Figure 4.12 shows the behavior of loose Ottawa sand tested under monotonic drained condition for the test with a constant minor principal stress (σ'_3) performed from the post peak portion of an undrained stress path. In this figure A-B-C represents the undrained stress path and C-D represents the drained loading at constant minor principal stress path. After reaching the peak at point B, the undrained stress path shows a strain softening behavior. Point C represents a stress state on the post peak portion of the undrained stress path and therefore a point on the state boundary. From C-D the sample was loaded fully drained under constant effective minor principal stress conditions. Hence, path C-D shows a typical behavior of an anisotropically consolidated sample of very loose sand tested under conventional triaxial compression test. From C to D, the deviator stress increases continuously and reaches a constant value. The volume change decreases continuously and reaches constant volume at D. Hence, stresses and void ratio at point D represent steady state condition.

Figure 4.13 shows the resulting stress paths of this constant minor principal stress path in deviator stress-effective mean normal stress and deviator stress-void ratio stress space. In this figure the effective mean normal stress and void ratio axis are reversed in order to compare these stress paths with the schematic shown in Figure 4.4. Along stress path C-D, the deviator stress, effective mean normal stress and void ratio change continuously and the change in deviator stress is 3 times the change in effective mean normal stress.

STATE BOUNDARY SURFACE FOR VERY LOOSE SAND

The main conclusions from the monotonic undrained triaxial compression loading or constant void ratio stress paths are:

(1) Samples with identical void ratio have essentially the same steady state regardless of their consolidation stresses.

(2) The post peak portion of constant void ratio stress paths can be approximated by a straight line for a given void ratio.

(3) The post peak portion of the constant void ratio stress path at different void ratio's can be approximated by straight lines with identical slope. This may not be true for loose sands consolidated to very high stress levels where the slope may flatten as the sand becomes less brittle.

A state boundary can be defined by the post peak portion of the undrained stress paths for very loose sand. Hence, these constant slope straight lines and the steady state line define the state boundary regardless of consolidation stress for a given void ratio. There are potentially an infinite number of these straight lines which forms a surface in deviator stress (q)- effective mean normal stress (p')- void ratio (e) space for very loose sands. In reality the state boundary is limited by the consolidation line of a very loose sand.

Figure 4.14 shows schematically the state boundary surface in deviator stress (q) -effective mean normal stress (p') -void ratio (e) space. The projection of this surface in q-p' space is shown in Figure 4.15. To define this surface mathematically, let;

$$\frac{q_{ss}}{p'_{ss}} = M \qquad [4.1]$$

and

$$\frac{q - q_{ss}}{p' - p'_{ss}} = s \qquad [4.2]$$

Where;

M = slope of the steady state line in deviator stress-effective mean normal stress space.

s = Approximate slope of the state boundary surface in deviator stress-effective mean normal stress space.

q_{ss} = deviator stress at steady state

p'_{ss} = effective mean normal stress at steady state

q = deviator stress of a stress state on state boundary

p' = effective mean normal of a stress state on state boundary

By substituting [4.1] in [4.2] and rearranging

[4.3] $$q = s\,p' + (M - s)\,p'_{ss}$$

It is often found that the void ratio (e) and effective mean normal stress at steady state (p'_{ss}) can be approximated by a straight line if plotted with a logarithmic scale for the effective mean normal stress at steady state (p'_{ss}) (Fig. 4.16). Hence, the equation relating void ratio and effective mean normal stress at steady state can be written as

[4.4] $$e = \Gamma - \lambda \ln p'_{ss}$$

[4.5] i.e. $$p'_{ss} = \exp\left(\frac{\Gamma - e}{\lambda}\right)$$

where;

λ = slope of the line.

Γ = the intercept of the line at $p'_{ss} = 1$.

By substituting [4.5] in [4.3]

[4.6] $$q = s\,p' + (M - s)\exp\left(\frac{\Gamma - e}{\lambda}\right)$$

Where M, s, Γ and λ are constants and can be obtained by performing undrained tests for loose sand as outlined below.

M- The slope of the straight line representing stresses at steady state (p'_{ss}, q_{ss})

s- The slope of the straight line approximation of the post peak portion of undrained stress paths with identical void ratio.

λ- The slope of the best fit straight line between void ratio (e) and logarithmic effective mean normal stress at steady state ($\ln p'_{ss}$). Here, the value of λ will depend on the unit chosen for the effective mean normal stress.

Γ- The intercept of the best fit straight line between void ratio (e) and logarithmic effective mean normal stress ($\ln p'_{ss}$) at $p'_{ss} = 1$ unit.

Equation [4.6] therefore, defines a plane in q-p'-e space that represents an approximation for the state boundary. Equation [4.6] defines a plane that extents in the direction of increasing p' from the steady state line until the state boundary flattens at very high stress. The actual state boundary for very loose sand is presented by the limit of void ratio (e) and effective mean normal stress (p'), as shown schematically in Figure 4.14. Equation [4.6] represents only an approximation for the actual curved state boundary for very loose sand.

INTERPRETATION OF DRAINED BEHAVIOR OF LOOSE OTTAWA SAND USING THE STATE BOUNDARY SURFACE

One of the main objectives of this study was to study the relationship between constant void ratio stress paths which can be obtained from undrained triaxial compression tests (Sasitharan *et al.*, 1993) and drained stress paths.

State Boundary Surface for Ottawa Sand

The state boundary surface for soils was introduced as a unifying concept to allow the behavior of the soil to be interrelated (Roscoe *et al.*, 1958). It has been shown in the previous section that a state boundary surface for loose sand can be approximately represented by [4.6] in deviator stress (q)-effective mean normal stress (p')-void ratio (e) space.

Figure 4.17 shows the relation between deviator stress at steady state (q_{ss}) and effective mean normal stress at steady state (p'_{ss}) for Ottawa (C109) sand obtained from the undrained tests. For the purpose of clarity the data obtained from the high pressure test is not shown in this figure. It may be noticed that the relation between q_{ss} and p'_{ss} can be approximated by a straight line with slope (M) equal to 1.197. This is equivalent to a friction angle of 30^{o}.

Figures 4.5 and 4.6 show the resulting stress paths of the undrained tests with identical void ratio at different consolidation stresses. It was assumed that the post peak portion of these stress paths forms a straight line and the slope of this straight line (s) is equal to 0.8.

Figure 4.18 shows the variation of void ratio with effective mean normal stress at steady state. Here, data are plotted with a logarithmic scale for the effective mean normal stress at steady state (p'_{ss}). It may be noticed that the e-ln p'_{ss} relationship can be approximated by a straight line in this logarithmic plot. The slope of this straight line (λ) is equal to 0.0168 and the intercept of this straight line at p'_{ss} = 1 kPa is equal to Γ= 0.864.

Hence, the state boundary surface of loose Ottawa sand can be represented in deviator stress (q)-effective mean normal stress (p')-void ratio (e) space by equation [4.6] using;

M = 1.197
s = 0.8
λ = 0.0168
Γ = 0.867

This section has defined an approximate state boundary surface using equation [4.6] for very loose sand in the normal engineering range of stress (0-700 kPa). The following section will evaluate this state boundary using the drained test results.

Monotonic Drained Loading

Figure 4.19 compares the results from the conventional isotropically consolidated drained triaxial compression test with the state boundary defined by equation [4.6]. The comparison is made in q-p' and q-e space. The state boundary is calculated using equation [4.6] for each value of e and p'. Figure 4.19 shows that in the conventional isotropically consolidated drained triaxial compression test the stress path gradually climbs until it reaches the state boundary surface. Then the stress path essentially travels along the state boundary surface until it reaches steady state conditions. Although equation [4.6] represents only an approximation of the actual curved state boundary, it is clear from Figure 4.19 that the drained stress path does not cross the state boundary but moves along it towards steady state.

This stress path shows that even when the initial stress state of a saturated sand is below the state boundary surface, with subsequent loading the stress state reaches the state boundary surface and then travels along the state boundary surface to reach steady state conditions. At steady state the stresses and void ratio remain constant with further loading or deformation. The length of travel along the state boundary surface will depend on the initial stress state and void ratio. For some initial smaller void ratio the stress path may not reach the state boundary but travel just below the surface until reaching the steady state condition.

Figure 4.20 compares the results from the drained constant effective mean normal stress path (C-D) from an anisotropic stress state (post peak portion of an undrained stress path) with the state boundary defined using equation [4.6]. The constant mean normal stress path closely follows the state boundary surface before reaching the steady state condition at D. At steady state the stress and void ratio remain constant. The initial anisotropic consolidation stress state (point C) lies on the state boundary and the constant effective mean normal stress path involves continuous increases in deviator stress. Hence, the subsequent stress path C-D remains on the state boundary surface since it cannot travel above the state boundary surface during compression loading.

Figure 4.21 compares the results from the drained constant effective minor principal stress path (C-D) from an anisotropic stress state (post peak portion of an undrained stress path) with the state boundary defined using equation [4.6]. The constant effective minor principal stress path closely follows the state boundary surface before it reaches the steady state condition at D. Figure 4.22 shows that even when all three variables q, p' and e change the stress path follows the state boundary surface until it reaches steady state. The initial anisotropic stress state (point C) lies on the state boundary surface and the constant effective minor principal stress path involves continuous increases in deviator stress. Hence, the subsequent stress path C-D remains essentially on the state boundary surface.

The important feature of the two drained test results shown in Figures 4.20 and 4.21 is that the initial anisotropic stress state was selected to lie on or very close to the state boundary. Hence, any drained loading would evaluate if the state boundary defined by equation [4.6] was realistic to describe drained behavior of fully saturated sand.

STATE BOUNDARY SURFACE FOR OTHER SANDS

It has been shown that a state boundary surface for very loose Ottawa sand can be defined by equation [4.6] with constants M, s, λ and Γ. Further it has been shown that these constants can be obtained from undrained triaxial compression test on very loose samples. Table 4.2 summaries the constants M, s, λ and Γ obtained from published results for various other sands. In Table 4.2, λ and Γ values for the other sands are specified for ranges of effective mean normal stress at steady state. These values were obtained by fitting a straight line approximation for what is sometimes a curved void ratio-effective mean normal stress relation over a wide range of effective mean normal stress at steady state.

Figures 4.22 and 4.23 show comparison of the state boundary surface based on equation [4.6] obtained for Toyoura sand with two conventional (constant minor principal stress) drained triaxial compression tests performed by Dr. R. Verdugo at The University of Tokyo (Ishihara, 1992). For both tests at different void ratios and isotropic consolidation stresses, the deviator stress gradually increases until the state boundary surface is reached. Then the stress path essentially travels along the state boundary surface similar to the behavior observed for Ottawa sand (Fig. 14). Similar results were obtained using data for Erksak sand presented by Been *et al.* (1991) and Jefferies and Been (1992) and shown in Figures 4.24 and 4.25.

The results presented in this study have shown that the post peak strain softening portion of undrained triaxial compression tests on a very loose sand define an approximate state boundary. This state boundary can be approximated using the planar representation using equation [4.6]. The results have also shown that triaxial compression loading along either drained or undrained stress paths for very loose sand will not cross this state boundary.

PRACTICAL IMPLICATIONS

Results presented in chapter 3 show that when a sample of very loose saturated sand is loaded under fully drained conditions in a direction of constant q and decreasing p' the sample collapsed undrained when the stress path tried to cross the state boundary. In chapter 3 it was also shown that collapse could be triggered during undrained cyclic loading when the cyclic stress path attempts to cross the state boundary. Hence, undrained strain softening and liquefaction for very loose saturated sand can be triggered by both static and cyclic loading when the resulting stress path attempts to cross the post peak strain softening portion of the monotonic undrained compression test. Figure 4.26 shows a schematic of two stress paths that can trigger strain softening behavior. The static loading (q = constant, p' decreasing) could represent a condition of rising ground water within a slope.

The results presented in this study have shown that when a very loose sample of saturated sand is loaded such that the stress path approaches the state boundary in stable loading, strain softening behavior will not occur and the stress state will travel along the state boundary and climb up toward a high ultimate steady state.

Figure 4.27 shows a schematic representation of the state boundary surface for very loose sand in q-p'-e space. Also shown in Figure 4.27 is an element of sand with a stress state on the state boundary. The actual state boundary is a curved surface dropping down to the steady state/critical state line. However, this study has shown that the actual curved state boundary can be simplified and represented as plane, as shown in Figure 4.27. If a stress state for a saturated loose sand exists on the state boundary, the response to loading will depend on the rate of loading and the rate of structural collapse of the sand structure. If the rate of loading is rapid (i.e., undrained) either monotonic or cyclic for fully saturated sand, the resulting stress path must travel down the state boundary towards steady state at the same void ratio. Since, the steady state strength is less than the initial stress state the sand element will strain soften towards steady state. If the initial deviator stress is constant (i.e., q= constant) such as would exist in a slope where q is induced by the gravity stresses, the element of sand could experience rapid collapse resulting in large strains .

If the rate of loading and loading conditions result in a stress path that tries to cross the state boundary surface, saturated loose sand would strain soften due to collapse of the sand grain. This sand grain rearrangement causes undrained conditions and an increase in pore pressure. Hence, saturated loose sands can strain soften. Dry sands would show a volume decrease when stress paths try to cross the state boundary due to the sand grain rearrangement. However, there would not be any increase in pore pressure. Hence, dry sands collapse with limited deformation and reach a new stable stress state and void ratio below the state boundary surface (Skopek, 1993).

If the rate of loading is very slow (i.e., drained) either monotonic or cyclic for fully saturated sand, the resulting stress path must travel along the state boundary towards steady state at a different void ratio. The structural collapse of the sand skeleton will result in a decrease in void ratio. Hence, the element will strain harden as it decreases in volume and climbs up the state boundary towards steady state at a lower void ratio. These two extreme stress paths are shown schematically in Figure 4.27.

The stability of the stress state on the state boundary can be visualized as a small ball located on a sloping surface. Provided the ball is pushed up the slope (i.e., stable stress path resulting in strain hardening response) the ball will travel up the slope. However, if the ball is pushed in a direction that will allow it to roll down the slope it will drop to a new stable level (i.e., unstable stress path resulting in strain softening response to steady state).

If a slope or embankment is comprised of very loose saturated sand it is possible to construct the slope in a drained condition such that elements of sand are on or very close to the state boundary surface. This drained construction is similar to the stress paths illustrated in Figures 4.19, 4.22, 4.23 , 4.25 and 4.26. Using conventional drained friction angle limit state analyses, the slope may have a factor of safety close to 2. However, very loose saturated sands that exist in this state are potentially unstable and may be on the verge of catastrophic collapse. Any small loading that could push the stress state toward or down the state boundary surface could result in a rapid undrained collapse as the saturated sand moves toward a lower steady state strength. Since, this collapse occurs at small strains there is little evidence of the potential slope failure. This condition was confirmed experimentally by Eckersley (1990) using a model embankment and increasing the level of the water table. In chapter 3 this condition was duplicated in the laboratory by performing drained triaxial tests on very loose sand with q constant and p' decreasing.

Gu *et al.* (1993) showed that the collapse of the lower San Fernado dam after the 1971 earthquake could be explained using a collapse surface concept similar to the state boundary surface presented in this study.

The existence of some elements of sand in a slope at or close to the state boundary may not necessarily result in complete failure of the slope. Complete failure of a slope can only result if a sufficient amount of loose strain softening soil exists to develop a complete failure mechanism. If a very small volume of loose sand exists in the slope it is possible that the failure mechanism may be contained by a sufficient quantity of strain hardening sand.

Conventional slope stability analyses that use the ultimate friction angle in a limit state approach can not account for the potential instability and strain softening behavior of soil elements close to the state boundary surface.

Summary and Conclusions

An experimental program to study the relationship between drained and undrained behavior of a very loose saturated sand has been presented. From monotonic undrained triaxial compression tests, it has been shown that the post peak strain softening portion of undrained stress paths of identical samples at the same void ratio can be approximated by a straight line for very loose sand. Further, it has been shown that the slope of this straight line remains approximately constant for samples at different void ratio's within the normal engineering range of stresses (0-700 kPa) for Ottawa sand. There are potentially an infinite number of these lines, which form a planar surface in q-p'-e space. In chapter 3 it was shown that the post peak portion of a monotonic undrained stress path defines a state boundary above which stress states of the sand at a given void ratio can not exist. Hence, this planar surface represents a state boundary surface for very loose sand.

In chapter 3 it was also shown that strain softening and liquefaction occurs when a stress path tries to cross the state boundary surface. Hence, whether a saturated very loose sand strain softens and collapses or strain hardens as it travels along the state boundary surface will depend on the rate of loading and the rate of structural collapse of the sand skeleton. If the rate of loading is rapid (i.e., undrained) either monotonic or cyclic for fully saturated very loose sand, the resulting stress path must travel down the state boundary towards steady state at the same void ratio. If the rate of loading is very slow (i.e., drained) either monotonic or cyclic and the rate of structural collapse is slow for fully saturated very loose sand, the resulting stress path can travel up the state boundary under drained conditions towards steady state at a different void ratio.

If the rate of loading and loading conditions result in a stress path that tries to cross the state boundary surface, saturated loose sand would strain soften due to collapse of the sand grains. This sand grain rearrangement causes undrained conditions and an increase in pore pressure. Hence, saturated very loose sands can strain soften. Dry sands would show a volume decrease when stress paths try to cross the state boundary. However, there would not be any increase in pore pressure. Hence, dry sands can collapse with limited deformation and reach a new stable stress state and void ratio below the state boundary surface (Skopek, 1993).

An analog similar to a small ball placed on a sloping surface was presented to explain the behavior of a sand element with a stress state on or closer to the state boundary surface under different rates of loading. If the sand element is loaded slowly such that volume changes occur, the sand will strain harden to reach the respective steady state. If the sand element is loaded rapidly such that no volume change can occur the sand will strain soften to reach the respective steady state. The critical rate of loading for collapse and strain softening may depend on the shape of the state boundary, initial void ratio and stresses, the rate of collapse of the sand skeleton structure and the permeability of the sand. Whether or not collapse failure of sand elements will result in a large mass movement of a soil slope may depend on the volume of collapsible material in the structure. If there is large volume of strain softening material then catastrophic failure could result. If there is only small amount of strain softening material then it is possible that the collapse mechanism may be contained by a sufficient quantity of strain hardening sand.

REFERENCES

Alarcon-Guzman, A., Leonards, G. A. and Chameau, J. L. 1988. Undrained monotonic and cyclic strength of sands. Journal of Geotechnical Engineering American Society of Civil Engineering, **114**: 1089-1109.

ASTM 1969. Standard test method for relative density of cohesionless soils (D2049-69). In 1969 Annual Book of ASTM Standards. American Society of Testing Materials, Philadelphia, pp. 622-630.

Been. K., Jefferies. M. G. and Hachey. J. 1991. The critical state of sand. Geotechnique, **41**: 365-381.

Castro, G. 1969. Liquefaction of sands. Harvard Soil Mechanics Series No. 81. 112 pp.

Castro, G ., and Enos, J. L., France, J. W. and Poulos, S. J. 1982. Liquefaction induced by cyclic loading. Report to National Science Foundation, Washington, DC, No. NSF/CEE-82018. 79 pp.

Eckersley, D. 1990. Instrumented laboratory flow slides. Geotechnique, **40**: 489-502.

Georgiannou, U. N., Hight, D. W. and Burland, J. B. 1991. Behavior of clayey sands under undrained cyclic triaxial loading. Geotechnique, **41**: 383-393.

Gu, W. H., Morgenstern, N. R. and Robertson, P. K. 1993. Progressive failure of lower San Fernando dam. Journal of Geotechnical Engineering American Society of Civil Engineering, **119**: 333 - 349.

Ishihara, K., Verdugo, R. and Acacio, A. A. 1991. Characterization of cyclic behavior of sand and post-seismic stability analysis. IX. Asian Regional Conference on Soil Mechanics and Foundation Engineering, Bangkok, Thailand. Vol. 2. pp. 17-40.

Ishihara, K. 1992. Personal communication.

Jefferies. M and Been. K. 1992. Undrained response of Nor-Sand. 45th Canadian Geotechnical Conference, Toronto. 2:1- 2:12.

Klohn Leonoff Report. 1984. Seismic investigation for Brenda mine sand. Vol. (1)- Vol. (3). Klohn Leonoff. Vancouver, BC. Canada.

Poulos, S. 1981. The steady-state of deformation. Journal of Geotechnical Engineering American Society of Civil Engineering, **107**(5): 553-561.

Roscoe, K. H., Schofield, A. N. and Wroth, C. P. 1958. On yielding of soils. Geotechnique, **8**: 22-53.

Sasitharan, S., Robertson, P. K., Sego. D. C. and Morgenstern. N. R. 1993. Collapse behavior of sand. Canadian Geotechnical Journal. Accepted for publication in August 1993

Skopek, P. 1993. Personal communication.

Sladen, J. A., D'Hollander, R. D. and Krahn, J. 1985. The liquefaction of sands, a collapse surface approach. Canadian Geotechnical Journal, **22**: 564-578.

Sladen, J. A. and Handford, G. 1987. A potential systematic error in laboratory testing of very loose sands. Canadian Geotechnical Journal, **24**: 462-466.

Stroud. M. A. 1971. The behavior of sand at low stress levels in the simple shear apparatus. Ph.D. thesis. University of Cambridge. UK.

Symes, M. J. P. R., Gens, A. and Hight, D. W. 1984. Undrained anisotropy and principal stress rotation in saturated sand. Geotechnique, **34**: 11-27.

Tatsuoka, F. and Ishihara, K. 1974. Yielding of sand in triaxial compression. Soils and Foundation, **14**: 63-67.

Tokimatsu, K. and Hosaka, Y. (1986). Effects of sample disturbance on dynamic properties of sand. Soils and Foundation, **26:** 53-64.

Vesic, A. S. and Clough, G. W. 1968. Behavior of granular materials under high stresses. Journal of Soil Mechanics and Foundation Engineering American Society of Civil Engineering, **94**: 661-688.

Worth C. P. and Bassett. R. H. 1972. A stress-strain relationship for the shearing behavior of a sand. Geotechnique, **15**: 32-56.

Table 4.1 Void ratio and stress state for undrained triaxial compression tests.

Void ratio (e)	Isotropic consolidation stress p'_o (kPa)
0.809	384
0.805	550
0.804	350
0.793	348
0.793	475
0.791	433
0.758	1470

Table 4.2 State boundary constants for various sands

Sand	Source	Mineralogy	emax	emin	Gs	M	s		λ	Γ	
							State boundary	Collapse surface			
Ottawa (C109)	present study	quartz (rounded to subrounded)	0.820	0.500	2.66	1.19	0.80	0.51	0.0168	0.864	
Erksak	Been et al (1991)	73 % quartz 22 % feldspar (rounded to subrounded)	0.753	0.527	2.66	1.24	0.97	0.70	0.0133 0.1346	0.820 1.167	p'ss < 1000 kPa p'ss > 1000 kPa
Toyoura	Ishihara (1992) and Tokimatsu et al (1986)	75 % quartz 25 % feldspar (rounded to subrounded)	0.973	0.635	2.64	1.24	0.93	0.58	0.0043 0.0283 0.1210	0.938 1.048 1.677	p'ss < 100 kPa 100 kPa < p'ss < 1000 kPa p'ss > 1100 kPa
Lornex	Castro et al (1982)	quartz (angular)	1.080	0.680	2.68	1.42	1.36	0.83	0.0220 0.1470	1.100 1.762	p'ss < 200 kPa p'ss > 200 kPa
Brenda	Klohn Leonoff Report (January 18, 1984)	85 % quartz 15 % mica	1.060	0.688	2.70	1.46	1.17	0.73	0.0420 0.1087	1.112 1.492	p'ss < 200 kPa p'ss > 200 kPa
Syncrude	Sladen and Hanford (1987)	95 % quartz	0.930	0.550	_	1.19	0.64	0.50	0.0170	0.847	
Nerlerk	Sladen et al (1985)	_	0.890	0.660	_	1.20	0.89	0.62	0.0145	0.885	
Leight Buzzar	Sladen et al (1985)	quartz	0.750	0.580	_	1.19	0.73	0.54	0.0347	1.000	

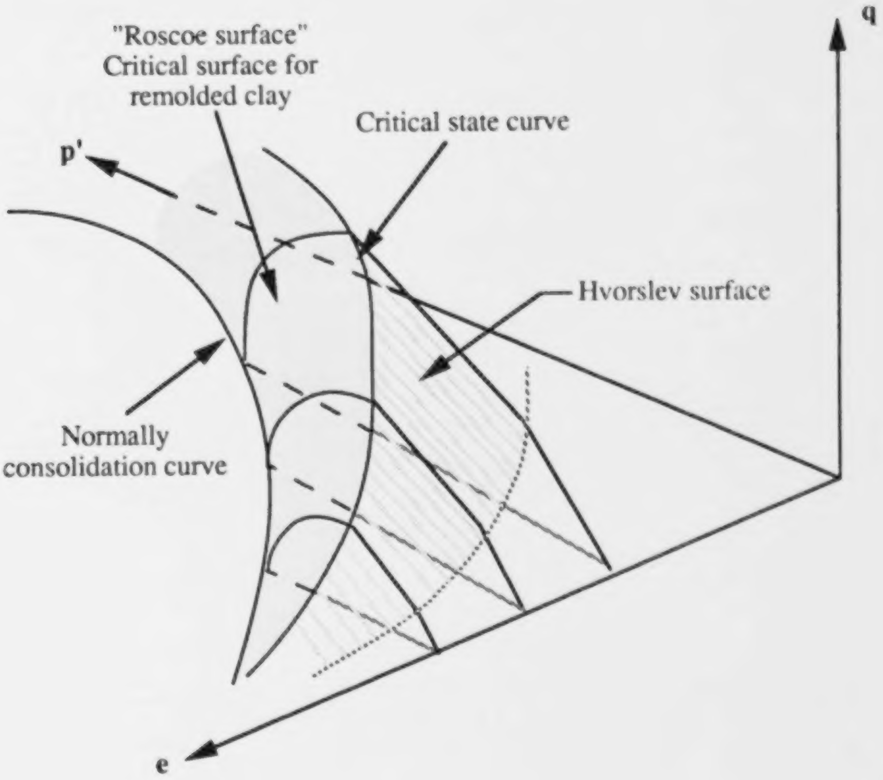

Figure 4.1 State boundary surface for remolded clay.

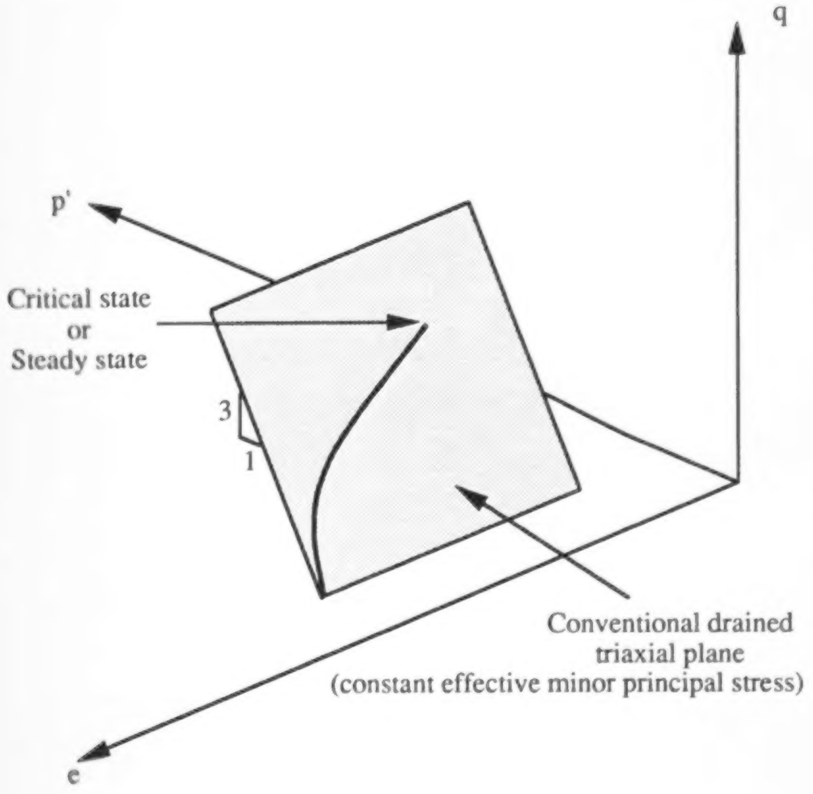

Figure 4.2 A schematic of a conventional drained triaxial compression stress path starting from an isotropic stress state.

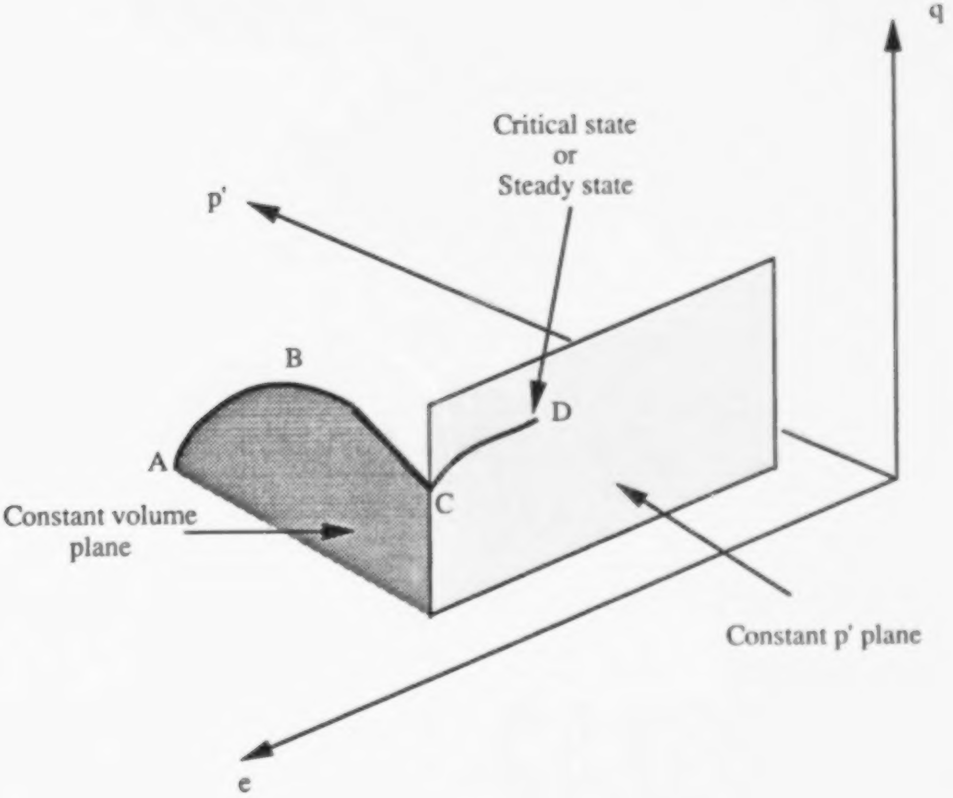

Figure 4.3 A schematic of the drained constant effective mean normal stress path from the post peak portion of an undrained stress path.

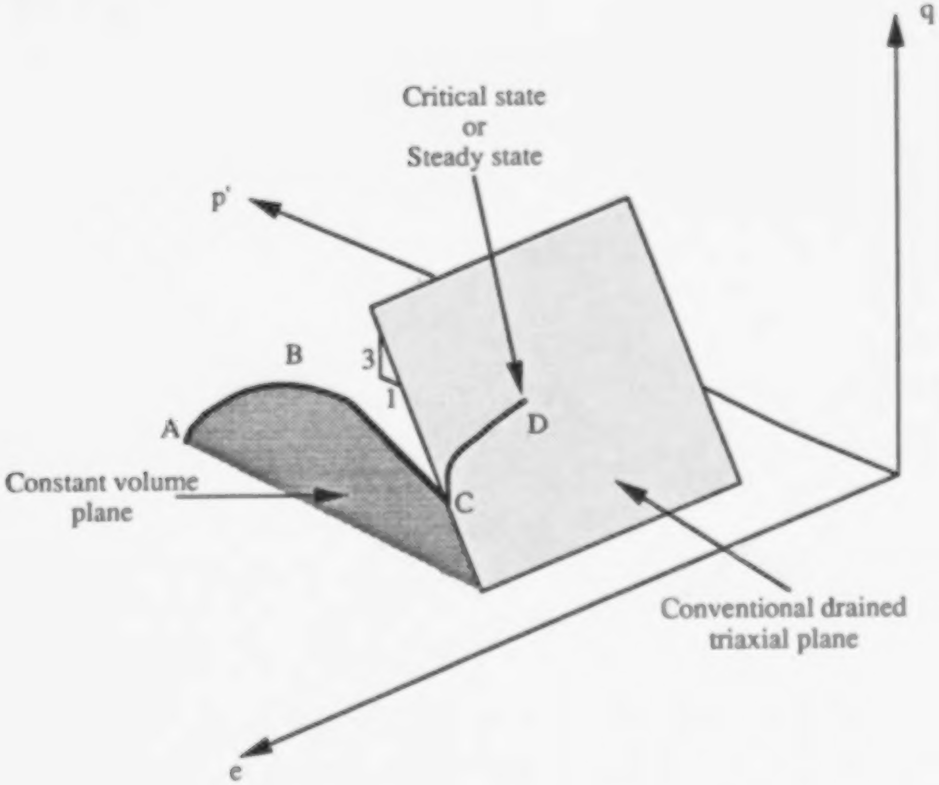

Figure 4.4 A schematic of the drained constant effective minor principal stress path from the post peak portion of an undrained stress path.

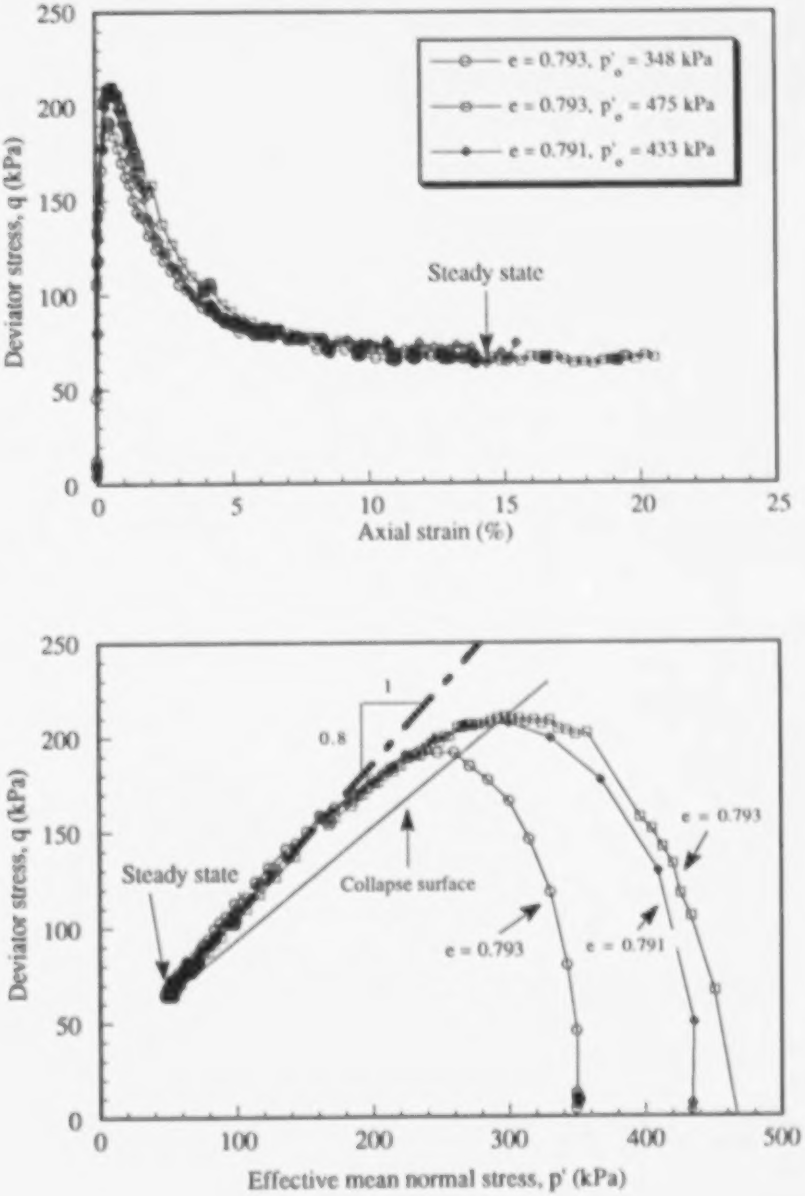

Figure 4.5 The deviator stress-axial strain response and resulting stress paths for themonotonic undrained triaxial compression test on samples consolidated to an identical void ratio of 0.793.

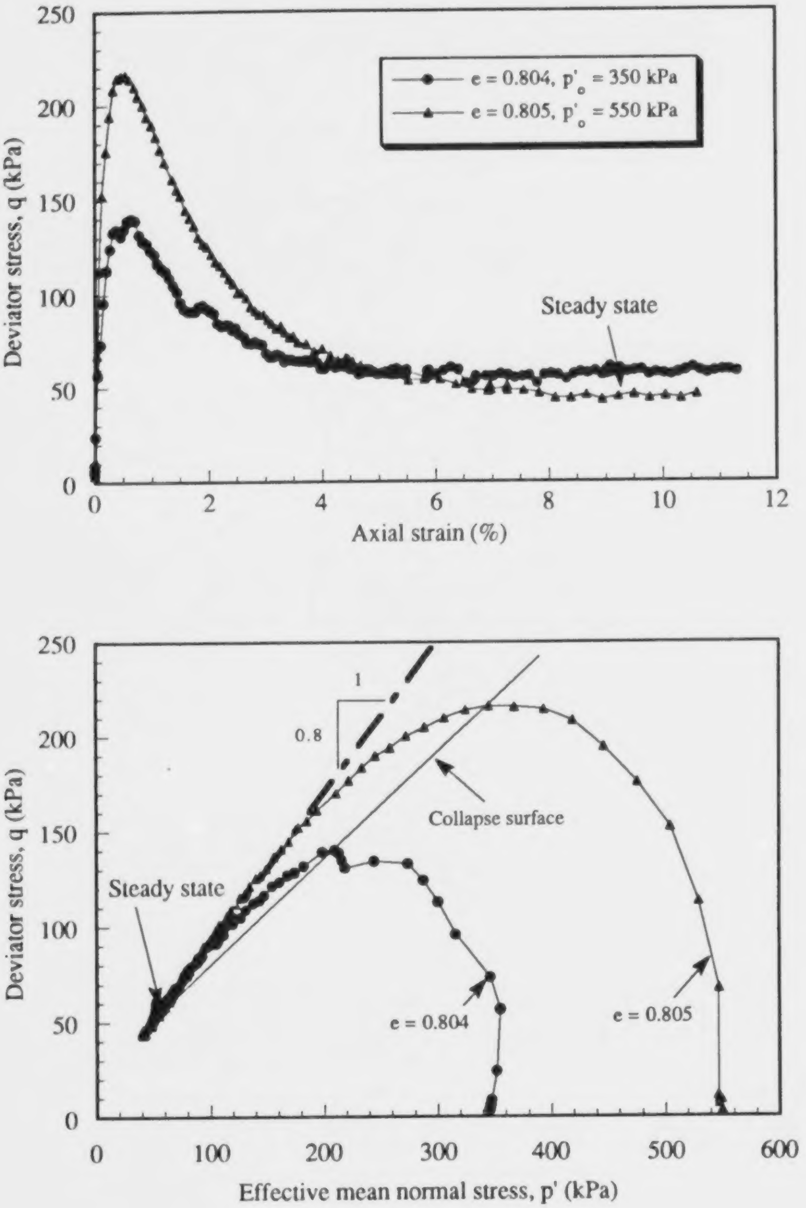

Figure 4.6 The deviator stress- axial strain response and resulting stress path for the monotonic undrained triaxial compression test on samples consolidated to an identical void ratio of 0.803.

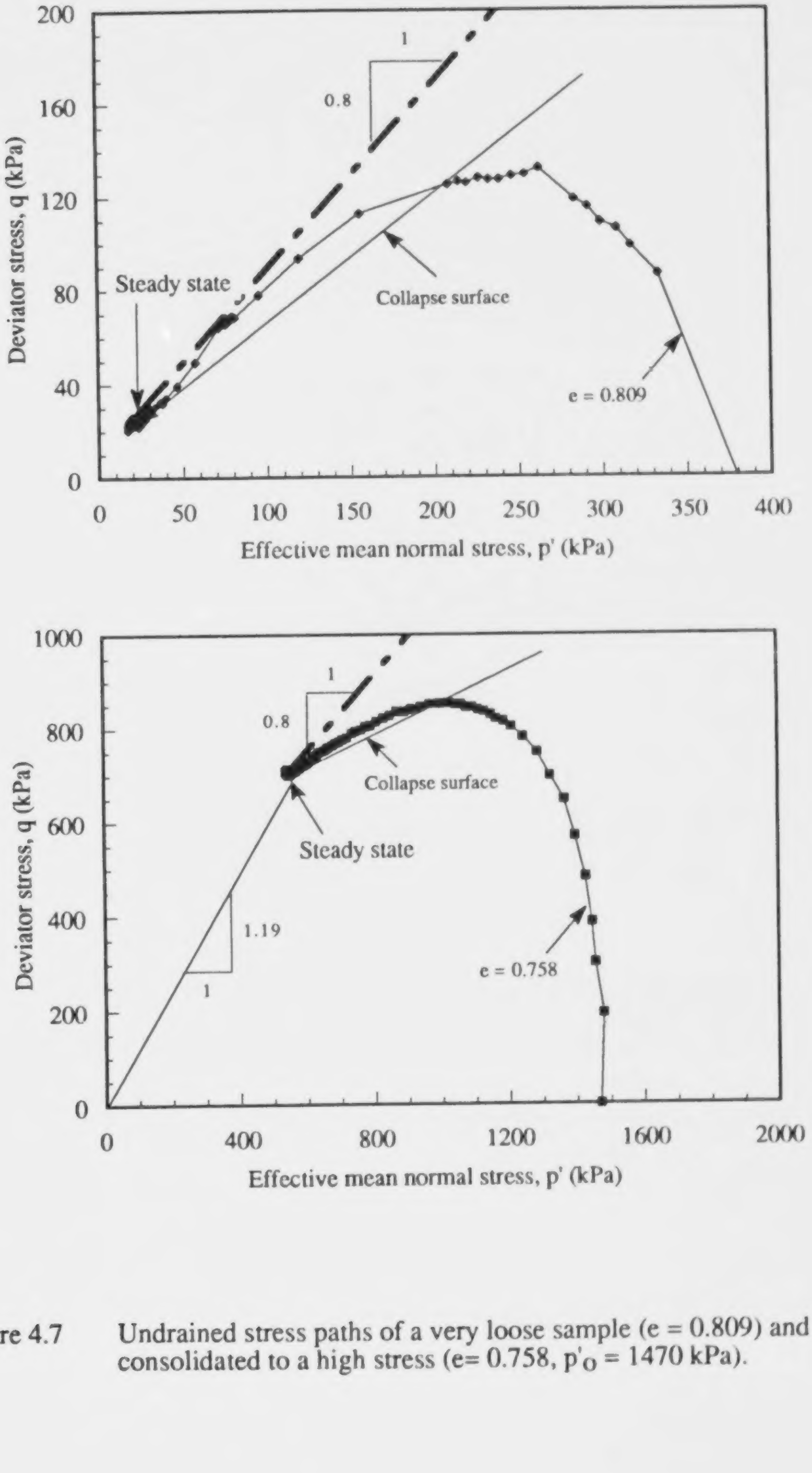

Figure 4.7 Undrained stress paths of a very loose sample (e = 0.809) and a sample consolidated to a high stress (e= 0.758, $p'_o = 1470$ kPa).

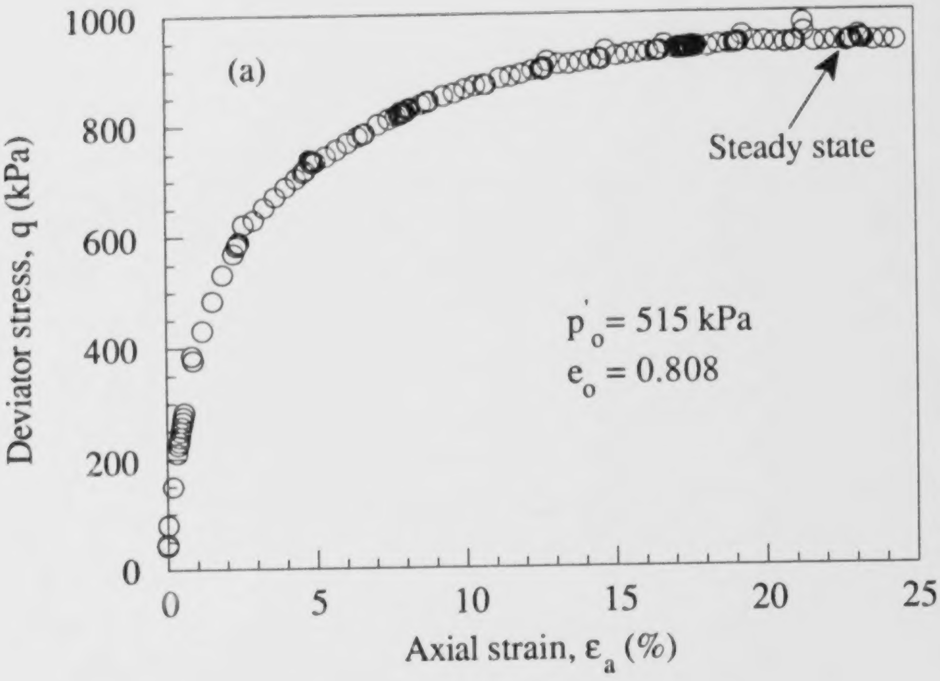

Figure 4.8(a) The deviator stress- axial strain behavior for the monotonic drained conventional triaxial compression test on a sample consolidated to an isotropic stress of 515 kPa and void ratio of 0.808.

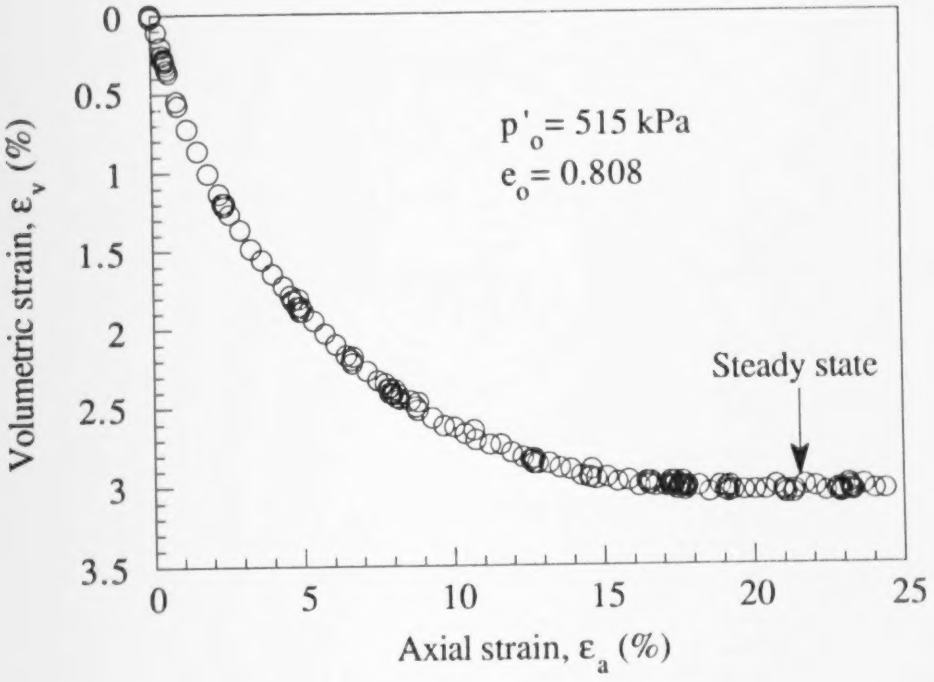

Figure 4.8(b) The volumetric strain- axial strain behavior for the monotonic drained conventional triaxial compression test on a sample consolidated to an isotropic stress of 515 kPa and void ratio of 0.808.

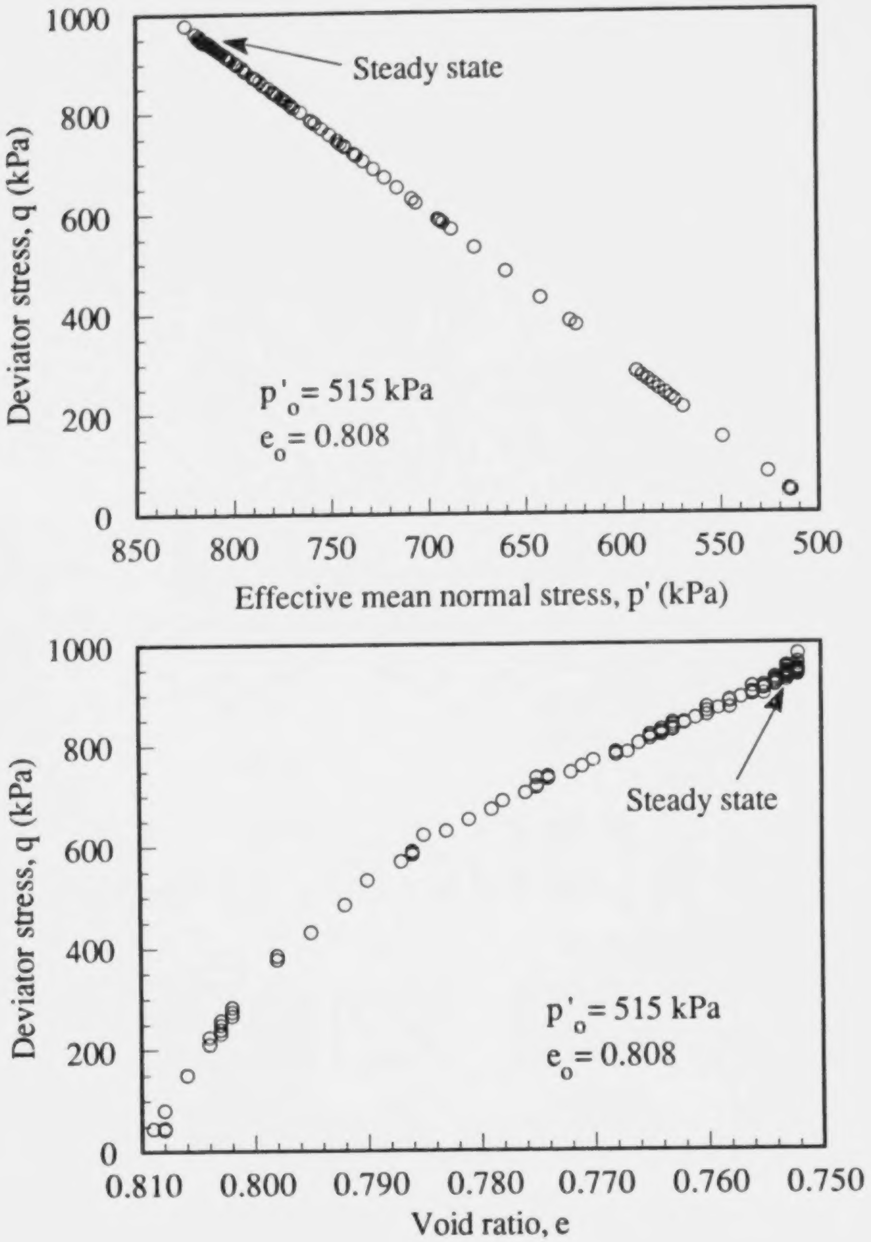

Figure 4.9 Resulting stress path for the monotonic drained conventional triaxial compression test on a sample consolidated to an isotropic stress of 515 kPa and void ratio of 0.808.

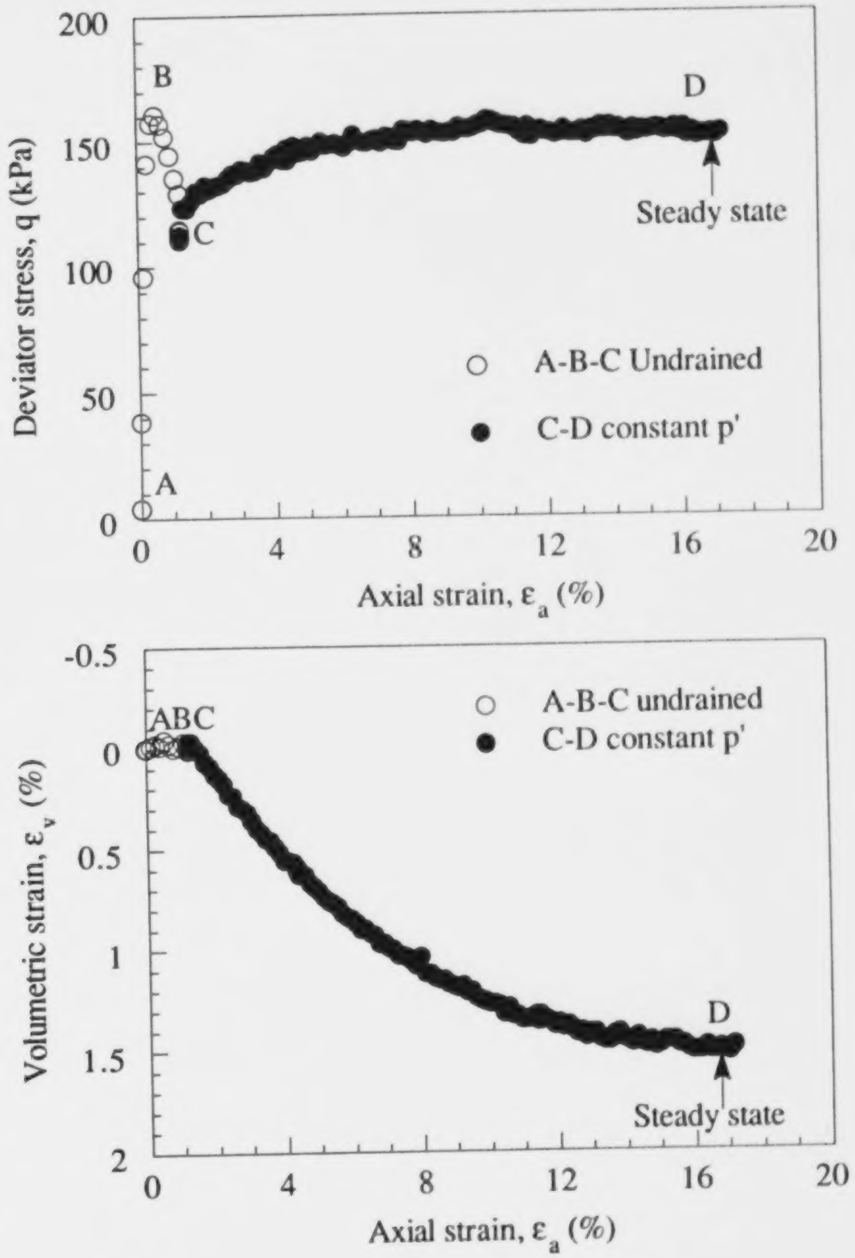

Figure 4.10 The stress-strain behavior for the monotonic drained triaxial compression constant effective mean normal stress test performed from the post peak portion of an undrained stress path.

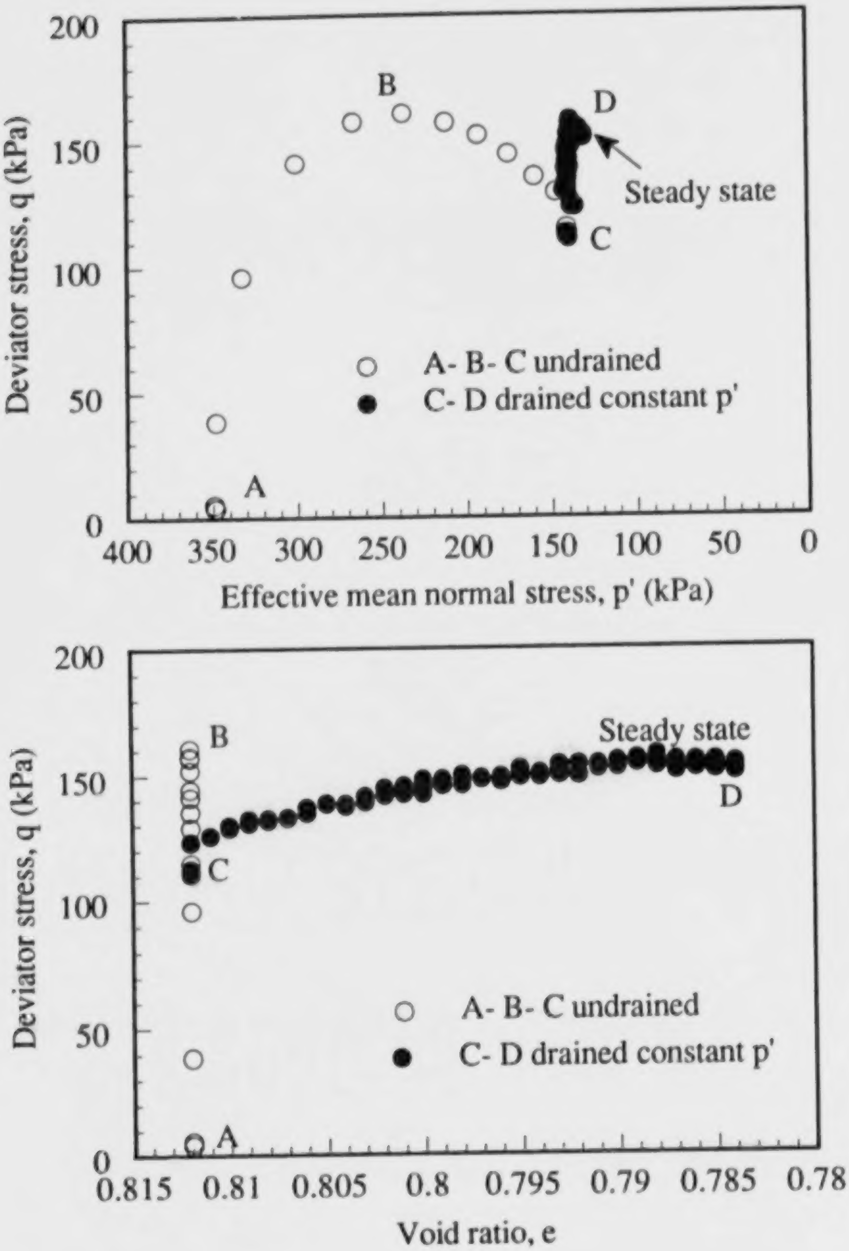

Figure 4.11 Resulting stress path for the monotonic drained triaxial compression constant effective mean normal stress test performed from the post peak portion of an undrained stress path.

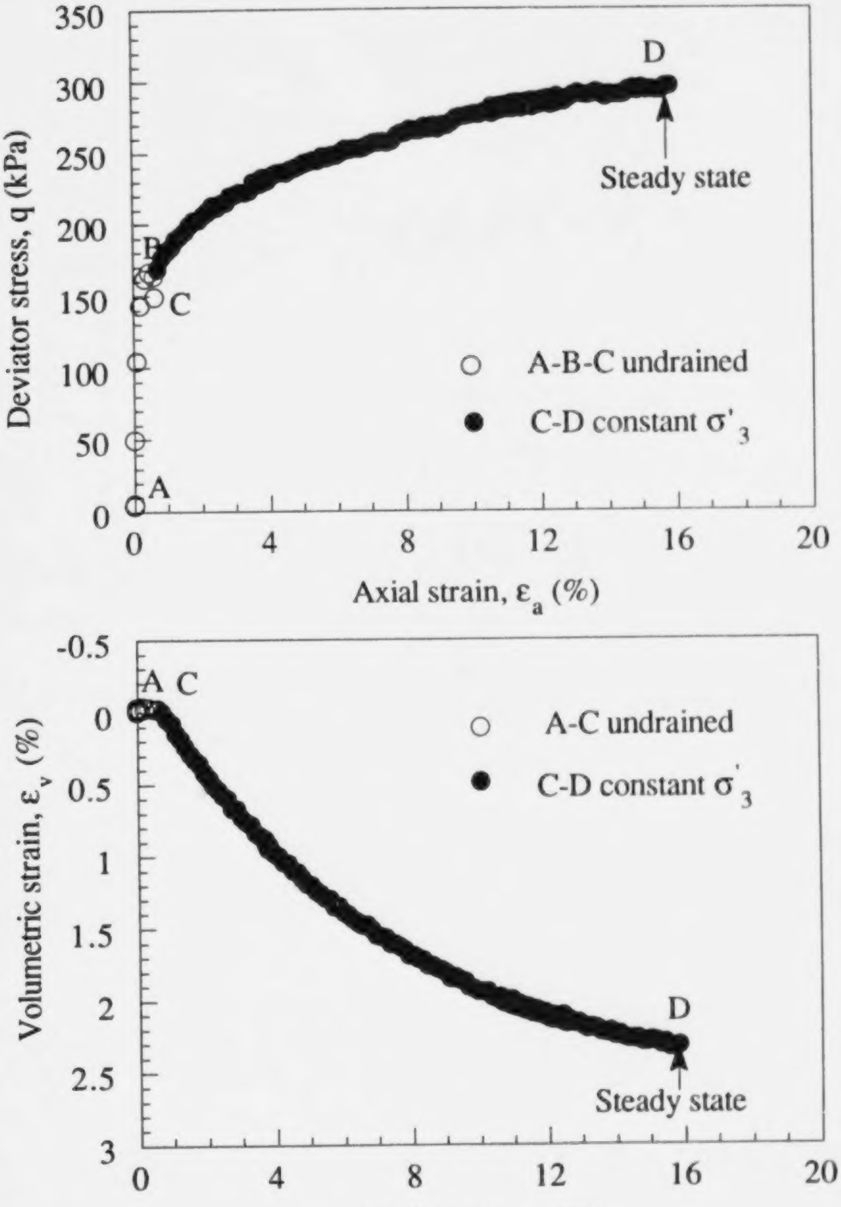

Figure 4.12 The stress-strain behavior for the monotonic drained conventional triaxial compression test performed from the post peak portion of an undrained stress path.

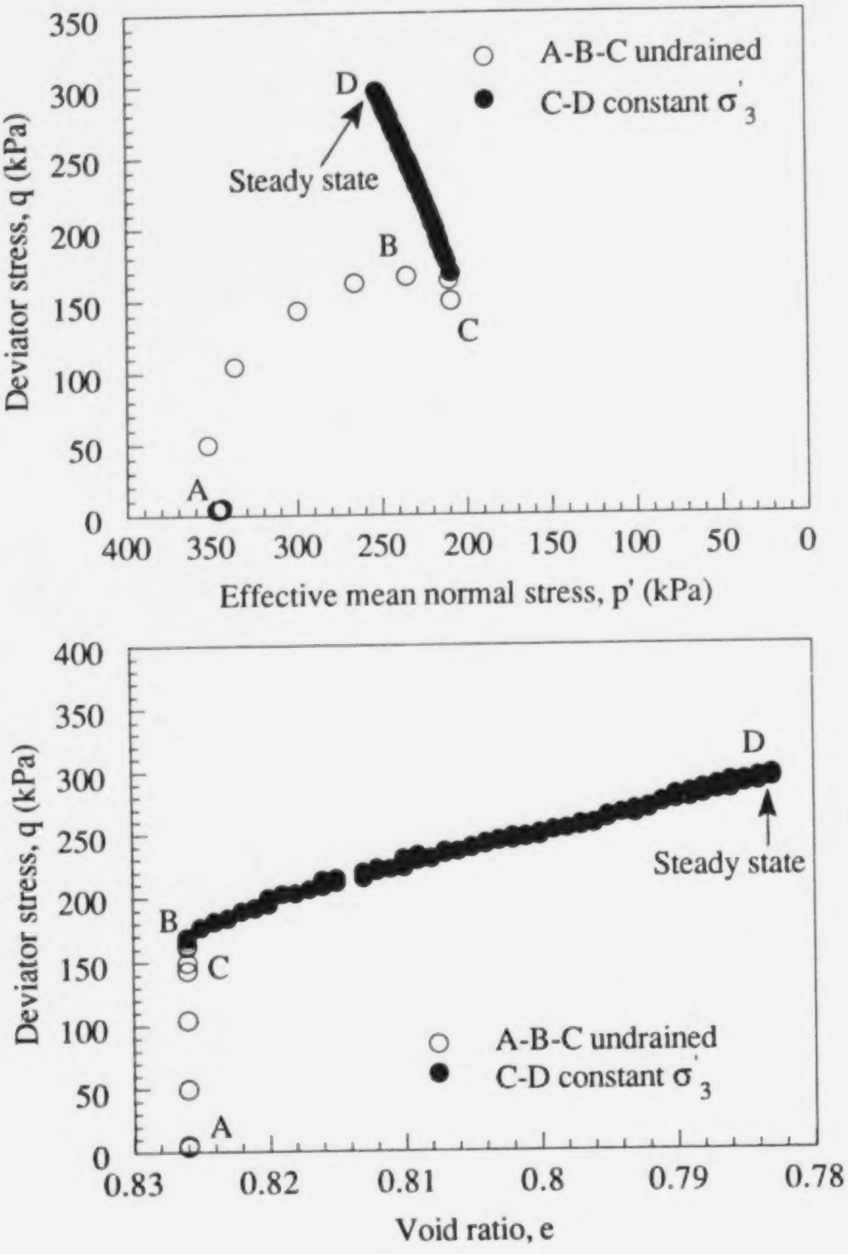

Figure 4.13 Resulting stress path for the monotonic drained conventional triaxial compression test performed from the post peak portion of an undrained stress path.

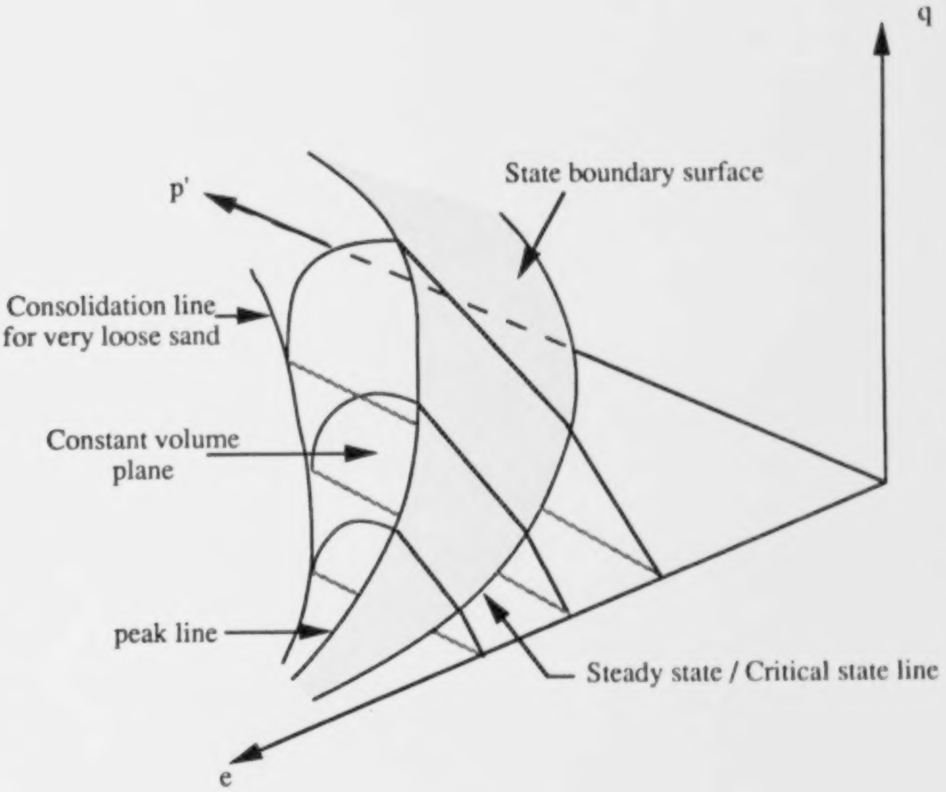

Figure 4.14 A schematic of state boundary surface for very loose sand.

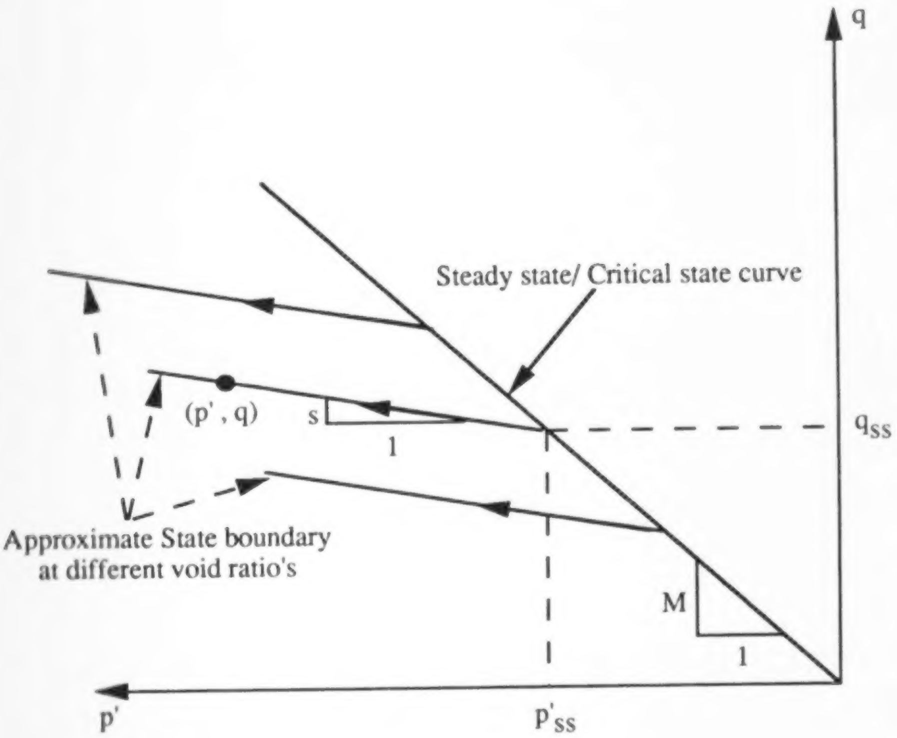
q
Steady state/ Critical state curve
(p' , q)
s
1
q_{ss}
Approximate State boundary
at different void ratio's
M
1
p'
p'_{ss}

Figure 4.15 Projection of the state boundary surface in deviator stress-effective mean normal stress space.

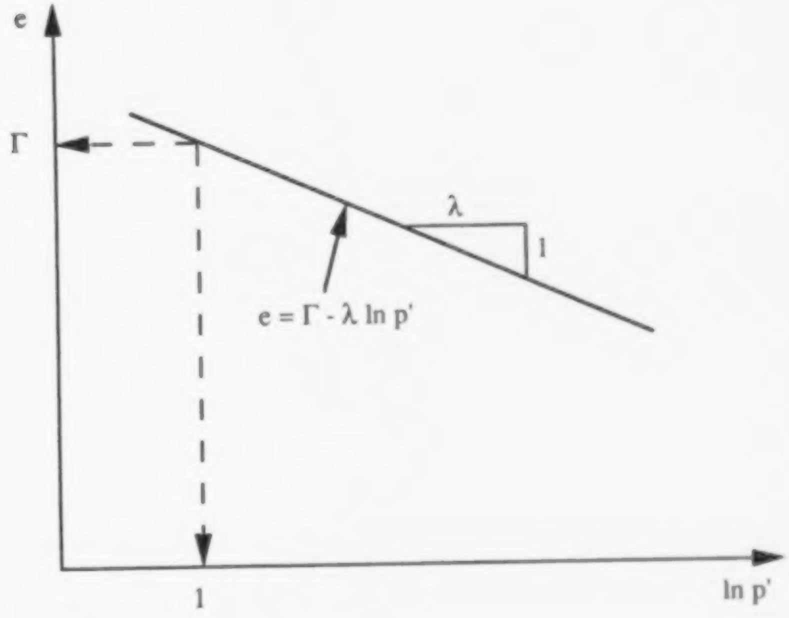

Figure 4.16 Projection of the steady state curve in void ratio-effective mean normal stress space.

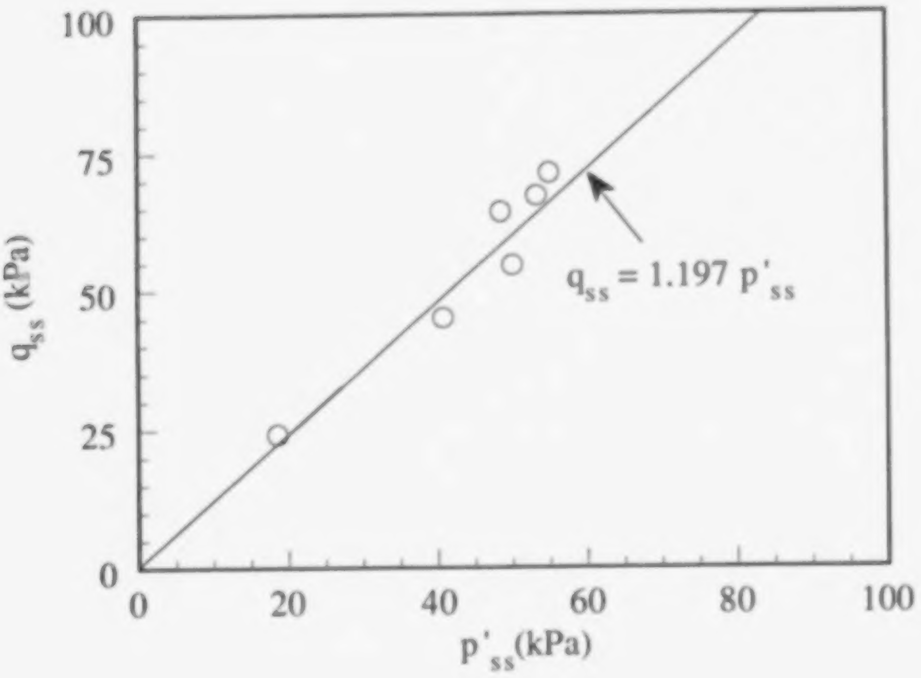

Figure 4.17 Steady state curve for loose Ottawa sand in deviator stress-effective mean normal stress space.

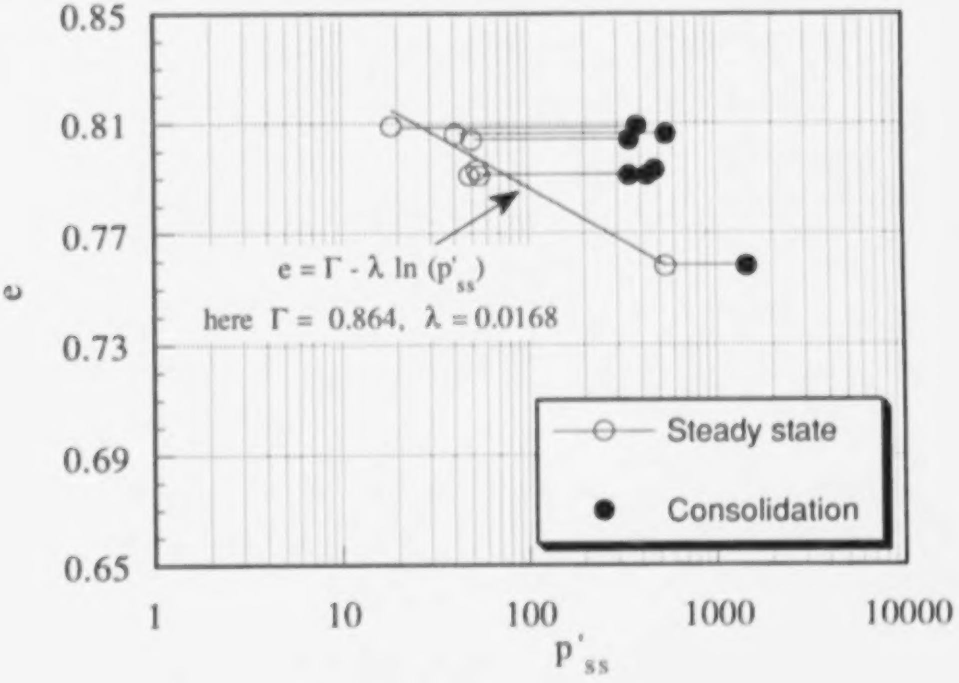

Figure 4.18 Steady state curve for loose Ottawa sand in void ratio-effective mean normal stress space.

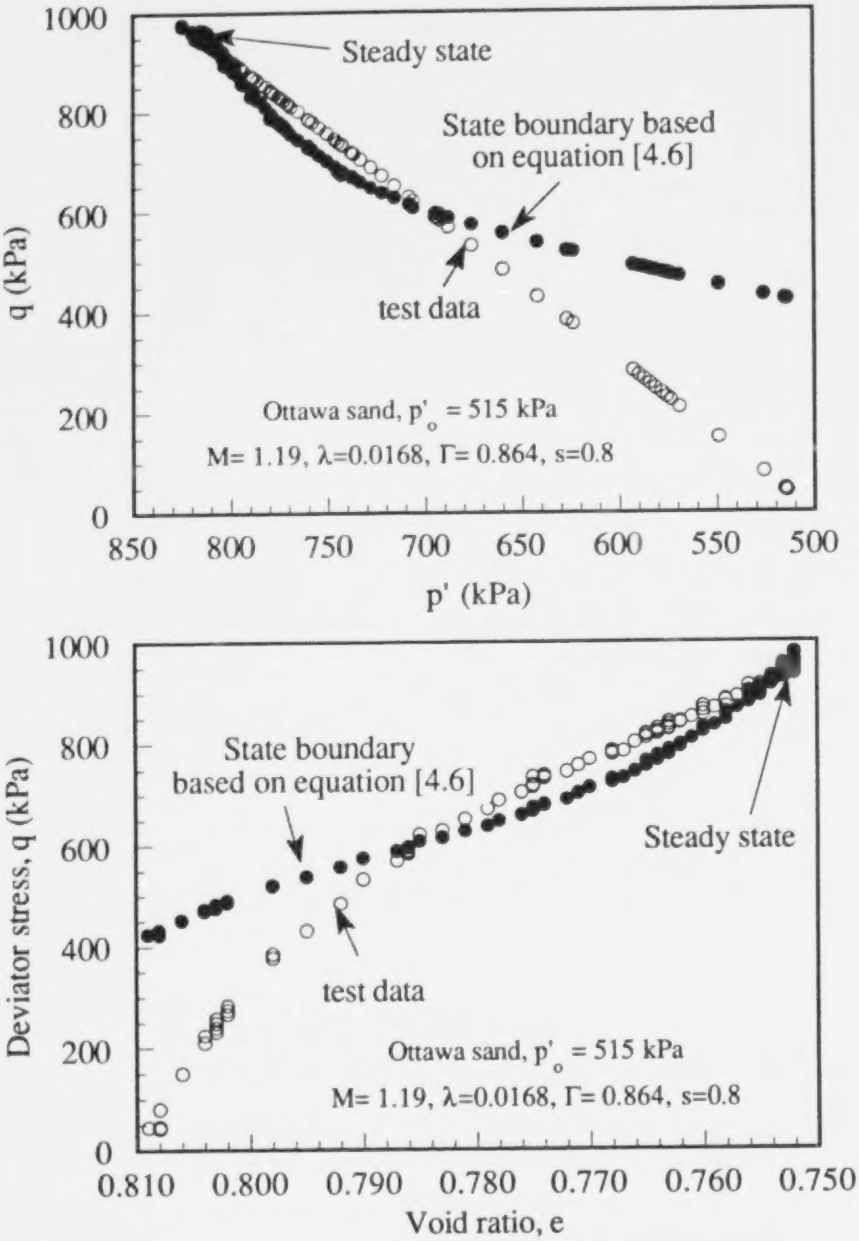

Figure 4.19 Comparison of the conventional isotropically consolidated drained triaxial compression stress path with the state boundary defined by equation [4.6] for Ottawa sand.

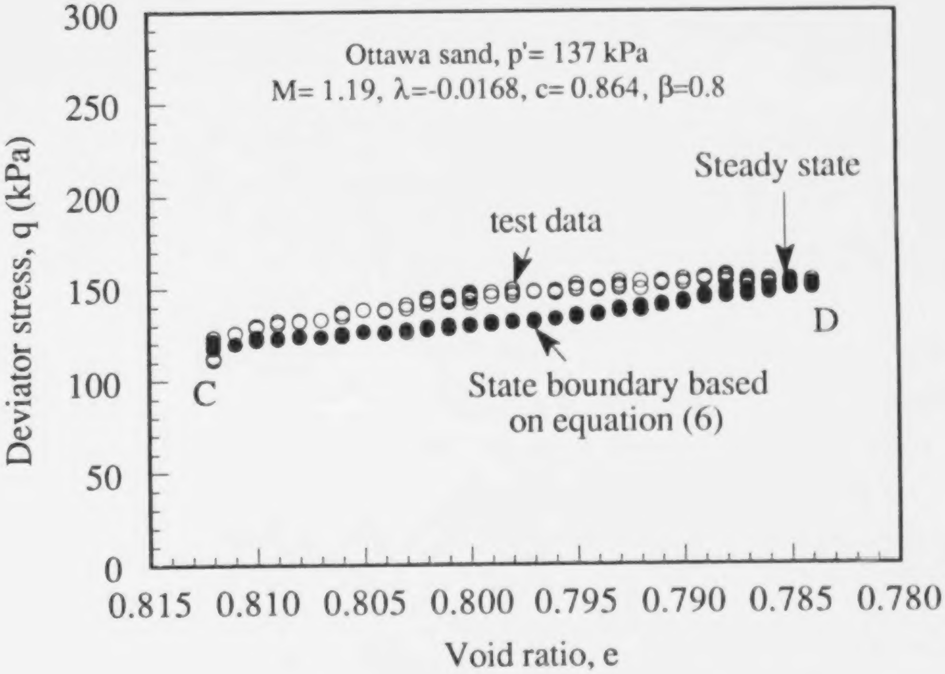

Figure 4.20 Comparison of constant effective mean normal stress test performed from the post peak portion of an undrained stress path with the state boundary defined by equation [4.6] for Ottawa sand.

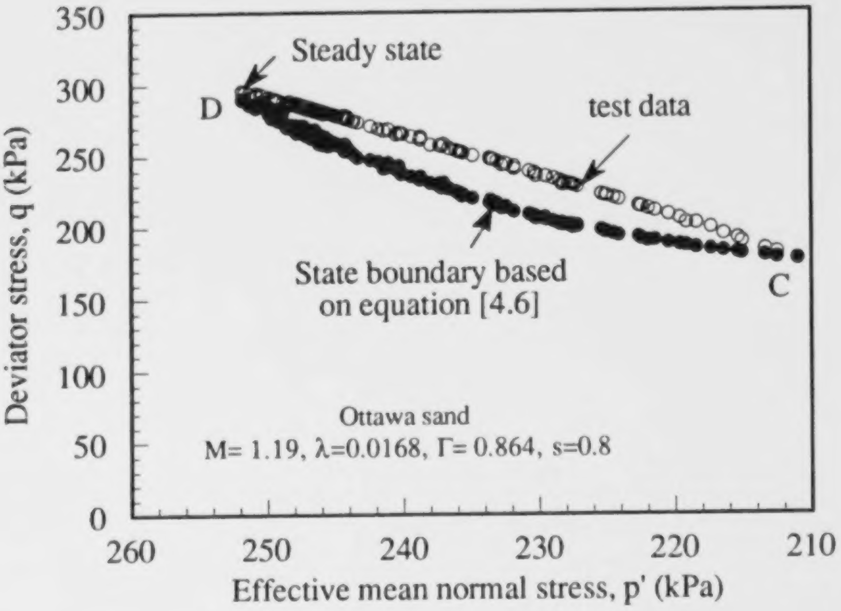

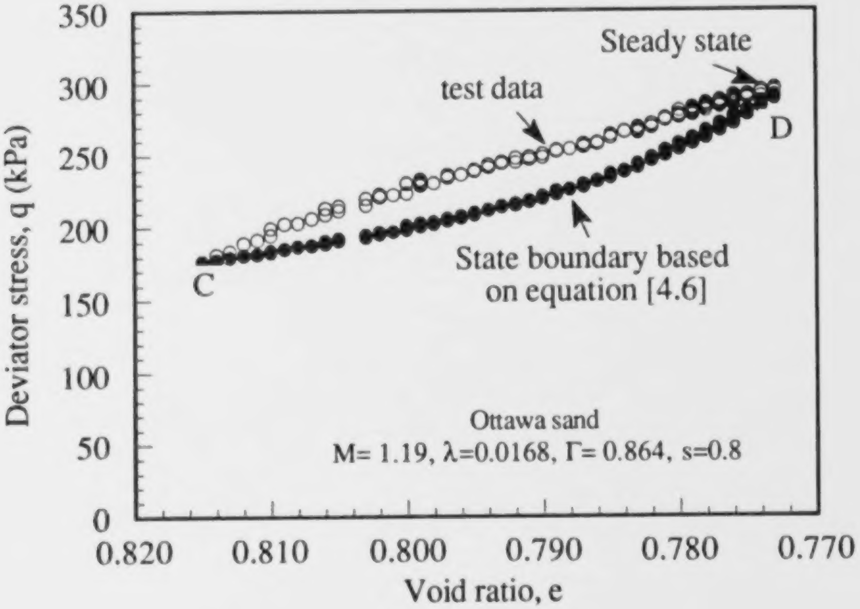

Figure 4.21 Comparison of conventional triaxial compression test performed from the post peak portion of an undrained stress path with the state boundary defined by equation [4.6] for Ottawa sand.

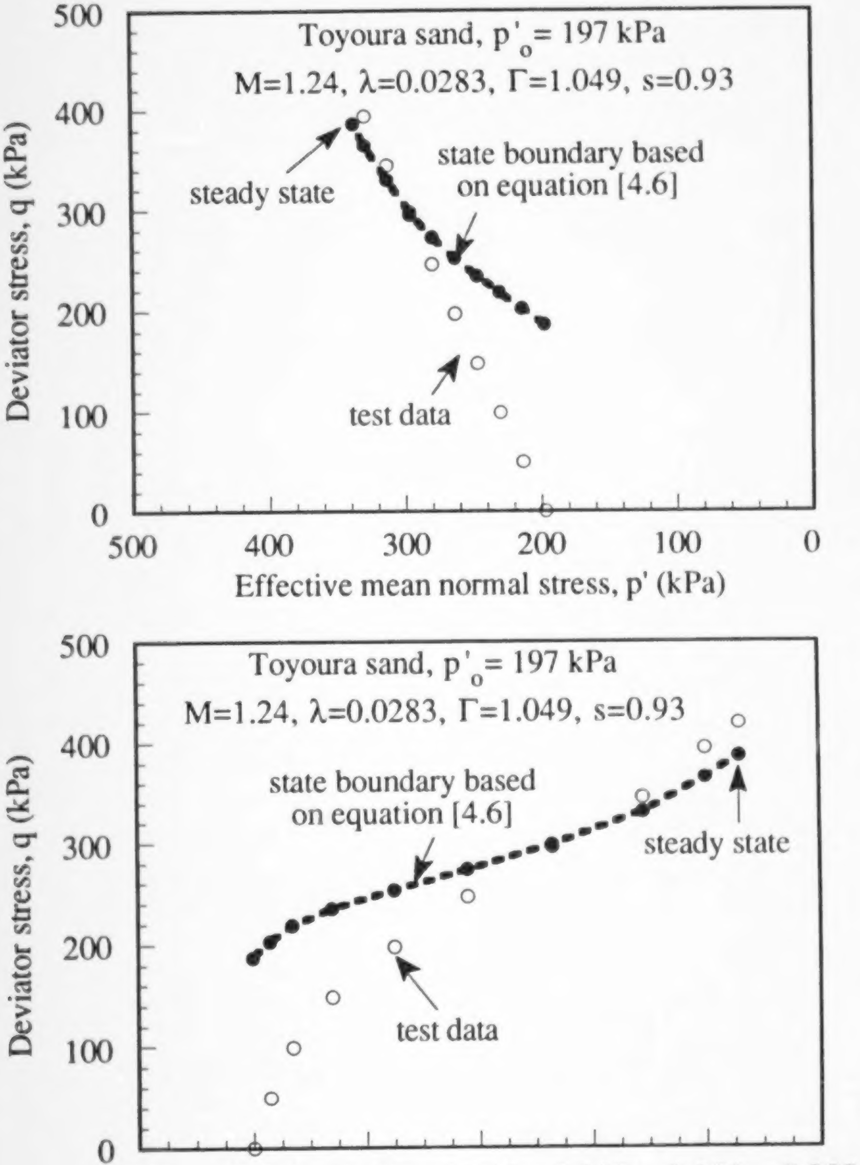

Figure 4.22 Comparison of the conventional isotropically consolidated drained triaxial compression stress path with the state boundary defined by equation [4.6] for Toyoura sand (Consolidation stress 197 kPa).

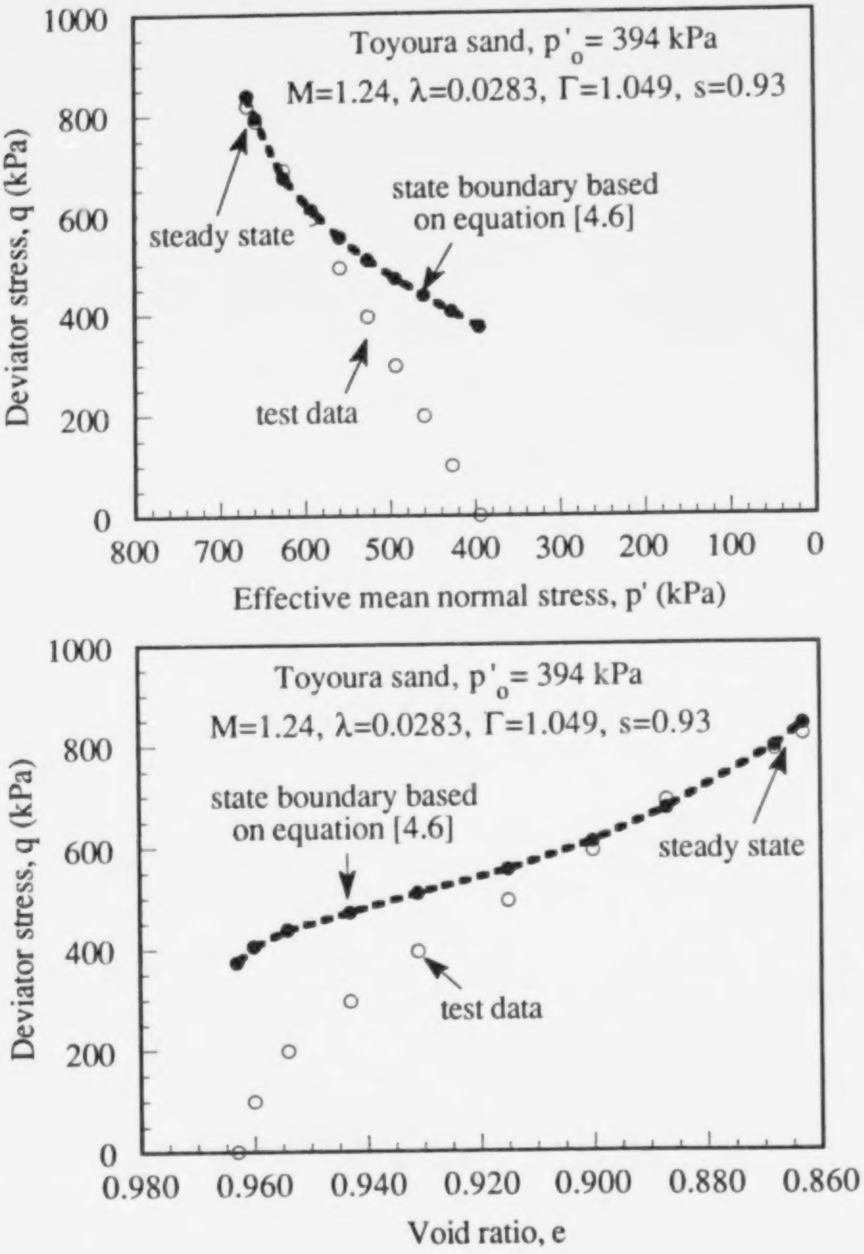

Figure 4.23 Comparison of the conventional isotropically consolidated drained triaxial compression stress path with the state boundary defined by equation [4.6] for Toyoura sand (Consolidation stress 394 kPa).

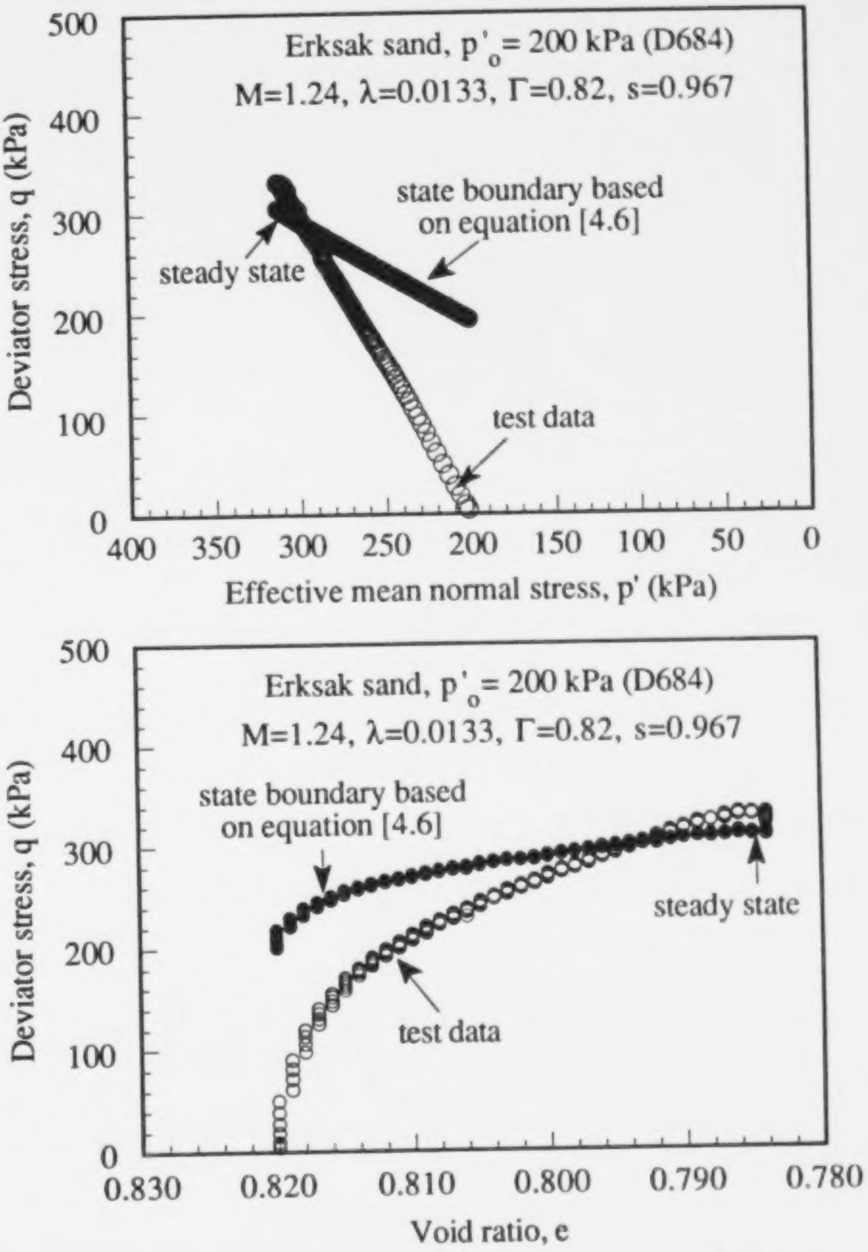

Figure 4.24 Comparison of the conventional isotropically consolidated drained triaxial compression stress path with the state boundary defined by equation [4.6] for Erksak sand (Consolidation stress 200 kPa, void ratio 0.820).

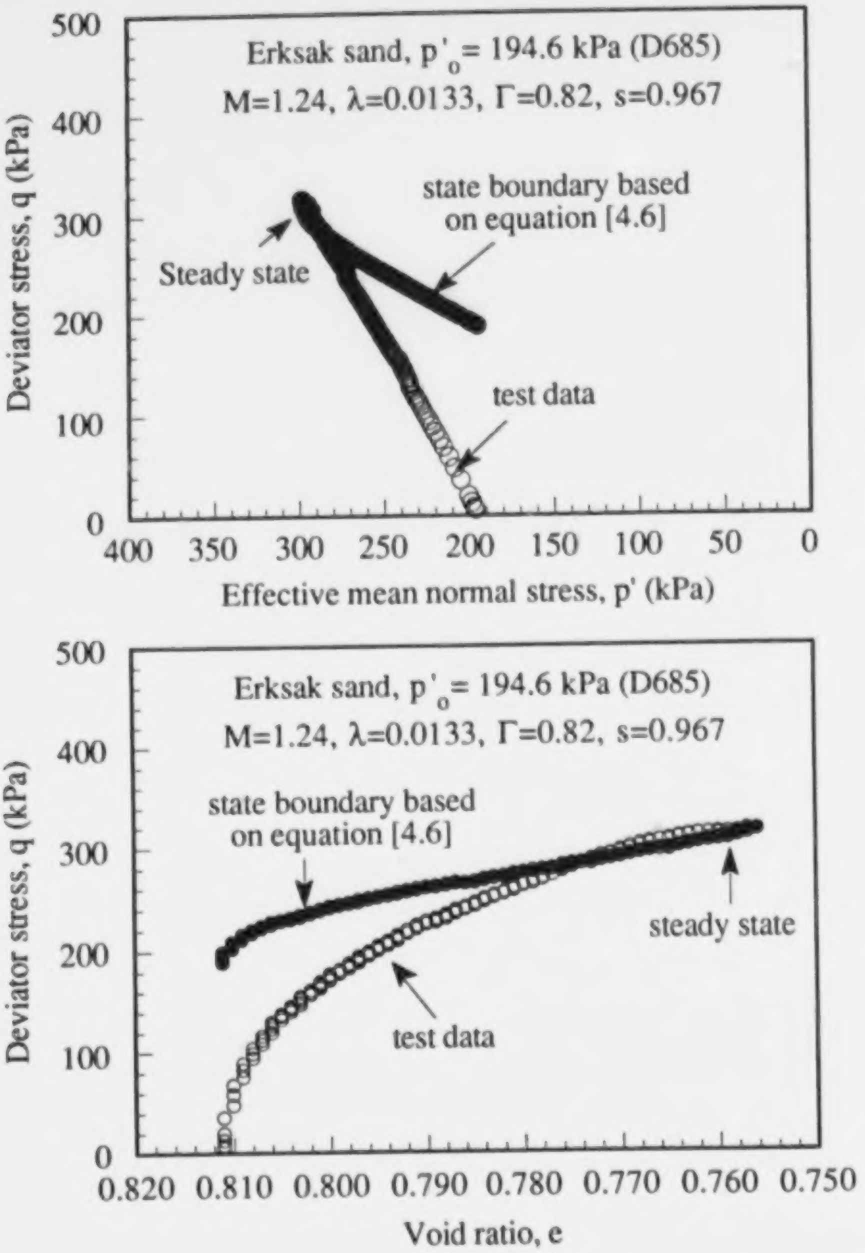

Figure 4.25 Comparison of the conventional isotropically consolidated drained triaxial compression stress path with the state boundary defined by equation [4.6] for Erksak sand (Consolidation stress 194 kPa, void ratio 0.815).

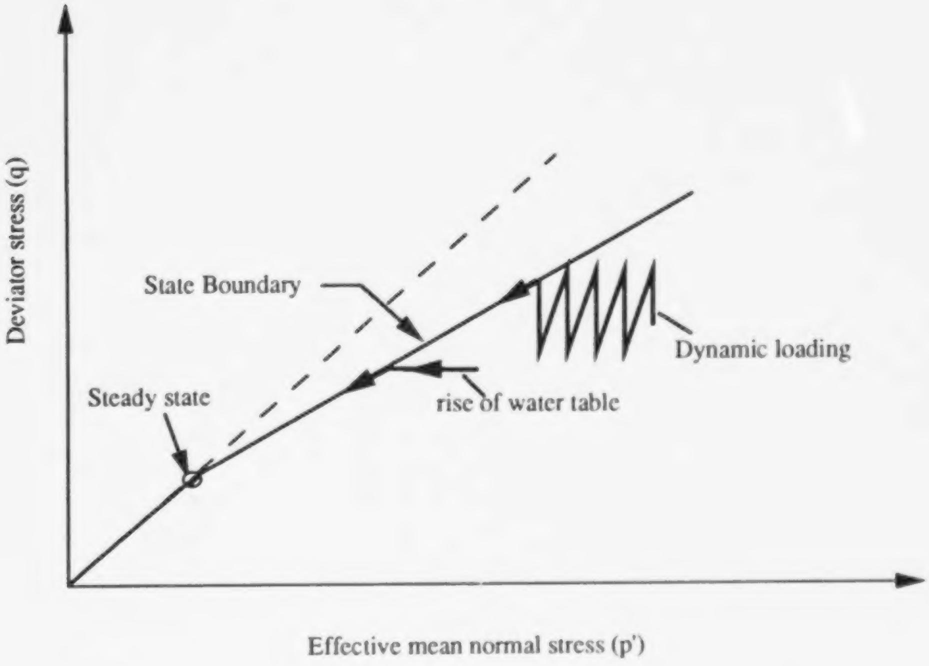

Figure 4.26 Schematic of two stress paths that can trigger collapse.

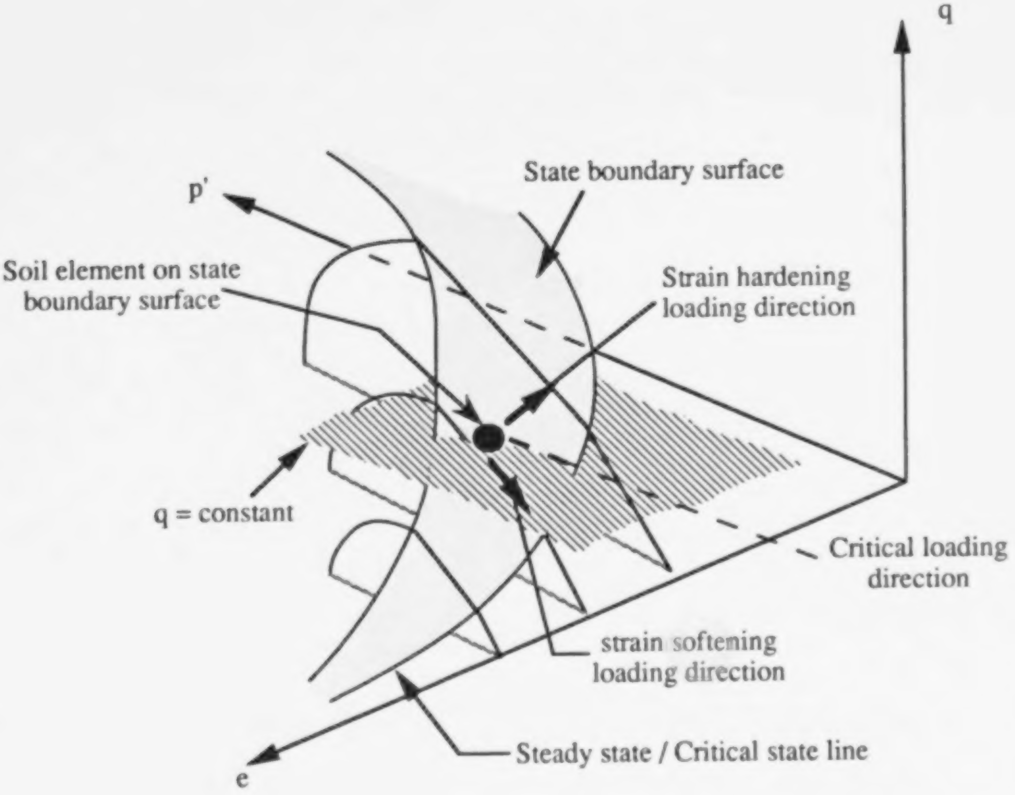
q
p'
State boundary surface
Soil element on state boundary surface
Strain hardening loading direction
q = constant
Critical loading direction
strain softening loading direction
Steady state / Critical state line
e

Figure 4.27 An element of sand with stress state on the state boundary.

CHAPTER 5

SHEAR WAVE VELOCITY TO EVALUATE FLOW LIQUEFACTION[*]

INTRODUCTION

During monotonic undrained loading a loose sand can reach a peak resistance and then rapidly strain soften to a constant resistance at which the effective stress state remains constant. Castro (1969) termed this ultimate constant state as the steady state and showed that it represents a state in the void ratio-effective mean normal stress-deviator stress space. If the gravitational shear stresses are larger than the ultimate strength at steady state, large flow deformations can occur. Castro (1969) defined this flow deformation as liquefaction. Been *et al*. (1991) showed that the ultimate steady state achieved during monotonic undrained loading is also a critical state implying that steady state is independent of the stress path followed, i.e., steady state is unique for a void ratio regardless of whether it was reached via drained or undrained loading.

---

[*] A version of this chapter has been submitted for publication: Sasitharan, S., Robertson, P.K. and Sego, D.C. 1993. Shear wave velocity to evaluate flow liquefaction. Journal of Geotechnical Engineering American Society of Civil Engineering.

Roscoe *et al.* (1958) and Been and Jefferies (1985) showed that large strain behavior of a soil can be expressed in terms of their initial state relative to the steady/critical state at the same stress level (see Fig. 5.1). Sands with an initial state above the steady/critical state would undergo a net contraction when sheared to the critical state. If the initial state of a sand lies below the critical state then a net dilation occurs when sheared to the critical state. Therefore, the initial state defined by the void ratio and mean normal stress, can be used to identify the large strain behavior. Hence, the state parameter, which uniquely relates the effect of void ratio and mean normal stress, can be used to describe the state of a sand (Been and Jefferies, 1985). Here the state parameter is defined as the difference between the current void ratio and the steady state void ratio at the same stress level, i.e., negative or positive state parameter would mean a dilative or contractive large strain loading response, respectively. In chapter 3 it was shown that a state boundary can be defined for sand that shows a collapsible, contractive behavior at large strains.

In practice, the generic term liquefaction is used to describe different mechanisms. Seed *et al.* (1983), using the results of extensive cyclic triaxial testing, defined liquefaction as the condition of zero effective confining stress due to cyclic loading with shear stress reversal. At zero effective stress a cohesionless soil has very little stiffness and large deformation can develop during the cyclic loading. In Japan (Ishihara, 1993) it is common to define liquefaction in terms of the magnitude of cyclic stress ratio required to produce a given level of strain, typically 5% double amplitude of the axial strain. Robertson (1993) suggested that liquefaction should be defined as either gravitational (flow) liquefaction or seismic liquefaction.

Gravitational (flow) liquefaction follows closely the definition of liquefaction suggested by Castro (1969). Flow liquefaction requires strain softening response in undrained shear loading and *in-situ* gravitational shear stresses greater than the ultimate critical/steady state strength. Seismic liquefaction results from cyclic loading and can be further subdivided into either cyclic liquefaction or cyclic mobility. Cyclic liquefaction occurs during undrained cyclic loading where shear stress reversal or zero shear stress can develop (i.e., where *in-situ* gravitational shear stress is low compared to the cyclic shear stress). Cyclic liquefaction also requires that sufficient undrained cyclic loading occurs to allow the effective confining stress to reach zero. At zero effective confining stress the soil has very little stiffness and large deformations can result even under very small gravitational shear stress. Cyclic mobility results when there is no shear stress reversal during undrained cyclic loading. Hence, the condition of zero effective stress does not develop and deformations tend to be smaller and eventually stabilize.

Figure 5.2 shows a flow chart suggested by Robertson (1993) for evaluating liquefaction potential (flow liquefaction, cyclic liquefaction and cyclic mobility). The first step is to evaluate the material characteristics in terms of strain softening and strain hardening response. If the soil is strain softening, flow liquefaction is possible if the soil can be triggered to collapse and if the gravitational shear stresses are larger than the ultimate steady state or residual strength. The trigger to cause collapse can be either monotonic or cyclic. Whether a slope or soil structure will slide or flow will depend on the amount of strain softening soil relative to the strain hardening soil within the structure and the brittleness of the strain softening soil. If the soil is strain hardening, flow liquefaction will not occur. However, cyclic liquefaction or cyclic mobility can occur due to cyclic (seismic) undrained loading.

The preferred method to evaluate the response of a soil to a given loading is to obtain high quality undisturbed samples and perform relevant laboratory testing following the appropriate stress path. However, this process is difficult in cohesionless soils such as sand. *In-situ* ground freezing has been recently used to successfully obtain high quality undisturbed samples of cohesionless soil (Yoshimi *et al.*, 1984; Hatanaka *et al.*, 1985; Yoshimi *et al.*, 1989; Sego *et al.*, 1993). However, the cost of these techniques is very high and is currently restricted to larger projects. For smaller projects and in the initial stages of large projects, *in-situ* testing such as the Standard Penetration Test (SPT) and the Cone Penetration Test (CPT) have been the most commonly used approaches to evaluate seismic liquefaction potential. Most of the existing methods to evaluate liquefaction potential from these *in-situ* tests are applicable to seismic liquefaction and are based on the cyclic stress ratio to trigger a given level of deformation (either cyclic liquefaction or cyclic mobility). Most methods are for level ground conditions and corrections are required for sloping ground (Seed *et al.*, 1983). In general, these methods have proven to be very good at predicting cyclic liquefaction for essentially level ground conditions (Kayen *et al.*, 1992). However, their application to predict the trigger of flow liquefaction in very loose sands for steeply sloping ground is uncertain. Robertson *et al.* (1992a) and Ishihara (1993) have suggested a range of values for penetration resistance from the SPT and CPT to evaluate if strain softening response and hence, the potential for flow liquefaction, is possible. Sladen and Hewitt (1989) also suggested a profile of CPT based on back analysis of several flow liquefaction failures of hydraulically placed sand used for construction of artificial islands in the Beaufort sea. Robertson *et al.* (1992a) also suggested values of normalized shear wave velocity to evaluate the *in-situ* state of cohesionless soils.

In the past, laboratory studies have shown that the shear wave velocity of a sand is controlled primarily by the confining stresses and void ratio. Hence, there is increasing interest in using the shear wave velocity to define the state (void ratio, confining stresses) of a soil, since the shear wave velocity can be measured both in the field and in the laboratory.

Based on resonant column test results, Hardin and Richart (1963) found that the shear wave velocity can be related to confining stress and void ratio by;

[5.1] $$V_s = (m_1 - m_2 e)(p')^{0.25}$$

where;

V_s = the shear wave velocity.

e = void ratio

p' = the effective mean normal stress

m_1 and m_2 = constants.

Hardin and Richart (1963) further suggested that m_1 and m_2 have values of approximately 111 and 51 when stress is measured in kPa and shear wave velocity is measured in m/s. However, the Hardin and Richart (opt. cit.) equation was based on observations made on isotropically consolidated sand. An alternative equation, called the individual stress method, was proposed by Roseler (1979) based on tests with cubic samples where stresses can be applied independently. His results suggested that individual stresses play an important role on the wave travel rather than the mean normal stress proposed by Hardin and Richart (1963). Hence, Roseler proposed that

[5.2] $$V_s = (m_1 - m_2 e)(\sigma'_a)^{ma}(\sigma'_p)^{mp}$$

where;

σ'_a = the effective stress in the direction of wave propagation

σ'_p = the effective stress in the direction of particle motion.

ma, mp, m1 and m2 = constants.

Yu and Richard (1984) and Stokoe *et al.* (1985) showed that the exponents ma, mp were equal with a value of 0.125. Further, for dense sands de Alba *et al.* (1984) found that the shear wave velocity is also influenced by the soil fabric created using different sample preparation methods. Here soil fabric refers to the micro structure of the sand that involves the orientation and the distribution of normal contacts between grains.

There have been several attempts in the past to correlate seismic liquefaction resistance to shear wave velocity (Bierschwale and Stokoe, 1984; Tokimatsu *et al.*, 1986; Tokimatsu and Uchida, 1990; Robertson *et al.*, 1992a and 1992b). Robertson *et al.* (1992a) used a normalized shear wave velocity given by;

[5.3] $$V_{s1} = V_s\left(\frac{P_a}{\sigma'_v}\right)^{0.25}$$

where

V_{s1} = the normalized shear wave velocity,
V_s = the shear wave velocity,
P_a = the reference pressure (usually 100 kPa),
σ'_v = the effective overburden pressure.

Based on cone penetration tests and field shear wave velocity measurements, Robertson *et al.* (1992a) suggested a critical value of the normalized shear wave velocity between 140 to 160 m/s that separates contractive strain softening response from dilative strain hardening behavior at large strains. However, evaluation of this critical value was limited to one site and did not fully incorporate the steady state concept.

Since the introduction of bender elements it is now possible to measure shear wave velocity in almost any laboratory testing apparatus. Hence, shear wave velocity and the large strain behavior of a sand can be measured for a given sample in a single test.

This paper presents results of an experimental study performed to evaluate whether shear wave velocity can be used to identify the behavior of a sand at large strain. It is shown that the shear wave velocity can be related to the effective confining stresses and void ratio regardless of soil fabric in a loose sand. Further, the shear wave velocity can be used to identify whether a given sand is contractant or dilatant at large strains.

TESTING APPARATUS

A modified Wykeham Farrance triaxial test apparatus described in chapter 3 was used throughout this study. Shear wave velocities were generated and received using bender elements (Shirley, 1978) in the triaxial sample. The bender elements, consisting of two thin plates of ceramic material rigidly bonded together, were installed at the top and bottom pedestal of the triaxial cell. Details are described in chapter 2. Hamdi and Taylor-Smith (1982) used bender elements to measure shear wave velocities in oedometer and triaxial apparatus. Dynik and Madshu (1985) evaluated and compared shear modulus obtained using the resonant column apparatus and using bender elements reporting excellent agreement between these methods. The introduction of bender elements facilitates shear wave velocity measurements in most laboratory testing apparatus.

A schematic layout of the shear wave velocity measuring system is shown in Figure 5.3. A pulse from the wave form generator provides the electrical pulse (± 15 V, 20 Hz) to the driving bender element and triggers the oscilloscope (Philips PM 3365A digital storage oscilloscope). The polarization of the ceramic material in each bender and the electrical connection is such that when a driving voltage is applied to the bender element, one plate elongates and the other shortens. Hence, one edge of the bender element protrudes into the specimen as a cantilever and deforms as shown on Figure 2.4. The surrounding soil particles move in the same direction as the tip of the bender element. This generates a shear wave that propagates vertically through the sample.

The bender element can also be used as a receiver. When the shear distortion reaches the receiving bender element embedded in the sample it creates a mechanical vibration, which causes one layer of the bender element to undergo extension while the other undergoes compression, hence, generating an electrical pulse that is displayed on the oscilloscope screen. The travel time of the shear wave through the sample is determined from the time lag of the pulse reaching the receiving bender element. Hence the shear wave velocity is calculated by

$$V_S = \frac{L}{t} \qquad [2.1]$$

where;

L = the travel length

t = the travel time.

Using this measuring system the change in shear wave velocities during consolidation and triaxial loading can be investigated for a given sample. All test variables were measured using electronic transducers which were also collected and stored on a microcomputer.

MATERIAL TESTED AND SAMPLE PREPARATION

Ottawa (C 109) sand obtained from Ottawa, Illinois was used in this study. Ottawa sand is a uniform sand with a mean grain size (D_{50}) of 0.35 mm and comprised primarily of quartz with a specific gravity of 2.67. The maximum and minimum void ratios of the sand determined using the ASTM method D2049 are 0.82 and 0.50 respectively.

Uniform Ottawa sand samples were prepared using water pluviation technique described by Negussey (1984) and Sasitharan (1989). However, it was observed that very loose sand samples could not be prepared by water pluviation. This is consistence with the observation made by various other researchers regarding water pluviated sand samples (e.g., Han and Vardoulakis, 1991). Hence, very loose uniform sand samples were also prepared using the moist tamping technique described in chapter 3.

TESTING PROGRAM

Ottawa sand samples prepared very loose (e = 0.82 - 0.83), medium dense (e = 0.66 - 0.68) and dense (e = 0.57 - 0.59) were initially consolidated to an isotropic consolidation stress of 50 kPa. Then the samples were isotropically consolidated by 50 or 100 kPa stress increments depending on the final consolidation stress. During consolidation dead loads were added to the top of the sample (Fig. 5.3) to compensate for the uplift force acting on the loading ram. This ensured that the samples were consolidated isotropically and that the bender element maintained contact with the sample. After applying a stress increment, the sample was allowed to fully consolidate. For Ottawa sand samples it was observed that the consolidation was complete within a minute from the application of the consolidation stress increment. However, a constant time interval of approximately five minutes was allowed before the shear wave velocity was measured across the sample at this consolidation stress. Then the next stress increment was applied. A similar test procedure was followed for each stress increment until the required consolidation stress or void ratio for triaxial compression loading was achieved. Then the samples were sheared in triaxial compression under drained or undrained loading condition. The behavior of the very loose Ottawa sand samples during drained and undrained loading was presented elsewhere in detail (chapters 3 and 4). For samples deformed to the critical /steady state (no change in stresses and volume), the shear wave velocity at steady state was also measured.

REPEATABILITY OF TEST RESULTS

The confidence level in experimental observation and results is enhanced by the ability to repeat tests. Repeatability of a test depends on consistence reproduction of void ratio, soil fabric, measurement accuracy and exact duplication of the test routine. The sample preparation technique described above ensured that this was achieved to the highest degree. Typical results of void ratio and shear wave velocity during consolidation of identical water pluviated samples of initial void ratio 0.685, is shown in Figure 5.4. Similarly typical results of void ratio and shear wave velocity during consolidation of identical moist tamped samples of initial void ratio 0.826 are shown in Figure 5.5. Excellent repeatability in results showing change in void ratio and shear wave velocity with consolidation pressure may be noted.

RESULTS AND INTERPRETATION

The consolidation stress, void ratio and shear wave velocity for all the tests are summarized in Table 5.1. Figure 5.6 shows the shear wave velocity and void ratio change during isotropic consolidation for very loose, medium dense and dense Ottawa sand. For clarity only one consolidation sequence from each void ratio range is shown in Figure 5.6. From Table 5.1 and Figure 5.6 it may be noticed that the shear wave velocity changes with consolidation stress and void ratio and the change in shear wave velocity reduces as consolidation stress increases, i.e., the shear wave velocity can be expressed as a function of void ratio and stress. Several researchers (e.g., Roseler, 1979; Yu and Richard, 1984; Stokoe *et al.*, 1985) have shown that the shear wave velocity can be related to void ratio and effective confining stresses by equation [5.2].

It may be observed from equation [5.2] that if the void ratio can be expressed in terms of stress or vise-versa, the constants m_1 and m_2 can be determined. At the ultimate steady state, the stresses and void ratio are uniquely related and independent of soil fabric (Been *et al.*, 1991 and Ishihara, 1993). Hence, shear wave velocities measured at steady state can be used to determine the constants m_1 and m_2.

For shear wave velocity measured along the axial direction during triaxial compression loading, $\sigma'_1 = \sigma'_a$ and $\sigma'_3 = \sigma'_p$. The mobilized friction angle (ϕ'_{ss}) at steady state is approximately 30° for Ottawa sand (chapter 4). Therefore, at steady state (subscribed 'ss' denotes variables measured at steady state in the following expressions);

$$[5.4] \qquad \frac{(\sigma'_1)_{ss}}{(\sigma'_3)_{ss}} = \frac{(\sigma'_a)_{ss}}{(\sigma'_p)_{ss}} = \frac{1 + \sin 30}{1 - \sin 30} = 3$$

$$[5.5] \qquad (p')_{ss} = \frac{(\sigma'_1)_{ss} + 2\,(\sigma'_3)_{ss}}{3} = \frac{(\sigma'_a)_{ss} + 2\,(\sigma'_p)_{ss}}{3}$$

substituting equations [5.4] and [5.5] in [5.2]

$$[5.6] \qquad (V_s)_{ss} = (m_1 - m_2\, e_{ss})\,(p'_{ss})^{0.25}$$

At steady state the relation between the void ratio and mean normal stress can be approximated by (chapter 4)

$$[4.5] \qquad p'_{ss} = \exp\left(\frac{\Gamma - e_{ss}}{\lambda}\right)$$

where;

λ = slope of the steady state line.

Γ = the intercept of the steady state line at $p'_{ss} = 1$.

Substituting equation [4.5] and rewriting equation [5.6]

$$[5.7] \qquad (V_s)_{ss} = (m_1 - m_2\, e_{ss})\left[\exp\left(\frac{\Gamma - e_{ss}}{\lambda}\right)\right]^{0.25}$$

Figure 5.7 shows the measured shear wave velocities at steady state versus measured void ratio. Also inserted in this figure is a curve fit using equation [5.7]. In chapter 4 it was shown that for Ottawa sand $\Gamma = 0.867$ and $\lambda = 0.0168$. This provides values for m_1 and m_2 of 100.2 and 57.3 respectively at the steady state in equation [5.7]. These values are very similar to $m_1 = 111$ and $m_2 = 51$ for consolidated sand obtained by Hardin and Richart (1963). Hence, the resulting relationship between the shear wave velocity, stresses and void ratio for Ottawa sand at steady state is;

$$[5.8] \qquad (V_s)_{ss} = (100.2 - 57.3\, e_{ss})\, (\sigma'_a)_{ss}^{0.125}\, (\sigma'_p)_{ss}^{0.125}$$

Equation [5.8] can be rewritten as

$$[5.9] \qquad V_s = (100.2 - 57.3\, e)\, (\sigma'_a)^{0.125}\, (\sigma'_p)^{0.125}$$

Assuming equation [5.8] can also be used to predict shear wave velocity for any given stresses and void ratio. The following section compares the shear wave velocity predicted by equation [5.9] with shear wave velocities measured during consolidation.

Shear wave velocities during consolidation

During isotropic consolidation $\sigma'_a = \sigma'_b = \sigma'_3 = p'_c$. Hence, equation [5.9] can be written as;

[5.10] $$V_s = (100.2 - 57.3\ e)\ (p'_c)^{0.25}$$

The above equation can be normalized in terms of stresses as proposed by Robertson *et al.* (1992)

[5.11] $$V^*_{s1} = V_s\left(\frac{100}{p'_c}\right)^{0.25} = (100.2 - 57.3\ e)\ (100)^{0.25}$$

where V^*_{s1} denotes shear wave velocity normalized by the effective mean normal stress.

Figure 5.8 shows the variation of measured normalized shear wave velocity during consolidation and normalized shear wave velocity predicted by equation [5.11] with void ratio for the very loose Ottawa sand. It may be noticed that equation [5.11] predicts the measured shear wave velocity closely and that the normalized shear wave velocity is essentially constant over this small void ratio range.

Equations [5.9] and [5.11] were derived using shear wave velocities measured at steady state. Therefore, equation [5.9] can be used to predict the shear wave velocities of very loose sand during consolidation and hence, for any stress and void ratio state of loose Ottawa sand.

The variation of measured normalized shear wave velocity during consolidation and that predicted from equation [5.9] for the entire range of void ratio is shown in Figure 5.9. Although equation [5.9] was based on shear wave velocities measured at steady state over a small void ratio range ($0.75 < e < 0.81$), the relationship provides a reasonable fit to the velocities measured during consolidation over a wider void ratio range. It may be noticed that the water pluviated medium dense ($e = 0.66 - 0.68$) and dense ($e = 0.57 - 0.59$) samples show slightly higher normalized shear wave velocities than those predicted by equation [5.11]. This observation may be consistence with the conclusion of de Alba *et al.* (1984) that the shear wave velocity is also slightly influenced by different soil fabric for a given sand. The moist tamping technique creates a soil fabric with random orientation whereas the water pluviation technique creates a fabric with a somewhat preferred orientation, usually along the deposition direction. However, the variation in shear wave velocity due to soil fabric appears to be only about 35 m/s for the dense sand and reduces as the sand becomes looser. This represents a variation of less than 15% for a dense sand and much less for a loose sand. It would appear that the fabric for the very loose Ottawa sand is similar to the fabric at steady state.

EVALUATING THE POTENTIAL FOR FLOW LIQUEFACTION USING SHEAR WAVE VELOCITY

Figure 5.10 shows a plot of void ratio against logarithm of effective mean normal stress. Included in this figure is the ultimate steady/critical state line for Ottawa sand obtained from triaxial compression tests and contours of shear wave velocity constructed using equation [5.10]. Also shown in Figure 5.10 are the individual shear wave velocity measurements from each test. The samples consolidated to a void ratio above the steady state line showed a contractant strain softening behavior at large strains during monotonic undrained triaxial compression loading. Samples consolidated to a void ratio below the steady state line showed a dilatant strain hardening response at large strain during undrained triaxial compression loading. The shear wave velocities measured at each state is shown adjacent to the associated data points. Excellent agreement is seen between the plotted contours using equation [5.10] and measured shear wave velocities. The dense sand samples show a slight deviation due to soil fabric, as discussed earlier.

Figure 5.11 shows the contours of shear wave velocity on a plot of void ratio against logarithm of effective mean normal stress over a wide range of void ratio and stress level. For a sand element with a mean normal stress of 100 kPa and shear wave velocity of 150 m/s (point C in Fig. 5.11) exhibites contractive response at large strain as shown in Figure 5.12. Whereas, a sand element with the same mean normal stress of 100 kPa but a shear wave velocity of 200 m/s (point D in Fig. 5.11) exhibites dilative behavior at large strain as shown in Figure 5.13. Hence, the shear wave velocity combined with effective mean normal stress can be used to identify *in-situ* state of a sand and therefore, estimate its large strain response.

The state parameter combines the influence of void ratio and stress level in a unique way to the critical/steady state. Negative and positive state parameter would mean strain hardening and strain softening undrained loading response, respectively. Been *et al.* (1985) defined the state parameter ψ as the void ratio difference between the current and steady state at the same stress level (Fig. 5.1).

[5.12] $$\text{i.e.,} \quad \psi = e - e_{ss}.$$

Current void ratio 'e' can be written as (rearranging equation 5.2)

[5.13] $$e = \frac{m_1}{m_2} - \frac{V_s}{m_2\,(\sigma'_a)^{0.125}\,(\sigma'_p)^{0.125}}$$

substituting equations [4.4] and [5.13] in [5.12]

[5.14] $$\psi = \left(\frac{m_1}{m_2} - \Gamma\right) - \left(\frac{V_s}{m_2\,(\sigma'_a)^{0.125}\,(\sigma'_p)^{0.125}} - \lambda \ln p'_{ss}\right)$$

m_1, m_2 and Γ are constants for a given sand. Hence, the term $(m_1/m_2 - \Gamma)$ is a constant.

If we define the following;

[5.15] $$C = \left(\frac{m_1}{m_2} - \Gamma\right) = \text{constant}$$

[5.16] $$V_{s\psi} = \left(\frac{V_s}{m_2\,(\sigma'_a)^{0.125}\,(\sigma'_p)^{0.125}} - \lambda \ln p'\right)$$

[5.17] $$\text{Then,} \quad \psi = C - V_{s\psi}$$

Where $V_{s\psi}$ is a state parameter shear wave velocity and is related to the state parameter for a given sand. $V_{s\psi}$ only depends on shear wave velocity and confining stresses for a given sand. Figure 5.14 shows the variation of $V_{s\psi}$ calculated from the measured shear wave velocity and stresses with the state parameter calculated from the steady state line and the consolidation void ratio. Due to soil fabric effects the dense sand samples show a slight deviation from the straight line relationship. The value of $V_{s\psi}$ at $\psi = 0$ can be used to differentiate net contractive behavior from net dilative behavior. At $\psi = 0$, $V_{s\psi} = 0.88$, i.e., Ottawa sand with $V_{s\psi}$ less than 0.88 would show a net contractive behavior, whereas, Ottawa sand with $V_{s\psi}$ greater than 0.88 would show a net dilative behavior, under triaxial compression loading.

Figure 5.15 shows the variation of shear wave velocity with vertical effective stress for $V_{s\psi} = 0.88$ under both isotropic ($\sigma'_p/\sigma'_a = K_o = 1.0$) and anisotropic ($\sigma'_p/\sigma'_a = K_o = 0.5$) stress conditions. The influence of consolidation state has a small effect on the contractive/dilative boundary when the vertical effective stress is less than 100 kPa. However, for high values of vertical effective stress, the difference in the boundaries between $K_o = 1$ and $K_o = 0.5$ starts to increase. At an effective vertical stress of 200 kPa the anisotropic consolidation with $K_o = 0.5$ would have a contractive/dilative boundary about 20 m/s less than the isotropic condition. For shallow depths where the vertical effective stress is less than about 200 kPa, the large strain behavior of Ottawa sand (contractive/dilative) can be estimated by measuring the *in-situ* shear wave velocity and estimating the vertical effective stress.

Yoshida *et al.* (1988) proposed a relationship between SPT, N values and shear wave velocity for Tonegawa sand ($D_{50} = 0.34$ mm) based on chamber test results. This relationship is given by;

$$[5.18] \qquad V_s = 94\, N^{0.25} \left(\frac{\sigma'_v}{Pa}\right)^{0.14}$$

For the shear wave velocities shown in Figure 5.15, the corresponding SPT N values can be calculated assuming equation [5.18] is also applicable to Ottawa sand ($D_{50} = 0.34$ mm). The Japanese SPT N values can be converted to a normalized SPT N value corrected to an energy level of 60% ($(N)_{60}$) using $(N)_{60} = 1.2$ N (Ishihara, 1993). Figure 5.16 shows the resulting equivalent SPT $(N)_{60}$ from shear wave velocity showing the net contractive/dilative boundary using equation [5.18].

Figure 5.17 compares the resulting equivalent SPT $(N)_{60}$ from shear wave velocity with the SPT $(N)_{60}$ values proposed by Robertson *et al.* (1992a) and Ishihara (1993) based on past flow failures. The SPT $(N)_{60}$ values obtained for both consolidation states for Ottawa sand fall within the rage of $(N)_{60}$ values suggested by Robertson *et al.* (1992a) and are close to the range suggested by Ishihara (1993).

Based on the shear wave velocity and the SPT $(N)_{60}$ correlation, it appears that the range of SPT $(N)_{60}$ values suggested by Robertson *et al.* (1992a) may be influenced by the different consolidation states of sands. From research with the SPT and CPT in large calibration chambers Jamiolkowski *et al.* (1989), Houlsby and Hitchman (1988) also found that penetration resistance is strongly influenced by the horizontal stress or the consolidation state in sands. Hence, it is reasonable to expect a range of penetration resistance values for a single vertical overburden pressure (σ'_v) depending on the consolidation state (K_o) of a sand. In general, it is quite likely that loose sands will have consolidation states close to $K_o = 0.5$. Hence, it would be appropriate to consider the lower bound SPT $(N)_{60}$ values proposed by Robertson *et* *al.* (1992a) when evaluating flow liquefaction potential of loose, uncemented young clean sand deposits. This lower bound SPT $(N)_{60}$ profile is also in close agreement with the $(N)_{60}$ values proposed by Ishihara (1993) for flow liquefaction.

Shear wave velocities can also be converted to cone penetration resistance (q_c) by (Robertson et al., 1992b);

$$[5.19] \qquad V_s = 102\, q_c^{\,0.23} \left(\frac{\sigma'_v}{Pa}\right)^{0.135}$$

where q_c is in MPa and V_s is in m/s. For the shear wave velocities shown in Figure 5.15, the corresponding q_c values can be calculated assuming equation [5.19] is also applicable to Ottawa sand. Figure 5.18 compares the resulting equivalent q_c values from shear wave velocities with the q_c values proposed by Sladen and Hewitt (1989), Robertson et al. (1992a) and Ishihara (1993). The q_c values for flow liquefaction obtained for Ottawa sand with $K_o = 0.5$ from shear wave velocity agrees very well with the values suggested by Sladen and Hewitt (1989) based on back analysis of several flow liquefaction failures. These values also fall within the range of values suggested by Robertson *et al.* (1992a) and are close to the range suggested by Ishihara (1993) for possible flow liquefaction.

FIELD APPLICATION

Ideally in order to evaluate *in-situ* strength and large strain behavior of sands, it is important to conduct laboratory tests on high quality undisturbed samples. There have been several successful attempts to obtain high quality undisturbed samples of sand by *in-situ* ground freezing (Yoshimi *et al.*, 1984; Hatanaka *et al.*, 1985; Yoshimi *et al.*, 1989 Sego *et al.*, 1993). Since the cost of *in-situ* ground freezing is high, the need to obtain high quality undisturbed samples would depend on the project requirements. However, it is possible to estimate the large strain behavior of a uniform loose sand deposit using *in-situ* shear wave velocity measurements.

Several methods currently exist to measure *in-situ* shear wave velocity profiles in a cost effective way (Stokoe and Hora, 1987; Woods, 1987; Robertson *et al.*, 1986; Addo and Robertson, 1992). As an initial screening, the relationship shown in Figure 5.15 can be used to estimate the large strain behavior of a clean uncemented, young sand. The boundary shown in Figure 5.15 represents a normalized shear wave velocity (V_{s1}), using equation [5.3], of between 160 m/s and 170 m/s depending on the *in-situ* K_o. This value is also supported by limited field evidence (Robertson *et al.* 1992). The equivalent SPT $(N)_{60}$ values estimated for both consolidation states of Ottawa sand using equation [5.18] are close to the range of $(N)_{60}$ values suggested by Robertson *et al.* (1992) and Ishihara (1993) for flow liquefaction failure. Further, the equivalent CPT q_c values estimated for Ottawa sand with a consolidation state of $K_o = 0.5$ shows excellent agreement with values of q_c obtained from back analysis of several liquefaction flow failures.

For a more detailed evaluation for a given sand, it should be possible to develop a material specific relationship between shear wave velocity, void ratio and effective confining stress based on a small number of undrained triaxial compression tests on very loose reconstituted samples of sand. The resulting relationship should look similar to that given in equation [5.9]. Based on the steady state and shear wave velocity relationship of the reconstituted sand, equation [5.14] can be developed. By substituting the *in-situ* stresses and *in-situ* shear wave velocity in this equation, the state parameter can be calculated. Hence, the large strain response can be estimated.

Provided the *in-situ* sand deposit is unaged and uncemented this approach should provide a reasonable estimation of *in-situ* state. For aged or cemented sands the relationship based on reconstituted samples may not be valid, since *in-situ* shear wave velocity can be sensitive to the effects of aging and cementation. However, frequently it is the young, uncemented sand deposits that represent the highest risk of flow liquefaction. Therefore, this approach should be applicable as an initial screening for these deposits.

SUMMARY

An experimental study has been presented for shear wave velocity interpretation of clean sand deposits based on steady/critical state concepts. Sand samples were prepared by water pluviation and moist tamping techniques. Shear wave velocities were measured on these samples during consolidation. Undrained and drained triaxial compression loading was performed on these samples to identify the large strain response (contractive/dilative). For samples that reached steady state the shear wave velocities were also measured at steady state.

Results present in this study show that shear wave velocities can be expressed in terms of void ratio and effective confining stresses for loose sands. However, for denser sands, variations in soil fabric appears to have a slight influence on the measured shear wave velocity.

The large strain behavior of a uniform sand deposit can be estimated using shear wave velocity measurements combined with a knowledge of the effective mean normal stress. When the effective vertical stress is less than 200 kPa, the contractive/dilative boundary is only slightly influenced by the consolidation state. Hence, for shallow depths the contractive/dilative behavior can be identified by shear wave velocity and estimating the vertical effective stress.

The following procedure can be applied when evaluating the potential for flow liquefaction of a clean sand using *in-situ* shear wave velocity measurements;

- As an initial screening, the relationship shown in Figure 5.15 can be used to estimate whether a contractant, strain softening response will result from undrained compression loading.
- For a more detailed evaluation, a relationship between shear wave velocity, void ratio and effective confining stress based on a small number of undrained triaxial compression tests on very loose reconstituted samples for a given sand can be developed. The resulting relationship should look similar to that given in equation [5.9].
- Based on the steady state and shear wave velocity relationship of the reconstituted sand, equation [5.14] can be developed. By substituting the *in-situ* stresses and *in-situ* shear wave velocity in this equation, the state parameter can be calculated. Hence, the large strain response can be identified.

This approach may be limited to young, uncemented, uniform clean sand deposits. For aged or cemented sands, the relationship based on reconstituted samples may not be valid. However, frequently it is the young, uncemented sand deposits that represent the highest risk of flow liquefaction. Therefore, this approach should be applicable to these deposits.

Further work is required to confirm and clarify the above conclusions for different sands and silty sands and for its field application.

REFERENCES

Addo, K. and Robertson, P.K. 1992. Shear wave velocity measurements of soils using Rayleigh waves. Canadian Geotechnical Journal, **29**: 558-568.

Been, K.H. and Jefferies, M.G. 1985. A state parameter for sands. Geotechnique, **35**: 99-112.

Been. K., Jefferies, M.G. and Hachey, J. 1991. The critical state of sand. Geotechnique, **41**: 365-381.

Bierschwale, J.G. and Stokoe, K.H. 1984. Analytical evaluation of liquefaction potential of sand subjected to the 1981 Westmoreland Earth quake. Geotechnical Engineering Report GR-84-15, Civil Engineering Department, University of Texas, Austin, Texas.

Castro, G. 1969. Liquefaction of sands. Harvard Soil Mechanics Series No. 81. 112 pp.

De Alba, P., Baldwin, K., Janoo, V., Roe, G. and Celikkol, B. 1984. Elastic wave velocities and liquefaction potential. Geotechnical Testing Journal, American Society of Testing Materials,. **7(2)**: 77-88.

Dynik, R. and Madshu, C., 1985. Laboratory measurements of G_{max} using bender elements. Proceedings, Advances in the art of testing soils under cyclic conditions, American Society of Civil Engineering, Detroit, MI, pp. 186-196.

Hamdi, F and Taylor-Smith, D., 1982. The influence of permeability on compressional wave velocity in marine sediments. Geophysical Prospecting, **30**: 622-640.

Han, C. and Vardoulakis, I.G. 1991. Plane strain compression experiments on water saturated fine grained sand. Geotechnique, **41**: 49-78.

Hardin, B.O. and Richart, F.E. Jr. 1963. Elastic wave velocities in granular soils. Journal of the Soil Mechanics and Foundation Engineering, American Society of Civil Engineering, **89**(1): 33-65.

Hatanaka, M., Sugimato, M. and Suzudi, Y. 1985. Liquefaction resistance of alluvial volcanic soils sampled by in situ freezing. Soils and Foundations, **25**(3): 49-63.

Houlsby, G.T. and Hitchman, R. 1988. Calibration chamber tests of a cone penetrometer in sand. Geotechnique, **38**: 39-44.

Ishihara. K. 1993. Liquefaction and flow failure during earthquakes. The 33rd Rankine lecture. March 24. London. UK. 105pp.

Kayen, R.E., Mitchell, J.K., Seed, R.B.B., Lodge, A., Nishio, S. and Coutinho, R. 1992. Evaluation of SPT-, CPT-, and Shear Wave-Based methods for liquefaction potential assessment using Loma Prieta data. US-Japan Workshop. pp.177-204.

Jamiolkowski, M., Lo Presti, D.C.F., Manfredini, G. and Rix, G.J. 1989. Italian experience in assessing shear wave velocity from CPT and SPT. XII international conference on Soil Mechanics and Foundation Engineering, Rio. Vol. 4.

Negussey, D. 1984. An experimental study of small strain response of sand. Ph. D. Thesis, The University of British Columbia, Vancouver, B.C., Canada.

Robertson, P.K. 1993. Design consideration for liquefaction. US-Japan Workshop, June 1993.

Robertson, P.K., Cambanella, R.G., Gillespie, D. and Rice, A. 1986. Seismic CPT to measure in-situ shear wave velocity. Journal of Geotechnical Engineering American Society of Civil Engineering, **112**(8): 791-803.

Robertson, P.K., Woeller, D.J. and Finn, W.D.L. 1992a. Seismic cone penetration test for evaluating liquefaction potential under cyclic loading. Canadian Geotechnical Journal, **29**: 686-695.

Robertson, P.K., Woeller, D.J., Kokan, M., Hunter, J. and Luternauer, J. 1992b. Seismic techniques to evaluate liquefaction potential. 45th Canadian Geotechnical Conference, Toronto. 5:1-5:7.

Roscoe, K.H., Schofield, A.N. and Wroth, C.P. 1958. On yielding of soils. Geotechnique, **8**: 22-53.

Rosler, S.K. 1979. Anisotropic shear wave modulus due to stress anisotropy. Journal of Geotechnical Engineering American Society of Civil Engineering, **105**(7): 871-880.

Sasitharan, S. 1989. Stress path dependency of dilatancy and stress-strain response of sand. M.A.Sc. Thesis. The University of British Columbia, Vancouver, BC., Canada.

Sasitharan, S., Robertson, P.K. and Sego, D.C. 1992. Sample disturbance from shear wave velocity measurements. 45th Canadian Geotechnical Conference, Toronto. 23:1-23:7.

Sasitharan, S., Robertson, P.K., Sego, D.C. and Morgenstern, N.R. 1993(a). Collapse behavior of sand. Canadian Geotechnical Journal. Accepted for publication in August 1993.

Sasitharan, S., Robertson, P.K., Sego, D.C. and Morgenstern, N.R. 1993(b). A State boundary surface for very loose sand and it's practical applications. Canadian Geotechnical Journal. (in press).

Seed, H.B., Idriss, I.M. and Arango, I. 1983. Evaluation of liquefaction potential using field performance data. Journal of Geotechnical Engineering American Society of Civil Engineering, **109**(3): 458-482.

Sego, D.C., Robertson, P.K , Sasitharan, S., Kilpatrick, B.I. and Pillai, V.S. 1993. Ground freezing and sampling of foundation soils at Duncan Dam. 46th Canadian Geotechnical Conference, Saskatoon.

Shirley, E.T. 1978. An improved shear wave transducer. Journal of Acoustical Society of America, **63**: 1643-1645.

Sladen, J.A., and Hewitt, K.J. 1989. Influence of placement method of the in-situ density of hydraulic fills. Canadian Geotechnical Journal, **26**: 453-466.

Stokoe, K.H. II., Lee, H.H.S. and Knox. D.P. 1985. Shear moduli measurements under true triaxial stresses. Proceedings, Advances in the art of testing soils under cyclic conditions, American Society of Civil Engineering, Detroit, MI, pp. 166-185.

Stokoe, K.H. II. and Hora, R.J. 1987. Variables affecting in-situ seismic measurements. Proceedings, Conference on Earthquake Engineering and Soil Dynamics, American Society of Civil Engineers, Vol. II. pp. 919-939.

Tokimatsu, K., Yamazaki, T. and Yoshimi, Y. 1986. Soil liquefaction evaluation by elastic shear moduli, Soils and Foundations, **26**(1): 25-35.

Tokimatsu, K. and Uchida, A. 1990. Correlation between liquefaction resistance and shear wave velocity. Soils and Foundations, **30**(2): 33-42.

Woods, R.D. 1987. In-situ tests for foundation vibrations. Proceedings, Conference on use of in-situ tests in geotechnical engineering, American Society of Civil Engineering, Special Publication 6, pp. 336-375.

Yoshida, Y., Ikemi, M. and Kokusho, T. 1988. Empirical formulas of SPT blow-counts for gravely soils. Proc. of penetration testing, Balkema, Rotterdam. Vol. 1. pp. 381-387.

Yoshimi, Y. Tokimatsu, K., Kaneko, O. and Makihara, Y., 1984. Undrained cyclic shear strength of a dense Niigata sand. Soils and Foundations, **24**(4):131-145.

Yoshimi, Y. Tokimatsu, K. and Hosaka, Y., 1989. Evaluation of liquefaction resistance of clean sands based on high quality undisturbed samples. Soils and Foundations, **29**(1):93-104.

Yu. P. and Richard, F.E. Jr. 1984. Stress ratio effect on shear modulus of dry sands. Journal of Geotechnical Engineering, American Society of Civil Engineering, **110**(3): 331-341.

Table 5.1 Summary of shear wave velocity measured during consolidation

Dense sand

Preparation	p' (kPa)	e	Vs (m/s)
WP	55.0	0.584	181
	105.0	0.580	235
	156.5	0.578	261
	207.3	0.575	284
	257.2	0.573	300
	306.6	0.570	320
	357.5	0.569	324
	405.1	0.568	333
WP	65.4	0.593	168
	110.1	0.588	259
WP	57.5	0.585	198
	107.1	0.582	231
	173.5	0.578	248
	207.4	0.577	278
	256.7	0.575	299
	307.7	0.574	322
	358.6	0.572	328
	419.1	0.571	336

Medium dense sand

Preparation	p' (kPa)	e	Vs (m/s)
WP	52.9	0.666	183
	76.5	0.663	198
	102.1	0.661	221
WP	52.1	0.689	172
	102.1	0.682	210
	152.4	0.678	236
	202.6	0.675	255
	253.7	0.672	278
	302.7	0.671	293
	354.0	0.669	306
	404.0	0.667	308
WP	32.2	0.683	147
	58.8	0.679	181
	108.3	0.674	222
WP	56.1	0.681	168
	107.2	0.675	212
	157.2	0.671	226
	207.5	0.667	265
	257.3	0.665	278
	307.8	0.663	282
	407.9	0.659	308

Loose sand

Preparation	p' (kPa)	e	Vs (m/s)
MC	100.6	0.814	175
	151.8	0.809	192
	200.8	0.805	212
	250.7	0.802	226
	300.4	0.799	234
	350.5	0.796	245
	400.2	0.794	253
	442.9	0.792	258
	500.7	0.791	267
MC	150.3	0.827	189
	250.7	0.819	207
	350.5	0.813	223
	450.9	0.809	246
	550.6	0.806	258
MC	50.1	0.833	158
	148.9	0.824	200
	248.9	0.817	228
	349.4	0.812	249
MC	55.6	0.828	137
	151.2	0.822	202
	254.9	0.816	227
MC	49.1	0.822	138
	148.2	0.813	184
	247.3	0.807	207
	348.8	0.803	224
MC	52.6	0.826	139
	147.7	0.816	184
	247.6	0.808	208
	346.1	0.804	227

WP = Water pulviation; MC = Moist tamping

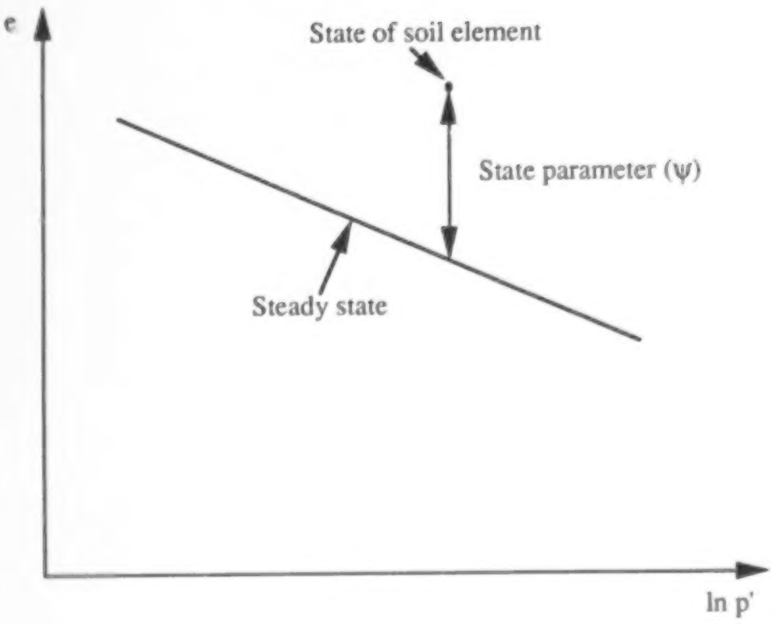

Figure 5.1 Initial state of a soil relative to steady/critical state.

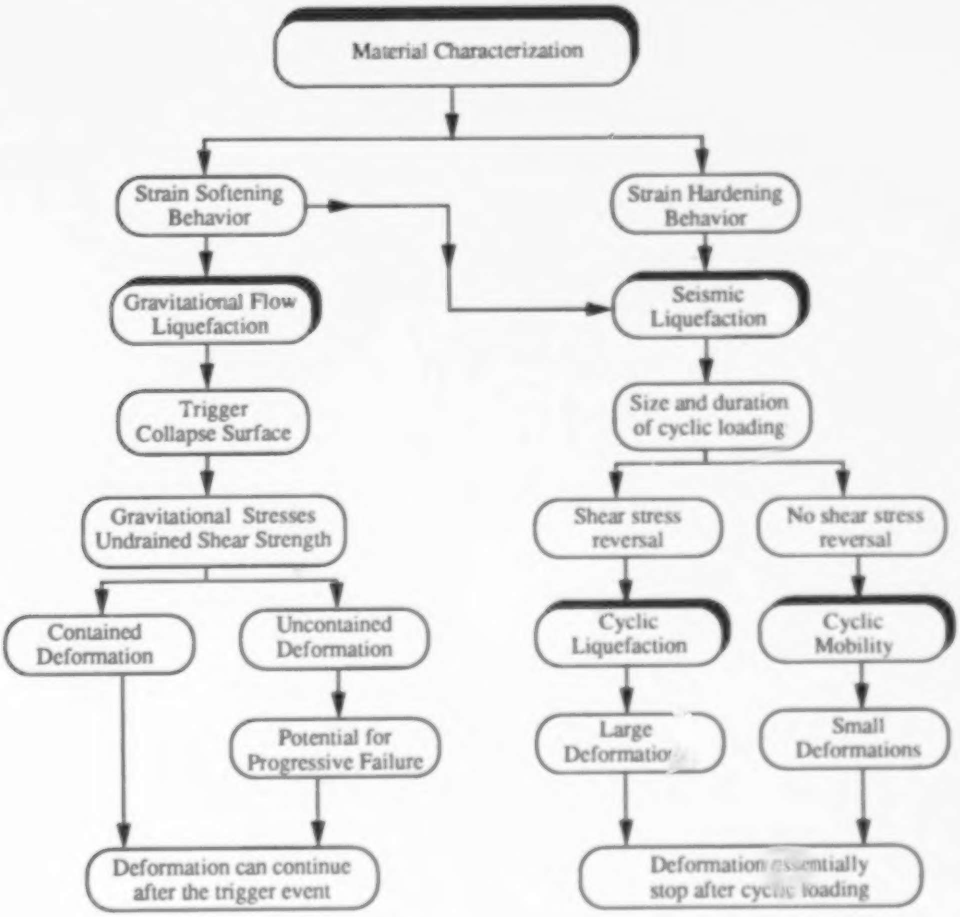
Material Characterization
Strain Softening Behavior
Strain Hardening Behavior
Gravitational Flow Liquefaction
Seismic Liquefaction
Trigger Collapse Surface
Size and duration of cyclic loading
Gravitational Stresses Undrained Shear Strength
Shear stress reversal
No shear stress reversal
Contained Deformation
Uncontained Deformation
Cyclic Liquefaction
Cyclic Mobility
Potential for Progressive Failure
Large Deformations
Small Deformations
Deformation can continue after the trigger event
Deformation essentially stop after cyclic loading

Figure 5.2 Flow chart for liquefaction evaluation. (After Robertson, 1993).

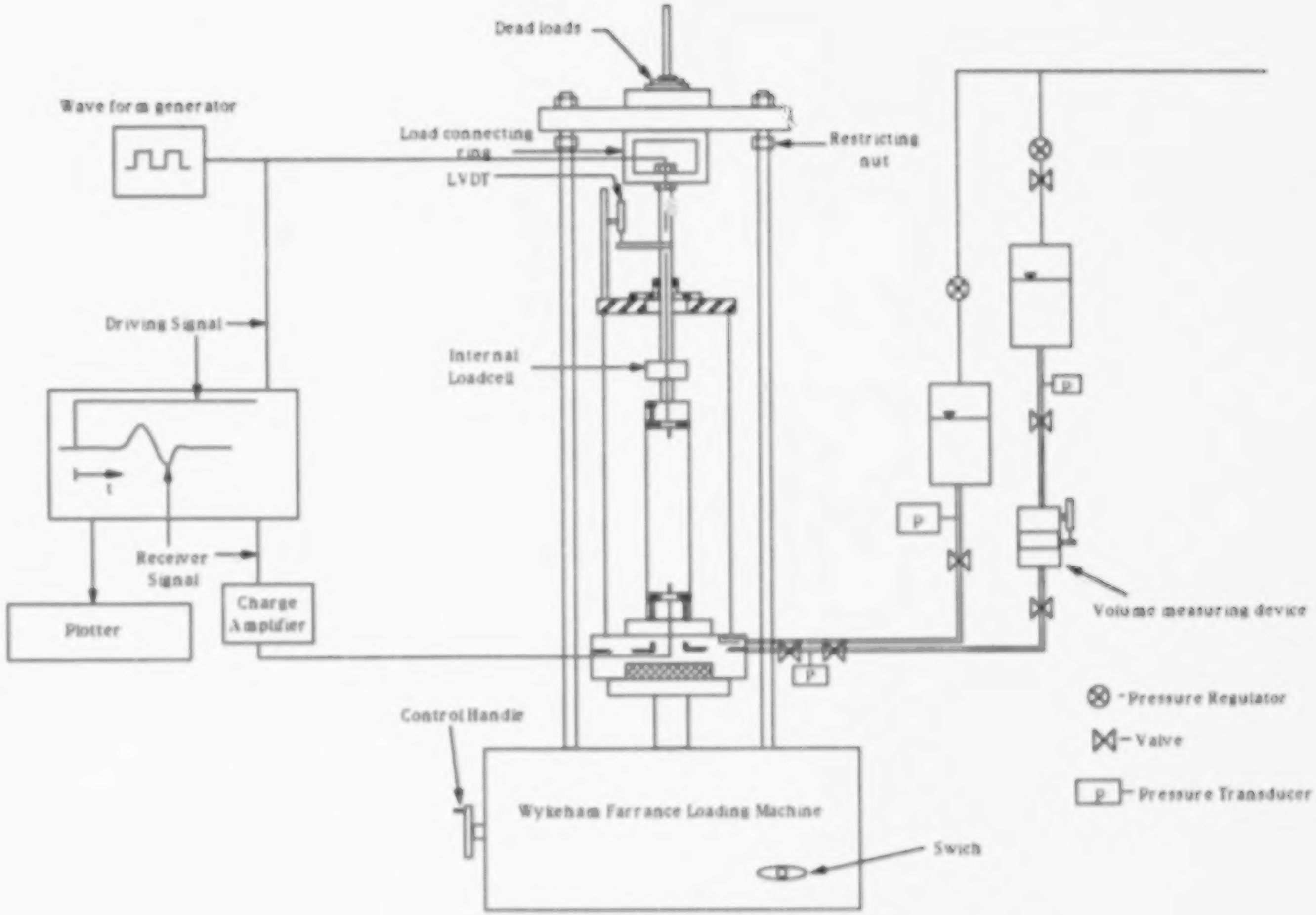

Figure 5.3 Schematic of testing apparatus

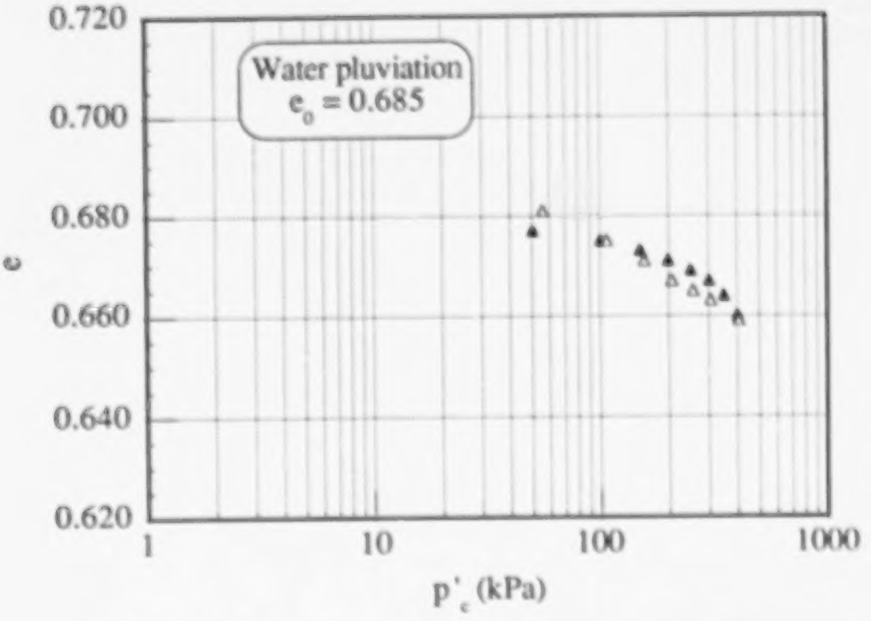

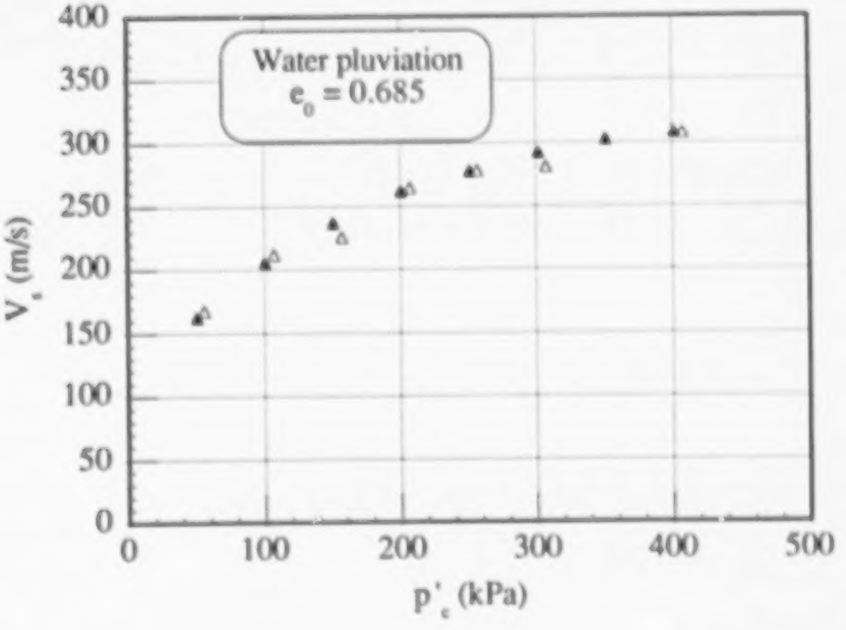

Figure 5.4 Repeatability of water pluviated samples interms of void ratio and shear wave velocity.

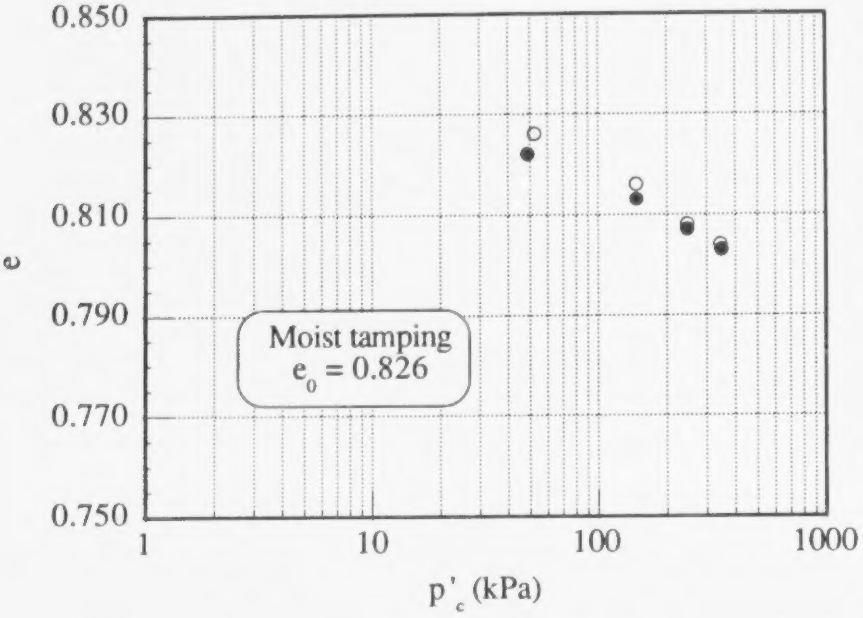

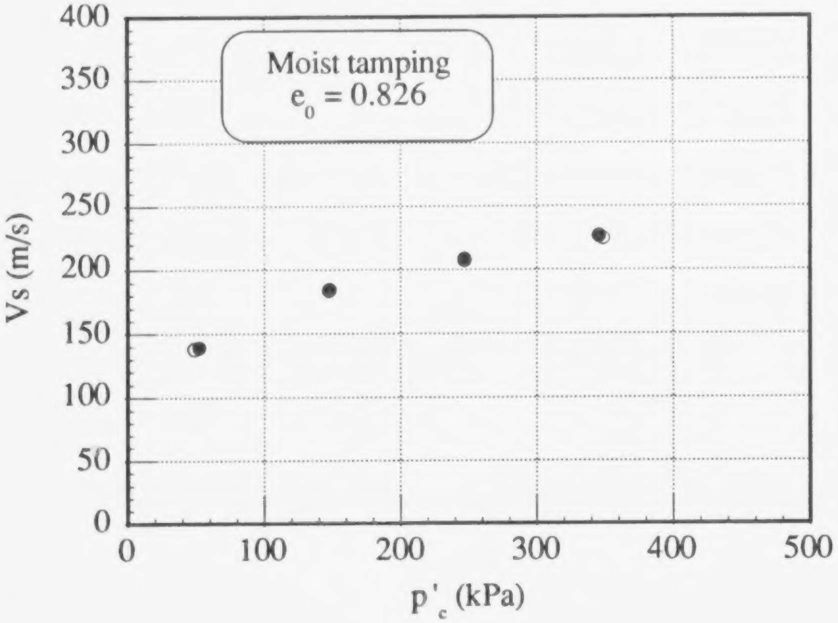

Figure 5.5 Repeatability of moist tamped samples interms of void ratio and shear wave velocity.

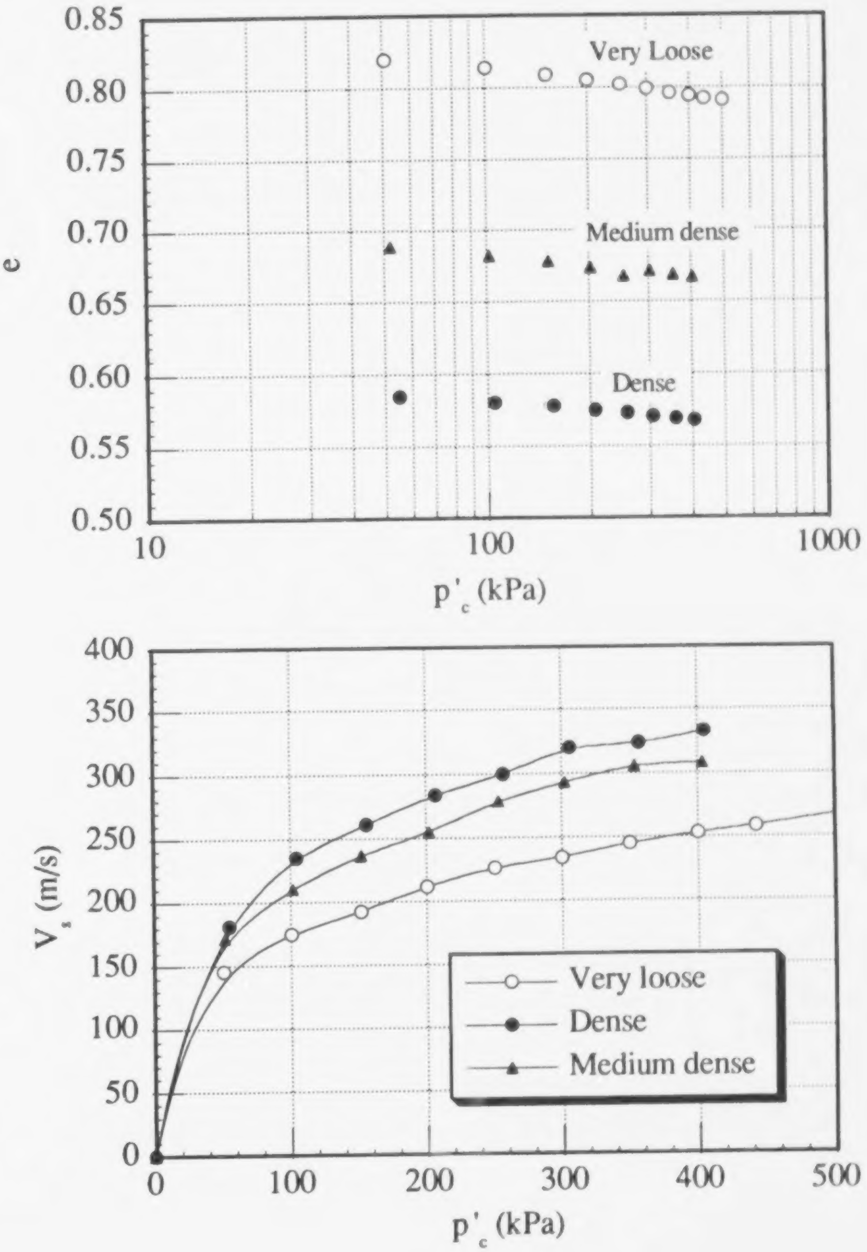

Figure 5.6 Shear wave velocity and void ratio changes during consolidation of loose, medium dense and dense Ottawa sand.

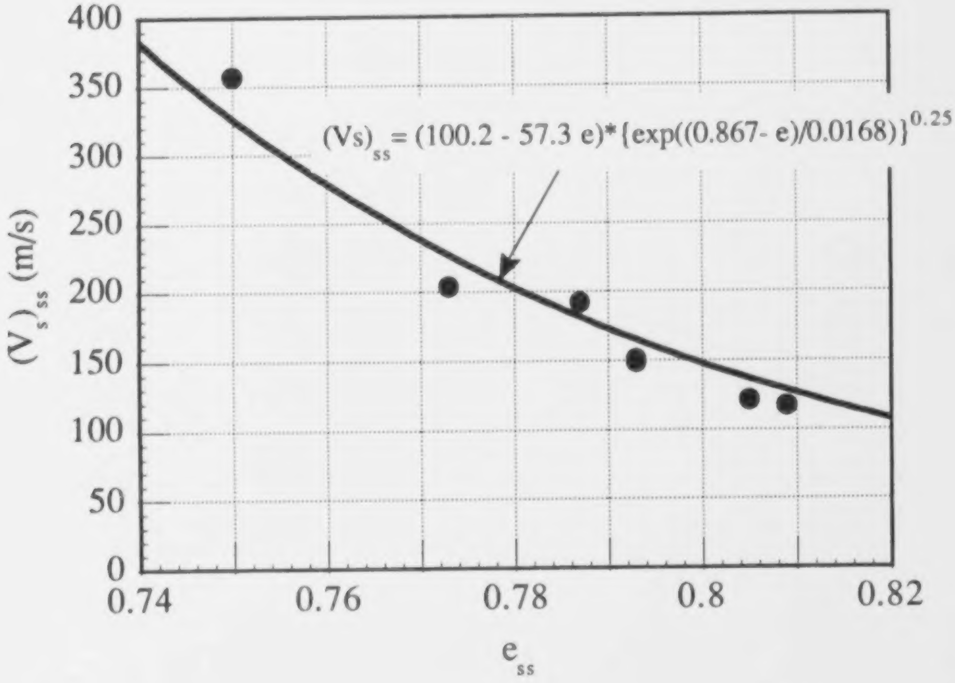

Figure 5.7 Steady state shear wave velocities and void ratio for Ottawa sand.

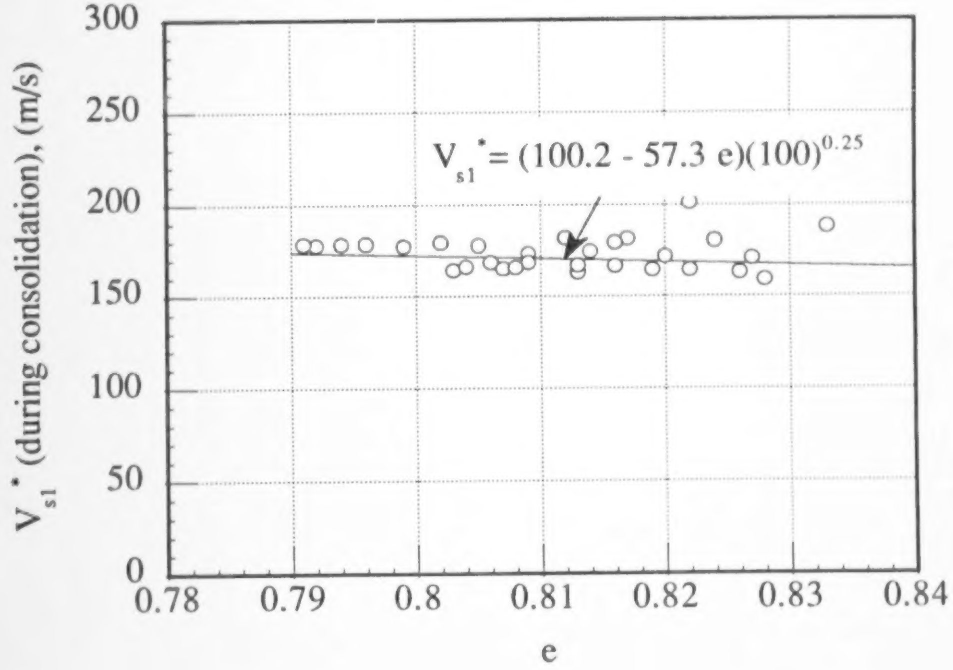

Figure 5.8 Normalized shear wave velocity during consolidation for very loose Ottawa sand.

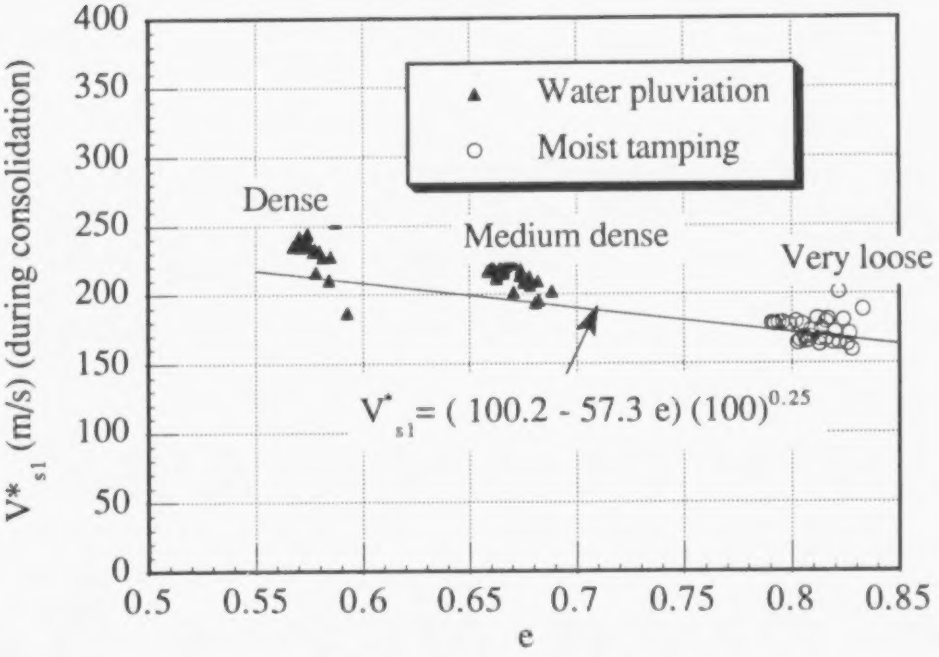

Figure 5.9 Normalized shear wave velocity during consolidation for very loose, medium dense and dense Ottawa sand.

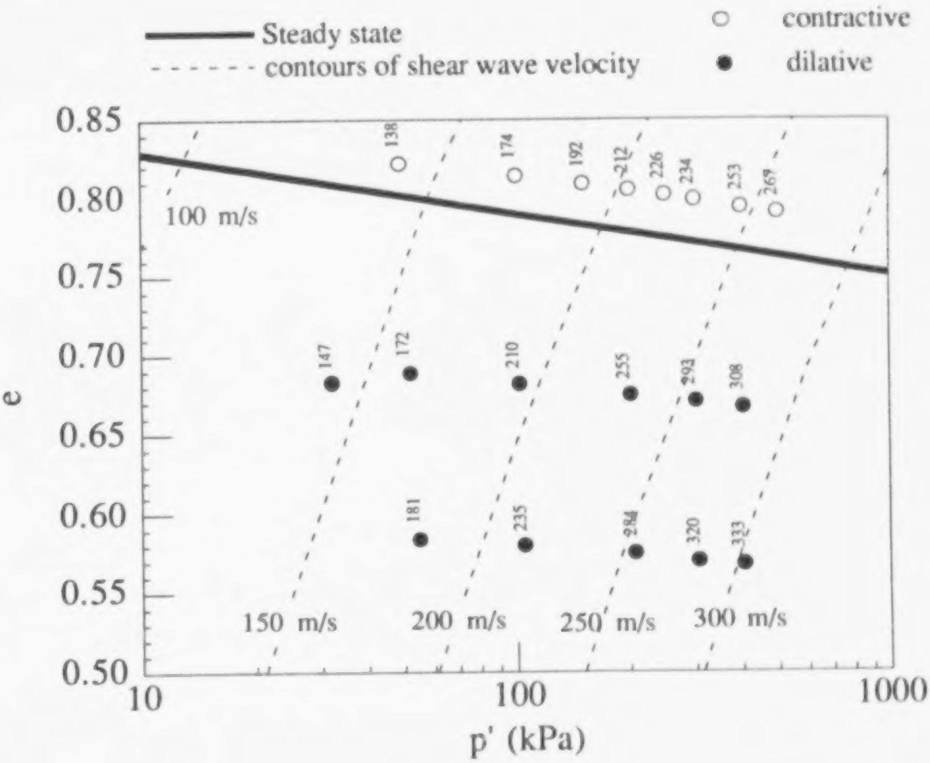

Figure 5.10 Void ratio against logarithm of effective mean normal stress, showing the steady/critical state line and contours of shear wave velocity constructed using equation [5.10] as well as measured shear wave velocities.

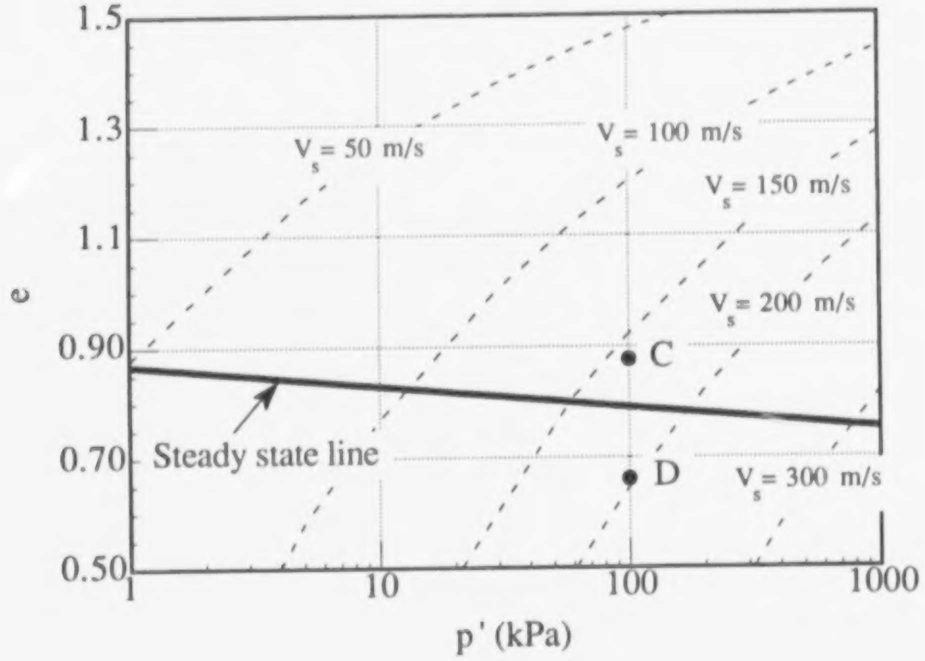

Figure 5.11 Contours of shear wave velocity on a plot of void ratio against logarithm of effective mean normal stress over a wide range of void ratio and stress level.

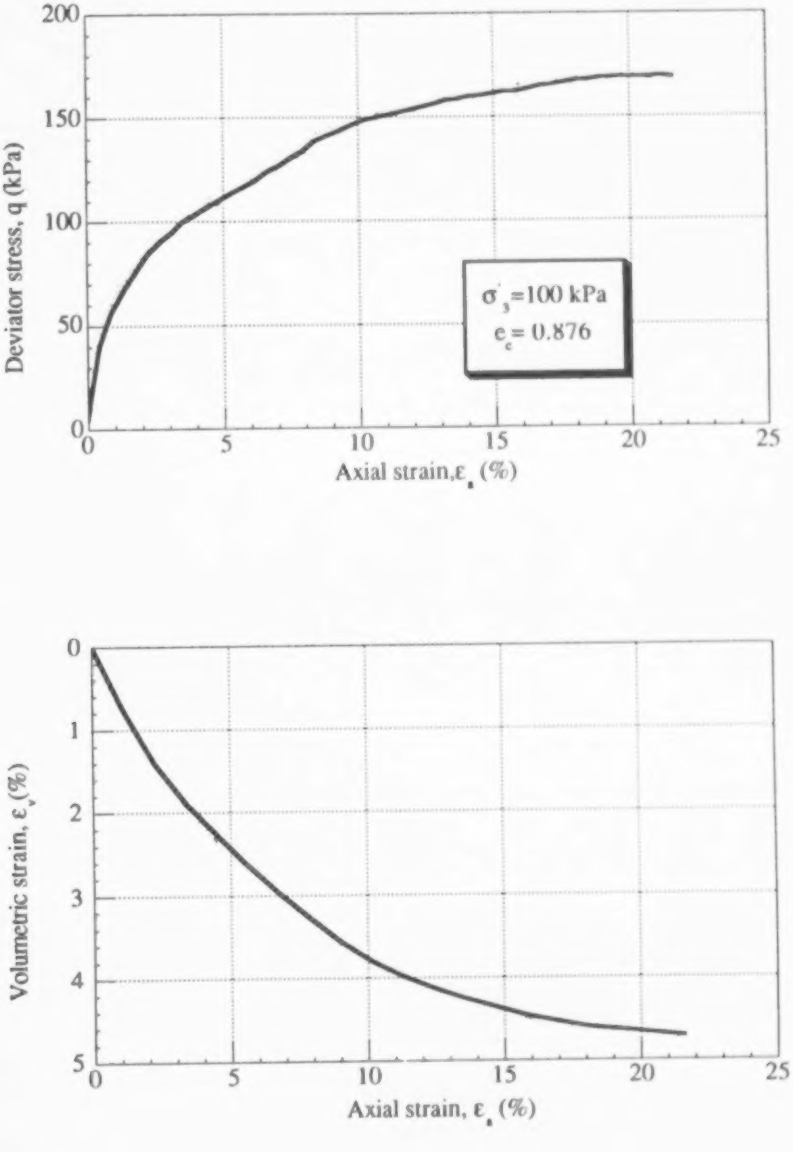

Figure 5.12 The stress-strain behavior for the monotonic drained conventional triaxial compression test on a sample consolidated to an isotropic stress of 100 kPa and void ratio of 0.876.

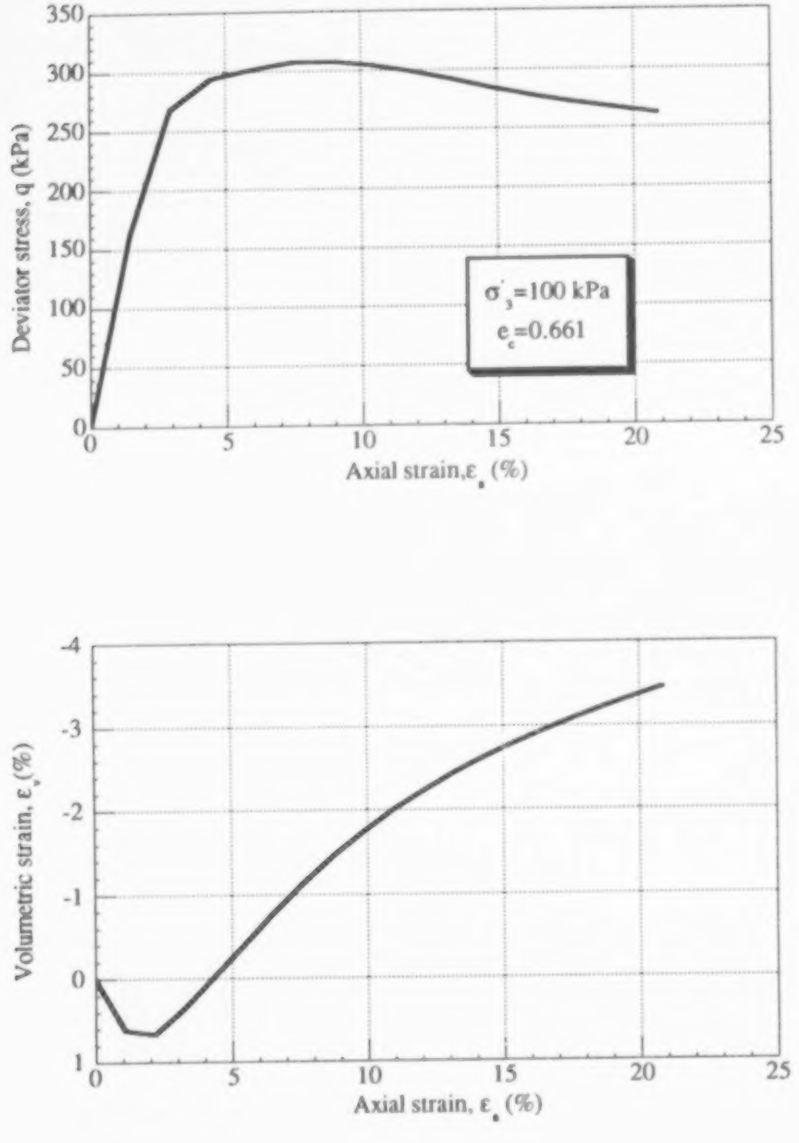

Figure 5.13 The stress-strain behavior for the monotonic drained conventional triaxial compression test on a sample consolidated to an isotropic stress of 100 kPa and void ratio of 0.661.

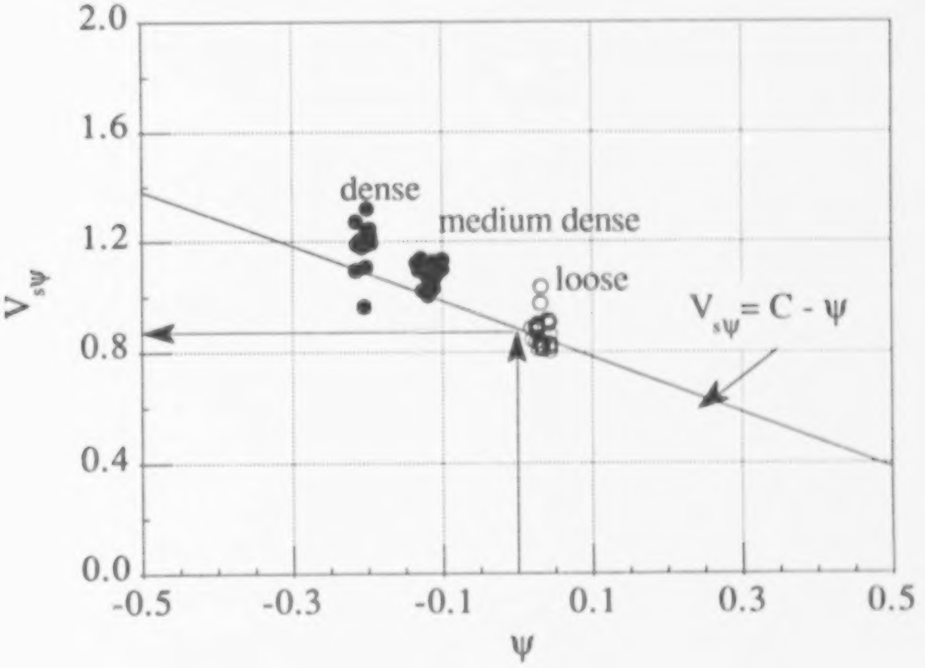

Figure 5.14 The variation of $V_{S\psi}$ calculated from the measured shear wave velocity and stresses with the state parameter calculated from the consolidation void ratio.

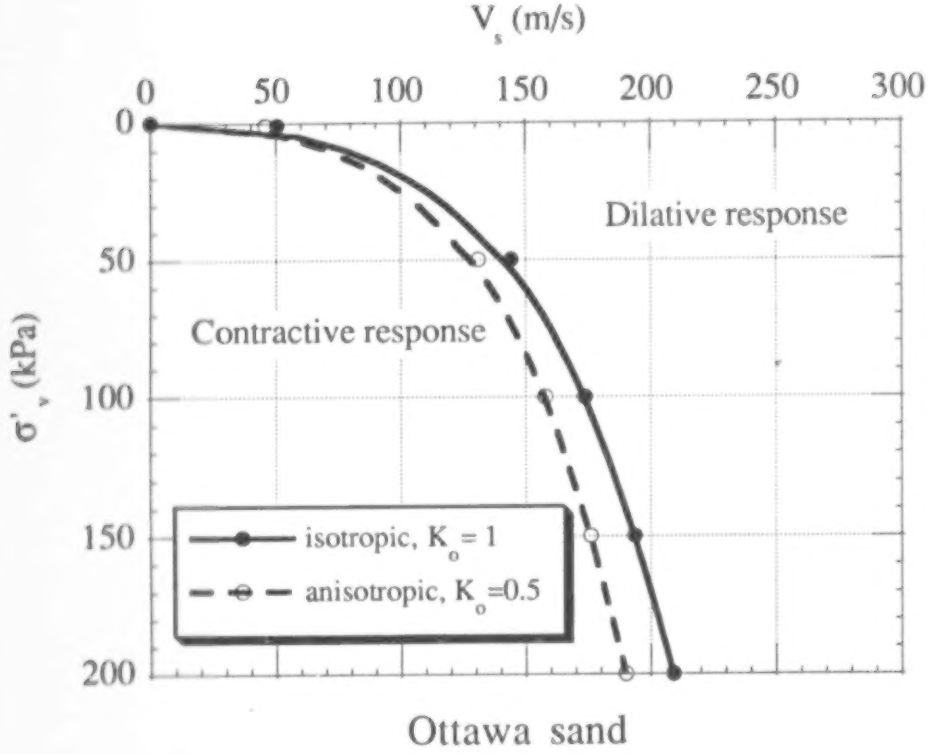

Figure 5.15 Boundary between contractive and dilative behavior at large strains based on shear wave velocity for Ottawa sand.

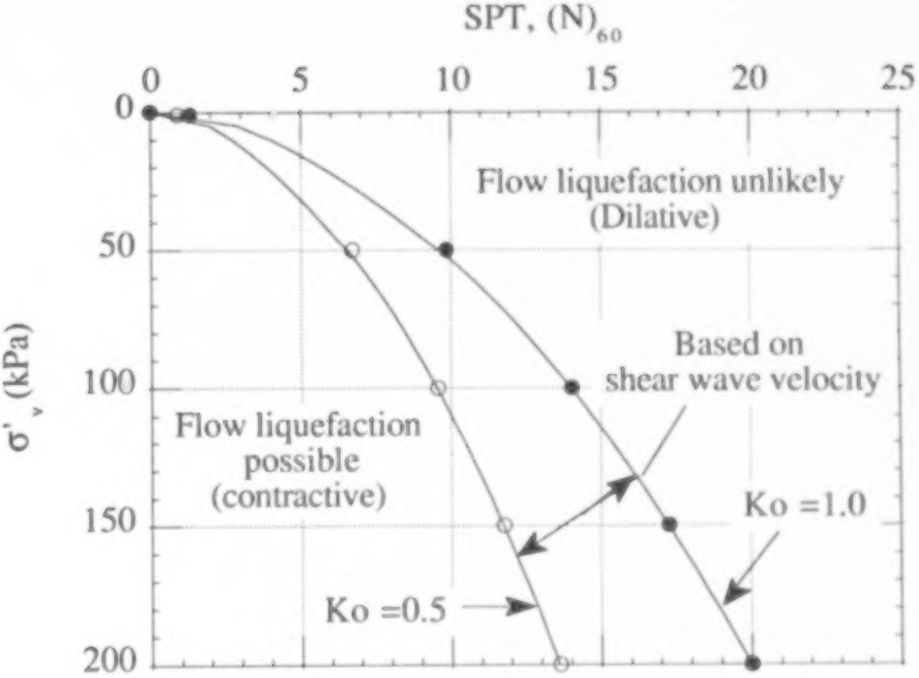

Figure 5.16 Boundary between contractive and dilative behavior at large strains using SPT $(N)_{60}$ based on shear wave velocity criteria for Ottawa sand.

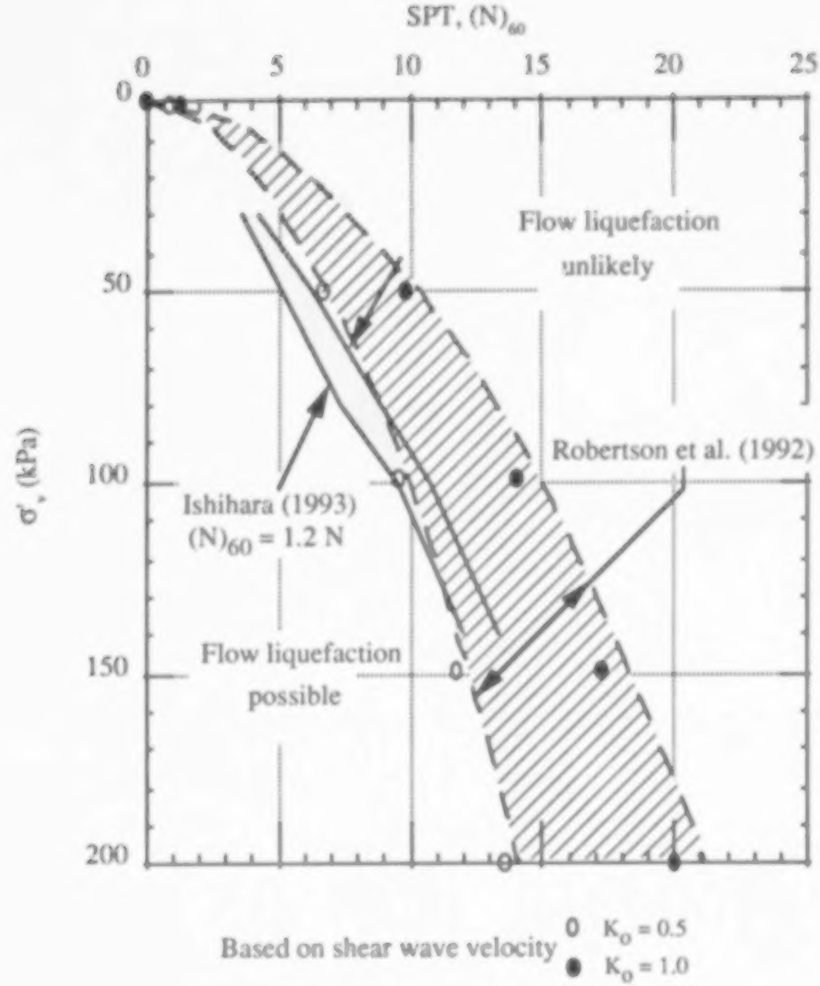

Figure 5.17 Comparison between contractive and dilative boundaries using SPT $(N)_{60}$ based on shear wave velocity and those proposed by Ishihara (1993) and Robertson et al. (1992a).

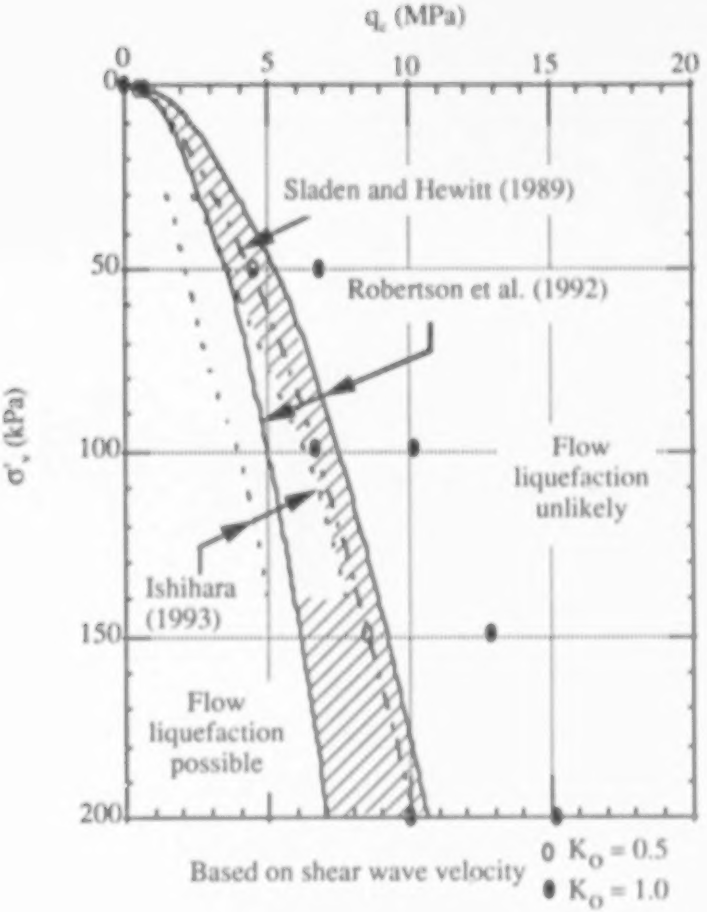

Figure 5.18 Comparison between contractive and dilative boundaries using CPT (q_c) based on shear wave velocity and those proposed by Sladen and Hewitt (1989), Robertson et al. (1992a) and Ishihara (1993).

CHAPTER 6

PRELIMINARY EVALUATION OF FLOW LIQUEFACTION OF SILTY SANDS USING SHEAR WAVE VELOCITY*

INTRODUCTION

Results presented in chapter 5 showed that shear wave velocities can be expressed in terms of void ratio and effective confining stresses for loose clean Ottawa sands using;

$$V_s = (100.2 - 57.3\,e)\,(\sigma'_a)^{0.125}\,(\sigma'_p)^{0.125} \qquad [5.9]$$

The following procedure was recommend in chapter 5 when evaluating the potential for flow liquefaction of a clean sand using *in-situ* shear wave velocity measurements;

---

* A version of this chapter has been accepted for publication: Sasitharan, S., Robertson, P. K. and Sego. D. C. 1993. Preliminary evaluation of flow liquefaction of silty sands using shear wave velocity. 46th Canadian Geotechnical Conference, Saskatoon.

- As an initial screening, the relationship shown in Figure 5.15 could be used to estimate whether a contractant, strain softening response will result from undrained compression loading.

- For a more detailed evaluation, a relationship between shear wave velocity, void ratio and effective confining stress based on a small number of undrained triaxial compression tests on very loose reconstituted samples for a given sand can be developed. The resulting relationship should look similar to that given in equation [5.9].

- Based on the steady state and shear wave velocity relationship of the reconstituted sand, the following can be developed.

$$\psi = \left(\frac{m_1}{m_2} - \Gamma\right) - \left(\frac{V_s}{m_2\,(\sigma'_a)^{0.125}\,(\sigma'_p)^{0.125}} - \lambda \ln p'_{ss}\right) \tag{5.14}$$

where;

ψ = the state parameter.

m_1 and m_2 = constants in equation 1.

λ = slope of the steady state line in e-lnp' space.

Γ = the intercept of the steady state line at $p'_{ss} = 1$.

- By substituting the *in-situ* stresses and *in-situ* shear wave velocity in equation [5.14], the state parameter can be calculated. Hence, the large strain response can be estimated (Been and Jefferies, 1985).

This approach will be limited to young, uncemented, uniform clean sand deposits. For aged or cemented sands, the relationship based on reconstituted samples may not be valid, since these factors can have a large effect on the shear wave velocity relationship. However, frequently it is the young, uncemented sand deposits that represent the highest risk of flow liquefaction. Therefore, this approach should be applicable to these deposits.

The above experimental investigation was based on clean Ottawa sand. Many natural sand deposits of sands contain some quantity of fines (< 74 μm). The fines can have an important effect on the sand fabric by developing a possible loose packing of the sand grains. Kuerbis and Vaid (1989) suggested that if the sand skeleton voids are filled with non-plastic fines then the resistance to liquefaction can remain unchanged. Georgiannous *et al.* (1990) found that undrained brittleness and strain at the phase transformation (contractive to dilative) increases as the clay content of a sedimented clayey sand increases from 4.6 to 10%, while the initial strain response was essentially unaffected by the clay content at identical intergranular void ratio. This trend reversed at clay fractions higher than 10%. Here, the intergranular void ratio is defined as

$$e_g = \frac{\text{Volume of voids + Volume of fines}}{\text{Volume of granular phase}} \tag{2.2}$$

In-situ testing such as SPT and CPT often show a substantial decrease in their measured penetration resistance with an increase in fines content for soils with the same liquefaction resistance. This rapid decrease in penetration resistance is probably due to the combined effects of increased soil compressibility and decreased drainage during penetration (Robertson *et al.* 1992). It has been common practice to correct the measured penetration resistance to an equivalent clean sand value (Seed *et al.*, 1984; Ishihara, 1985; Tokimatsu and Yoshimi, 1983; Olson and Farr, 1986; Shibata and Teparaksa, 1988). However, these corrections can become larger than the measured penetration resistance for sands with a high fines content.

This chapter presents results of an experimental study performed to evaluate whether the shear wave velocity can be used to identify the large strain behavior of a sand with a small amount of fines content (< 5%).

TESTING PROGRAM

A modified Wykeham Farrance strain controlled loading triaxial test apparatus and a triaxial cell in which bender elements were mounted within the top and bottom pedestals were used throughout the study. A detail description of the test apparatus is presented in chapter 5.

Ottawa (C 109) sand obtained from Ottawa, Illinois was used in this study. Ottawa sand is a uniform sand with a mean grain size (D_{50}) of 0.35 mm and comprised primarily of quartz with a specific gravity of 2.67. The maximum and minimum void ratios of the sand determined using the ASTM method D2049 are 0.82 and 0.50 respectively. Kaolinite with plastic index of 32%, liquid limit of 50% and specific gravity of 2.6 was used as the fine material in this study. 5% Kaolinite by weight was added to Ottawa sand in order to create a sand with some plastic fines. Uniform, very loose samples of Ottawa sand with 5% Kaolinite were prepared using the moist tamping technique described in chapter 3.

Very loose samples of Ottawa sand with 5% Kaolinite were then isotropically consolidated and sheared in triaxial compression. Test Dr4505k which contained 5% Kaolinite was consolidated to an isotropic consolidation stress of 450 kPa and sheared under drained conditions. Tests Un2505k, Un5005k and Un6505k were isotropically consolidated to 250, 500 and 650 kPa respectively and sheared under undrained conditions. Isotropic consolidation of these samples were performed in 100 kPa stress increments. During each of these stress increments, the shear wave velocity of the sample was measured. The shear wave velocities at various stress levels were also measured when the samples were sheared under drained or undrained conditions. When the sample was deformed to the ultimate critical/steady state, the shear wave velocity at steady state was also measured.

RESULTS AND INTERPRETATION

The deviator stress-axial strain response and resulting stress path for the monotonic undrained triaxial compression test of very loose samples of Ottawa sand with 5% Kaolinite sample consolidated to 650 kPa and void ratio of 0.800 is shown in Figure 6.1. The stress path shows a decrease in effective stress, until the process of deformation brings the sample to the steady state or critical state condition. The deviator stress-axial strain response of this sample reached a peak deviator stress at a very small axial strain (0.4-0.6 %). Then the sample showed a marked strain softening response with increase in axial strain until the shear stress stabilized at the steady state strength. A similar behavior, of strain softening before reaching a steady state, was also observed for very loose Ottawa sand with 5% Kaolinite samples consolidated to 505 kPa and void ratio of 0.817, 250 kPa and void ratio of 0.890, as shown in Figure 6.2 and 6.3, respectively.

Figure 6.4 shows the behavior of very loose Ottawa sand with 5% Kaolinite tested under monotonic drained conditions after consolidating to an isotropic stress of

450 kPa and void ratio of 0.830. The deviator stress increases steadily and the volume of the sand gradually decreases continuously until they reach constant values. The deformation under constant stress and volume was referred as steady state by Poulos *et al*. (1981).

The shear wave velocities measured during consolidation, shear loading and at steady state are summarized in Table 6.1. For clean sands the intergranular void ratio and conventional void ratio are the same, i.e., $e = e_g$ (See eqn. 2.2). Hence, equation [5.9], based on extensive testing (chapter 5) on clean Ottawa sand can be written in terms of intergranular void ratio as

[6.1] $$V_s = (100.2 - 57.3\, e_g)\, (\sigma'_a)^{0.125}\, (\sigma'_p)^{0.125}$$

The above equation can be normalized in terms of stresses as proposed by Robertson *et al*. (1992)

[6.2] $$V^*_{s1} = V_s \left(\frac{100}{\sigma'_a}\right)^{0.125} \left(\frac{100}{\sigma'_p}\right)^{0.125} = (100.2 - 57.3\, e_g)\, (100)^{0.25}$$

The variation of measured normalized shear wave velocity during consolidation for very loose Ottawa sand with 5% Kaolinite is shown in Figure 6.5. Also included in Figure 6.5 is equation [6.2] based on the tests using clean Ottawa sand with 0% fines. Although equation [6.2] was based on shear wave velocities measured for clean Ottawa sand, the relationship provides a reasonable fit to the velocities measured during consolidation of Ottawa sand with 5% Kaolinite.

Figure 6.6 compares the normalized shear wave velocities measured at steady state with the normalized shear wave velocity predicted by equation [6.2]. It may be noticed that equation [6.2] predicts the measured shear wave velocity at steady state quite closely. Hence, it appears that the fabric of very loose Ottawa sand with 5% Kaolinite had not changed appreciably during consolidation, shear loading and at steady state. This observation is consistence with the conclusion in chapter 5 that the fabric of very loose sand appears to be similar to the fabric at steady state.

Figure 6.7 shows the variation of intergranular void ratio with effective mean normal stress at steady state. Here, data are plotted with a logarithmic scale for the effective mean normal stress at steady state (p'_{ss}). It may be noticed that the e_g-log p'_{ss} relationship can be approximated by a straight line in this logarithmic plot. The slope of this straight line is equal to 0.056 and the intercept of this straight line at p'_{ss} = 1 kPa is equal to 0.934. Hence, the e_g-log p'_{ss} relationship can be written as

[6.3] $$e_g = 0.934 - 0.056 \log p'_{ss}$$

[6.4] $$e_g = 0.934 - 0.024 \ln p'_{ss}$$

Hence, λ and Γ in equation [5.14] take values of 0.024 and 0.934, respectively and it was shown that m_1 and m_2 take values of 100.2 and 57.3, respectively. Therefore, the contractive/dilative boundary ($\psi = 0$) can be calculated using equation [5.14] with the known values of λ, Γ, m_1 and m_2.

In chapter 5 it was shown that consolidation state had only a small effect in the net contractive/dilative boundary when the vertical effective stress is less that than 200 kPa (Fig. 5.14). Hence, the net contractive/dilative boundary can be conservatively calculated for one consolidation state (σ'_a/σ'_p) = K_o =0.5.

Figure 6.8 compares the net contractive/dilative boundary calculated using equation [5.14] for Ottawa sand with 5% Kaolinite with the contractive/dilative boundary of clean Ottawa sand in chapter 5. It may be noticed that the contractive/dilative boundary for clean Ottawa sand is similar to the boundary for Ottawa sand with 5% Kaolinite fines.

SUMMARY AND CONCLUSIONS

An experimental study has been presented for shear wave velocity interpretation of clean Ottawa sand deposits compared to that of Ottawa sand with 5% Kaolinite fines. Uniform Ottawa sand samples with 5% Kaolinite fines were prepared very loose by the moist tamping technique. Shear wave velocities were measured on the samples during consolidation, shear loading and at steady state.

Results presented in this study shows that;

(1) The shear wave velocity of Ottawa sand with a small amount of fines (< 5%) can be expressed by the same relationship as clean Ottawa sand in terms of confining stress and intergranular void ratio.

(2) The very loose sand fabric appears to remain essentially unchanged during consolidation, shear loading and at steady state.

(3) The contractive/dilative boundary suggested in chapter 5 for clean Ottawa sand is similar to the boundary for Ottawa sand with 5% Kaolinite fines.

The present study and above conclusions are limited to Ottawa sand with fines content up to 5%. Further similar work is underway to clarify the above conclusion for sands with larger amounts of fines.

REFERENCES

Georgiannou, V. N., Burland, J. B. and Hight, D. W. 1990. The undrained behavior of clayey sands in triaxial compression and extension. Geotechnique, **40**: 431-449.

Ishihara. K. 1985. Stability of natural deposits during earthquakes. Proc. of 11th international conference on soil mechanics and foundation engineering, San Francisco, vol. 1. pp 312- 376.

Kuerbis, R.H. and Vaid, Y.P. 1989. Undrained behavior of clean and silty sands. Proc. of discussion session on influence of local conditions on seismic response, XII International Conference on Soil Mechanics and Foundation Engineering, Rio de Janeiro, pp. 91-100.

Olsen, R.S., and Farr, J.V. 1986. Site characterization using the cone penetration test. Proc. In-situ 86, ASCE specialty conference, Blacksburg, VA.

Poulos, S. 1981. The steady-state of deformation. Journal of Geotechnical Engineering American Society of Civil Engineering, **107**(5): 553-561.

Robertson, P.K., Woeller, D.J. and Finn, W.D.L. 1992. Seismic cone penetration test for evaluating liquefaction potential under cyclic loading. Canadian Geotechnical Journal, **29**: 686-695.

Seed, H.B., Idriss, I.M. and Arango, I. 1983. Evaluation of liquefaction potential using field performance data. Journal of Geotechnical Engineering American Society of Civil Engineering, **109**(3): 458-482.

Seed, H.B., Tokimatsu, K., Harder, L.F. and Chung, R.M. 1984. The influence of SPT procedures in soil liquefaction resistance evaluations. Report No. UBC/EERC-84/15, Earthquake engineering research center, University of California, Berkeley, California.

Shibata, T. and Teparaksa, W. 1988. Evaluation of liquefaction potential of soil using cone penetration tests. Soils and Foundation, **28**(2); 49- 60.

Tokimatsu, K. and Yoshimi, Y. 1983. Empirical correlation of soil liquefaction based on SPT N-values and fines content. Soils and Foundations, **23**(4):

Table 6.1 Summary of Test Results.

Un6505k

	σ_1 (kPa)	σ'_3 (kPa)	V_s (m/s)	e_g
Consolidation	50.9	50.9	144	0.832
	151.2	151.2	186	0.822
	252.7	252.7	210	0.815
	352.2	352.2	230	0.810
	451.5	451.5	243	0.806
	556.0	556.0	257	0.803
	650.4	650.4	268	0.800
undrained loading	372.3	155.7	237	0.800
	263.5	102.1	219	0.800
	204.3	73.6	199	0.800
	189.9	62.5	190	0.800
	199.8	74.2	187	0.800
	173.2	59.0	186	0.800
	168.6	56.7	186	0.800
steady state	167.2	56.7	184	0.800

Un5005k

	σ_1 (kPa)	σ'_3 (kPa)	V_s (m/s)	e_g
Consolidation	53.6	53.6	138	0.852
	150.6	150.6	180	0.840
	253.3	253.3	206	0.831
	300.8	300.8	221	0.827
	356.3	356.3	229	0.825
	450.0	450.0	246	0.820
	505.1	505.1	256	0.817
undrained loading	485.4	274.5	239	0.817
	319.5	140.6	206	0.817
	234.7	96.3	189	0.817
	179.6	71.2	175	0.817
	143.8	57.3	167	0.817
	133.3	52.0	165	0.817
	135.2	52.6	169	0.817
steady state	136.2	52.6	166	0.817

Un2505k

	σ_1 (kPa)	σ'_3 (kPa)	V_s (m/s)	e_g
Consolidation	50.1	50.1	145	0.908
	150.0	150.0	185	0.899
	250.4	250.4	204	0.890
undrained loading	276.8	172.5	195	0.890
	155.7	72.3	165	0.890
	90.2	35.6	133	0.890
	66.4	23.4	118	0.890
	44.2	14.6	103	0.890
	38.2	11.7	96	0.890
	34.3	9.4	96	0.890
	32.6	8.2	95	0.890
	31.2	7.6	93	0.890
	28.8	5.9	94	0.890
	29.5	7.1	98	0.890
steady state	24.4	7.1	98	0.890

Dr4505k

	σ_1 (kPa)	σ'_3 (kPa)	V_s (m/s)	e_g
Consolidation	49.8	49.8	146	0.856
	151.3	151.3	175	0.846
	249.9	249.9	197	0.839
	350.3	350.3	228	0.834
	450.5	450.5	233	0.830
drained loading	1010.4	448.7	257	0.820
	1084.2	448.7	255	0.812
	1177.0	448.7	251	0.801
	1215.5	448.7	282	0.796
	1241.5	450.4	272	0.793
	1245.2	450.4	293	0.792
steady state	1248.8	450.4	306	0.791

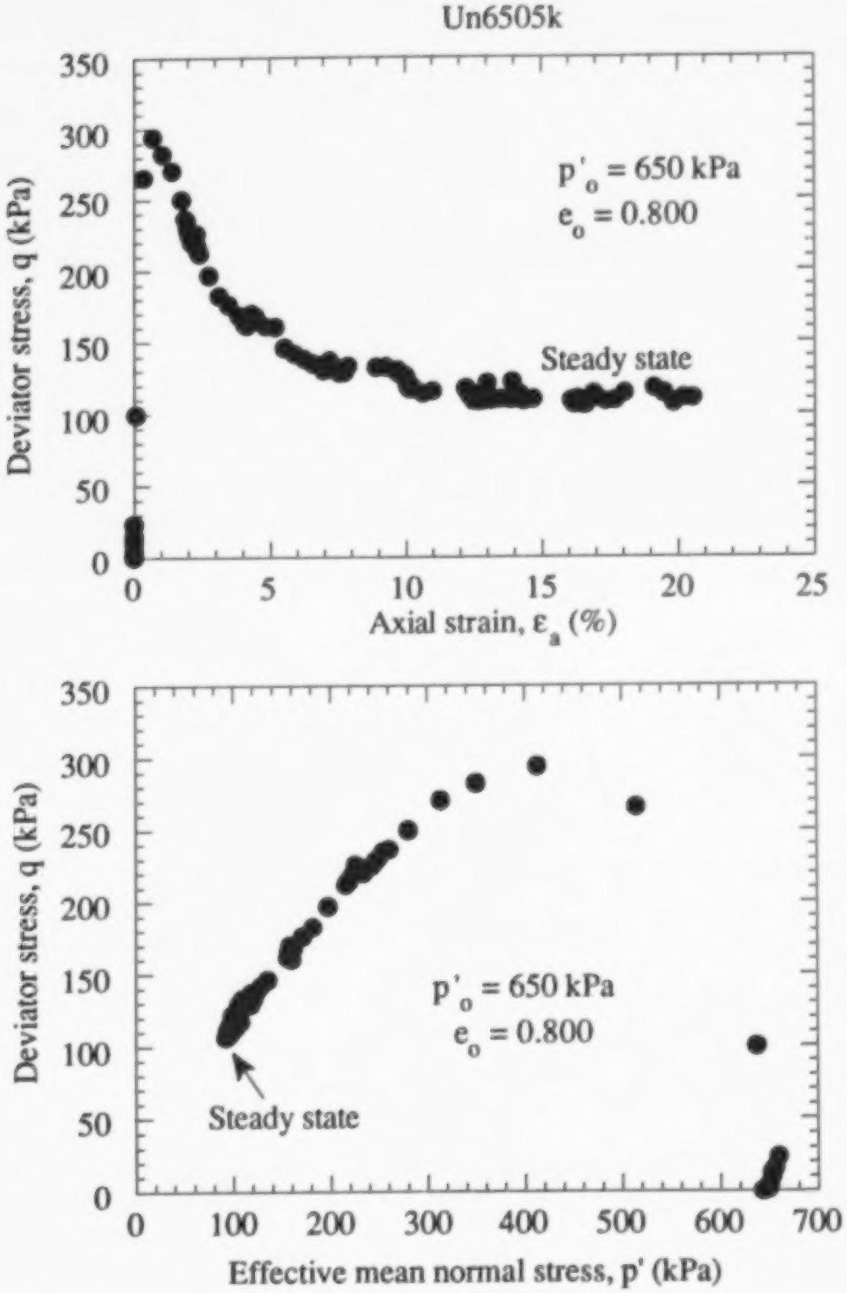

Figure 6.1 The stress-strain behavior and resulting stress path for the monotonic undrained triaxial compression test performed on very loose Ottawa sand with 5% Kaolinite (isotropic consolidation stress of 650 kPa and void ratio of 0.800)

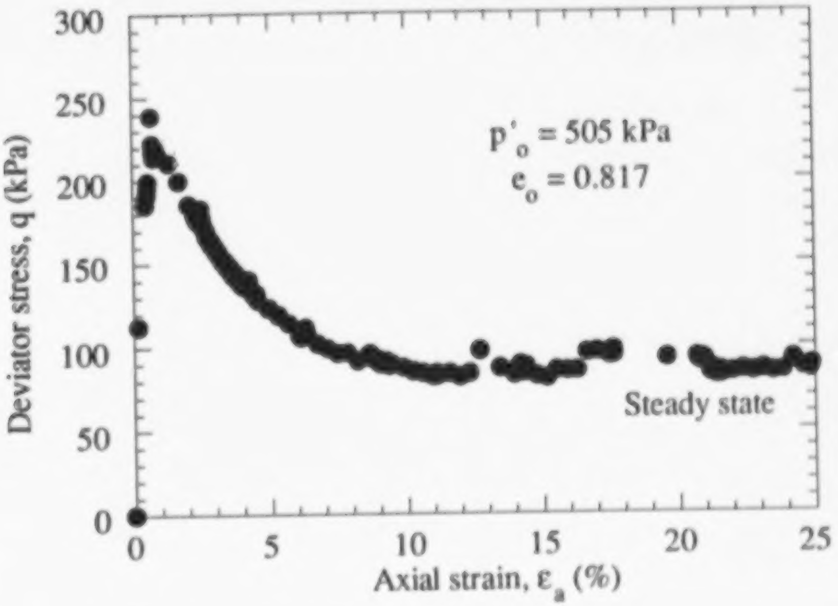

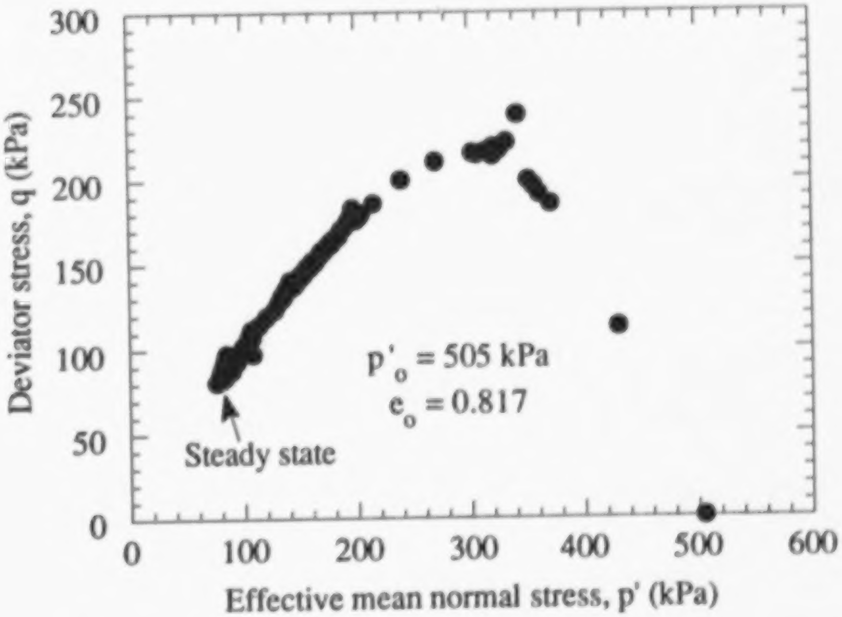

Figure 6.2 The stress-strain behavior and resulting stress path for the monotonic undrained triaxial compression test performed on very loose Ottawa sand with 5% Kaolinite (isotropic consolidation stress of 500 kPa and void ratio of 0.817)

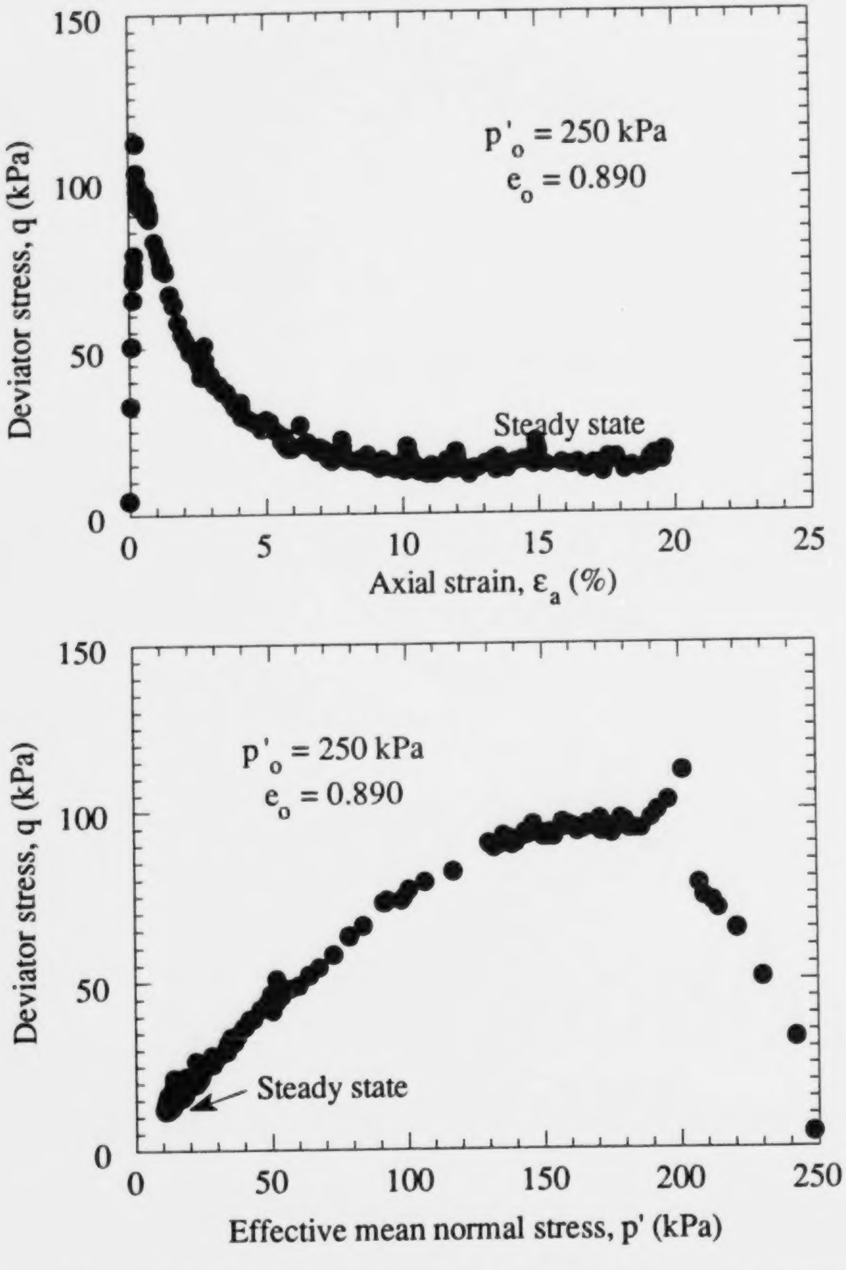

Figure 6.3 The stress-strain behavior and resulting stress path for the monotonic undrained triaxial compression test performed on very loose Ottawa sand with 5% Kaolinite (isotropic consolidation stress of 250 kPa and void ratio of 0.890)

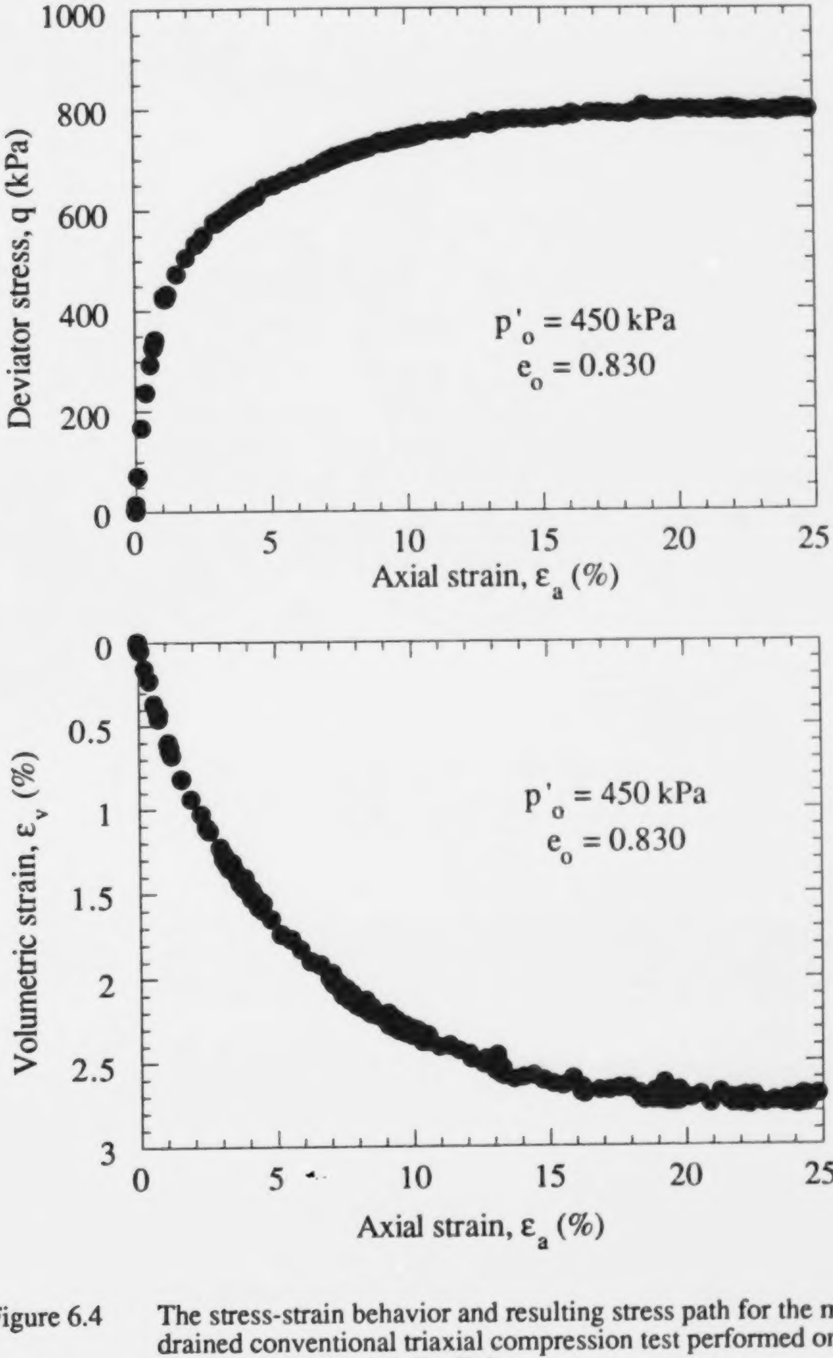

Figure 6.4 The stress-strain behavior and resulting stress path for the monotonic drained conventional triaxial compression test performed on very loose Ottawa sand with 5% Kaolinite.

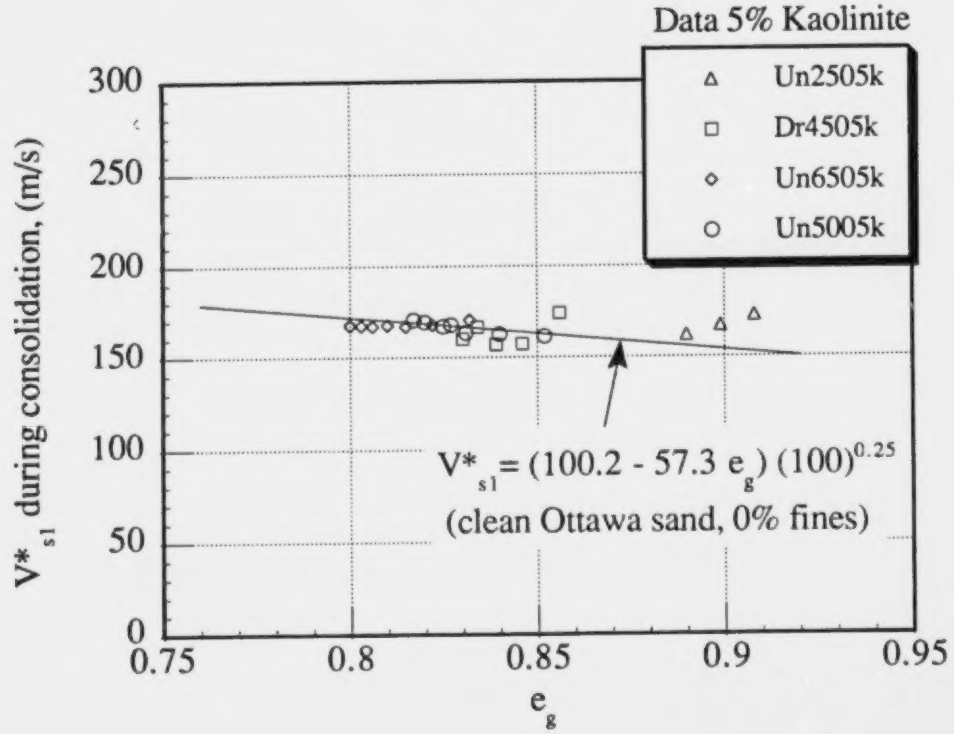

Figure 6.5 Normalized shear wave velocity during consolidation for very loose Ottawa sand with 5% Kaolinite.

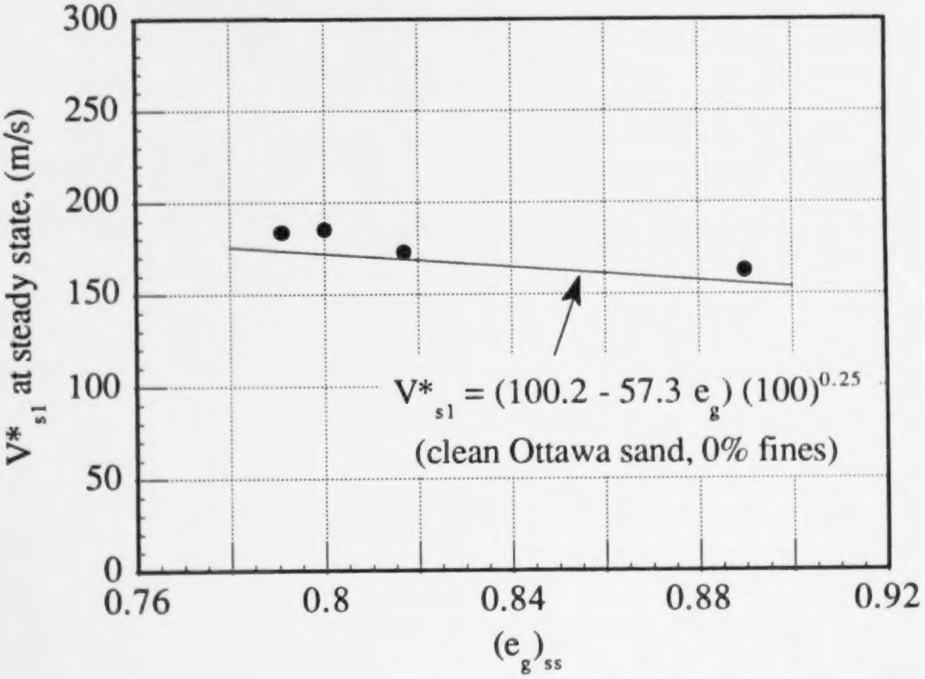

Figure 6.6 Normalized shear wave velocity at steady state vs. intergranular void ratio for Ottawa sand with 5% Kaolinite.

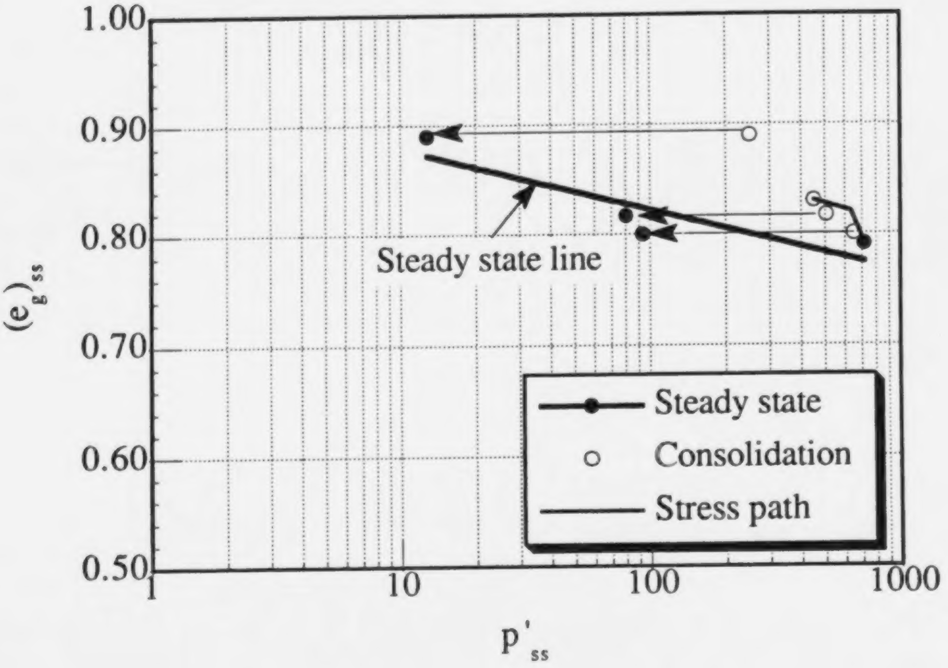

Figure 6.7 Steady state line in terms of intergranular void ratio against logarithm of effective mean normal stress for Ottawa sand with 5% Kaolinite.

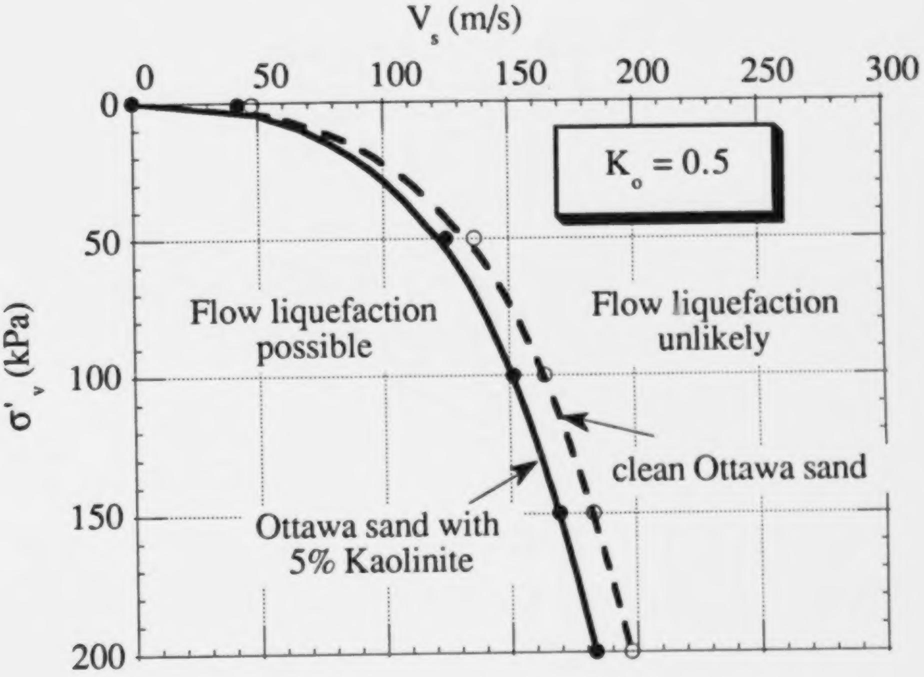

Figure 6.8 Boundary between contractive and dilative behavior at large strain based on shear wave velocity for clean Ottawa sand and Ottawa sand with 5% Kaolinite.

CHAPTER 7

FABRIC STUDIES ON VERY LOOSE SAND

INTRODUCTION

Only a limited number of studies relating the mechanical behavior of cohesionless materials to the fabric has been performed in the past twenty years. Various definitions of fabric exist in the literature. Geologists and soil scientists separate 'fabric' meaning particle arrangement and orientation from the term 'structure' which combines the fabric and the size and shape of the individual grains and void within a soil. The engineering community tends to use these terms inter changeably (Mahmood and Mitchell, 1974). In this study fabric is defined as the sand particle arrangement and orientation. Hence, the fundamental parameters needed to describe fabric would be number and orientation of contact, displacement of individual particles and distribution of contact force within the soil (Oda, 1974).

Oda and Konishi (1974) testing photo elastic cylinders and sand in simple shear apparatus showed that the normal to the contact planes tend to reorientate towards the maximum principal stress axis during an increase of shear force. The continuous reconstruction of the initial fabric with increasing deformation has been attributed to sliding and rolling of the particles relative to one another in many theoretical works (Skinner, 1969; Oda, 1972; Konishi *et al.* 1982). Horn (1965) stated that "deformation occurs as a relative motion between instantaneously rigid groups of particle, these groups continuously reforming by division and coalescence". Arthur *et al.* (1977) suggested that a distribution of isolated local failures will occur during overall strain hardening. These local failures are strain softening and can be visualized as the shedding of load carried by grains involved onto other elements of the granular structure within the soil. Strain hardening is brought about by some of the rearrangements of particle geometry and particle contact following local failures.

Various ways of quantifying the fabric have been put forward. Oda (1974, 1982) introduced a fabric tensor that is closely related to the three distributions of the contact normal in the soil assembly. He assumed that for an assembly of spheres the corresponding fabric is represented by the distribution and geometrical arrangement of lines connecting centers of adjacent particles that are in contact. Nemate Nasser (1982) showed that different fabric tensors can be obtained according to assumptions made for the microscopic or macroscopic state. However, he agrees that for non complex shear loading the fabric can be completely defined by the distribution of the orientation of the unit contact normal at the active contact points.

This chapter describes some qualitative observations of very loose sand grain arrangement after consolidation and at steady state. Based on these observed fabrics at consolidation and steady state, an explanation for the collapse of sands behavior is postulated.

TEST PROGRAM

Undisturbed segments of Ottawa sand samples for scanning electro microscope analysis were formed by freezing the sand samples with no disturbance. The sand sample will remain undisturbed during freezing provided the water can freely flow away from the advance freezing front and the volume of water expelled equals the volume of the ice which develops in pores. Clean sands have sufficiently high permeability to allow drainage and can be frozen without disturbance (Davila *et al.*, 1992; Sasitharan *et al.*, 1992). A loose sand sample was formed using moist tamping technique described in chapter 3. After the sample was saturated and consolidated to 350 kPa, the sample was frozen using the freezing technique described in chapter 2. The frozen sample was then removed from the triaxial cell and was cut into sections. The middle section of the triaxial sample was analyzed using the scanning electron microscope to study the grain arrangement (fabric) after consolidation.

Another moist tamped very loose Ottawa sand sample was prepared, saturated and consolidated to 350 kPa. This sample was sheared undrained until the sample reached steady/critical state. When the sample was deforming at steady state, the loading was stopped. Then the back pressure applied to the sample was increased to the current steady state excess pore pressure. The drainage value was opened and the sample was brought to a free draining condition without any change in stresses and void ratio. Then the sample with steady state stresses and void ratio was frozen using the same procedure described in chapter 2. The frozen steady state sample was then removed from the triaxial cell and was cut into sections. The middle section of the triaxial sample was analyzed using the scanning electron microscope to study the grain arrangement (fabric) at steady state.

RESULTS OF SCANNING ELECTRON MICROSCOPE ANALYSIS

Figure 7.1 shows packing of particulate group of loose Ottawa sand after consolidation. It may be noticed that very loose Ottawa sand contains holes within its grain arrangement. The hole shown in this figure is stable under static conditions. However, the stability would be rather marginal if the particulate group were to deform during shear loading. During shear loading, at certain load and deformation these particles may collapse into these holes and due to this particle collapse suddenly the sample would experience large measurable external deformations.

Figure 7.2 shows packing of particulate group of loose Ottawa sand at steady state. It may be noticed that sand grains are arranged in a critical packing. This particle arrangement shows how particles deform at steady state as a unit without any increase or decrease in external measured volume and stresses.

DISCUSSION

When deformation occurs in a granular sand under unequal principal stresses, the initial fabric changes with increasing axial strain in order to withstand the continuously increasing stresses. In this case relative displacement constitutes grain particle rearrangement and these particles must come to contact with each other by newly formed contact points or surfaces with a gradual decrease of contact that previously existed.

The most important problem concerning the microscopic picture of the deformation of randomly packed granular sand is the mechanical role of sliding and rolling of grains during deformation to form new contact points. It may be observed from Figure 7.1 that very loose sand grains arrangement contains holes. When the particles deform under load they roll and slide to form a new grain particle arrangements. At certain loads due to the deformation or stresses it is possible that some of these sand grains would start to collapse into these holes.

If this grain collapse is rapid and the rate of collapse is greater than the permeability of the sand, the sand particles may experience an internal undrained condition although the external drainage is opened and water could flow freely. Hence, the pore pressure inside the sample increases. Due to increase in pore pressure the effective stress decreases. Then at this new decreased effective stress more sand grains may collapse, hence, the pore pressure continues to increase and the effective stress continues to decrease. This process may continue until the effective stress and grain structure collapse reaches a stable condition. A stable stress and deformation state was defined as steady state by Castro (1969).

If the rate of particle collapse is slower than the permeability of the sand then there would be internal drained condition and the sand grains will form a more stable structure as it deforms to the ultimate steady state. Whether the sand deforms to the ultimate state by strain softening or by strain hardening depends on the rate of loading and sand permeability.

At the ultimate steady/critical state the sample deforms with constant external volume and stresses, i.e., the sand grains had rearranged such that with further straining, the newly formed steady state grain arrangement may start to deform as a unit rather than forming new contacts. Hence, the external volume remains constant. There are no new contacts formed during the deformation, hence, the internal stresses at the grain contacts remain constant. Therefore, the external stresses also remain constant during the steady state deformation.

CONCLUSIONS

Based on the preliminary study of the loose sand fabric, the following conclusions can be made;

(1) One dimensional freezing technique used in this study yielded good quality samples for scanning electron microscope study.

(2) The very loose Ottawa sand after consolidation shows holes in the grain arrangement that provides an explanation for collapse and flow behavior of very loose sand.

(3) At steady state, very loose Ottawa sand shows a unique grain arrangement. The sand grain arrangement is such that it can deform as a unit rather than forming new grain contacts.

All the above observations were based on qualitative analysis of the scanning electron microscope photographs. Currently there are image analyzing programs that can provide quantitative analysis of the sand grain arrangements. The observations made in the present study are limited to small representative specimens (normally 15mm square). However, this may not be a representative quantitative measure of the fabric in large samples that may exhibit heterogeneous fabric. Hence, there were no quantitative analysis performed in this study. It is recommend to obtain small representative specimens from different location of the large sample, hence, obtain quantitative values for the sand fabric through out the sample.

Further research is recommend to study the fabric formed by different sample preparation technique such as moist tamping, water pluviation and dry deposition. To verify the uniqueness of the steady state, the steady state fabric achieved from these sample preparation techniques can be compared.

REFERENCES

Davila , R. S., Sego, D. C. and Robertson, P. K. 1992. Undisturbed sampling of sandy soils by freezing. 45th Canadian Geotechnical Conference, Toronto, paper 13A.

Konishi, J., Oda, M. and Nemat-Nasser, S. 1982. Inherent anisotropy and shear strength of an assembly of oval cross-section rods. IUTAM conference on deformation and failure of granular materials, Delft.

Mahmood, A. and Mitchell, J.K. 1974. Fabric property relationships in fine granular materials. Clays and Clay Minerals, **22**(516): 397 - 408.

Oda, M. and Konishi, J. 1974. Microscopic deformation mechanism of granular material in simple shear. Soils and Foundations, **14**(4): 25 - 38.

Oda, M. 1972. The mechanism of fabric change during compressional deformation of sand. Soils and foundations, **12**(2): 1 - 18.

Oda, M. 1974. A mechanical and statistical model of granular material. Soils and foundations, **14**(1): 13 - 27.

Oda, M. 1982. Fabric tensor for discontinuous geological materials. Soils and foundations, **22**(4): 96 - 108.

Sasitharan, S., Robertson, P. K. and Sego. D. C. 1992. Sample disturbance from shear wave velocity measurements. 45th Canadian Geotechnical Conference, Toronto. 23:1-23:7.

Skinner, A.E. 1969. A note on influence of inter particle friction on shear strength of a random assembly of spherical particles. Geotechnique, **19**(1): 150 - 157.

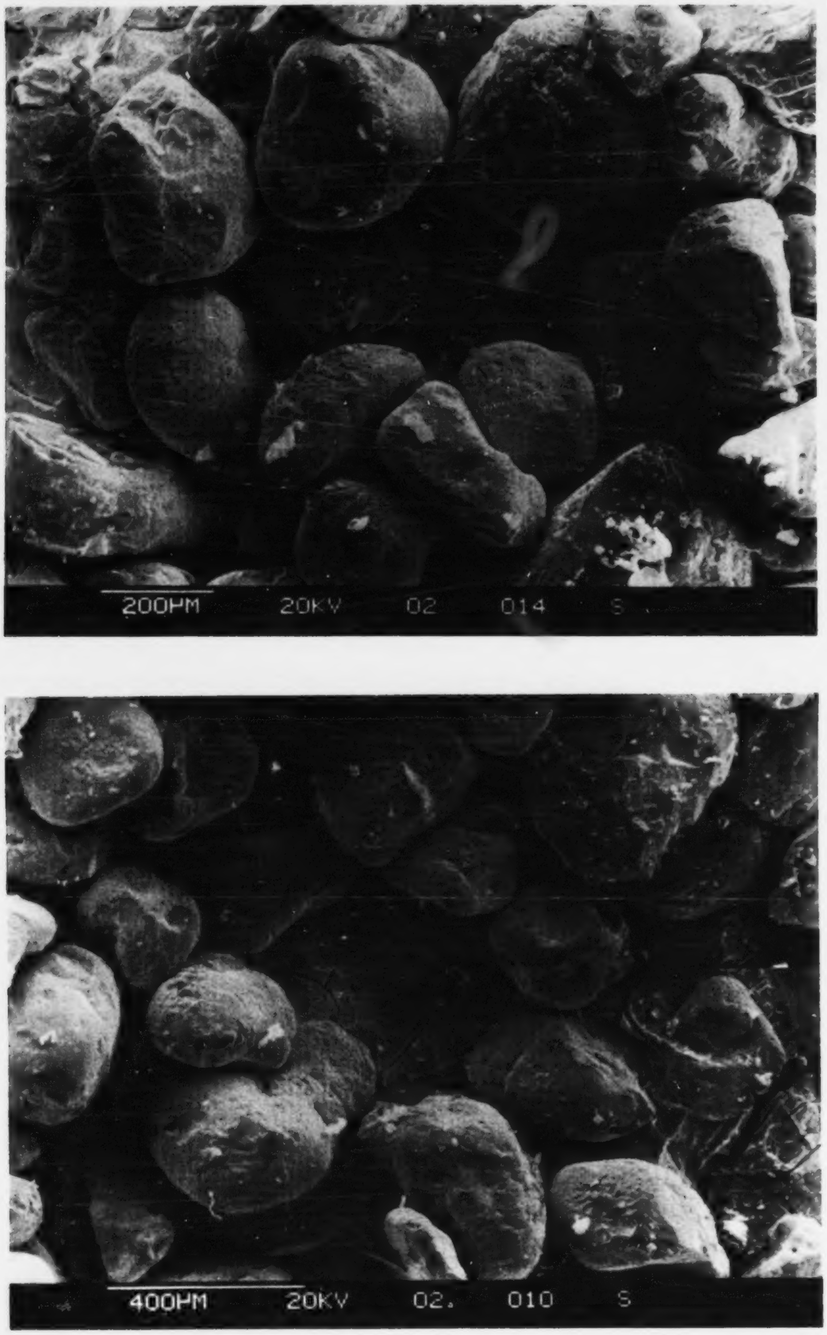

Figure 7.1. SEM photographs of very loose Ottawa sand after consolidation.

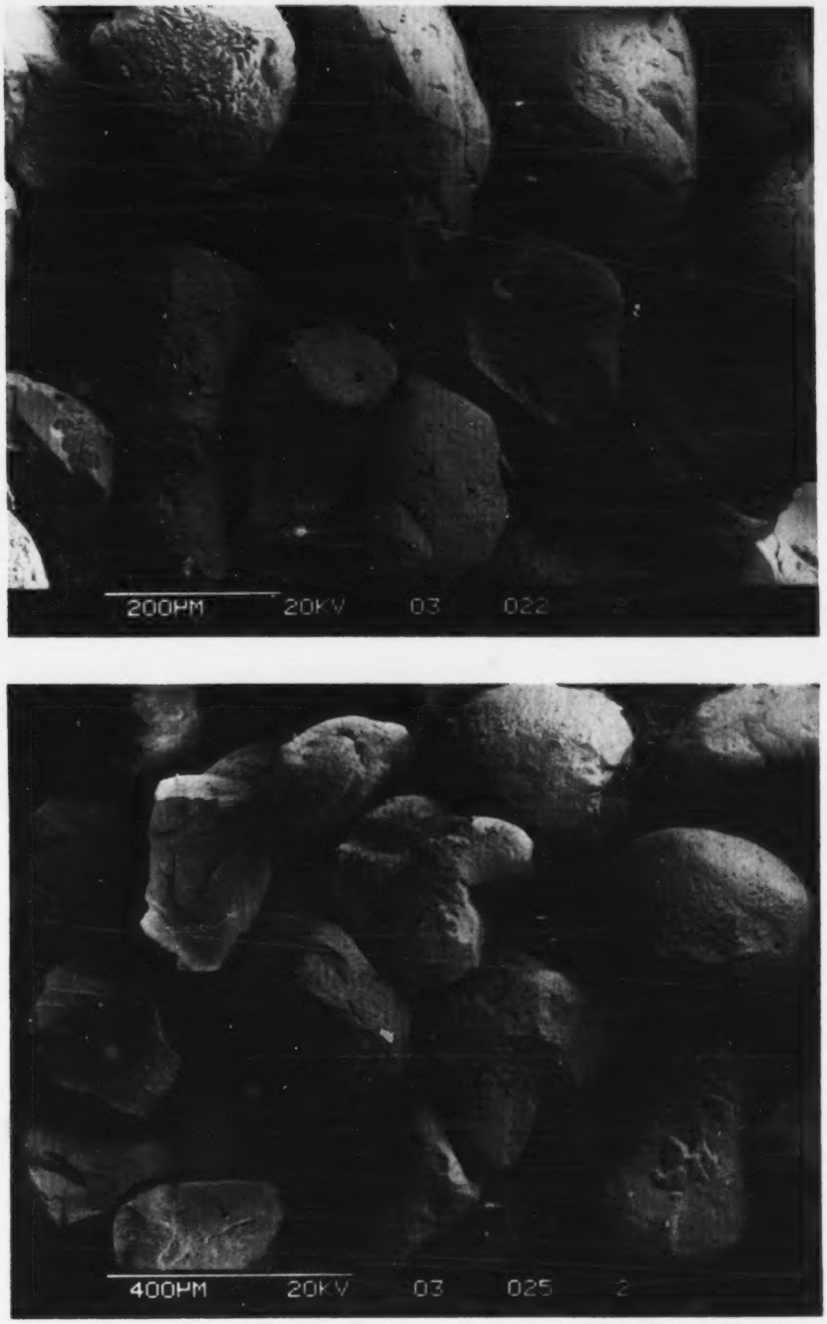

Figure 7.2. SEM photographs of very loose Ottawa sand at steady state.

CHAPTER 8

SUMMARY AND CONCLUSIONS

The objective of the present research was to investigate the collapse and flow liquefaction of very loose sand and to identify sands that can collapse and flow when loaded slowly (drained) or rapidly (undrained).

In the first chapter, attention was paid to the fact that very loose sand can not be sampled for testing purpose without inducing void ratio change and particle rearrangements by conventional sampling techniques. Artificial *in-situ* ground freezing which can be used to obtain undisturbed samples of very loose sand was described. However, there is still concern regarding the possibility of disturbance during the freezing and thawing of these samples. A laboratory study was performed to evaluate the use of shear wave velocity measurements to detect sample disturbance due to freezing and thawing of cohesionless soils. Samples prepared with different amounts and type of fines were frozen using uniaxial freezing techniques and subsequently thawed. Shear wave velocity measurements were made before and after freezing and thawing of the reconstituted samples. The measured shear wave velocities were unchanged for samples that did not heave (undisturbed) during the freeze-thaw cycle. Samples that heaved (disturbed) showed an associated change in shear wave velocity. Hence, measurement of shear wave velocities *in-situ* and in the laboratory has the potential to identify sample disturbance in granular soils.

Since the cost of in-situ ground freezing is high, the need to obtain high quality undisturbed sample would depend on the project requirements. Hence, the next obvious step was to study collapse behavior by reconstituting very loose samples. Collapse behavior of these reconstituted samples was studied by performing specially designed stress path testing in chapter 3. Results from this test program and previously published data showed that a state boundary could be defined when a cohesionless material moves from peak to steady state along a constant void ratio stress path regardless of whether it is loaded drained or undrained. Further, it was demonstrated that the state boundary represents a surface in the effective mean normal stress-deviator stress-void ratio space. Hence, flow slides and liquefaction can be initiated when the stress path followed during either drained or undrained loading attempts to cross this state boundary surface.

An experimental study relating drained and undrained behavior of loose saturated sand was presented in chapter 4. It was shown that the post peak portion of undrained stress paths travels along a state boundary and that the state boundary could be approximated by a straight line. The slope of this straight line appeared to stay constant for very loose sand. There are potentially an infinite number of these lines, which form a three dimensional surface in deviator stress-effective mean normal stress-void ratio space. Previously published results by various researchers were used to confirm the existence of the state boundary. This surface was mathematically defined in deviator stress-effective mean normal stress-void ratio space. Loose saturated sand samples loaded drained from a stress state on or very close to the state boundary surface essentially travel along the state boundary surface. Loose saturated sand samples loaded drained from a stress state below the state boundary reach the state boundary and then essentially travel along the state boundary to reach the steady state or critical state.

The initial state was used to identify sand that could show collapse behavior in chapter 5. In this chapter, an experimental study of shear wave velocity interpretation for a clean sand based on steady/critical state concepts was presented. Results presented in this study showed that shear wave velocities could be expressed in terms of void ratio and effective confining stresses for loose sand. Hence, the large strain behavior of a uniform sand deposit could be estimated using shear wave velocity measurements combined with a knowledge of the *in-situ* effective mean normal stress. Further, it was shown that, when the effective vertical stress is less than 200 kPa, the strain softening or strain hardening (net contractive/net dilative) boundary is only slightly influenced by the consolidation state. Hence, for shallow depths the strain softening/hardening behavior of a clean sand could be evaluated using *in-situ* shear wave velocity. Based on these findings, a method to evaluate the potential for flow liquefaction using shear wave velocity measurements was presented. Further, it was shown that this method was consistent with the existing indirect *in situ* measuring methods.

Many natural deposits contain some quantity of fines (< 74 μm). Fines can affect the sand fabric. Hence, an experimental study of shear wave velocity interpretation for a sand with small amount of fines (< 5%) based on steady/critical state concepts was carried out. Results presented in chapter 6 showed that shear wave velocity of sands with a small amount of fines (< 5%) could be expressed by essentially the same relationship as a clean sand in terms of confining stress and inter granular void ratio. Further, by comparing the shear wave velocities measured during consolidation, shear loading and at steady state it was shown that very loose sand fabric appears to remain essentially unchanged during the entire loading process. The contractive to dilative boundary suggested in chapter 5 for clean sand could also be used for sands with small amount of fines (< 5%) without any corrections for fines content. Note: For sands with small amount of fines (< 5%), the shear wave velocity and steady state line were expressed in terms of inter granular void ratio and confining stresses .

Finally, the fabric of very loose sand was studied. By comparing sand fabric after consolidation and at steady state qualitatively it was shown that loose sand fabric contains holes. Collapse and flow deformation could occur when sand grain falls into these holes.

RECOMMENDATIONS FOR FUTURE WORK

The present study has attempted to investigate experimentally the collapse behavior of very loose sand and identify sands that can show collapse and flow behavior. However, the present study has neither covered all the natural deposits that can show collapse behavior nor uniquely answered all the questions relating to flow and collapse behavior. In this view it would be highly desirable to extend the present work in the following areas.

(1) All the collapse behavior investigations were performed on reconstituted samples. It is recommened to repeat the tests described in this study on very loose natural samples obtain by *in-situ* ground freezing.

(2) Collapse behavior of sand containing more than 5% fines was not investigated in this study. It is recommend to perform similar study with various amounts

of plastic fines (e.g., Kaolinite) and non plastic fines (e.g., crushed silica) at percentage greater than 5%.

(3) Study fabric rearrangement during collapse by performing constant deviator stress triaxial tests on dry sand.

(4) Extent the state boundary surface concept for coarse grain natural materials such as mine waste , gravel.

(3) Extent the shear wave velocity interpretation presented in chapter 5, to various other natural sands.

(4) Verify the shear wave velocity interpretation presented in chapter 5 for sands containing high fines content (both plastic and non plastic fines).

(5) Compare the shear wave velocity interpretation presented in chapter 5 with existing *in-situ* shear wave velocity measurements of deposits that have showed flow liquefaction behavior.

(6) Quantitative fabric studies to investigate the effect of initial grain arrangement on collapse behavior.

APPENDIX A

EXPERIMENTATION

EXPERIMENTATION

This appendix describes the testing apparatus and laboratory procedures that were utilized in this study. Specially detail explanation of the loading system, sample preparation methods and testing procedure for various tests are given.

TESTING APPARATUS

Introduction

Soils are tested under triaxial condition in order to simulate field loading conditions or to study fundamental material response. Most often, triaxial tests are used to determine shear strength parameters when the vertical stress increase while the horizontal stress is kept constant. The vertical stress can be increased either by monotonic axial loading or by straining the soil continuously. Monotonic axial loading under stress control condition had been used to study the time dependent deformation of soils. Earthquake effects on soils are simulated by stress controlled cyclic axial loading. On the other hand, axial loading under strain control condition can be used to study post peak behavior. The use of advanced electronic equipment will enable the laboratory soil sample to be subjected more closely to the same stresses and stress changes as in the field under triaxial conditions (Lade et al. 1976; Atkinson et al. 1988; Sasitharan 1989).

A electro-pneumatic cyclic triaxial loading system was first developed by Chan (1981) using a function generator to control a electro-pneumatic pressure transducer. However, a computer controlled electro-pneumatic loading system can simulate any described loading patterns. Such a computer controlled electro-pneumatic loading system has been developed at University of Alberta. This loading system permits stress controlled monotonic loading or cyclic loading, enables to switch from monotonic loading to cyclic loading or vice-versa way into the test. Further, this system also permits to change the amplitude and frequency of cyclic loading, the rate of monotonic loading in a single test. This system combined with Wykeham Farrance loading machine can be used to follow strain control loading stress paths where major and minor principal stress changes continuously.

Loading System

The schematic of the loading system is shown in figure (2.1). The computer (IBM 286) is connected to a Metrabyte 16/16F card. This card is capable of converting signals from Digital to Analog (D/A) or vice-versa (A/D). The computer interacts with a D/A portion of the card and provides a described loading pattern as a electrical current to the electro-pneumatic pressure transducer (E/P). The E/P is a force-balanced instrument. The force of the out put pressure acting over a nozzle is balanced by the force produced on the input coil by interaction of the in put current and the permanent magnetic field. An increases in the current to the coil creates a down ward thrust, which in turn restricts the flow of air out of the nozzle, causing an increase in the out put pressure. The out put pressure is directly proportional to the change in input electrical current up to 100 kPa. This relatively low pressure and very limited flow capacity is then amplified by the 1:4 pneumatic amplifier, which is a pneumatic force balance instrument that uses 1:4 ratio of diaphragm area. A restriction valve is introduced before the volume booster relay (1:2) to reduce over shoots of the wave traces. The volume booster relay (1:2) further increases the pressure by a factor of two: more importantly it relays the out put pressure that now has a larger flow capacity. The maximum out put pressure from the volume booster relay (1:2) is about 800 kPa which is large enough to test any soils under normal working confining pressure (approximately < 700 kPa).

Load Control Axial Loading

The volume booster relay (1:2) supplies pressure to the one chamber of the air piston. For the cyclic loading, the air piston should operate in a push and pull mode. Therefore, the non cyclic(steady) side of the air piston is pressured through another volume booster relay (1:1) controlled by a manual pressure regulator (Figure A.1).

Most of the soil tests are performed after consolidating the soil at a confining pressure. By adjusting the steady side air pressure, the soil samples can be isotropically or anisotropically consolidated.

Isotropically or anisotropically consolidated samples can now be loaded by increasing the supply pressure from the volume booster (1: 2) in many different loading patterns. The time dependent deformation of soil can be studied by

(1) loading the soil sample at different monotonically increasing loading rate.

(2) loading the soil sample to different load levels and keeping it constant in a single test. The load increments can be performed automatically at described time intervals.

The soil sample can also be subjected to cyclic loading

(3) until it collapses or the amplitude and frequency of the cyclic loading can be changed after certain number of cycles.

(4) In a sample that exhibits cyclic mobility, the cyclic loading can be stop after sufficient number of cycles and the sample may be loaded monotonically to the steady state.

Most importantly all these loading. i.e., time dependent loading and cyclic loading can be performed in a single test.

Strain Control Axial Loading

In addition the loading system combined with Wykeham Farrance loading machine can be used to shear the triaxial samples along stress paths where the horizontal stress (σ'_h) and the vertical stress (σ'_v) changes continuously under strain controlled loading conditions. Wykeham Farrance loading machine is modified such that dead loads can be added at the top of the loading frame. Hence the triaxial sample can be isotropically or anisotropically consolidated by adding dead loads at the top of the loading frame. Now the isotropically or anisotropically consolidated samples can be sheared along various desired stress paths by shearing the sample under strain controlled loading.

Along a stress path the changes in vertical stress ($\Delta\sigma'_v$) and horizontal stress ($\Delta\sigma'_h$) can be related by

$$\Delta\sigma'_h = S\,\Delta\sigma'_v$$

The constant 'S' is characteristic of the desired stress path. For example this constant 'S' equals - 0.5 for the constant mean normal stress path, i.e.,

$$\Delta\sigma'_h = -0.5\,\Delta\sigma'_v$$

In a triaxial test the horizontal stress is given by

$$\sigma'_h = P_C - P_B$$
$$\Delta\sigma'_h = \Delta P_C - \Delta P_B$$

where P_C= Cell pressure

P_B= Back pressure

i.e., the change in horizontal stress ($\Delta\sigma'_h$) can be achieved by maintaining the cell pressure constant and changing the back pressure or vice-versa.

Hence, the changes to the horizontal stress can be performed by setting the cell or back pressure regulator manually or it can be automated by connecting the supply pressure from volume booster (1:2) to cell or back pressure reservoirs.

The fully automated stress path control system requires a servo control system. A computer control program can be developed such that the experimental data is continuously scanned, following each scan the change in $\Delta\sigma'_v$ due to straining is computed. This determines the required adjustments $\Delta P_B = -S\ \Delta\sigma'_v$ or $\Delta P_C = S\ \Delta\sigma'_v$ to the back or cell pressure in order to follow the desired stress path. The computer then converts this new pressure as voltage (174.07 kPa= 1 volt) and sends this voltage to the electro-pneumatic pressure transducer (E/P) causing the change $\Delta\sigma'_h$. Another data scan is now taken and the process is repeated until the sample reaches the steady state stress where there will be no stress changes with further straining.

For the present study such a computer program was not developed. The change to the σ'_h to follow a desired stress path were performed manually by adjusting the back pressure regulator.

INSTRUMENTATION

Data Acquisition

It is crucial to measure all the variables accurately during any type of loading. Therefore, all test variables are measured using electronic transducers. These transducers were selected with careful consideration as to their stability and sensitivity. The soil sample is loaded axially. Therefore, the loading pattern is more sensitive to the axial load. Hence, axial load is measured by an internal load cell. This eliminates the need to consider loading ram friction and other external loads when calculating the axial load acting on the sample.

The test data from all the transducers are collected by the A/D portion of the Metrabyte 16/16F card. This unit is interfaced with the computer so that all the test data are directly recorded in a floppy disk or in the hard drive of the computer. The test data is recorded continuously at 2s interval during the monotonic loading and the constant load phase (static loading) in load control loading. During the cyclic loading phase, the test data is recorded at 10 ms interval. This high speed data recording is necessary in order to measure rapidly changing stresses and strains during the cyclic loading(dynamic loading). For strain controlled loading test data was stored at prescribed time interval. This time interval was adjusted manually during the shearing process depending on the time interval at which data was desired.

SAMPLE PREPARATION

Water pluviation

(1) Calculate the required weight (approximate) of sand by assuming e(deposition)=e(max.).

(2) Take 20-30 g less than that was calculated.

(3) Mix sand with water and boil it in a flask to de-air the water sand mixture..

(4) Cool the boiled sand to room temperature by placing in water bath for about 15 min..

(5) Fill the flask with de-aired water to the top and seal it with a rubber stopper.

(6) Take dial gauge(1) reference reading at the top pedestal by placing a dummy sample of known height between bottom and top pedestal with the porous stones.

(7) Take dial gauge(2) reference reading at the top of the loading ram.

(8) Boil the porous stones and cool it.

(9) Push de-aired water through the cell base drainage lines to saturate all the drainage lines.

(10) Check membrane for leak.

(11) Place the bottom porous stone and place same water on the top of the porous stone such that it remains saturated.

(12) Wrap Teflon tape around the edge of the porous stone.

(13) Insert the membrane into the bottom pedestal.

(14) Seal the membrane to the bottom pedestal with an 'O' ring and push water through the bottom drainage to ensure bottom drainage lines and the porous stone are fully saturated.

(15) Place the vacuum mold around the bottom pedestal and make sure not to pinch the membrane.

(16) Screw in all the four nuts for the vacuum mold.

(17) Pull the membrane and flip it around the top of the vacuum mold.

(18) Apply vacuum to the mold through the vacuum out lets. Make sure the membrane is stretched to the vacuum mold so that uniform samples can form in the cavity.

(19) Fill the membrane cavity with de-aired water.

(20) Apply vacuum to the sand flask and remove any air that escaped in to the boiled sand and water.

(21) Remove the flask from the vacuum and attach a rubber stopper (conical) with a glass nozzle.

(22) Add de-aired water through the nozzle until it over flows.

(23) Invert the flask by sealing the top of the nozzle with a finger.

(24) Keep the flask at the inverted position until all the sand in the flask has settled.

(25) Remove the finger and start deposition of the sand by allowing the nozzle tip to make shallow penetration into the membrane cavity filled with de-aired water.

(26) Move the flask in a circular motion so that sand would get deposit equally in all direction while maintaining the flask 1" above the top of the sample formation.

(27) After depositing all the sand remove the flask and level the top surface of the sample.

(28) Place the top porous stone in the top cap and wrap Teflon tape around the edge.

(29) Place the top cap on the sample surface by checking the level by with level tube.

(30) Place the dial gauge(1) at the top cap.

(31) Open the top drainage line.

(32) Increase the density of the sample (the desired height) by vibrating the cell base.

(33) Pull the membrane and seal it with the top cap. (apply a small load on the cap by pressing it while pulling the membrane).

(34) Plug the top drainage line.

(35) Apply 20 kPa vacuum through the bottom drainage line. note: the vacuum is being applied to a saturated sample. Hence, it should always be applied through a water reservoir.

(36) When the drainage valve is open you would notice small amount of water going into the reservoir. However, it would stop and stabilize if there is no leak. If water is continuously goes into the reservoir and air bubbles starts to appear, there is a leak, hence, no point in continuing the test.

(37) After the water in the vacuum reservoir stabilizes, remove the vacuum connection to the mold and carefully dismantled the mold.

(38) Measure the perimeter of the sample at top, middle and bottom.

(39) If you feel it is necessary to have a second membrane, install the second membrane.

(40) Assemble the cell.

(41) Fill the cell with the cell fluid.

(42) Take the final height of the sample with dial gauge(2) at the top of the loading ram.

(43) Close the drainage value and remove water reservoir connection.

Test procedure for water pluviated samples

(1) Set the LVDT to desired reading.

(2) Connect the cell pressure line to the cell pressure system.

(3) Apply a cell pressure of 25 kPa.

(4) Remove sample drainage and connect it to the drainage line. Note: the connection should be saturated, hence, allow water drops from both end of the tubing while connecting them. If no water appears from the sample drainage then the vacuum applied was greater than 25 kPa, hence, increase the cell until water drops appear. But make sure to calibrate the vacuum before next test.

(5) Take a reference reading of all the transducers.

(6) Measure 'B' value by increasing the cell and the back pressure at 50 kPa effective stress.

(7) When 'B' value of 0.99 or greater is achieved stop increasing the back pressure and increase the cell pressure in 50 kPa increments by allowing 5 min. at each stage until the desired effective consolidation stress is achieved.

(8) At each consolidation stage apply the load necessary for isotropic stress by dead loads at the top of the sample.

(9) Take a second reference reading of all the transducers and start shearing.

Moist tamping

(1) Fill the de-airer with boiled water.

(2) Apply vacuum and de-airer the water.

(3) Calculate the required weight (approximate) of sand by assuming e(deposition)=e(max.).

(4) Take approximately 100 g less than that was calculated.

(5) Mix sand with 5% (by weight) water.

(6) Take dial gauge reference reading at the top of the loading ram by placing a dummy sample of known height between bottom and top pedestal with the porous stones.

(7) In order to saturate the sample it is necessary to have top drainage and a small vacuum should be applied to the sample before removing the vacuum mold. Hence, it is always convenient to have the top drainage through the cell top.

(8) If it is necessary to use two membrane then the second membrane and the 'O' rings should be attached to the split vacuum cylinder and the top drainage line should be inserted through the vacuum cylinder before the top drainage line is attached to the top cap.

(9) Place the bottom porous stone and wrap Teflon tape around the edge of the porous stone.

(10) Insert the membrane into the bottom pedestal.

(11) Seal the membrane to the bottom pedestal with an 'O' ring.

(12) Place the vacuum mold around the bottom pedestal and make sure not to pinch the membrane.

(13) Screw in all the four nuts for the vacuum mold.

(14) Pull the membrane and flip it around the top of the vacuum mold.

(15) Apply vacuum to the mold through the vacuum out lets. Make sure the membrane is stretched to the vacuum mold so that uniform samples can form in the cavity.

(16) Divide sand in to four equal volume.

(17) Place first equal volume and compact the sand. Place the next equal volume and repeat compacting. For this layer the amount of compacting should be higher than previous one. Repeat the procedure for the next two equal volumes. The amount of compacting (No of drops for each layer) can be decided by performing several trial sample.

(18) Level the top surface of the sample.

(19) Place the top porous stone in the top cap and wrap Teflon tape around the edge.

(20) Place the top cap on the sample surface by checking the level with level tube.

(21) Pull the membrane and seal it with the top cap. (apply a small load on the cap by pressing it while pulling the membrane).

(22) Connect the top drainage line.

(23) Apply 20 kPa vacuum through the bottom drainage line.

(24) Remove the vacuum connection to the mold and carefully dismantled the mold.

(25) Measure the perimeter of the sample at top, middle and bottom.

(26) If you feel it is necessary to have a second membrane, put the second membrane.

(27) Assemble the cell.

(28) Fill the cell with the cell fluid.

(29) Take the final height of the sample with dial gauge at the top of the loading ram.

(30) Close the bottom drainage value .

Saturating the moist tamped samples

(1) Set the LVDT to desired reading.

(2) Apply 20-30 kPa cell pressure.

(3) Open the top drainage valve.

(4) Adjust CO_2 in let pressure to 5 kPa.

(5) Connect the CO_2 in let to the bottom drainage and open the drainage valve.

(6) After 15 min. remove CO_2 connection and connect the other bottom drainage to CO_2.

(7) After 15 min. remove CO_2 connection.

(8) Percolate de-aired water through the bottom drainage.

(9) Repeat percolation with the other drainage port.

(10) Take a reference reading of all the transducers.

(11) Measure 'B' value by increasing the cell and the back pressure at 50 kPa effective stress.

(12) When 'B' value of 0.99 or greater is achieved stop increasing the back pressure and increase the cell pressure in 50 kPa increments by allowing 5 min. at each stage until the desired effective consolidation stress is achieved.

(13) At each consolidation stage apply the load necessary for isotropic stress by dead loads at the top of the sample.

(14) Take a second reference reading of all the transducers and start shearing.

Reference

Atkinson, J.H., Richardson, D. and Robinson, P.J. 1987. Compression and extension of Ko normally consolidated Kaolin clay. Journal of Geotechnical Engineering, American Society of Civil Engineering. **113**(12): 1468-1481.

Chan, C.K. 1981. An electronic cyclic loading system. Geotechnical Testing Journal, American Society of Testing Materials. **4**(4): 183-187.

Lade, P.V. and Duncan, J.M., 1976. Stress path dependent behavior of cohesionless soils. Journal of Geotechnical Engineering, American Society of Civil Engineering. **102**(1): 51-68.

Sasitharan, S. 1989. Stress path dependency of dilatancy and stress-strain response of sand. M.A.Sc. Thesis. The University of British Columbia, Vancouver, BC., Canada.

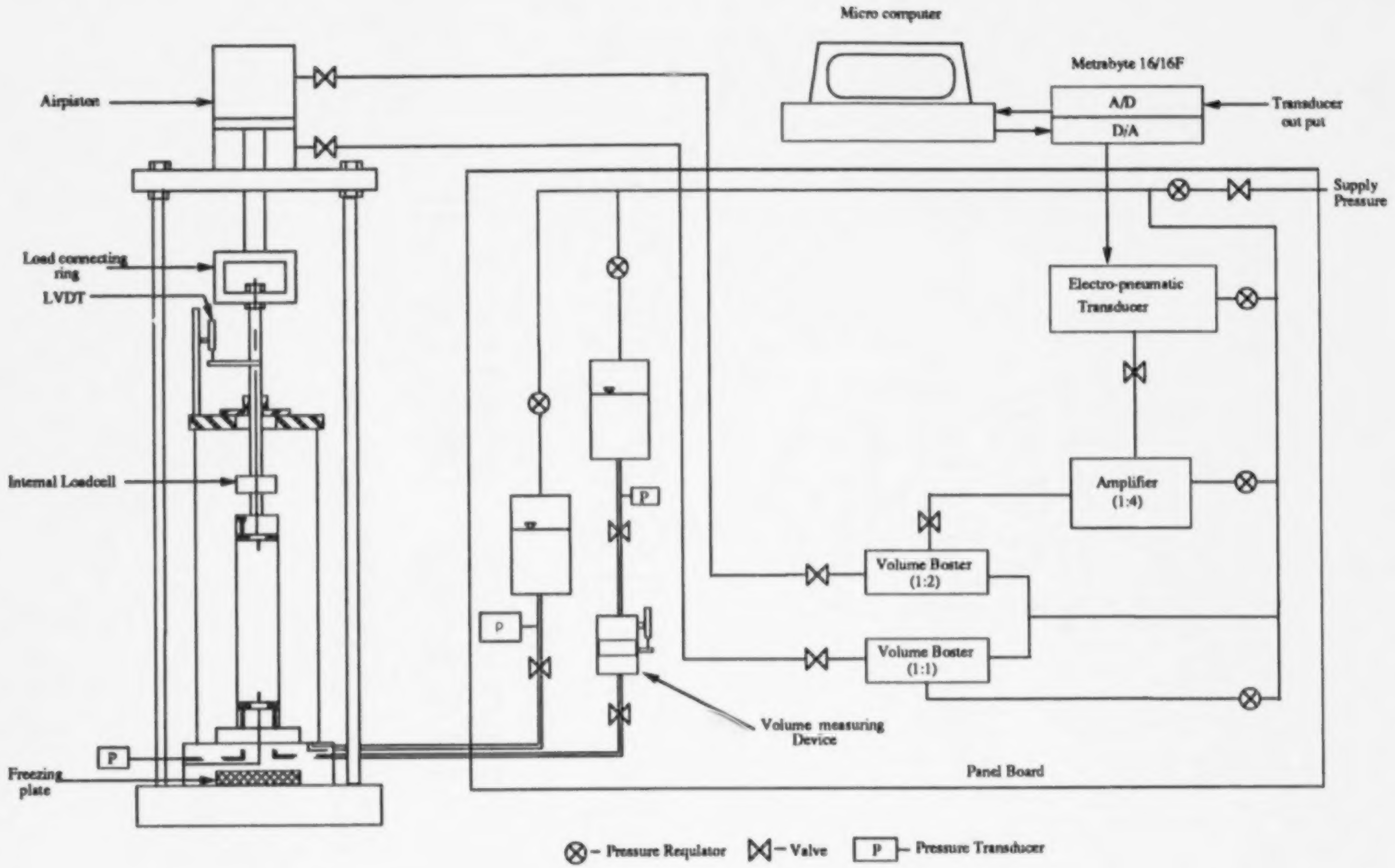

Figure A1 Schematic of the monotonic and cyclic triaxial testing system

APPENDIX B

FREEZ THAW TEST RESULTS

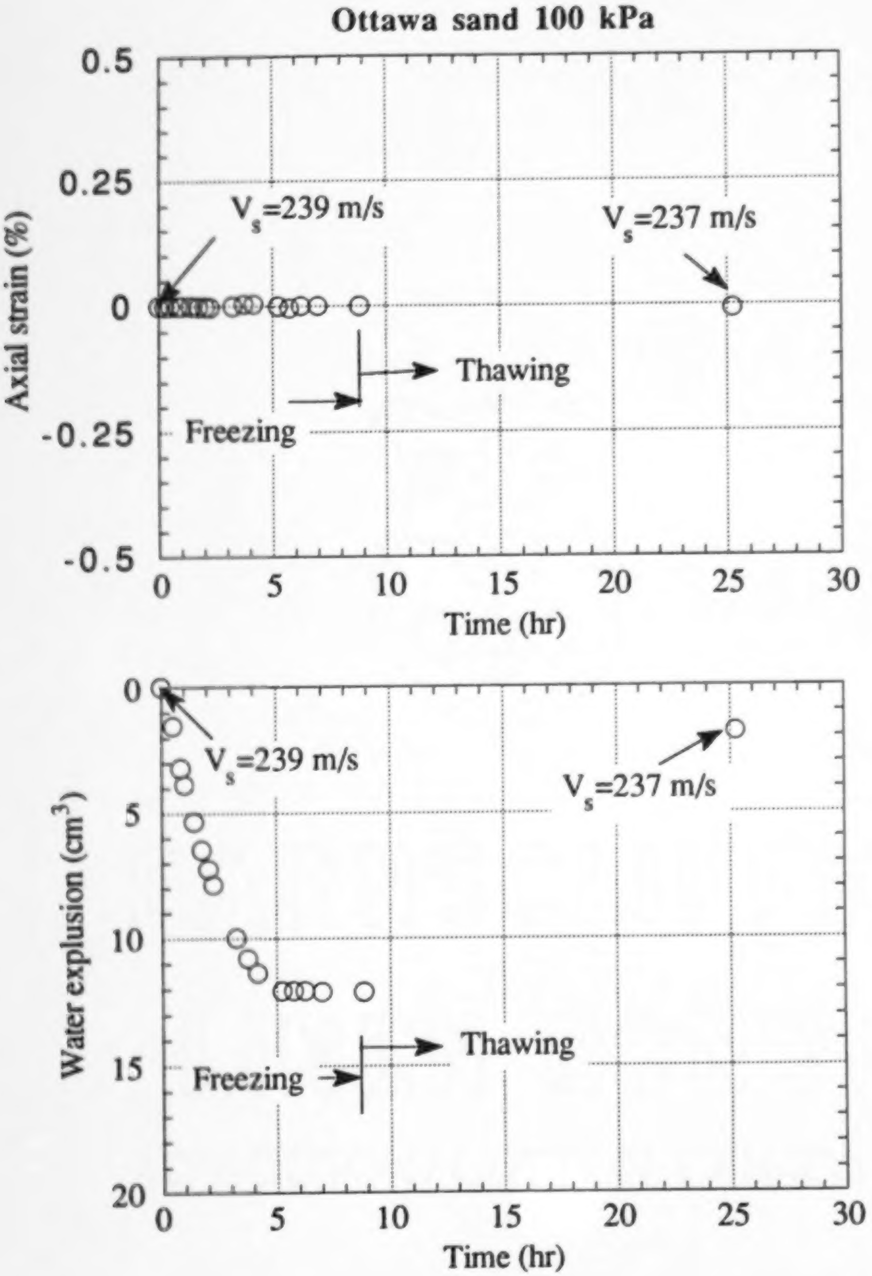

Figure B.1. Typical axial strain and water explusion behavior of a Ottawa sand sample at 100 kPa confining stress during freezing and thawing.

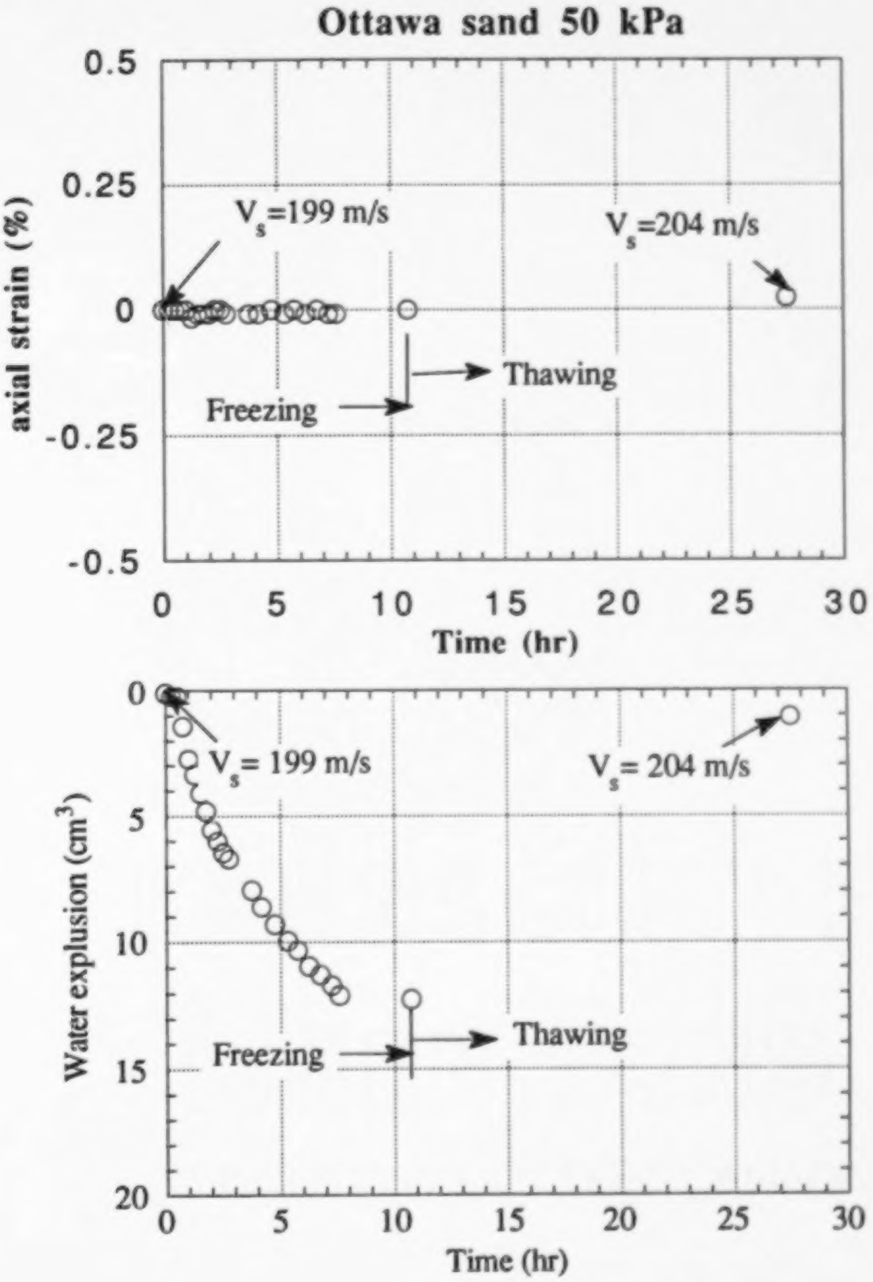

Figure B.2. Typical axial strain and water explusion behavior of a Ottawa sand sample at 50 kPa confining stress during freezing and thawing.

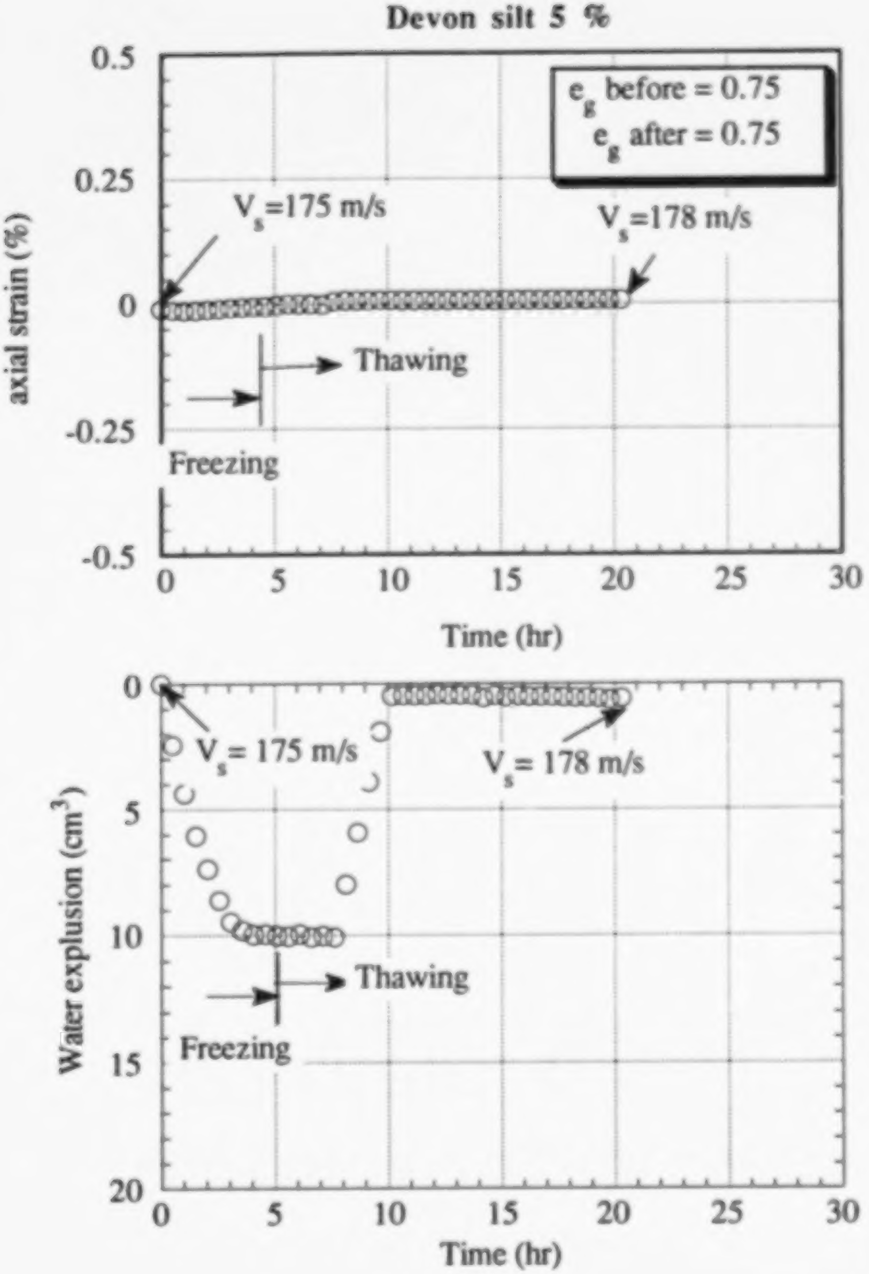

Figure B.3. Typical axial strain and water explusion behavior of a sample comprised of Ottawa sand and 5% Devon silt during freezing and thawing.

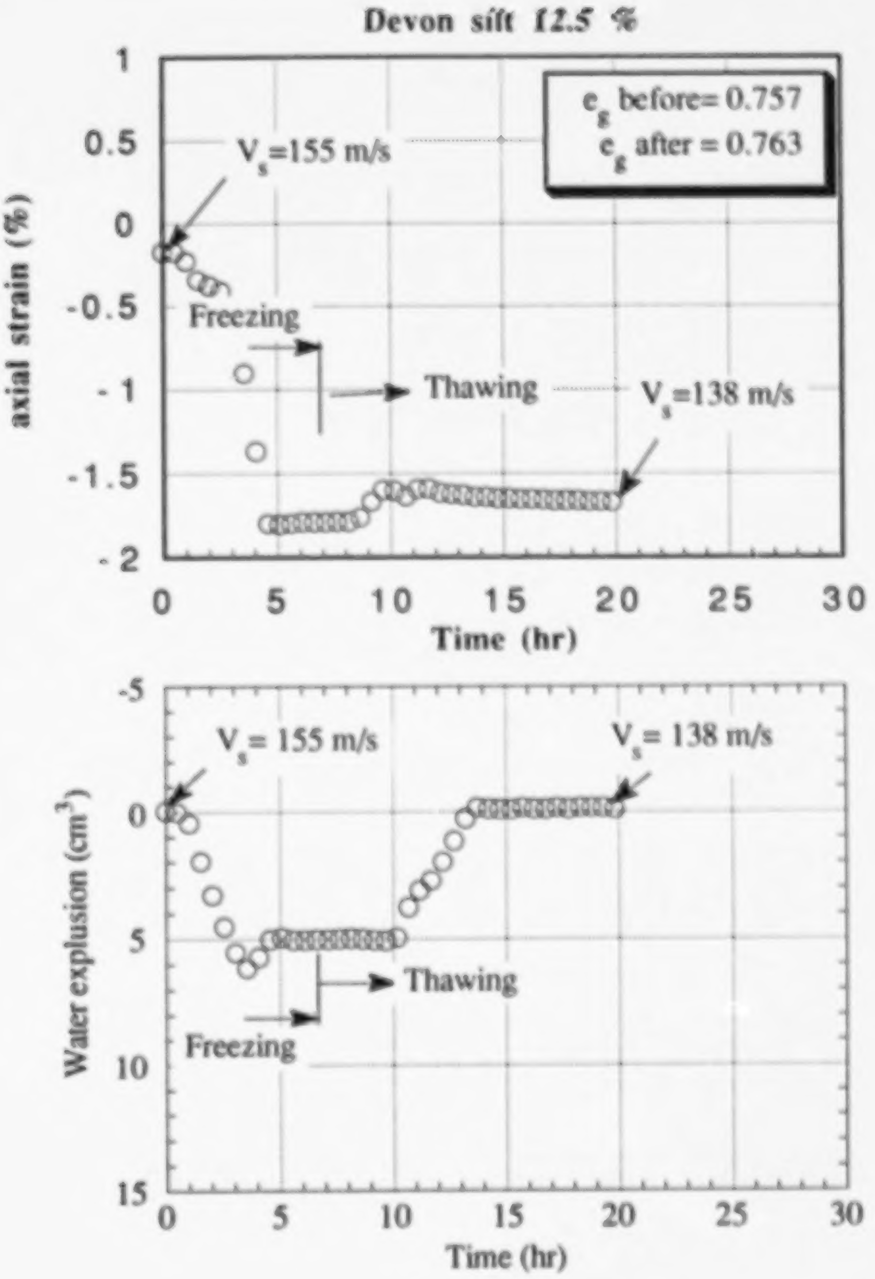

Figure B.4. Typical axial strain and water explusion behavior of a sample comprised of Ottawa sand and 12.5% Devon silt during freezing and thawing.

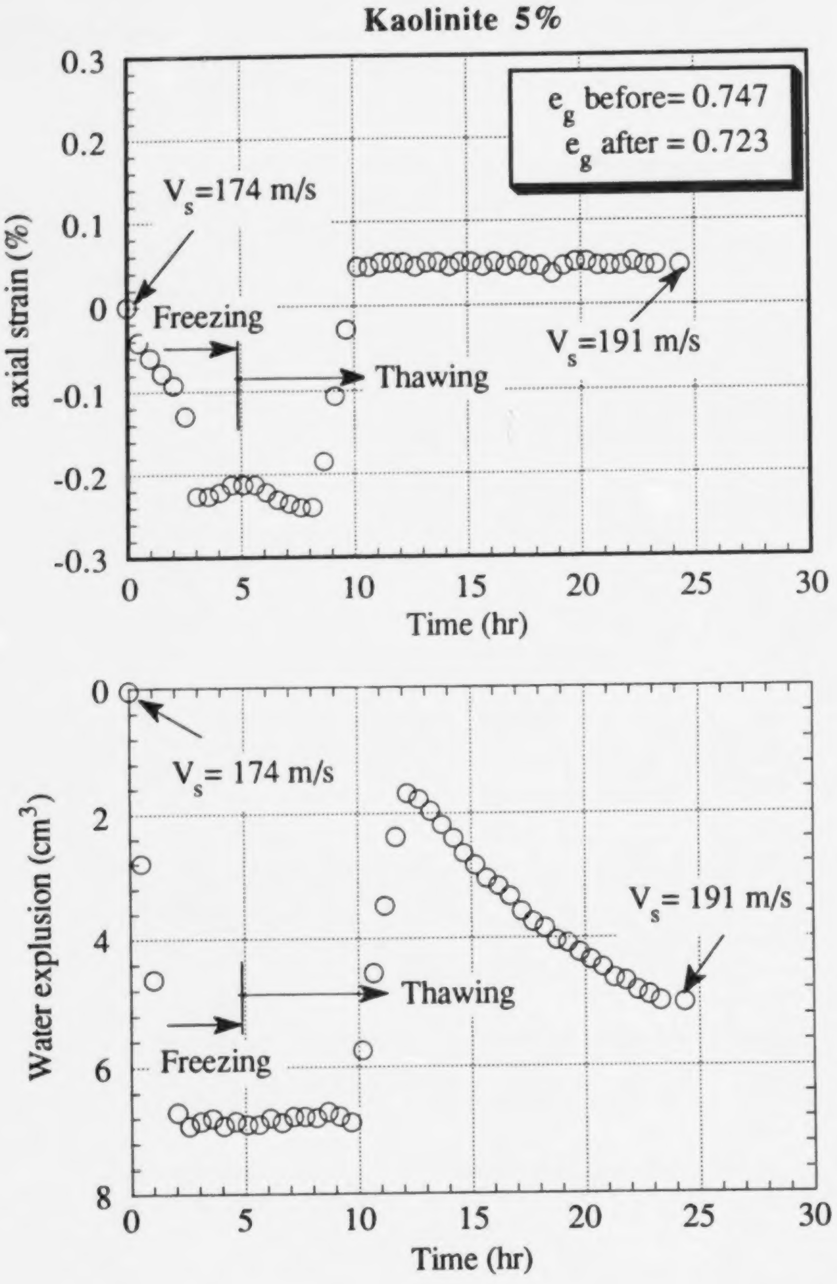

Figure B.5. Typical axial strain and water explusion behavior of a sample comprised of Ottawa sand and 5% Kaolinite during freezing and thawing.

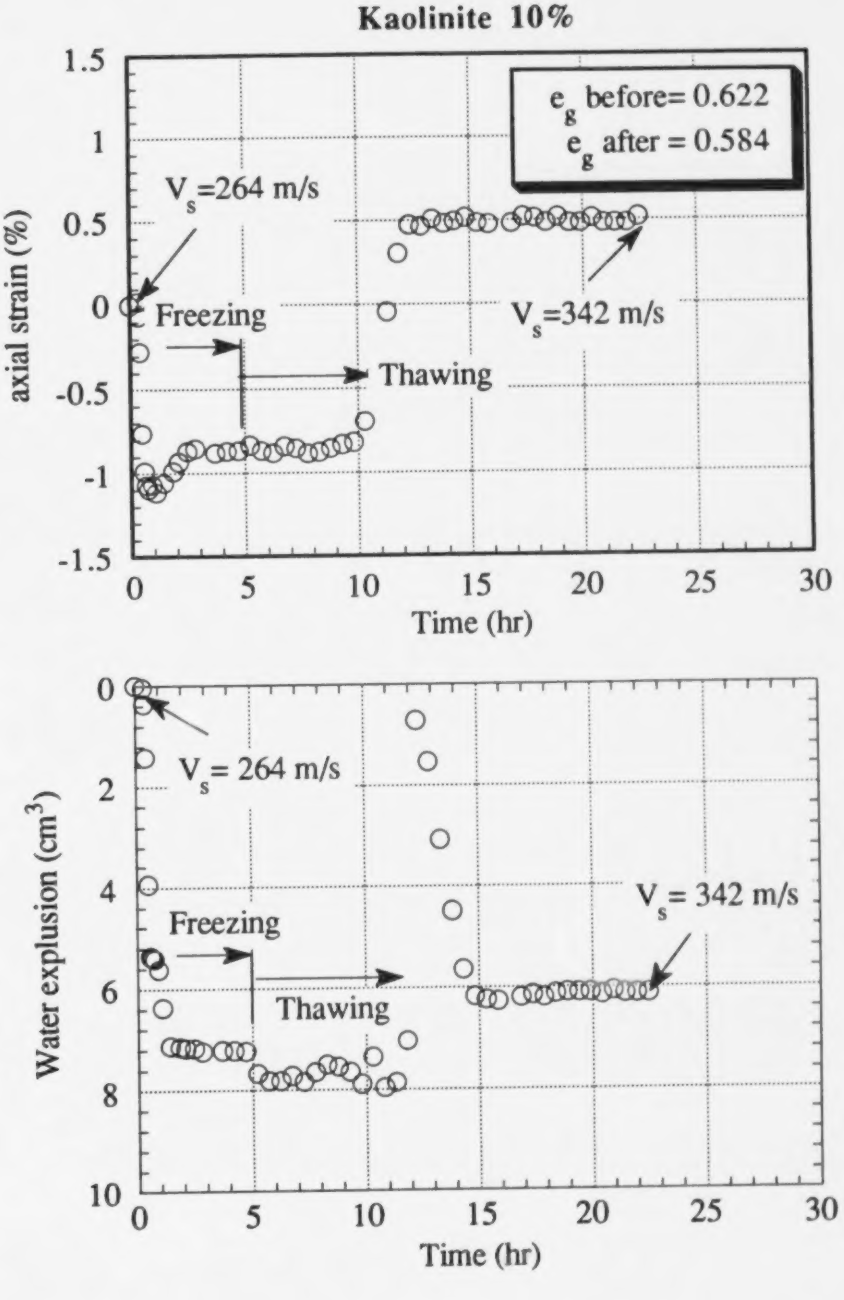

Figure B.6. Typical axial strain and water explusion behavior of a sample comprised of Ottawa sand and 10% Kaolinite during freezing and thawing.